EXPERIMENTAL AND NUMERICAL STUDY OF CONTINUOUS GALVANIZING GAS JET WIPING VIA A MULTI-SLOT AIR KNIFE

EXPERIMENTAL AND NUMERICAL STUDY OF CONTINUOUS GALVANIZING GAS JET WIPING VIA A MULTI-SLOT AIR KNIFE

By

ALI YAHYAEE SOUFIANI, B.A.Sc., M.A.Sc.

A Thesis

Submitted to the School of Graduate Studies
In Partial Fulfilment of the Requirements

For the Degree

Doctor of Philosophy

McMaster University

Title: Experimental and numerical study of continuous galvanizing gas jet wiping via a multi-slot air-knife

Author: Ali Yahyaee Soufiani, M.ASc.

Supervisors: Dr. Joseph R. McDermid, Dr. Andrew N. Hrymak

Pages: xxi-226

Abstract

This thesis investigates a novel configuration of a multi-slot jet, through numerical simulation and experimental measurements, for coating thickness reduction and noise elimination in the continuous galvanizing gas jet wiping process. Gas jet wiping is an effective hydrodynamic method for controlling the final zinc coating thickness on a moving steel substrate during continuous hot dip galvanizing (CHDG). In this process, an impinging jet, which is referred to as an air knife in the industry, is used to wipe excess zinc alloy from the steel substrate and control the final coating thickness through the combined effects of a pressure gradient and shear stress distribution on the moving strip emerging from the molten zinc bath.

In this study, a novel configuration of a multi-slot air-knife, comprising one main jet with two auxiliary jets, symmetrically located on each side of the main jet, was investigated as an alternative to the conventional single slot jet geometry. For this purpose, computational fluid dynamics was used to determine the wall pressure profile and wall shear stress distributions produced by the multi-slot jet, and these results were used in an analytical model to estimate the final zinc coating thickness on the substrate.

An operating region, which was relatively robust to air knife geometry changes, was determined through numerical simulations. Based on the CFD results, a modified geometry for the multi-slot air knife was proposed which led to lighter coating weights compared to the single slot jet. Numerical simulations over a wide range of gas wiping parameters was then performed in order to evaluate the wiping efficiency of the modified design of multi-slot jet at different operating conditions.

It was shown that for higher jet to wall distances ($Z/D \geq 8$) and at high strip velocities ($V_s \geq 1$ m/s), lighter coating weights can be obtained through use of the multi-slot jet design compared to that of the conventional single slot jet.

Moreover, a cold laboratory-scale model of the continuous galvanizing gas jet wiping process was designed and manufactured with the objective of validating numerically modelled coating weights for the prototype multi-slot air knife. Experimental measurements under a variety of knife geometries and process conditions agreed with the coating weight predictions of the analytical model. It was determined that the final coating weight was significantly affected by the auxiliary jet width, D_a, where lighter coating weights at higher strip velocities (up to 5.4 % at V_s = 1.5 m/s) could be achieved by using the multi-slot air knife prototype versus the conventional single-slot configuration. The effects of various operating conditions, such as: main jet Reynolds number (Re_m), auxiliary jet Reynolds number (Re_a) and jet-to-substrate distance (Z/D) on the final coating weight were also determined experimentally. The results showed that the final coating weight produced by the multi-slot air knife, with a relatively low flow for the auxiliary jet (i.e. $Re_a/Re_m \leq 0.5$), was lower than the final coating weight utilizing a similar main jet Reynolds from the single slot jet design.

Finally, the acoustic properties of the multi-slot prototype design were experimentally investigated. It was observed that the auxiliary jets had the ability to either attenuate or eliminate the tonal noise produced by the main jet. The measurements were performed for various main jet Reynolds number (Re_m), auxiliary jet Reynolds number (Re_a), jet to strip distance (Z/D) and strip velocities (V_s). It was found that the high intensity tonal noise

observed for the single jet was eliminated when using the multi slot-jet working with the same main jet condition and with relatively low auxiliary jet flows (i.e. $Re_a/Re_m \leq 0.5$). The coating weight measurements carried out under the same operating conditions also showed that multi-slot jet resulted in lighter coating weights compared to the single slot jet.

Acknowledgements

It would be my honor to express my sincere gratitude to my supervisors, Dr. Joseph R. McDermid and Dr. Andrew N. Hrymak for their precious guidance and patience through my studies at McMaster University. Also, I gratefully appreciate my lovely parents and my brothers Hamid, Saeed and Vahid for their love and support. Additionally, my thesis could not have been completed without funding support from Dr. Frank E. Goodwin, Executive Vice President of Technology and Market Development at the International Lead-Zinc Research Organization. Finally, I deeply thank the generosity of my friends at McMaster University, particularly Dr. Omid Dadoo, Dr. Yousef Tabatabai and Ali Khoei.

Table of Content

List of Figures

Nomenclature

a: Wall distance between the main and auxiliary jet (m)

b_p*:* Half width of pressure profile (m)

b_τ*:* Half width of shear stress profile (m)

B_X: Instrumental bias error for variable X

c: Speed of sound (m/s)

Ca: Capillary number

C_μ: Standard k-ε turbulence model constant

$C_{1\varepsilon}$: Standard k-ε turbulence model constant

$C_{2\varepsilon}$: Standard k-ε turbulence model constant

C_f : Skin friction coefficient

D: Main jet width (m)

D_a: Auxiliary jet width (m)

g: Gravitational acceleration (m/s^2)

G: Non-dimensional pressure gradient

h_f : final film thickness (m)

k: Turbulence kinetic energy (m^2/s^2)

L: Computational domain length (m)

L_s: Strip Width (m)

$\dot{m}_{cl}$: Mass flow rate of removed oil (kg/s)

M_w: Molecular weight of gas (g/mol)

P_∞: Ambient pressure (Pa)

P_s: Inlet Pressure (Pa)

P: Static pressure (Pa)

P_{max}: Maximum pressure (Pa)

P_X: Precision (random) error for variable X

$P_{0:}$ Nozzle pressure (Pa)

q: Volumetric flow rate per unit of film width (m^2/s)

Q: Non-dimensional withdrawal flux

R: Universal gas constant (J/mol.K)

Re_m: Main jet Reynolds number, $Re_m = \frac{\rho V D}{\mu}$

Re_a:Auxiliary jet Reynolds number, $Re_a = \frac{\rho V D_a}{\mu}$

s: Main jet and auxiliary jet standoff distance (m)

S: Non-dimensional shear stress

T: Temperature (K)

u: Fluid velocity (m/s)

u' : Fluctuating velocity (m/s)

u_τ: Shear velocity (m/s) ($u_\tau = (\tau_w/\rho)^{1/2}$)

V_s: Strip Velocity (m/s)

$w(x)$: local film thickness (m)

x: Cartesian coordinate (m)

y: Cartesian coordinate (m)

y^+: Non-dimensional distance from the wall ($y^+ = \frac{\rho u_\tau y}{\mu}$)

Z: Impinging distance (m)

Greek Symbols

γ: Ratio of specific heats of air

δr: Overall uncertainty of a dependent variable r

δX: Uncertainty for measured variable X

ε: Turbulence dissipation rate (m^2/s^3)

θ: Auxiliary jet inclination angle

μ: Dynamic Viscosity (kg/m.s)

μ_t: Turbulence viscosity (kg/m.s)

ξ_p: Non-dimensional distance, $\xi_p = x/b_p$

ξ_τ : Non-dimensional distance, $\xi_\tau = x/b_\tau$

ρ: density (kg/m^3)

ρ_{cl} : Density of coating liquid (kg/m3)

σ_k: Standard k-ε turbulence model constant

σ_ε: Standard k-ε turbulence model constant

τ: Shear stress (Pa)

Abbreviations

CHDG: Continuous hot dip galvanizing

EOC: Edge over coating

LES: Large eddy simulation

VOF: Volume of fluid

Chapter 1: Introduction

1.1 Thesis statement

A numerical and experimental investigation was performed on a novel multi-slot air knife to determine the effect of the wiping parameters and the air knife geometry on the wall pressure gradient, wall shear stress, film coating weight and noise generation during the continuous galvanizing gas jet wiping process. In order to carry out this project, numerical simulations were performed using FLUENT commercial code and a laboratory scale wiping setup was designed, manufactured, tested and utilized to verify the computational predictions. The numerically derived wall pressure gradient and wall shear stress distributions were used in an analytical model developed by Elsaadawy et al. [1] to predict film coating thickness and the results were compared with experimental measurements over a range of operating conditions and geometrical parameters.

1.2 The objectives of this study

At present, only single-slot jets are used in the continuous galvanizing industry. A recent trend within the automotive industry has been to reduce zinc coating weights applied to their steels as part of their efforts to reduce the overall mass of the body-in-white, thereby increasing vehicle fuel efficiency and reducing costs.

However, according to the below literature review, the current generation of single slot air knives are close to meeting their limit and are not capable of wiping to the desired low coating weights (less than 6 μm) at line speeds which are desired by the steel industry to

maintain productivity. In this study, a novel configuration for the air-knives comprising two symmetrically inclined auxiliary jets adjacent to the main jet will be investigated numerically and experimentally to determine if the novel design has significant advantages over the traditional single slot geometry in terms of decreased coating weights.

The motivations for the current research can be summarized as:

1) Improving robustness of the zinc coating control process:
   - Assess the sensitivity of the coating weight to the multi-slot jet pressure and shear stress profiles to determine if there are operating regions that are reasonably robust to air knife profile changes.

2) Operating at high line speeds:
   - Determine if lower coating weights at high line speeds can be obtained by the use of alternative configurations for the multi-slot air knife.

3) Applicability of the analytical coating model:
   - Investigate if the analytical lubrication model is valid for the new multiple slot air-knife configuration.

4) Noise elimination and coating thickness reduction:
   - Investigate if using the multi-slot air knife can simultaneously lead to noise elimination and lighter coating weights compared to the traditional single jet wiping geometry.

1.3 Thesis outline

This thesis comprises eight chapters: an Introduction, a Literature Review, followed by four journal papers discussing the experimental and numerical research undertaken as part of this thesis followed by a Global Discussion (Chapter 7) which discusses the results of the four journal papers and a Conclusions chapter. Chapters 3 has been published in the Journal of Coating Technology and Research, Chapter 4 has been accepted in final form in Metallurgical and Materials Transactions B (MMTB) and Chapter 5 has been submitted to the journal Iron and Steel Institute of Japan (ISIJ) International. Chapter 6 will be submitted for publication shortly.

The contents and the role of each chapter in the thesis are described briefly below.

Chapter 1: "Introduction". This chapter provides a general introduction to the research; describing the motivation for this study, defining detailed research objectives and presenting an outline of this thesis.

Chapter 2: "Literature Review". This chapter reviews the relevant literature in the area of gas jet wiping via the conventional single slot jet configuration. The limitations of single jet wiping discussed in the literature are then reviewed and the chapter finishes with a literature survey on previous work on the multi-slot air jet geometry.

Chapter 3: "Numerical investigation of multiple slot jets in air knife wiping". In this chapter, the multi-slot air-knife was investigated through numerical simulations. The aim of this study was to investigate the sensitivity of the coating weight to the pressure and shear stress profiles in order to determine if there were operating regions that were reasonably robust to air knife geometry changes.

Chapter 4: “Experimental and Numerical Study of Coating Thickness using Multi-Slot Air-Knives”. This chapter presents an experimental investigation and numerical analysis of the prototype multi-slot air-knife, which offers an increase in wiping efficiency relative to the traditional single-slot jet geometry in the continuous galvanizing process. The applicability of the analytical coating weight model of Elsaadawy et al. [1] to predict the final coating weight was determined for the multi-slot air-knife, where particular focus was devoted to the effect of the air-knife geometric parameters.

Chapter 5: “A Parametric Study of Multi-Slot Air Knives for Coating Thickness Reduction”. The main goal of this chapter was to identify the operating window for which lighter coating weights can be achieved with multi-slot air-knives at higher strip velocities. The effects of various operating conditions on the final coating thickness were determined experimentally. Numerical simulations of multi-slot jet wiping were also performed under the same conditions using computational fluid dynamics modeling to predict the final coating thickness.

Chapter 6: “Experimental study on coating thickness reduction and noise attenuation via multiple slot air-knives”. This chapter investigates the simultaneous effect of the multi-slot air knife on noise elimination and coating thickness reduction within the gas jet wiping process. Noise and coating thickness measurements were performed over a wide range of operating parameters for the gas jet wiping process via multi-slot air-knife to compare the results with the traditional single slot air-knife.

Chapter 7: “Global Discussion”. This chapter draws together the important findings from each of the previous chapters illustrating how each one contributes to the overall research objectives.

Chapter 8: Finally, some general conclusions are drawn and suggestions for future work are offered.

Chapter 2: Literature review

This chapter begins with a brief introduction to the continuous hot-dip galvanizing process, and continues with a description of the gas jet wiping process used to control the Zn-alloy coating thickness – usually referred to as coating weight in the literature – in the CHDG process. It then presents some industrial difficulties regarding traditional single slot jet wiping and, finally, discusses an alternative configuration of the multi-slot air knife for use in the continuous galvanizing line for controlling the coating thickness of liquid zinc on a steel substrate.

2.1 Introduction

Continuous hot-dip galvanizing is a coating technique widely used in the steel industry. In this process, a steel strip is annealed in a N_2-H_2 process atmosphere in order to control its properties and surface chemistry, after which it is continuously immersed in a bath of molten liquid zinc, usually at 460°C, during which the liquid metal alloy reactively wets the moving sheet substrate (Figure 2-1). When the substrate emerges from the bath, it carries out a relatively thick layer of liquid zinc due to viscous drag. The molten zinc coating thickness on the sheet substrate is controlled above the bath by using opposing planar turbulent gas jets or air knives, in a single-slot configuration. This process is called gas jet wiping. The coating is then allowed to cool and solidify before contacting the tower roll (Figure 2-1) to avoid transferring or damaging the coating. Finally, it is either coiled or sheared into cut lengths at the exit of the line [2]. The coating weight – usually expressed

as a mass of zinc per unit area of substrate, i.e. g/m^2/side – is monitored continuously using X-ray or gamma ray coating thickness measurement equipment.

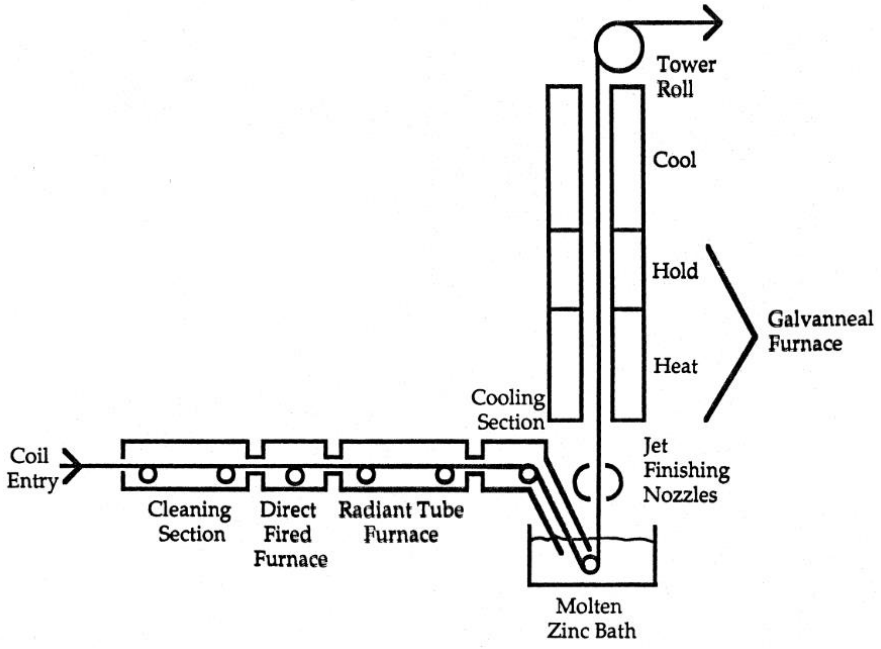

Figure 2-1) Schematic of a continuous hot-dip dip galvanizing line [2].

Gas jet wiping is based on the action of an impinging slot jet on a liquid film carried by a moving substrate. The impinging slot jet has been studied extensively, with a focus on the heat transfer to the substrate ([3]–[6]). Due to the high Nusselt number near the wall region, which leads to a high rate of heat transfer, impinging jets have found many applications in various industries such as the drying of textiles and paper, cooling of electronic devices, and cooling of turbulent blades ([7]–[9]). Also, the complex flow structure of impinging jets has been the subject of several investigations ([10]–[12]).

It has been shown that the velocity field of an impinging jet comprises three zones [10]. These are the potential core, the intermediate zone and the impinging zone (Figure 2-2). In

the potential core zone, the centerline velocity of the gas jet does not change significantly from the jet exit velocity and remains constant over the length of this zone (Figure 2-3). The length of the potential core varies between 3D and 6D (where D is the jet width). In the transition zone, the axial velocity profile begins to decay and, eventually, in the impinging zone as the flow reaches to the plate, the value of velocity normal to the plate becomes zero and the flow turns along the impingement plate (Figure 2-3). The flow builds up the higher pressure and shear stress on the wall [10].

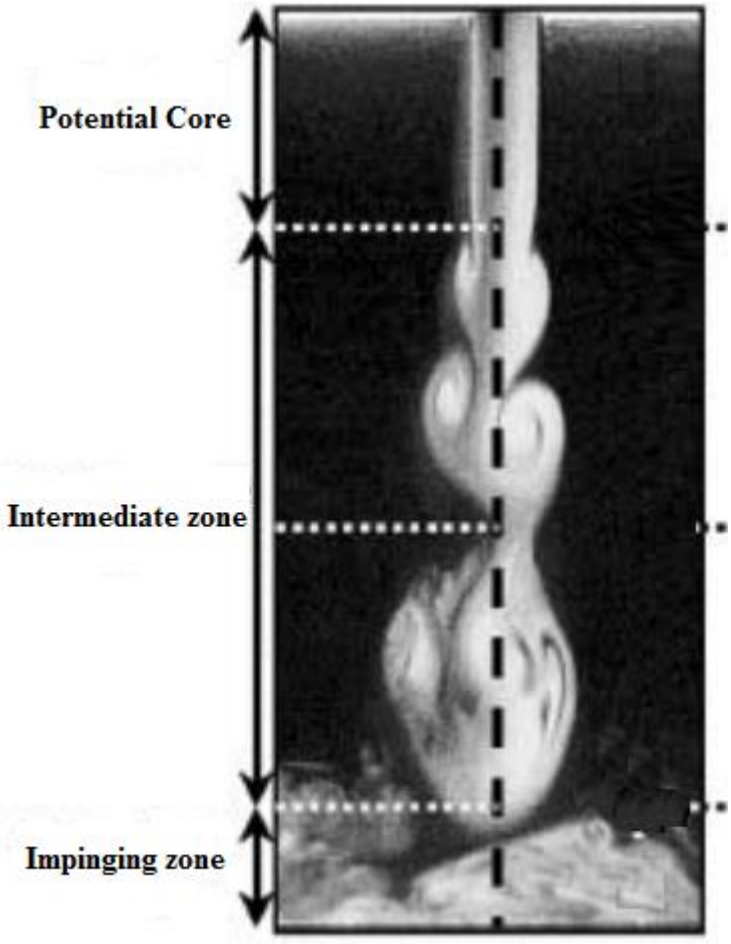

Figure 2-2) Visualization of an impinging jet flow field [10]

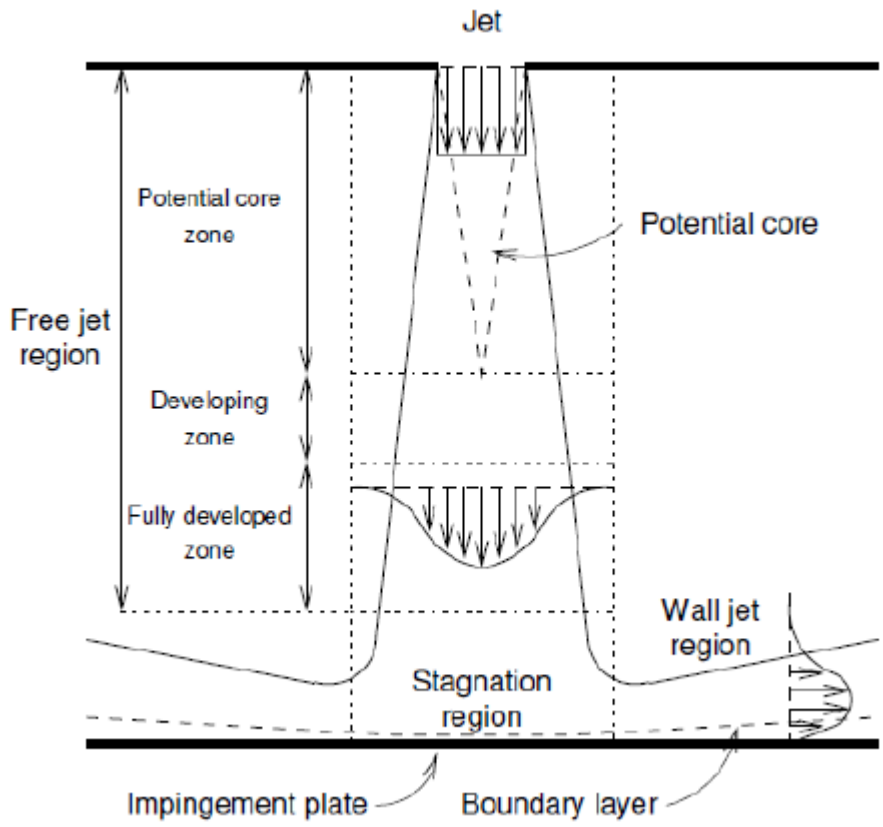

Figure 2-3) impinging jet flow regimes [13].

In addition to the above mentioned applications, one of the important industrial uses for impinging jets is in the gas jet wiping process in the continuous hot dip galvanizing line. This application is the subject of the current study and is discussed in more detail below.

In continuous hot dip galvanizing, a pair of opposing impinging jets – commonly referred to as air knives – are located above the molten zinc bath (Figure 2-1) to control coating thickness of liquid zinc on the steel substrate. These air knives remove the excess zinc by applying a pressure gradient (dp/dx) and shear stress (τ) to the coating layer and return the excess molten Zn liquid to the bath (Figure 2-4). The film thickness after wiping (h_f) depends on the substrate velocity V_s, wall pressure gradient and shear stress, the nozzle

to substrate standoff distance *Z*, the nozzle slot width *D*, and the physical properties of the liquid zinc ([14], [15]).

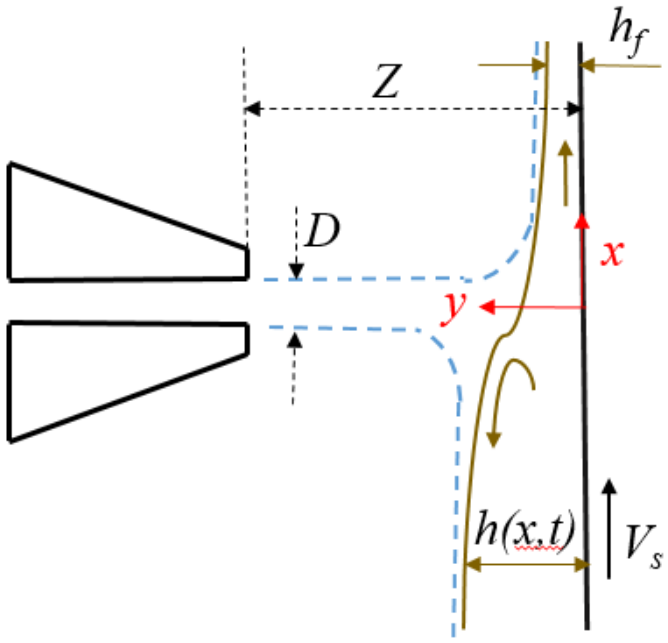

Figure 2-4) Schematic of the gas wiping process.

2.2 Gas jet wiping via the single slot jet geometry

At present, single-slot jets are commonly used in the continuous galvanizing industry. There are several studies available in the literature on using a single slot turbulent impinging jet for controlling the liquid zinc coating thickness on a metallic strip during continuous galvanizing ([1], [14]–[19]). The early work on this subject assumed a decoupled model – i.e. a thin liquid coating film, with boundary conditions on the surface coupled to the impinging flow field (i.e. pressure gradient and shear stress gradient). Fundamental analytical work was done by Thornton and Graff [14] to predict the Zn alloy film coating thickness after wiping by an air-knife. They postulated that only the maximum

wall pressure gradient played a major role in the determination of the final film thickness and the predicted coating thickness by this model was proportional to the square root of the strip velocity and the inverse square root of the maximum wall pressure gradient (Equation 2.1).

$$h_f = 4.57\left(\frac{\mu V_s}{(dp/dx)_{\max}}\right)^{1/2} \tag{2.1}$$

Where h_f is final coating thickness, μ is coating liquid viscosity, V_s is the strip velocity and $(dp/dx)_{\max}$ is the maximum wall pressure gradient.

Ellen and Tu [15] incorporated the effect of shear stress applied to the film surface by the jet, and improved the coating weight model of Thornton and Graff [14]. The assumptions and details of the model will be discussed in the introductory sections in Chapters 3-5. They showed that using the wall shear stress in the analytical model improved the model's applicability over a wider range of operating conditions. In that sense, their model increased the accuracy of the analytical model for the estimation of final coating weight.

Tuck and Broeck [20] investigated the influence of surface tension on gas jet wiping, which was neglected in the previous studies. By comparing the models of Thornton and Graff [14] and Tuck and Brock [20] (Figure 2-5), it can be inferred that the surface tension effect became negligible for larger value of the pressure gradient as the jet action then overcame the coating liquid capillary force. Following Tuck and Broeck [20], Yoneda [21] further numerically analyzed the gas jet wiping process, including the effect of surface

tension and shear stress in the mathematical model, showing in general a small contribution of surface tension with larger pressure gradient (Figure 2-5).

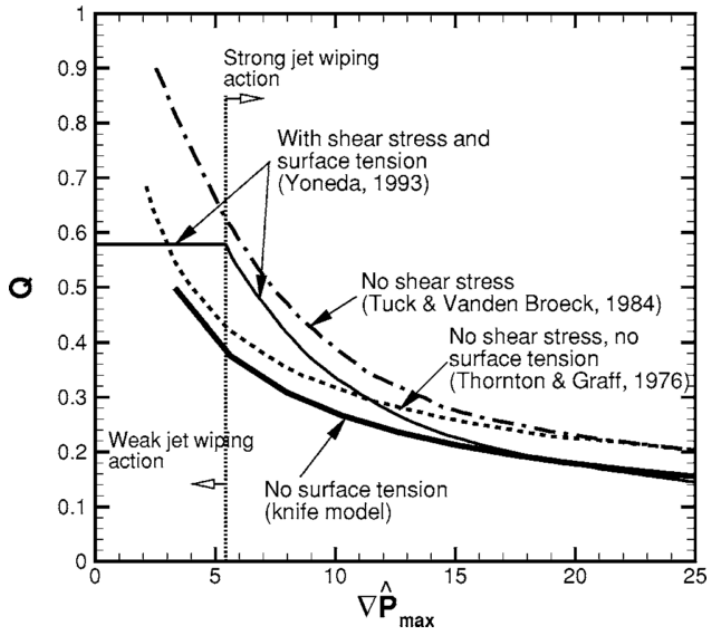

Figure 2-5) Comparison of the dimensionless volumetric film flow rate predicted by the knife coating weight model developed by Ellen and Tu [15] and various models from literature for Ca=0.01 [19].

Tu and Wood [22] experimentally measured the wall pressure and shear stress distribution beneath an impinging jet for a wide range of plate to nozzle ratios of $2 \leq Z/D \leq 20$ and gas jet Reynolds numbers of $3000 \leq Re \leq 11000$, where the nozzle width was $0.97 \leq D \leq 6.4$ mm. They concluded that the length of the potential core was approximately $5D$. They also examined a range of Preston and Stanton tubes for measuring the shear stress, and found that a 0.05 mm-high Stanton tube gave the most accurate results. They also found that the non-dimensional shear stress profile was dependent on the plate-to-nozzle ratio and Reynolds number.

Hrymak et al. [23] numerically predicted the wall pressure and wall shear stress distribution for low impingement ratios (i.e. $2 \leq Z/D \leq 6$). The range of coating weight studied was between 45-75 g/m^2. The coating weight model developed by Ellen and Tu [15] was used to calculate final coating thickness of the film and the results were in an excellent agreement with the industrial data for the targeted range of coating weights with 8% discrepancy.

Naphade et al. [16] used the mathematical model proposed by Ellen and Tu [15] to estimate the coating weight as a function of strip velocity, jet nozzle pressure, plate to nozzle distance and nozzle gap width. The results were validated with industrial line data and the experimental results of Buchlin [24]. They showed that, for a fixed pressure and strip velocity, the coating weight was a function of *Z/D* and increaased with increasing *Z/D* s (Figure 2-6). As the slope of the curve for $Z/D \leq 19$ was less compared to the steep slope of the curve for high *Z/D* ratios, they deduced that coating weight was less sensitive to *Z/D* variations over this range of wall to jet distances. Thus, operation in relatively low *Z/D* region was more robust in the gas jet wiping process to achieve uniform coating weight for $Z/D \leq 19$.

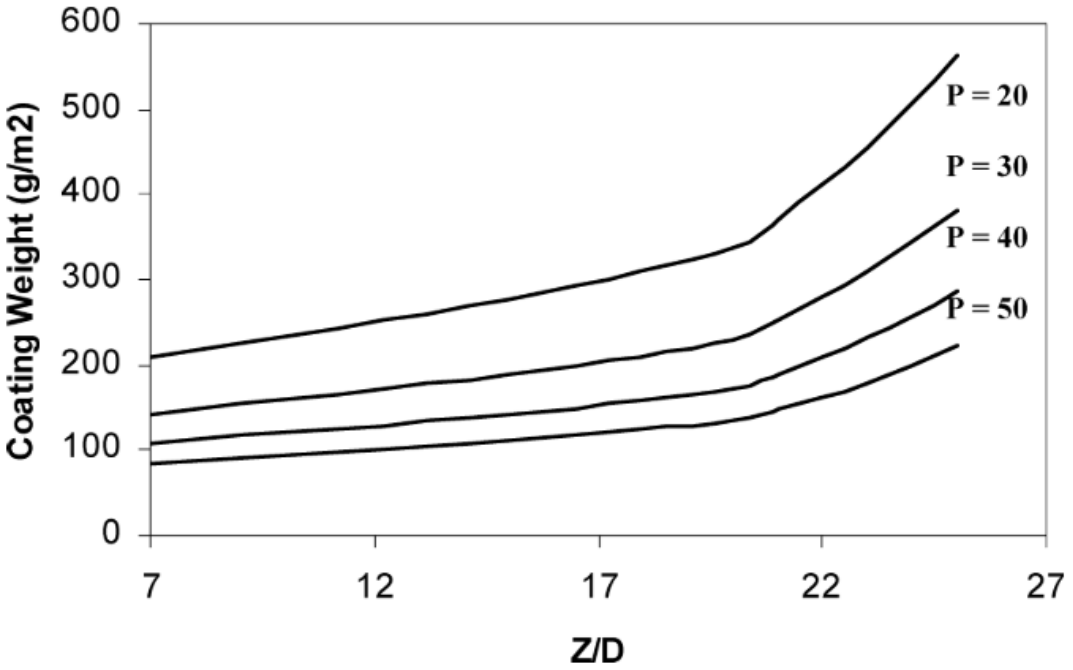

Figure 2-6) Coating weight versus Z/D, V_s = 1.5 m/s, P in kPa [16].

Gosset et al. [25] studied the wiping performance of a gas jet at small standoff distances ($Z/D \leq 8$). Such a study was of great interest for practical applications, because a small variation of Z due to substrate vibration results in a negligible variation of the coating thickness. They developed wall pressure gradient and shear stress correlations based on experimental measurements (Equations 2.2-2.3).

$$\frac{d}{d\xi}\left(\frac{P}{P_{\max}}\right) = -2.607\xi^2\left(1+0.55\xi^3\right)^{-2.58} \tag{2.2}$$

$$100\frac{\tau_{\max}.Z/D}{P_{Nozzle}} = a\left(Z/D\right)+c \tag{2.3}$$

Where $\xi = x/b$ in which b is the location of $P_{max}/2$. And a and c are constants which are functions of jet Re. The correlations were then implemented in the analytical model developed by Ellen and Tu [15] for the prediction of film thickness. It was observed that

the final coating thickness remained almost constant as long as the normalized standoff distance (*Z/D*) did not exceed 7, i.e. the impingement wall was in the jet potential core.

Elsaadawy et al. [1], developed a coating weight model based on the work of Ellen and Tu [15] as a function of the jet operating parameters for $Z/D \leq 8$. By combining experimental and computational methods they improved the pressure and shear stress correlations using the *k-ε* turbulence model. (Equations 2.4-2.6)

$$\frac{d}{d\xi_P}\left(\frac{p}{p_m}\right) = -3.6\xi_p^3[1+0.6\xi_p^4]^{-2.5} \tag{2.4}$$

$$\begin{cases} \dfrac{\tau}{\tau_{\max}} = erf(0.41\xi_\tau) + 0.54\xi e^{-0.22\xi_3^3} & for \quad 0 \leq \xi_\tau \leq 1.73 \\ \dfrac{\tau}{\tau_{\max}} = 1.115 - 0.24\ln(\xi_\tau) & for \quad \xi_\tau > 1.73 \end{cases} \tag{2.5}$$

Where $\xi = x/b$ and

$$\begin{cases} \dfrac{b_p}{D} = 0.0453\left(\dfrac{Z}{D}\right) + 0.7921 \\ \dfrac{b_\tau}{D} = 0.0443\left(\dfrac{Z}{D}\right) + 1.1687 \end{cases} \tag{2.6}$$

The Elsaadawy et al. [1] coating weight model represented a significant improvement , where the model was in good agreement with industrial data for coating weights of less than 75 g/m^2 in which the maximum deviation was 8% between the predicted coating weight and measured data.

Kweon and Kim [26] numerically investigated the effect of the single jet width on final coating thickness. They simulated a two-dimensional steady compressible flow by using *k-ε* turbulence model. The slot gap varied in the range of 0.6 mm to 1.7 mm. They showed

that for a given jet to wall distance, an effective nozzle width exists which lead to thinner coating thicknesses (Figure 2-7).

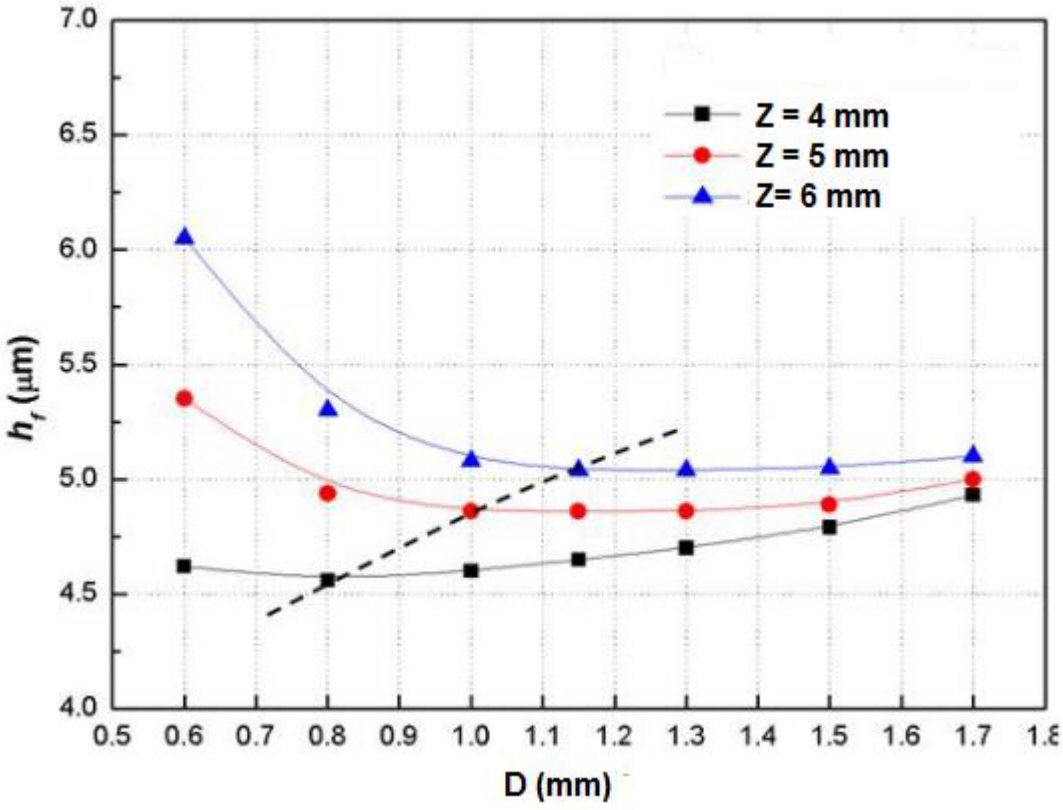

Figure 2-7) Variation of final coating thickness with *D* [26].

In addition to the decoupled approaches to model final coating thickness, the fully coupled simulation approach was investigated by Lacanette et al. [27] with the impinging jet on a moving strip with a liquid film. The two phase simulation was carried out in order to determine the free surface of the coating liquid and to visualize the shape of the liquid on the moving substrate for the impingement region and its vicinity. Analyzing the time evolution of the film thickness throughout the wiping process showed that, after 0.5 s, the film thickness did not change significantly and reached to steady state condition.

In other work, Lacanette et al. [28] used a LES turbulence model in order to obtain the mean pressure gradient and shear stress distributions induced by a single slot jet on a dry wall. The verified profiles were then applied in the coating weight model of Ellen and Tu [15] for determination of the final film thickness. Lacanette et al. [28] also used the VOF method coupled with the LES model in order to determine the effect of a turbulent jet on a moving wall containing a liquid film layer. By comparing the decoupled lubrication model and the two phase model (Figure 2-8), they concluded that the model developed by Ellen and Tu [15] was a good estimator for the final film thickness. It was also shown that for $2 < Z/D < 8$ – i.e. within the jet potential core – the film thickness after wiping was not dependent on the nozzle to plate distance in both the experimental and numerical results.

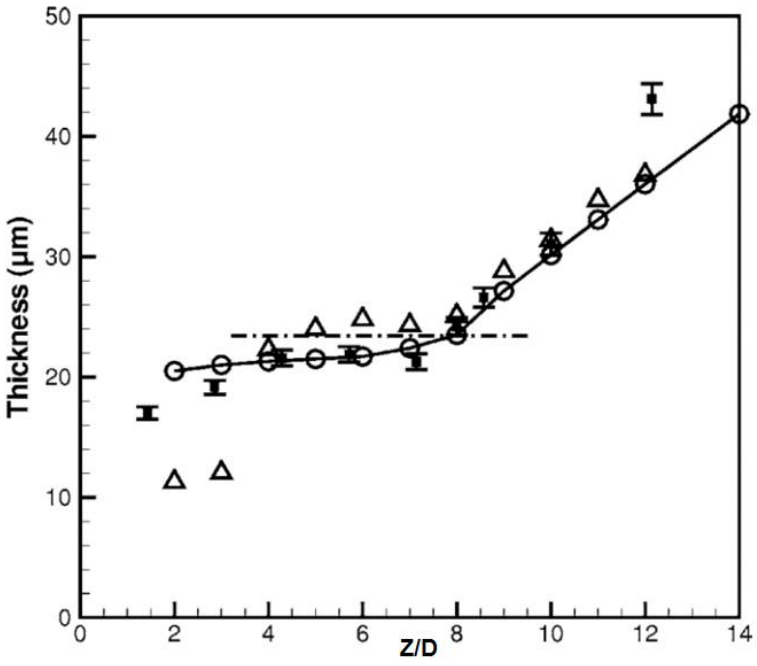

Figure 2-8) Effect of the nozzle to plate distance on coating thickness for D = 1.4 mm and Re = 4500 (□: Experimental data with error bars, Δ: two-phase flow simulations, O: Ellen and Tu [15] analytical model) [28].

2.3 Limitations of gas jet wiping process via the single slot-jet geometry

Thin steel sheet products are generally used by the automotive industry for either structural members or closure panels. A recent trend within the automotive industry has been to reduce the zinc coating weights applied to steel sheets, as part of their efforts to reduce the overall mass of the body-in-white to meet regulation requirements for higher fuel efficiency [29] and reduce costs while continuing to meet consumer anti-corrosion, vehicle safety and durability expectations. However, the current generation of single slot air knives are very close to their limit with respect to having the capability of wiping to the desired low coating weights of less than 40 g/m^2 at higher line speeds desired by the steel industry [18].

To obtain lower coating weights using a traditional single slot air-knife at reasonable strip velocities, the wiping pressure would have to be increased significantly. However, increasing the pressure can cause some industrial difficulties such as higher tonal noise generation, splashing and coating non-uniformity. Moreover, zinc coating quality is an important industrial issue, especially in the automobile industry, which requires exposed (i.e. parts exposed directly to the consumer view – e.g. closures such as hoods and door panels) sheet steels to have a defect-free, uniform coating and excellent corrosion resistance. One of the coating defects in the continuous hot-dip galvanizing process affecting final coating quality is a localized non-uniform coating known as check mark [30]. Check marks which appear on the steel strip may be caused by flow instabilities arising from gas jet flow flapping. The mentioned industrial difficulties are briefly summarized below.

2.3.1 Splashing

One of the phenomena which limits wiping efficiency of impinging slot jets in the continuous galvanizing process is splashing. Splashing is characterized by the ejection of zinc droplets from the strip which results in unacceptable coating defects in the final product, nozzle blockage due to solidification of liquid zinc droplets on the air-knife nozzle and, therefore, increasing of equipment maintenance [18].

Gosset and Buchlin [19] studied splashing experimentally using two different impinging slot jet configurations on a water-model facility and the effect of strip speed, nozzle pressure, standoff distance, and the tilt angle of the nozzle (α) on splashing was investigated. At constant jet pressure, the substrate velocity was increased until splashing occurred along the strip. The onset of splashing occurs when the shearing effect of the wall jet flow overcomes the stabilizing effect of surface tension [31]. The critical jet Weber number above which splashing developed was correlated with the film Reynolds number based on the strip velocity, V_s, and the final coating thickness (Figure 2-9). It was shown that tilting the nozzle downward can delay splashing and allows for higher line speeds. A tilt angle of 30° was found as an optimal angle at which the strip velocity could increase by 40%.

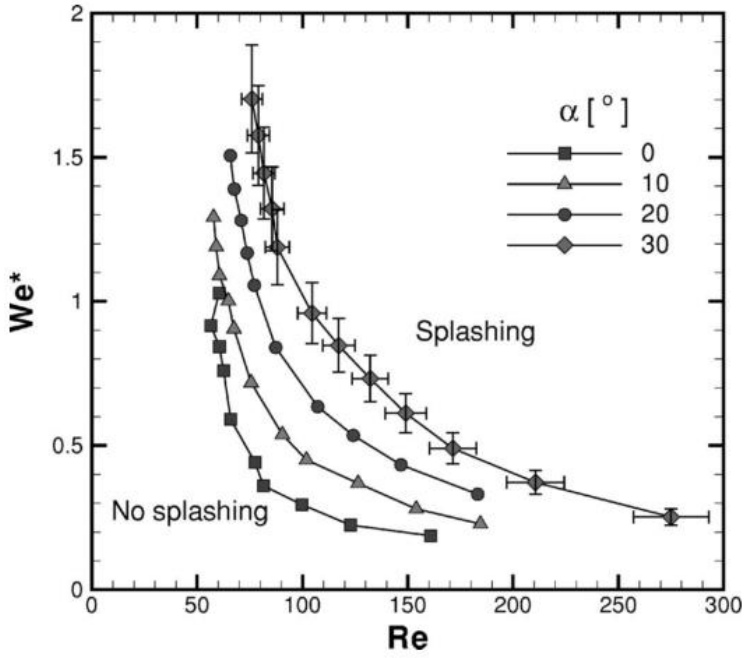

Figure 2-9) Dimensionless splashing curves for *Z/D* = 10, *D* = 1.4 mm and tilting angle of $0 \leq \alpha \leq 30°$ [19].

Cho et al. [31] also studied the effect of jet tilting angle on delaying full splashing. They showed that tilting the air knife alleviates the splashing problem. However, by increasing the jet inclination for angles higher than 5°, the coating thickness increased up to 11%. For jet angles less than 5°, a significant difference was not observed.

2.3.2 Edge over coating (EOC)

Edge over coating (EOC), in which the coating thickness at the edge of the sheet is thicker than the middle of the strip, is another undesirable outcome of the gas jet wiping process. EOC causes difficulties in coiling or results in inadequate galvanealing at the edge of sheet substrate. Kim et al. [32] numerically studied edge over coating of a galvanized steel substrate. They showed that the coating weight was 1.4-1.8 times larger than at the

middle of the strip for D = 1 mm, Z/D = 24 and nozzle pressure of P_0 = 13 kPa. It was shown that the increase in coating thickness at the edge of the substrate was due to the vortices arising from the collision of the two opposing slot jets. In this case, the vortices created a local pressure drop at the edge and, therefore, an increase in coating weight was observed. Installing a baffle plate parallel to the strip has been shown to be an effective method to cope with EOC as it prevents the appearance of vortices.

Hrymak et al. [23] studied the effects of bow tie profiled air-knives, essentially variable slot width profiles, on coating weight. A single bow-tie air-knife, with symmetric and asymmetric gap profiles, as shown in Figure 2-10, was investigated experimentally. They showed that bow-tie air-knives can modify the pressure distribution profiles along the strip as both the symmetric and asymmetric gap configurations resulted in higher pressures at the edge of the static plate than those at the center of the plate. Therefore, having a higher pressure impinging jet at the edge of strip can alleviate EOC.

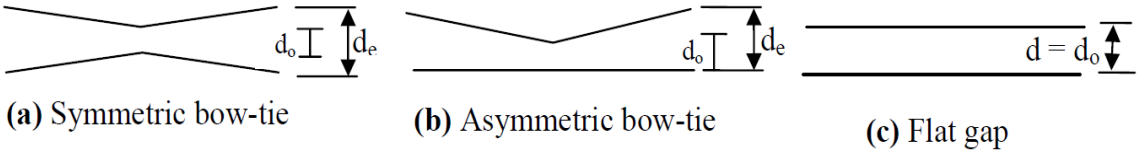

Figure 2-10) Bow tie air-knife configurations [23].

To prevent EOC, Ahn and Chung [33] changed direction of the jet flow by adding a small diameter cylinder at the lower lip of the impinging jet (Figure 2-11). Accordingly, the opposing jets collided at an angle lower than 180°, which resulted in the vortex structures disappearing at the edge of the substrate.

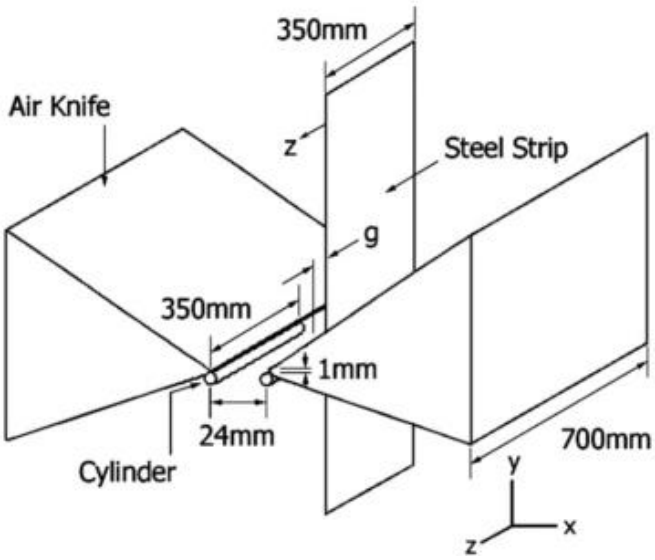

Figure 2-11) Schematic of air knife system used by Ahn and Chung [33].

2.3.3 Coating film non-uniformity and check marks

Due to the unsteadiness of gas flow of an impinging jet, the pressure gradient developed on the sheet will oscillate, with some coupling between the liquid flow and the oscillating gas jet [34]. This phenomenon induces a wavy coating and/or check marks. The main cause for the check mark on the substrate is the stream wise vortices which periodically impinge on the sheet [18].

So et al. [35] numerically studied the flow structures of a plane impinging jet with Reynolds number of 11000 and nozzle width of 1.5 mm while the nozzle to plate distance was varied between 4 mm and 24 mm. In this study, the check mark patterns observed on the coating layer were attributed to static pressure variations on the impinging substrate which were caused by a series of vortices moving along the horizontal impinging stagnation line.

Yoon and Chung [30] designed an impinging jet configuration with one main slot jet which operated as a wiping actuator and a guide jet to decrease the flow instabilities of the main jet. The guide jet prevented the formation of vortical structures on the impinging surface. By removing the vortical structures on the flat surface, the check mark defects decreased significantly.

Pfeiler et al. [36] numerically investigated the coating non-uniformity resulting from impinging jet during gas jet wiping process. It was shown that the coating uniformity was insensitive to the jet flapping with high frequency. Conversely it was found that gas jet flapping with considerably high period resulted in production of waves on the coating layer. In this study, the influence of a slight nozzle tilting on the film waviness was also investigated. For the studied case, tilting nozzle was found to produce a coating with less waviness.

2.3.4 Noise generation

High levels of tonal noise generation during the gas wiping process is another industrial issue when using air-knives as a wiping actuator in continuous galvanizing. According to Dubois [18], it is common to reach more than 100 dB, 1m away from the zinc pot when high wiping pressure was used while the regulated limit is 85 dB at 1 m [37]. Noise generation by gas jets impinging on solid surfaces has been the subject of a number of experimental studies ([38]–[43]). Petrie [39] experimentally investigated the noise generated by an axisymmetric gas jet impinging on a flat surface for flow velocities between V = 82 and 213 m/s. The author reported that the sound pressure level was, in general, inversely proportional to the jet impingement ratio Z/D and, for specific distances,

increased to more than 27 dB above the noise of a free jet were produced, with a "distinct tonal character" of the noise being reported.

Nosseir and Ho [40] focused on the noise generation and feedback mechanism of an axisymmetric jet impinging normally on a flat plate. The authors concluded that a aeroacoustic feedback mechanism existed for axisymmetric jets impinging on a flat surface for impingement ratios of less than $Z/D \leq 7.5$. The feedback mechanism consisted of coherent structures generated within the jet shear layer which travel downstream and impinged on the flat surface. The impingement of these structures resulting in pressure fluctuations and distortion to the vorticity field. These fluctuations propagated upstream to the nozzle lip, exciting subsequent perturbations in the shear layer, completing the feedback cycle and causing large acoustic tones to be generated.

An experimental study of noise generation in the continuous galvanizing gas jet wiping process was carried out by Arthurs and Ziada [41] to determine the effect of various process parameters on overall noise levels and the generation of discrete acoustic tones. The effect of plenum pressure and impingement ratio on the noise generated by gas jet wiping, in particular, were investigated. A semi-empirical model was developed to predict the frequency (f) of the tones based on the process parameters used (Equation 2.7).

$$f = 0.462\left(\frac{Z}{D}\right)^{-1.146}\left(\frac{V_{Jet}}{D}\right) \tag{2.7}$$

In addition, noise maps of tone intensity were constructed to aid operators in optimizing gas wiping process to minimize noise production. According to Figure 2-12 there were no significant tones generated for plenum pressures of 7 and 10 kPa (1.0 and 1.5 psi). Significant acoustic tones were present for plenum pressures of P = 14 kPa (2.0 psi) and

greater starting at an impingement ratio of *Z/D* = 6. The generation of this tone occurred for successively larger ranges of impingement ratios for increasing plenum pressures, and appeared to occur over two distinct regions.

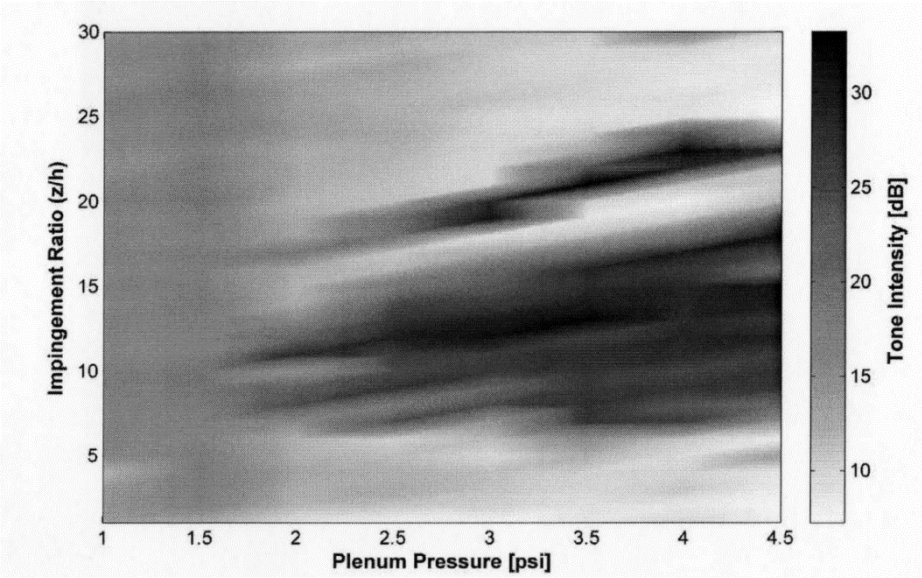

Figure 2-12) Tone intensity as a function of plenum pressure and impingement ratio (*z/h* or *Z/D*) single slot jet-plate impingement with *D* = 1 mm [41].

2.4 Multi-slot air knife

With the objective of impoving final coating quality, Tu [44] filed a patent and proposed a variety of new air knife designs with multiple nozzles for application to the continuous hot dip galvanizing process (Figure 2-13). In all instances, the apparatus comprised an auxiliary nozzle releasing a low velocity smoothing jet stream and a higher velocity striping jet which was located above the smoothing jet stream. The step of smoothing the surface comprised impinging a lower velocity jet stream of gas on the coating material in an amount and at a pressure sufficient to smooth the layer of material, and the step of stripping surplus material comprised impinging a higher velocity stripping jet stream of gas in an amount

and at a pressure sufficient to reduce the thickness of the smoothed layer to a targeted final thickness.

According to Tu [44], in Figure 2-13a) the stripping was effected by the lower jet stream 11 issuing from a dual nozzle. The upper jet stream 14 only cooperated with the stripping jet stream 11 to maintain a stabilizing gas pressure in the space 16 between the dual nozzle and the strip. It had no significant effect on the thickness of the coating layer 12. In Figure 2-13b) there was a smoothing nozzle 17 located slightly below the main nozzle 10. The jet stream 18 was of a significantly lower velocity and only affected the outer layer of material and served to replace the wave pattern below the jet stream 18. In Figure 2-13c) the dividing wall 21, allowed the jets pressure to be adjusted separately. In this manner, the upper jet stream 11 wiped the extra coating layer and smoothing function was performed by the jet stream 18. Figure 2-13d shows another configuration in which the surface modifying jet was combined with a dual nozzle pad assembly discussed in Figure 2-13a.

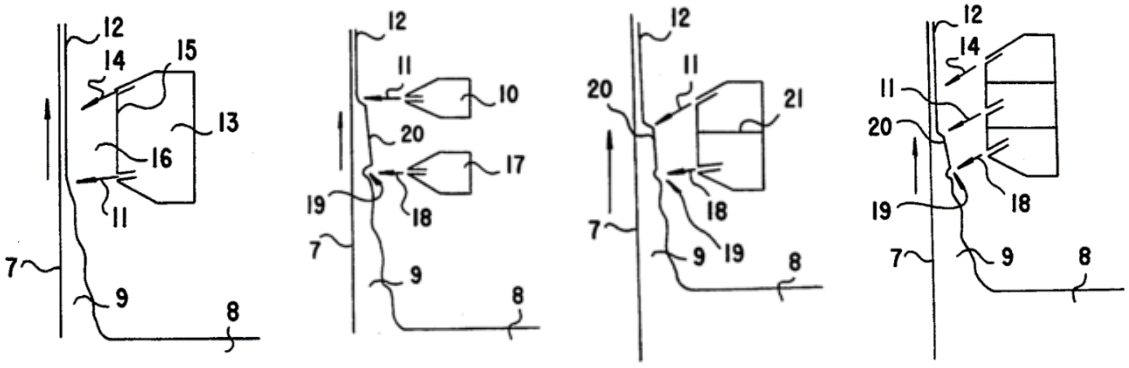

Figure 2-13) Proposed multi-slot air-knife configurations by Tu [44].

Two of the proposed models, a main jet with inclined auxiliary impinging slot jets and two parallel impinging slot jets (Figure 2-14a and Figure 2-14b), were studied numerically

by Tamadonfar et al. [45]. The maximum wall pressure gradient and shear stress distribution were obtained for these two configurations. The obtained profiles were implemented in the coating weight model developed by Elsaadawy et al. [1] in order to calculate the final coating thickness. Tamadonfar's numerical results did not show any advantage for using these two multi-slot configurations over the single slot air-knives in term of coating thickness reduction.

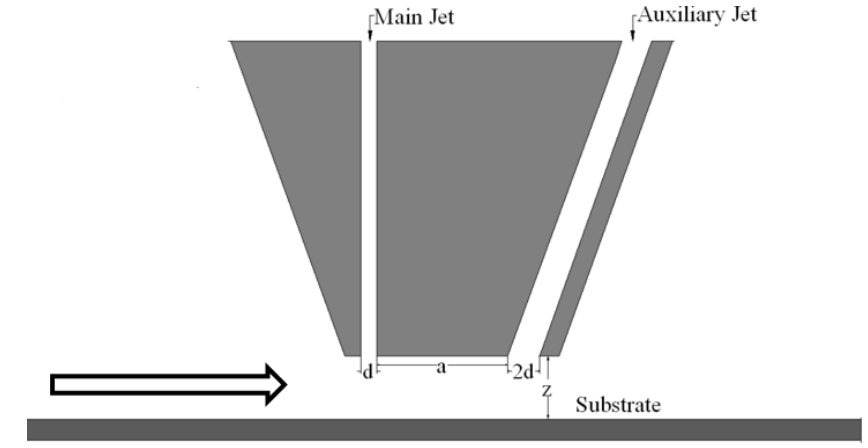

a)

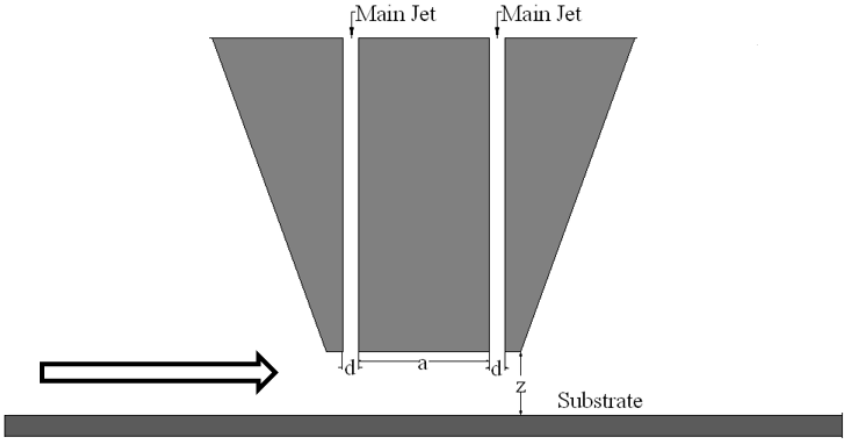

b)

Figure 2-14) Schematic for a) a main with an inclined auxiliary impinging slot jets and b) two parallel impinging slot jets used in the Tamadonfar et al. study [45].

Kim et al. [46] proposed a multiple-slot jet design to solve the splashing problem and enhance coating quality. The proposed air-knives comprised one main jet and four symmetrically placed auxiliary inclined jets discharging air at a lower velocity in comparison with the main slot jet (Figure 2-15). The configuration was for application to the continuous hot dip galvanizing process for coating weight control. The intent of the patent was that the gas discharging from the main and inner jets were to provide the necessary force for wiping excess molten zinc from the sheet. The outer auxiliary jets were used to prevent splashing by mixing the gas particles of the main jet and auxiliary jets, resulting in the lower speed of the jet wall along the length direction of the substrate. However, the effect of the proposed jet configuration on the wall pressure and wall shear stress distributions, and consequently the film coating thickness, were not reported.

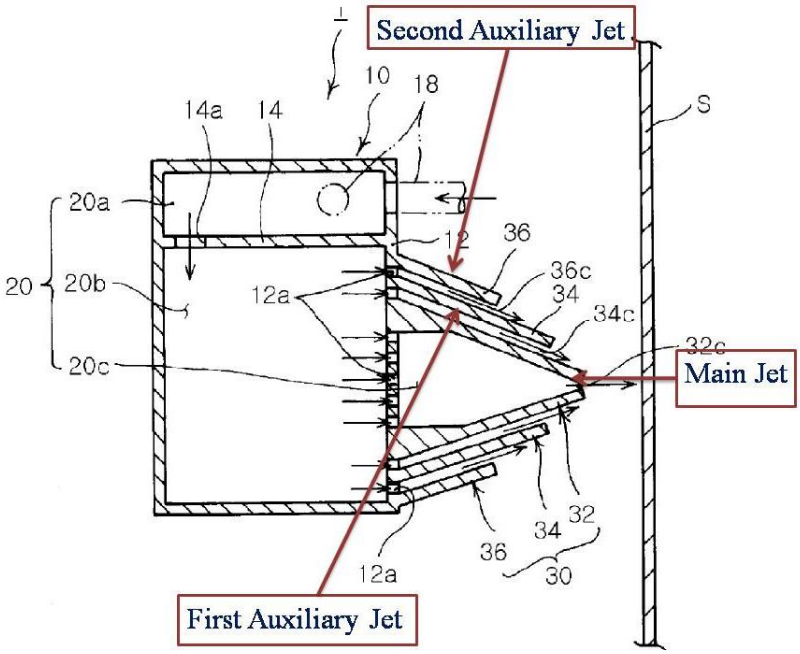

Figure 2-15) Proposed multiple jet of Kim et al. [46].

Tamadonfar et al. ([45], [47]) also numerically simulated a multiple slot jet composed of a main jet and two inclined auxiliary jets symmetrically situated around the main jet (Figure 2-16) with jet width of d = 1.52 mm, the auxiliary jet width held constant at $a = 2d$ and S = 20 mm. The numerical simulations were carried out for the plate to nozzle ratios of $2 \leq z/d \leq 12$ and the jet operating conditions were limited to one main and auxiliary jet Reynold's number ($Re_m = Re_a$ = 11000). For the range of parameters explored in the study, the multiple slot air-knives did not produce a thinner coating thickness compared to a conventional single slot air-knife for each z/d ratio.

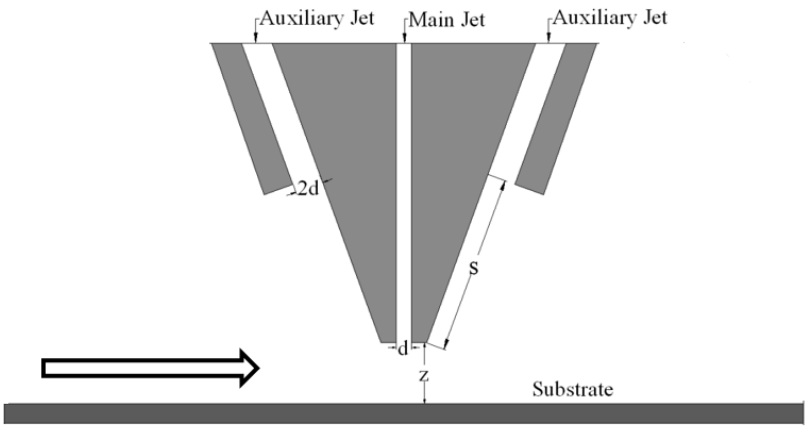

Figure 2-16) Schematic for a main with two adjacent inclined auxiliary impinging slot jets used in the studies of Tamadonfar et al. ([45], [47]) .

Alibeigi et al. [48] later extended the work of Tamadonfar et al. [refs] by experimentally investigating the wall pressure distribution of the prototype multiple slot jet shown in (Figure 2-17). In this study the main jet width was fixed at D = 1.5 mm, the auxiliary slot jet width was held constant at 3 mm (i.e. $a = 2D$) and the auxiliary jet stand-off distance was set at S = 20 mm. The wall pressure distribution was measured for $4 \leq Z/D \leq 12$, 9000

$\leq Re_m \leq 13000$ and $11000 \leq Re_a \leq 15000$ in this study [48]. It was observed that adding auxiliary jets to the main jet changed the wall pressure profile distribution compared to the single slot impinging jet wall pressure profile and a secondary peak was seen for $Z/D \leq 6$ at $x/D \approx 5$ (Figure 2-18). The authors reported that the impingement plate for a single jet at $Z/D = 6$ was located in the potential core of the jet, while for the multi-slot jet the length of potential core was reduced to $Z/D = 4$ [48].

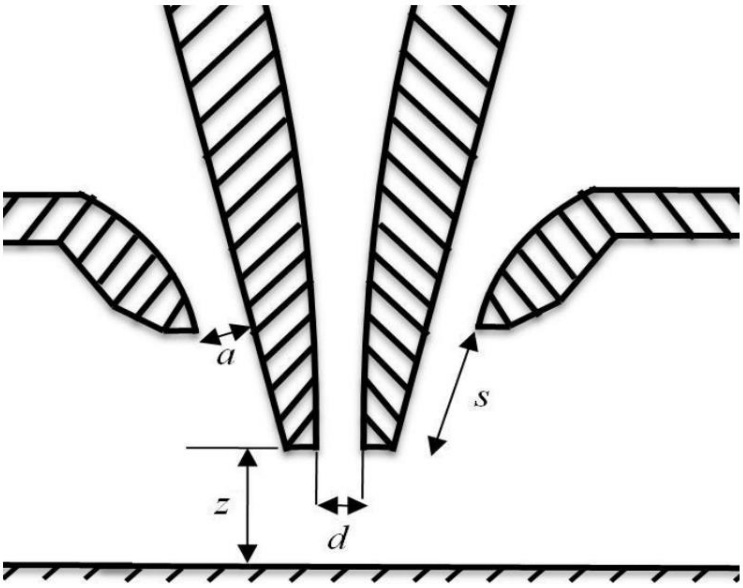

Figure 2-17) Multiple-slot impinging jet schematic [48].

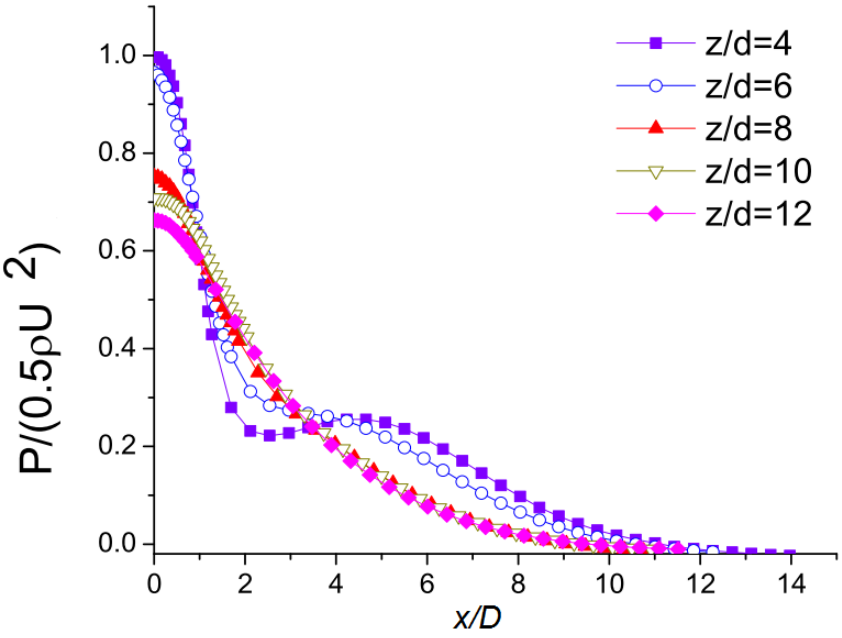

Figure 2-18) Non-dimensional wall pressure distribution as a function of *Z/D* at Re_m = 9000 and Re_a = 11000 [48].

Alibeigi et al. [48] also investigated the effect of auxiliary jet Reynolds number (Re_a) on the wall pressure distribution (Figure 2-19) and wall pressure gradient (Figure 2-20) for a fixed main jet Reynolds number of Re_m = 11000 and *Z/D* = 4. It was shown that the wall stagnation pressure was insensitive to the changes of auxiliary jet Reynolds number, as the plate was located within the potential core of the main jet. However, by increasing Re_a, the shoulder observed in the pressure profile became more pronounced [48]. The author also reported a lower maximum pressure gradient as a result of increasing auxiliary jet Reynolds number (Figure 2-20) due to the pressure profile broadening arising from the secondary auxiliary jet pressure peaks [48].

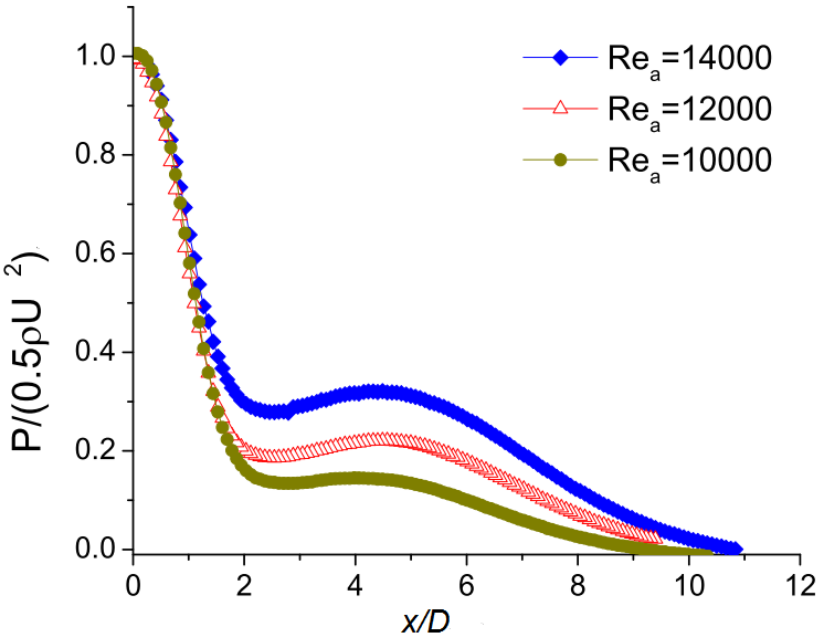

Figure 2-19) Experimental non-dimensional wall pressure distribution for different Rea with Re_m = 11000 and Z/D = 4 [48].

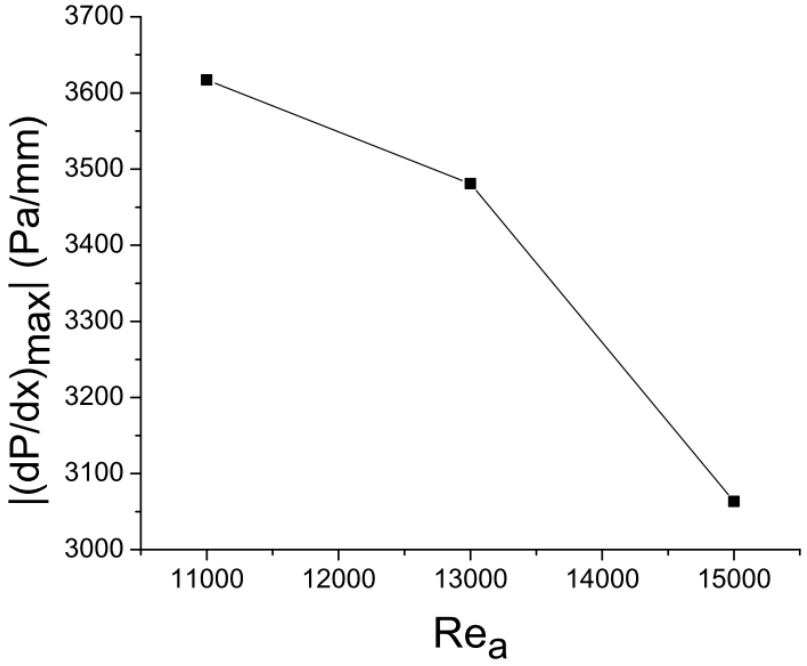

Figure 2-20) Experimental maximum pressure gradient as a function of auxiliary jet Reynolds number (Re_a) with Re_m = 11000 and Z/D = 4 [48].

Myrillas et al. [49], experimentally studied the effect of an additional side jet to the main wiping jet on final coating thickness through use of light absorption technique (Figure 2-21). They showed that using a side jet can stabilize the runback flow and resulted in a lower value of coating thickness. They placed the side jet parallel to the main jet at a distance of 1 mm away from the main jet, which could be operated at higher pressure while delaying splashing. Therefore, because of higher pressure gradients and shear forces applied by the jets, a13% reduction in coating thickness could be obtained.

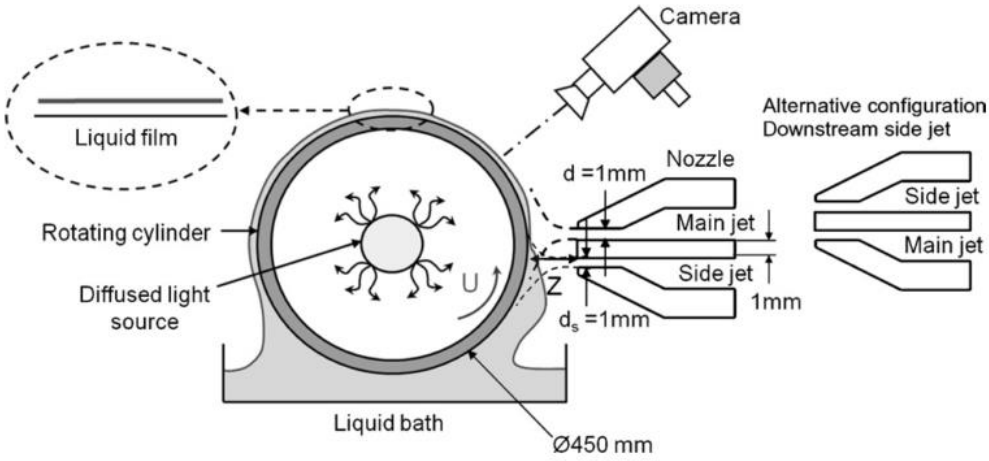

Figure 2-21) Schematic of the experimental facility using the light absorption technique with a main jet and side jet width of 1 mm, for nozzle pressure of P_0 = 600 Pa and $5 \leq Z/D \leq 15$ [49].

Finnerty et al. [42], recently experimentally studied the effect of auxiliary jets on noise reduction by using the prototype multiple slot air knives shown in Figure 2-17. In this study, the main jet velocity was held at 250 m/s for all experiments and the auxiliary jet flows were varied between 0 m/s and 60 m/s in 20 m/s intervals. The authors showed that the multiple slot jets were able to decrease the magnitude of the tonal noise to the point of near complete suppression when the auxiliary jet velocity was set at approximately a quarter velocity of the main jet (Figure 2-22). They also showed that the auxiliary jets also introduced broadband noise at low frequencies which was not of a sufficient magnitude to present a hazard to workers on continuous galvanizing lines.

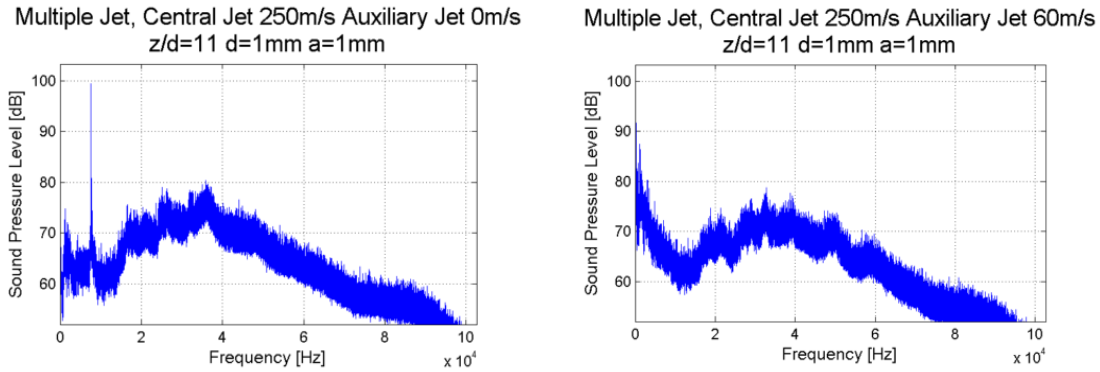

Figure 2-22) Acoustic measurements for an impingement distance of 11mm with varying auxiliary jet velocities and a constant main jet velocity of 250m/s [42].

At present, only single-slot jets are widely used in the continuous galvanizing industry. As stated above, the current generation of single slot jet is not capable of wiping to the desired low coating weights at line speeds which are consistent with the production schedule and profitability outcomes desired by the steel industry.

The multi-slot jet could be promising to alleviate some the limitations mentioned in section 2.2 for single slot jets. However, there is a serious lack in the literature, to explore the operating window and geometric parameters of the multi-slot jet configuration that would allow for thinner coatings at higher line speeds by shaping the pressure and shear stress distributions. In the present study, the capability of the multi-slot air knife in coating thickness reduction and tonal noise attenuation will be investigated numerically and experimentally.

Chapter 3: Numerical investigation of multiple slot jets in air knife wiping

Ali Yahaee Soufiani, Joseph R. McDermid, Andrew N. Hrymak, Frank E. Goodwin, Journal of Coating Technology and Research, 14 (5), pp 1015-1028, 2017. (DOI: https://doi.org/10.1007/s11998-017-9963-0)

In this paper, all the numerical simulations were carried out entirely by me, under the supervision of Dr. McDermid and Dr. Hrymak. The manuscript was initially drafted by me and reviewed to the final version by Dr. McDermid and Dr. Hrymak. Dr. Goodwin was included as an author of this paper as a courtesy for his provision of the industrial sponsorship.

3.1 Abstract

Gas jet wiping using an air-knife is an effective hydrodynamic method to control the coating thickness of zinc on a moving steel substrate in the continuous hot dip galvanizing process (CHDG). The current generation of single slot air knives are widely used in the galvanizing industry, but have limitations in producing low coating weights at the higher line speeds desired for the current generation of automotive sheet steel products. In this work, a novel configuration of a multiple slot jet (multi-jet) air-knife is investigated through numerical simulations as an alternative to the traditional single slot air-knife. The aim of this study is to investigate the sensitivity of the coating weight to the pressure and shear stress profiles in order to determine if there are operating regions that are more robust to air knife geometry changes. A modified geometry for the multi-slot air knife is proposed based on computational fluid dynamics results obtained from a parametric study. The effects of different operating conditions such as the main jet Reynolds number (Re_m), auxiliary jet Reynolds number (Re_a) and jet to wall distances (Z/D) on the final coating thickness were investigated. The results of the modelling showed that by setting the auxiliary jet Reynolds number at a fraction (25%) of the main jet Reynolds number, lighter coating weights can be achieved for higher strip velocities and higher wall to jet distances as compared to the single slot jet design. It is believed that this geometry will provide a robust operating window to enable the prototype design to be employed in the industrial setting.

3.2 Nomenclature

C_f	Skin friction coefficient
D_a	Auxiliary jet width (mm)
D	Main Jet Width (mm)
g	Gravitational acceleration (m/s^2)
G	Non-dimensional pressure gradient
h_f	Final film thickness (μm)
p	Static pressure (Pa)
q	withdrawal flux ($1/m^3$)
Q	Non-dimensional withdrawal flux
Re_a	Auxiliary Jet Reynolds Number
Re_m	Main Jet Reynolds Number
s	Auxiliary jet offset (mm)
S	Non-Dimensional Shear Stress
u	Fluid Velocity (m/s)
V_s	Strip velocity (m/s)
w	Local film thickness (μm)
W	Non-dimensional film thickness
Z	Main Jet Exit to wall Distance (mm)
μ	Fluid Dynamic Viscosity (kg/m.s)
ρ	Fluid Density (kg/m^3)
τ	Shear stress (Pa)
θ	Auxiliary jet tilt angle relative to Main Jet Centerline
ρ	Density of gas
R	Universal gas constant (J/mol.K)
M_w	Molecular weight of the gas (g/mol)
T	Temperature (K)

3.3 Introduction

Continuous hot-dip galvanizing is a coating technique which is widely used in the steel industry. In this process, a steel strip is continuously immersed in a bath of molten liquid zinc, usually at 460°C, during which the liquid metal alloy reactively wets the moving sheet substrate [1].When the substrate emerges from the bath, it carries out a relatively thick layer of liquid zinc due to viscous drag. The molten zinc coating thickness on the sheet substrate is usually controlled just above the bath through the use of a planar turbulent gas jet or air knife, typically in a single slot configuration (Figure 3-1). The pressure gradient and shear stress applied to the liquid film by the jet controls the film thickness above the air knife, and the majority of the liquid returns to the bath as a runback flow [2-5]. The film thickness after wiping (h_f) depends on the substrate velocity V_s, the nozzle pressure P_0 , the nozzle to substrate standoff distance Z, the nozzle slot width D and the physical properties of the liquid zinc ([6],[7]). In industry the general ranges of $0.8 \leq D \leq 1.5$, $8 \leq Z/D \leq 12$ and $5000 \leq Re \leq 25000$ are commonly being used.

Thornton and Graff [2] proposed a model for calculating the final liquid film thickness by assuming that the reduction of film thickness was due solely to the pressure gradient created by the impinging jet. Tuck [3] used a similar approach and checked the stability of the solutions for long wavelength perturbations. Ellen and Tu [4] subsequently incorporated the effect of wall shear stress distribution into the coating weight model. Tu and Wood [6] experimentally measured the wall pressure and shear stress distribution beneath an impinging jet for a wide range of plate to nozzle ratios of $2 < Z/D < 20$ and Reynolds

numbers $3000 \leq Re_m \leq 11000$. Guo and Wood [8] measured the wall shear stress for a jet with a free stream turbulence intensity of approximately 0.35% at the jet exit. They compared their results with Tu and Wood [6], where their turbulence level was approximately 4%. By comparing these results they concluded that the turbulence intensity had only a second order influence on the wall shear stress within the jet stagnation region.

Naphade et al. [9] proposed a model to estimate the coating weight as a function of strip velocity, jet nozzle pressure, plate to nozzle distance and nozzle gap width. The proposed correlation was validated with industrial line data. Gosset et al. [7] presented a model to predict the gas jet wiping performance at small standoff distances and showed that the final coating thickness did not change significantly for $Z/D < 7$ for a given jet velocity. Elsaadawy et al. [10] developed a coating weight model as a function of operating parameters for $Z/D \leq 8$. By combining experimental and computational methods they improved the pressure and shear stress correlations using the k-ε turbulence model in the FLUENT code. The model showed good agreement with industrial data, particularly at lower coating weights, where the maximum deviation was 8% between the predicted coating weight and measured data. Lacannette et al. [11] used a LES turbulence model in order to obtain the mean pressure gradient and shear stress distribution induced by a single slot jet on a dry wall. The obtained profiles were then applied in a knife model. The authors also used VOF method coupled with LES model in order to study the effect of turbulent jet on a moving wall containing a layer of liquid film. By comparing the decouple lubrication model and the two phase model, the concluded that the knife model is demonstrated to be a good estimator for the final film thickness.

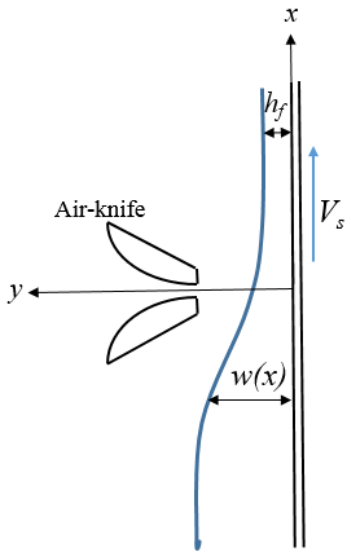

Figure 3-1) Schematic of the gas jet wiping process

In order to obtain lighter coating weights at reasonable strip velocities, the usual practice would be to increase the wiping pressure (i.e. increase the jet velocity) significantly. However, increasing the wiping pressure can result in increased noise, an industrial hygiene issue, or splashing. Splashing is characterized by the ejection of zinc droplets from the strip which can be deposited on or around the jet nozzle or on the strip itself, resulting in defects. Dubois [12] showed that full splashing occurs for a zinc coating thickness of 20 μm produced at line speeds of 160-170 m/min when $Z/D < 6$. Splashing is initiated at the edge of the strip and spreads toward the center of the strip. Therefore, full splashing occurs throughout the whole sheet width and makes the running back flow to detach from the substrate and causes defects on the final product. Kim et al. [13] proposed a multiple-slot air knife design which comprised a main jet and four inclined auxiliary jets discharging air at lower velocity in comparison with the main slot jet. In this design, the gas discharging

from the main and auxiliary jets provided the necessary force for wiping the excess molten zinc from the sheet. It was claimed that the second auxiliary jets prevented splashing where the auxiliary jets restrained zinc droplets from splashing by mixing the gas particles of the main jet and lower speed auxiliary jets such that the wall shear stress was reduced, thereby preventing splashing.

In this study, a novel multi-jet configuration based on the proposal of Kim et al. [13] was studied through numerical simulations as the zinc wiping apparatus in the continuous hot dip galvanizing (CHDG) process. In particular, the objective of this paper is to investigate the sensitivity of the coating weight to the pressure and shear stress profiles to determine if there are operating regions that are robust to the prototype air knife operating parameter changes and to also determine if lower coating weights at high line speeds can be obtained through the use of the proposed multi-slot air knife.

3.4 Analytical model of film thickness

Calculation of the liquid zinc volumetric flux on the steel strip, q, is the first step in the modeling of coating thickness [10]. A condensed summary of the analysis is provided below to demonstrate the assumptions applied to calculating the thickness of the liquid film. A simplified form of the Navier-Stokes equation can be used for calculating q based on the assumptions of steady-state, isothermal, incompressible flow of the liquid film, where it is assumed that surface tension can be neglected and that the no-slip condition of the liquid on the steel strip is valid [4]. Fluid properties, such as viscosity and density, were

assumed to be constant. By considering the above assumptions, the two-dimensional Navier-Stokes equation for a thin film on a flat plate reduces to:

$$\mu\frac{d^2u}{dy^2}-(\rho g+\frac{dp}{dx})=0 \tag{3-1}$$

Using the coordinate system in Figure 3-1, the boundary conditions can be written as:

$$u=V_s \qquad \text{at} \quad y=0 \tag{3-2}$$

$$\mu\left(\frac{\partial u}{\partial y}\right)=\tau \qquad \text{at} \quad y=w \tag{3-3}$$

Where τ is the shear stress imposed by the turbulent impinging slot jet on the strip, V_s is the strip velocity and w is the local film thickness. Integrating equation (3-1) and applying the boundary conditions in equations (3-2) and (3-3) yields:

$$u=V_s\left[1+\frac{y}{w}SW-\frac{y}{w}\left(2-\frac{y}{w}\right)\frac{GW^2}{2}\right] \tag{3-4}$$

Where $W=w\sqrt{\frac{\rho g}{\mu V_s}}$ is the non-dimensional film thickness, $S=\frac{\tau}{\sqrt{\rho\mu V_s g}}$ is the non-dimensional shear stress and $G=1+\frac{1}{\rho g}\frac{dp}{dx}$ is the effective gravitational acceleration. The liquid volumetric flux, q, can then be calculated as:

$$q=\int_0^w u dy=V_s w\left(1+\frac{SW}{2}-\frac{GW^2}{3}\right) \tag{3-5}$$

The non-dimensional withdrawal flux, $Q=\frac{q}{V_S}\sqrt{\frac{\rho g}{\mu V_S}}$ can be derived from equation (3-5) by substitution and rearrangement as:

$$Q = -\frac{GW^3}{3} + \frac{SW^2}{2} + W \tag{3-6}$$

From Elsaadawy et al. [10], the non-dimensional film thickness *W*, corresponding to the maximum withdrawal flux, Q_{max}, can be determined by solving $\frac{dQ}{dW} = 0$ and employing the quadratic formula such that:

$$W = \frac{S \pm \sqrt{S^2 + 4G}}{2G} \tag{3-7}$$

Using the above formalism, the non-dimensional film thickness is a function of dp/dx and τ at any coordinate *x*. Due to mass continuity, the minimum value of Q_{max} corresponding to every *x* value is the physically available withdrawal flux, Q. The final film velocity is assumed equal to the substrate velocity and the final coating thickness, h_f, is given by

$$h_f = \frac{q}{V_S} = \frac{(Q_{max})_{min}}{\sqrt{\frac{\rho g}{\mu V_S}}} \tag{8}$$

The distribution of shear stress and pressure gradient along the wall can be used in equations (3-7) and (3-8) to estimate the final coating thickness on a moving substrate. Higher values for the *dp/dx* and τ distributions in the vicinity of wiping region can lead to a lower coating thickness according to equations (3-6) through (3-8). In this study, the pressure gradient and shear stress distributions induced by both the single and multiple jet geometries on a dry, fixed surface were determined through numerical simulations.

3.5 Numerical modeling

A computational approach was used to model the pressure distribution and shear stress on the wall. The computations were carried out using FLUENT 14.0 commercial software. The solver was pressure-based and all of the simulations were run in steady mode. The SIMPLE method was used for pressure-velocity coupling. Fluid flow can be represented by the Navier-Stokes equations which contain the mass and momentum balance equations. In Cartesian form they are as follows:

$$\frac{\partial \rho}{\partial t} + \frac{\partial (\rho u_i)}{\partial x_i} = 0 \tag{9}$$

$$\frac{\partial \rho u_i}{\partial t} + \frac{\partial \rho u_i u_j}{\partial x_i} = -\frac{\partial p}{\partial x_i} + \mu \frac{\partial}{\partial x_i}\left[\left(\frac{\partial u_i}{\partial x_j} + \frac{\partial u_j}{\partial x_i}\right)\right] \tag{10}$$

The well-known two-equation model was used to capture turbulence properties. One of the transport equations solved for the turbulent kinetic energy (k) and the other solved for the turbulent dissipation rate (ε). The turbulence model which was used in this study for all cases was the standard (k-ε) model, which includes the following two equations:

$$\frac{\partial \rho k}{\partial t} + \frac{\partial \rho k u_i}{\partial x_i} = \frac{\partial}{\partial x_j}\left[\left(\mu + \frac{\mu_t}{\sigma_k}\right)\frac{\partial k}{\partial x_j}\right] + G_k - \rho\varepsilon \tag{11}$$

$$\frac{\partial \rho \varepsilon}{\partial t} + \frac{\partial \rho \varepsilon u_i}{\partial x_i} = \frac{\partial}{\partial x_j}\left[\left(\mu + \frac{\mu_t}{\sigma_\varepsilon}\right)\frac{\partial \varepsilon}{\partial x_j}\right] + C_{1\varepsilon}\frac{\varepsilon}{k}(G_k) - C_{2\varepsilon}\rho\frac{\varepsilon^2}{k} \tag{12}$$

where the turbulent viscosity for the standard k-ε turbulence model is written as:

$$\mu_t = \rho C_\mu k^2 \big/ \varepsilon \tag{13}$$

where C_μ is a model constant. Table 1 provides the standard k-ε model constants for equations (11) through (13) from Launder and Sharma [14].

Table 3-1) Standard k-ε turbulence model constants

C_{μ}	$C_{1\varepsilon}$	$C_{2\varepsilon}$	σ_k	σ_ε
0.09	1.44	1.92	1	1.3

A double precision solver was used for all simulations. A segregated solver was used for the governing equations. The standard method was used for the pressure term with a first order up-winding scheme for the turbulent kinetic energy (k), turbulent dissipation rate (ε) and momentum. The governing equations were solved until the root-mean-square (RMS) residuals for all governing equations fell below 10^{-6}. A constant viscosity for the air was assumed and the air density was computed as a function of pressure and temperature based on the ideal gas law:

$$\rho = \frac{P}{\frac{R}{M_w}T} \tag{14}$$

3.6 Boundary conditions and grid generation

Schematics of the two nozzle geometries are illustrated in Figure 3-2. For the initial numerical simulations and for validation purpose, the auxiliary jet width (D_a), distance between the exit of the main and auxiliary jets (s), and the main jet slot width (D) were fixed at 3 mm, 20 mm and 1.5 mm respectively. The inclination of the auxiliary jets relative to the main jet centerline was 20°. The boundary conditions were the no slip condition at the impingement and nozzle walls, a pressure inlet at the nozzle inlets and a pressure outlet at the exit of the computational domain. The mesh used for the impinging jets comprised a

mixture of quadrilaterals and triangles. The full physical domain was solved, not taking into account geometric symmetry. Grid clustering was used adjacent to the wall and around the centerline where large gradients in the velocity field, pressure field and turbulent parameters were present. Four grids with differing numbers of nodal points were tested to verify mesh independence of the numerical results. In order to capture the severe pressure gradients and rapid changes of flow in the near wall region, the mesh was refined such that the first node located in the viscous sub-layer ($y^+ \sim 1$) and the mesh size near the wall is approximately 4 μm. The computational domain size was L/D=-85 to L/D=85.

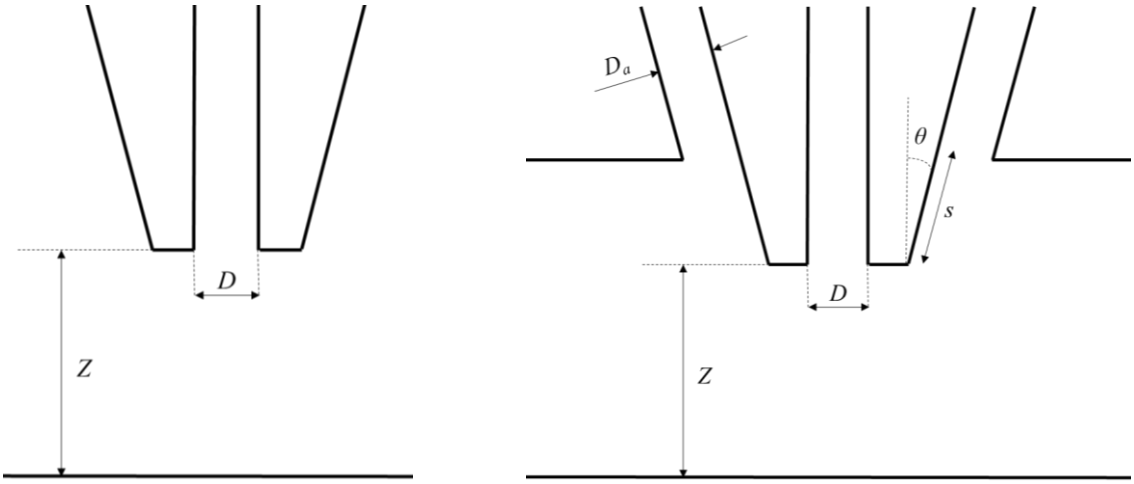

a) b)

Figure 3-2) Schematic of a) the single-slot jet and b) multiple-slot jet geometries.

3.7 Validation

Numerical simulations versus experimental wall pressure distribution and pressure gradient data for different wall to jet distances at Re_m = 11000 are presented in this section. Figure 3-3 presents a comparison of numerical non-dimensional wall pressure profiles

versus the experimental data of Alibeigi [15] for a short nozzle single-slot planar impinging jet as function of Z/D. It can be seen that the value of the predicted maximum non-dimensional pressure and pressure distribution were in good agreement with the experimental data. Figure 3-4 compares the numerical and experimental results for the wall skin friction $C_f = \tau_w \big/ \left(0.5\rho U^2\right)$. From this, it can be seen that the numerical skin friction results compare very well with the corresponding experimental measurements of Ritcey et al. [16]. It can also be seen that the maximum C_f value decreased with increasing *Z/D*. The decreasing skin friction can be attributed to the decaying velocity of the jet and momentum losses due to fluid entrainment. Figure 3-5 shows a comparison of the numerical wall pressure profile versus the experimental data of Alibeigi [15] for a the multi-slot impinging jet where $Re_m = Re_a = 11000$. From Figure 3-5, it can be seen that the numerical models of the multi-slot jet geometry also agree well with the experimental measurements. From the above, it can be concluded that the numerical models for both the single and multi-slot geometries have been experimentally verified.

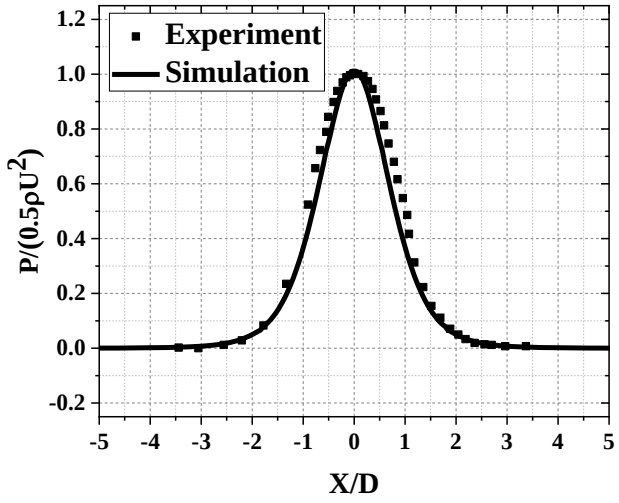

a)

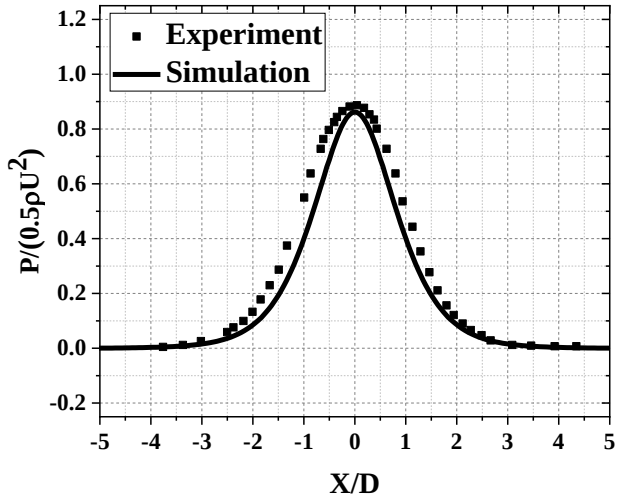

b)

Figure 3-3) Comparison of numerical pressure distribution and pressure gradient versus the experimental measurements of Alibeigi [15] for a single slot jet with a) *Z/D* = 6 and b) *Z/D* = 8.

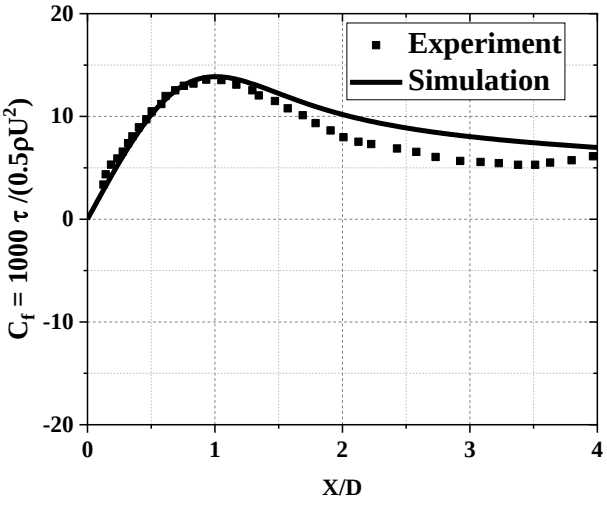

a)

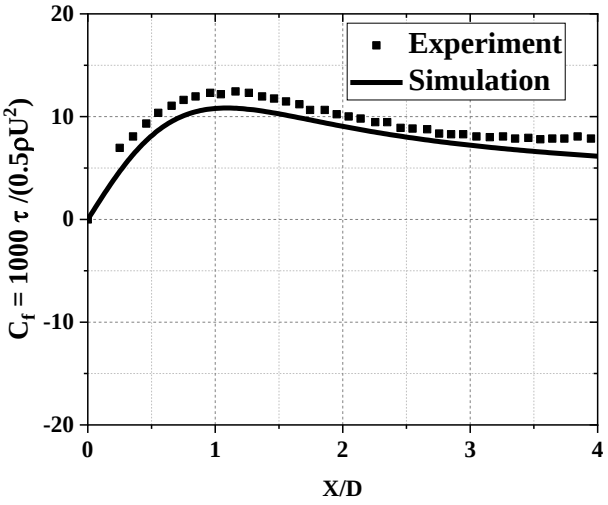

b)

Figure 3-4) Comparison of wall shear stress profiles predicted by numerical simulations versus the experimental measurements of Ritcey et al. [16] for a single slot jet for a) *Z/D* = 4 and b) *Z/D* =8.

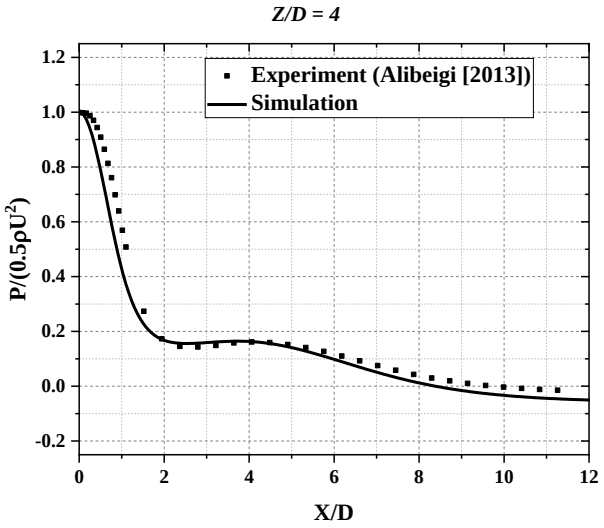

a)

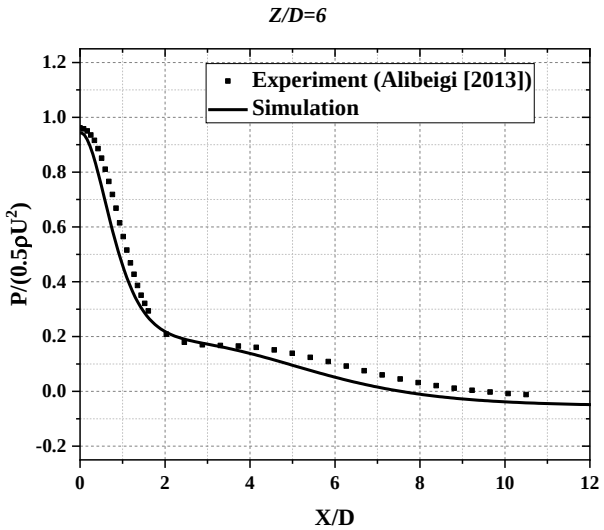

b)

Figure 3-5) Comparison of numerically predicted non-dimensional wall pressure distribution versus the experimental measurements of Alibeigi [15] for the multi-slot jet geometry where D = 1.5 mm, D_a = 3 mm and s = 19.7 mm for a) Z/D = 4, b) Z/D = 6.

3.8 Results and discussion

Figure 3-6 illustrates the wall pressure gradient and wall shear stress distribution for both the single and multiple slot air-knife geometries. According to this figure, lower values of the pressure gradient and shear stress are distributed in the vicinity of the wiping point for the multi-slot air knife design. This leads to a higher coating liquid flow rate *Q* from the bath which remains on the substrate after wiping, as described by equation (6). Accordingly, in Figure 3-7, which shows the variation of coating weight as a function of strip velocities between 0.5 m/s and 2.5 m/s, the single slot air-knife has a better performance in term of coating weight reduction versus the examined configuration of multi-slot air-knife. The same results were obtained for a wide range of operating conditions.

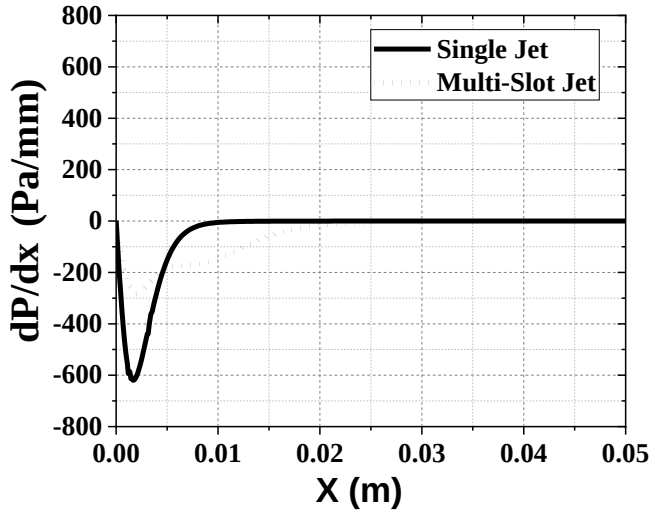

a)

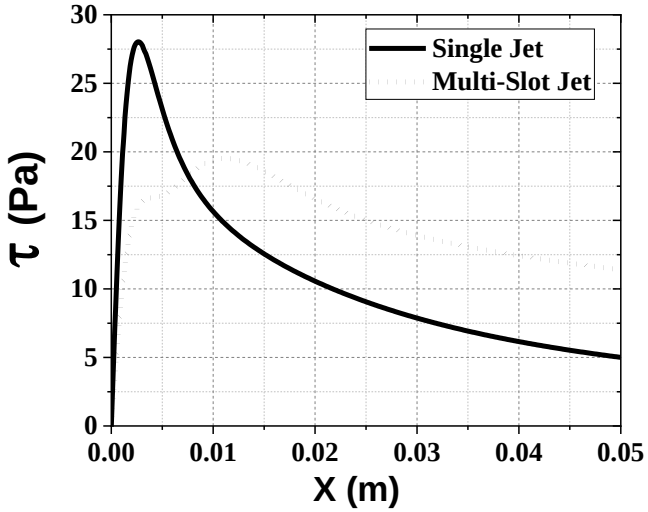

b)

Figure 3-6) Comparison of numerical results for the pressure gradient and wall shear stress for the single and multi-slot air knife geometries where $Re_m = Re_a = 11000$, $D = 2.5$ mm, $D_a = 3$ mm, $s = 19.7$ mm and $\theta = 20°$ for $Z/D = 8$.

By comparing the wall pressure profiles for the two air knife geometries, as shown in Figure 3-8, it can be seen that the auxiliary jets not only increased the maximum impingement pressure, but they can broaden the pressure distribution along the wall, resulting in a lowering of the pressure gradient (*dp/dx*) distribution.

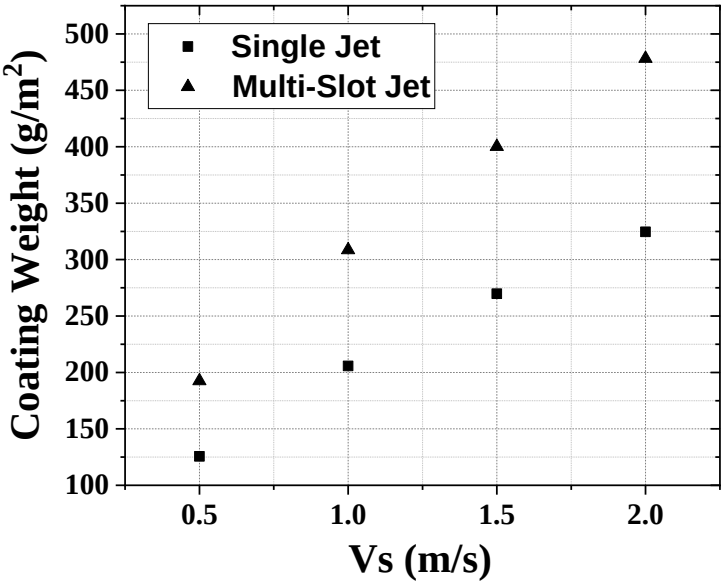

Figure 3-7) Coating weight as a function of strip velocity for the single and multi-slot jet air knives for Re_m = 11000, Re_a = 11000 and Z/D = 8.

Subsequent simulations investigated the effects of changing various geometric parameters such as D_a, a, s and θ per Figure 3-2 in order to modify the multi-slot air knife geometry such that the pressure profile and pressure gradient conformed more closely to the single slot air knife shape without losses in (dp/dx), the results of which discussed in the following sections.

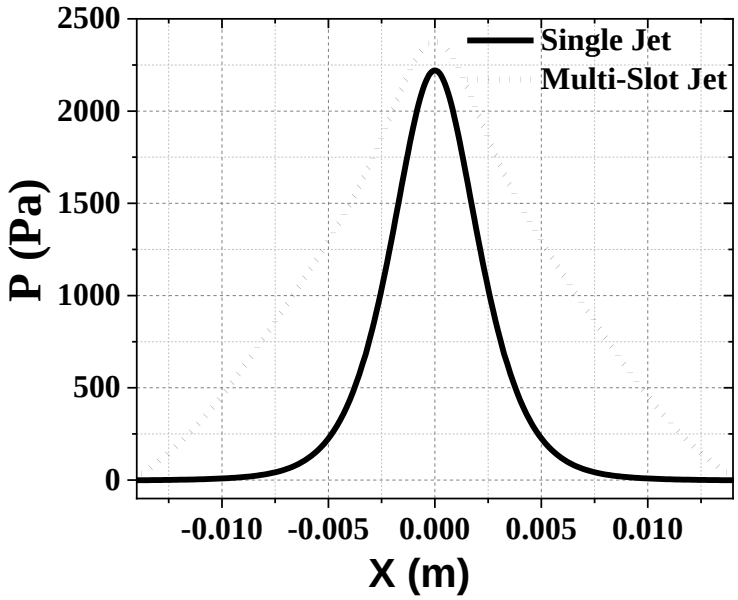

Figure 3-8) Comparison of the typical pressure profiles for the single and multiple slot jets for Re_m = 11000, Re_a = 11000 and Z/D = 8.

3.8.1 Effect of D_a

The effect of the auxiliary jet gap, D_a, on the wall pressure distribution was studied numerically. The main slot jet Reynolds number was fixed at 11000, which corresponds to an air velocity of 110 m/s. Three different values of D_a = 1.5 mm, 2 mm and 3 mm were examined while *a* and *s* were fixed at 3 mm and 5 mm respectively.

Figure 3-9 shows the wall pressure distribution as a function of the auxiliary jet gap width, D_a, where Z/D, Re_m, Re_a, *a* and *s* were held constant as documented in the figure caption. It can be seen that adding auxiliary jets to the main jet changed the wall pressure profile distribution as compared to the single-slot impinging jet wall pressure. The secondary peak that was observed for higher D_a values disappeared by decreasing D_a and

pressure profile became sharper. According to Figure 3-10, for high D_a values, the auxiliary jet flow could not be merged effectively with the main jet flow in vicinity of wiping region. Instead, the auxiliary nozzles gas particles, which have the lower speed compared to the main nozzle, collide with the main jet gas particles in downstream of imping point and it results in the overall gas speed decrease along the length of the steel substrate. However, for lower D_a the streamlines of the auxiliary jet merged with the main jet flow and therefore more momentum has been added in vicinity of the main jet centerline. This leads to higher pressure gradient in the impingement region.

Figure 3-11 illustrates the wall pressure gradient for the pressure profiles presented in Figure 3-9. According to this figure, the pressure gradient distribution in the vicinity of the wiping region remained significantly higher for the single slot jet relative to the multi-slot air-knife. From this result, the multi-slot air-knife geometry needs to be modified in order to obtain a thinner coating when using the multiple jet design.

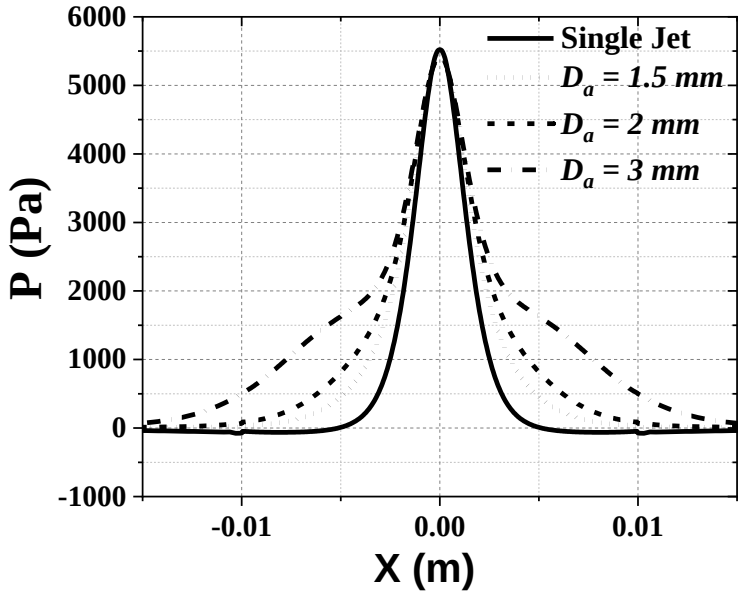

Figure 3-9) Effect of D_a on wall pressure profile for Z/D = 8, Re_m = 11000, Re_a= 6000, a = 3 mm and s = 5 mm

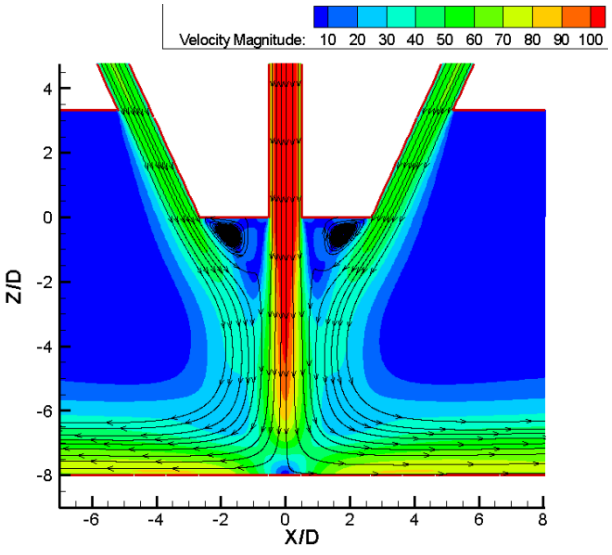

a)

b)

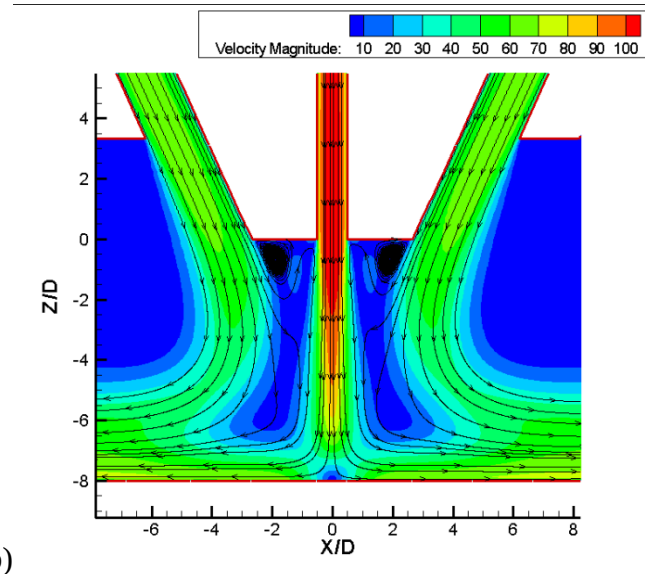

Figure 3-10) Velocity contour and streamlines with Z/D = 8, Re_m = 11000, Re_a = 6000, a = 3mm and s = 5mm for a) D_a=1.5 mm and b) D_a = 3 mm

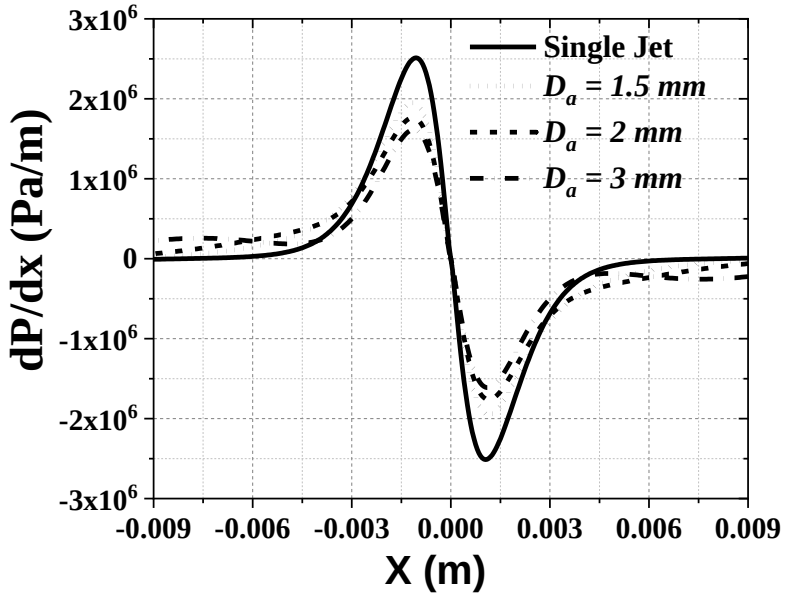

Figure 3-11) Effect of D_a on wall pressure gradient for Z/D = 8, Re_m = 11000, Re_a = 6000, a = 3mm and s = 5mm

3.8.2 Effect of auxiliary jet tilt angle (θ)

In this section, the effect of the auxiliary jet tilt angle (θ) on the wall pressure distribution and wall pressure gradient were investigated. The main and auxiliary jet Reynolds numbers were fixed at Re_m = 11000 and Re_a = 6000, respectively, and $D = D_a$ =1.5 mm, a = 3 mm, s = 5mm and Z/D = 12. The main jet was perpendicular to the impingement plate and the auxiliary jets were inclined at θ = 0°, 8° and 15° relative to the main jet centerline as defined in Figure 3-2 (please recall that θ = 20° in the computations documented above). In order to compare the results, mesh was reset to keep similar refinement near the wall and jet centerlines for each of the case studies. Figure 3-12 shows the resultant wall pressure distributions and wall pressure gradients for the various θ documented above.

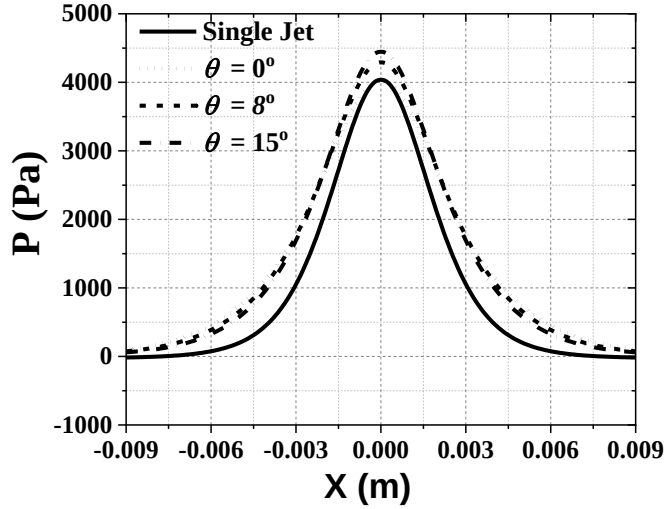

a)

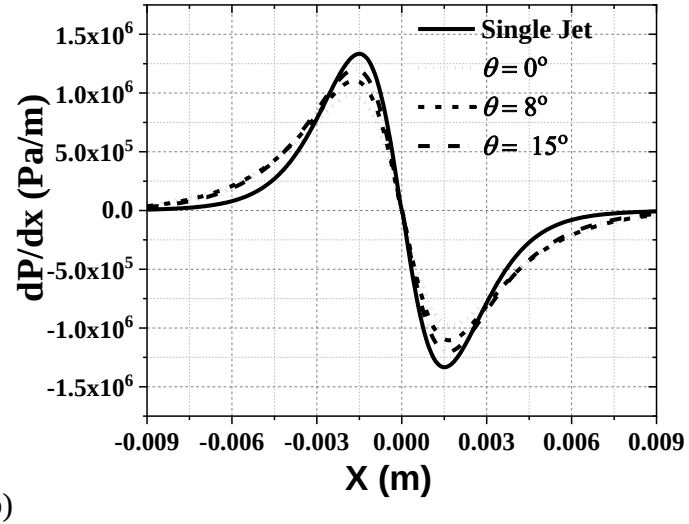

b)

Figure 3-12) Effect of θ on wall pressure profile and wall pressure gradient for Z/D = 12, Re_m = 11000, Re_a = 6000, a = 3 mm, s = 5 mm and $D = D_a$ = 1.5 mm

According to Figure 3-12a, the maximum pressure value was sensitive to the auxiliary jet tilt angle and, by inclining the auxiliary jet toward the main jet centerline, a higher maximum pressure could be achieved. For Z/D = 12 and a = 3 mm, the highest maximum pressure and maximum pressure gradient distribution were obtained for θ = 15° in which

the main and auxiliary jet centerlines were coincident at a same point on the impingement wall. In this arrangement for the multi-slot air-knife, the auxiliary jet flows merge with the main jet flow and formed a single flow field. Thus, the additional momentum from the auxiliary jets aided in increasing the main jet flow field momentum and a higher $(dp/dx)_{\max}$ could be achieved, as is shown in Figure 3-12b. However, it can also be seen that the maximum pressure gradient value continued to be lower for the multi-slot air-knife design as compared to the single slot jet under these operating conditions.

3.8.3 Effect of *a*

Figure 3-13 illustrates the effect of main jet to auxiliary jet distance (*a*, Figure 3-2) on the wall pressure profile and wall pressure gradient. The main and auxiliary jet Reynolds numbers were fixed at Re_m = 11000 and Re_a = 6000, respectively, and the jet to wall distance was fixed at *Z/D* = 12, and "*a"* varied between *a* = 1 mm and *a* = 3 mm while *s*, D_a and were fixed at 5 mm and 1.5 mm, respectively, where θ was varied between 8° and 15° in a way that the jet centerlines were coincident at a same point on the wall.

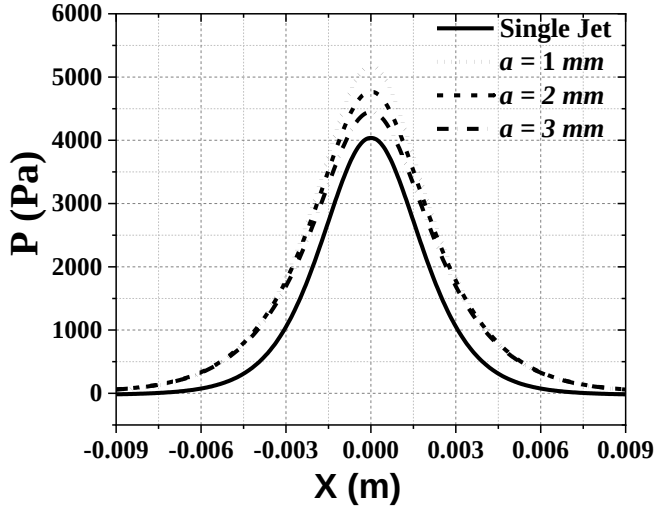

a)

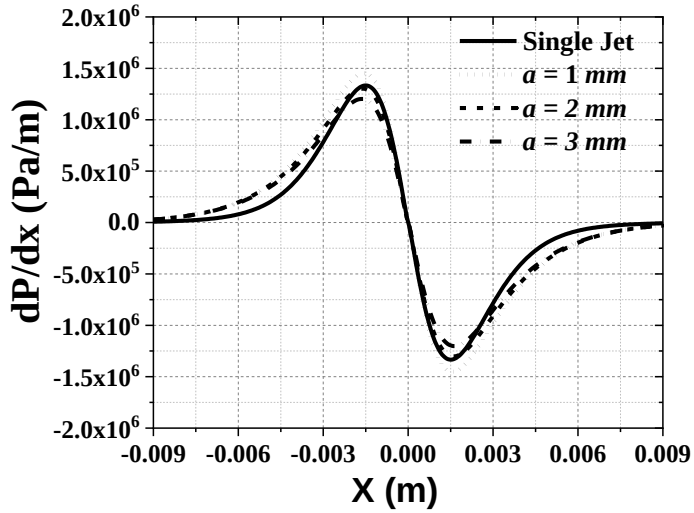

b)

Figure 3-13) Effect of a on wall pressure profile and wall pressure gradient for Z/D = 12, Re_m = 11000, Re_a = 6000, s = 5 mm, and $D = D_a$ = 1.5 mm.

It was observed that by decreasing the distance between the main jet and auxiliary jets (a), a higher maximum pressure value could be achieved while increasing the pressure profile gradient. Consequently, in Figure 3-13, the pressure gradient distribution increased

by decreasing "*a"* and, for a = 1 mm, the multi-slot air-knives had a higher $(dp/dx)_{max}$ as compared to the single slot jet.

3.8.4 Effect of *s*

In this section, the effect of the auxiliary jet offset (*s*, Figure 3-2) on the wall pressure gradient and wall shear stress profiles was investigated. The main and auxiliary jet Reynolds numbers were fixed at Re_m=11000 and Re_a=6000, respectively, and the jet to wall distance was fixed at Z/D = 12, a = 2 mm, $D = D_a$ = 1.5 mm and *s* ranged between 0 mm to 10 mm. According to Figure 3-14 there was no significant effect on the pressure gradient profiles for the range of *s* values investigated.

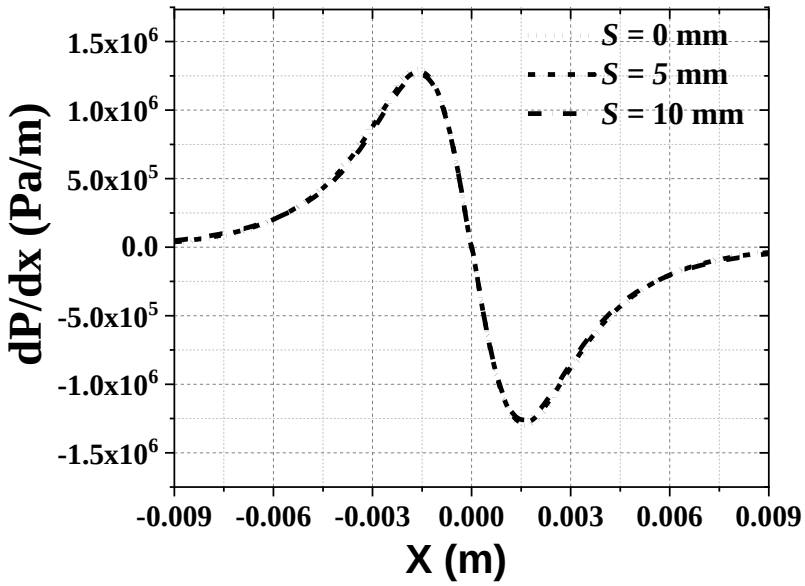

Figure 3-14) Effect of *s* on the wall pressure gradient for Z/D = 12, Re_m = 11000, Re_a = 6000, a = 2 mm and $D = D_a$ = 1.5 mm

Based on the above numerical simulation results, the dimensions for the multiple slot air-knives were modified such that $D=D_a$=1.5 mm, a=1 mm, s=0, and θ varied between 8° to 16° for various Z/D ratios to facilitate convergence of the main and auxiliary jets at the wall along the centerline of the main jet.

3.8.5 Effect of jet to wall distance

According to Dubois [14] coating thickness reduction through gas jet wiping strongly depends on the nozzle to strip distance in the range of line speeds of over 100 m/min and Z/D ≥ 7. In this section, the effect of Z/D on the wall pressure gradient and shear stress distribution for the modified multi-slot air-knife design were investigated and their resultant coating weights on a moving substrate computed. Results of the flow field and coating weight for the modified multi-slot air-knife were compared with the results of the traditional single slot jet air-knife. In the modified design, for each specific Z/D, θ was set in a way that all the three jet centerlines converged on the wall at the centerline of the main jet.

Figure 3-15 illustrates the wall pressure distribution for different values of Z/D for Re_m=11000 and Re_a=3000. It can be seen that the maximum pressure decreased significantly with increasing Z/D. Moreover, by comparing wall pressure distribution for the single jet and multi-slot jets in Figure 3-16, it can be seen that for high Z/D ratios, higher maximum pressure can be obtained for the multi-slot jets. This can be explained by the pressure contour and streamlines in Figure 3-17. According to this figure, the flow from the auxiliary combine with the main jet flow and increase its momentum. This increment can compensate some part of the jet momentum loss due to locating of the wall outside the jet potential core.

Therefore, higher stagnation pressure was observed for the multi-slot jets compared to the single jet. However, this trend was not seen for low Z/D=6 where the impingement wall was already located within the potential core.

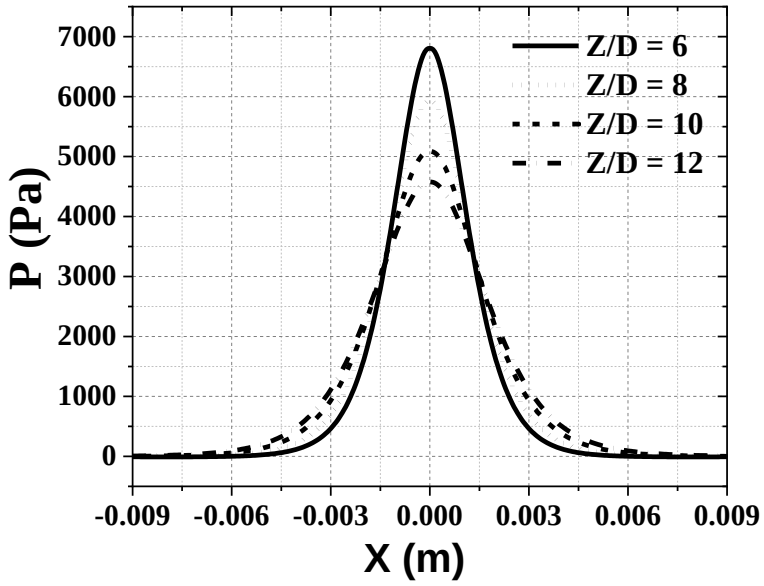

Figure 3-15) Wall pressure distribution of the modified multi-slot air knives for different *Z/D*, where Re_m = 11000 and Re_a = 3000 for D_a = 1.5 mm *D* = 1.5 mm, *a* = 1 mm, *s* = 0.

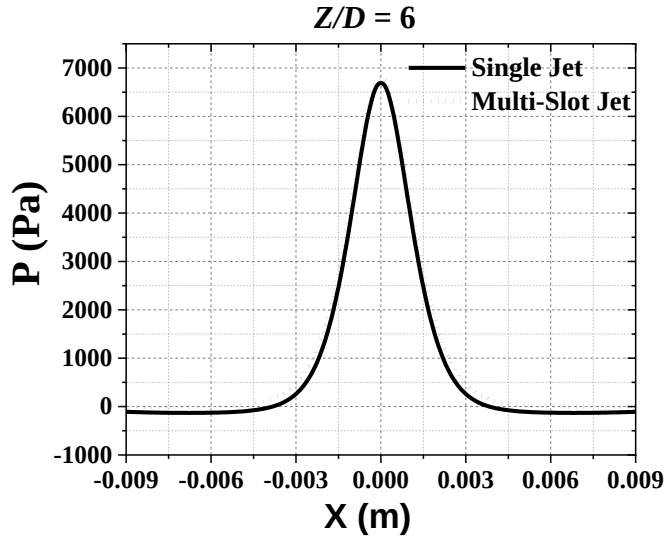

a)

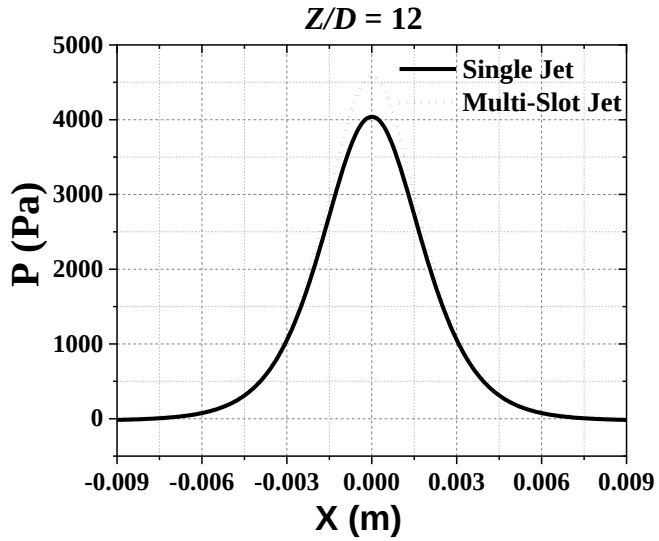

b)

Figure 3-16) Comparison of wall pressure distribution for Z/D = 6 and Z/D = 12, where Re_m = 11000 and Re_a = 3000 for D_a = 1.5 mm D = 1.5 mm, a = 1 mm, s = 0.

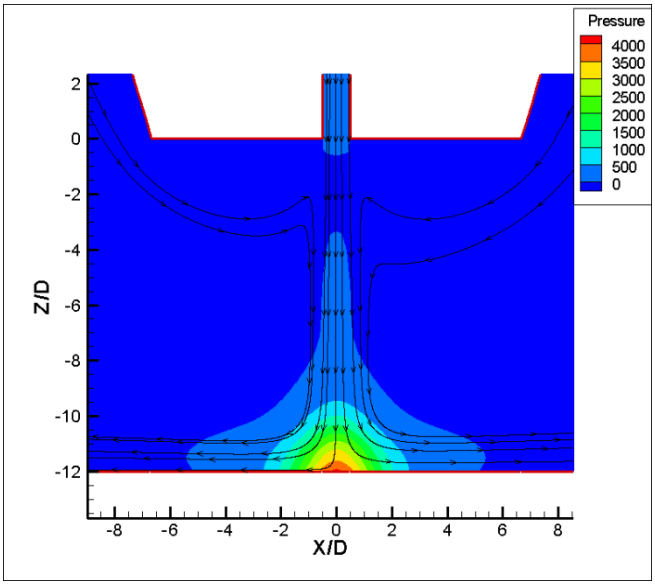

a)

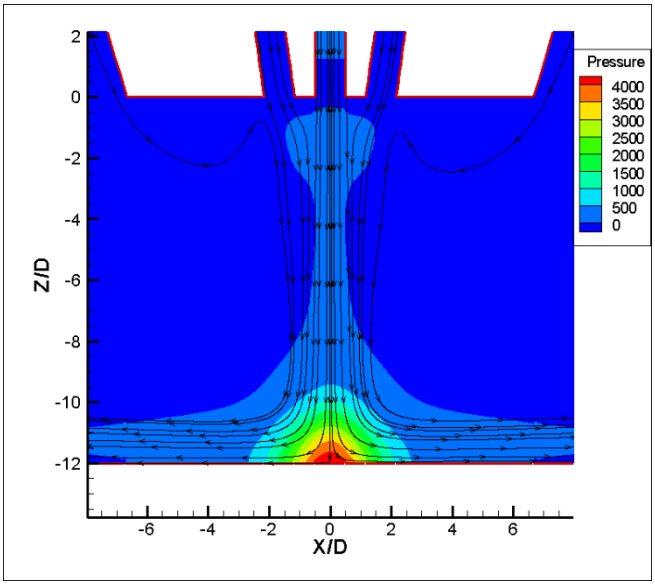

b)

Figure 3-17) Pressure contour and streamlines for Z/D = 12, for a) single slot jet, b) multi-slot jets where Re_m = 11000 and Re_a = 3000 for D_a = 1.5 mm, D = 1.5 mm, a = 1 mm, s = 0.

Figure 3-18 illustrates the maximum wall pressure gradient and shear stress for different Z/D ratios for both the single slot jet and modified version of the multi-jet geometry for Re_m=11000 and Re_a=3000, D_a=D=1.5 mm, a=1 mm and s=0. It is shown in this Figure that the non-dimensional maximum wall pressure gradient for the multiple slot jets was higher compared to the single slot jet for Z/D ≥ 8 and decreased continuously with increasing Z/D where the largest difference between the two configurations was approximately 18% for Z/D = 12.

Figure 3-18b compares the maximum wall shear stress at Re_m=11000 and Re_a=3000. For both configurations the maximum wall shear stress decreased with increasing Z/D ratio, where the rate of shear stress decrement for the single slot jet geometry was higher than for the modified multi-slot design. The value of the maximum shear stress was higher for the single jet geometry for Z/D ≥ 8. The largest difference between the maximum wall shear stress was approximately 11% for Z/D =12.

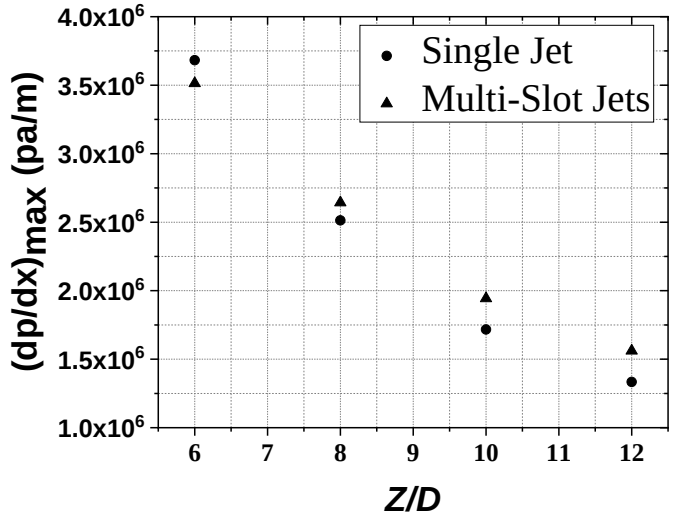

a)

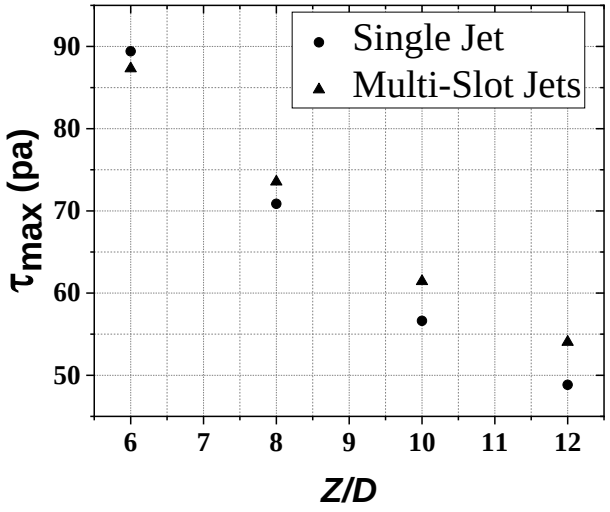

b)

Figure 3-18) Comparison of maximum (a) wall pressure gradient and (b) shear stress for different *Z/D* ratios for D_a=1.5 mm, *D* = 1.5 mm, *a* = 1 mm, *s* = 0.

Figure 3-19 shows a comparison of the coating weights for a single jet and the modified multi-slot jet as a function of *Z/D* ratio with V_s = 0.5 m/s, Re_m = 11000, Re_a = 3000, $D = D_a$ = 1.5 mm, *a* = 1 mm and *s* = 0. It is shown that the coating weight for both geometries is sensitive to the *Z/D* ratio and, as expected, increased with increasing *Z/D*. According to Gosset et al. [7] the final coating thickness varies linearly by the jet to strip distances for *Z/D* > 7 for the single jet. The current study also showed the same trend for the multi-jet slot air-knives. According to the results in Figure 3-19, the coating weight for this configuration of the multi-slot geometry is less than the single slot jet for *Z/D* > 6, with the largest difference being approximately 10% for *Z/D* = 12 and with no significant difference in the coating weight between the two geometries for *Z/D* ≤ 8.

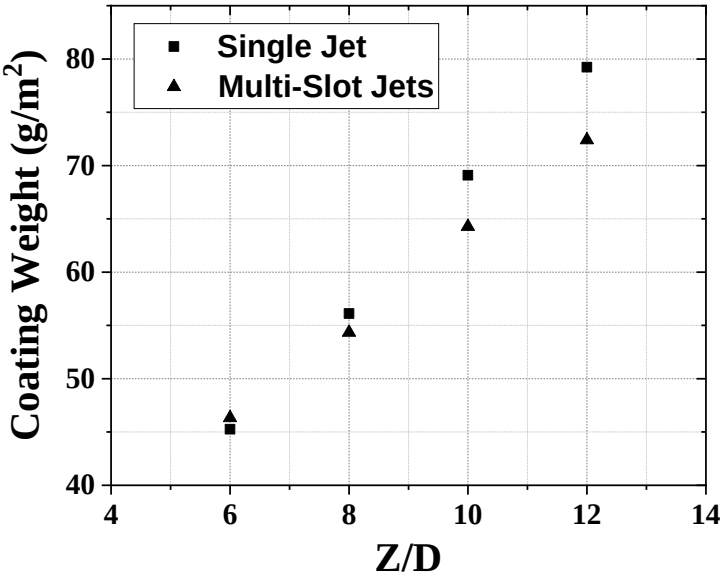

Figure 3-19) Comparison of coating weight for a single slot jet and modified multiple slot jets for different *Z/D* ratios, with V_s = 0.5 m/s, Re_m = 11000 and Re_a = 3000 for D_a = 1.5 mm *D* = 1.5 mm, *a* = 1 mm, *s* = 0.

3.8.6 Effect of main jet Reynolds number

The effect of main jet Reynolds number on the final coating weight is investigated in this section. Re_m was varied between 9000 and 13000 with *Z/D* = 12 and Re_a = 3000. The gas flow rate are 0.16 kg/m.s, 0.19 kg/m.s and 0.24 kg/m.s for *Re* = 9000, *Re* = 11000 and

Re = 13000 respectively. The wall pressure gradient and wall shear stress are shown in

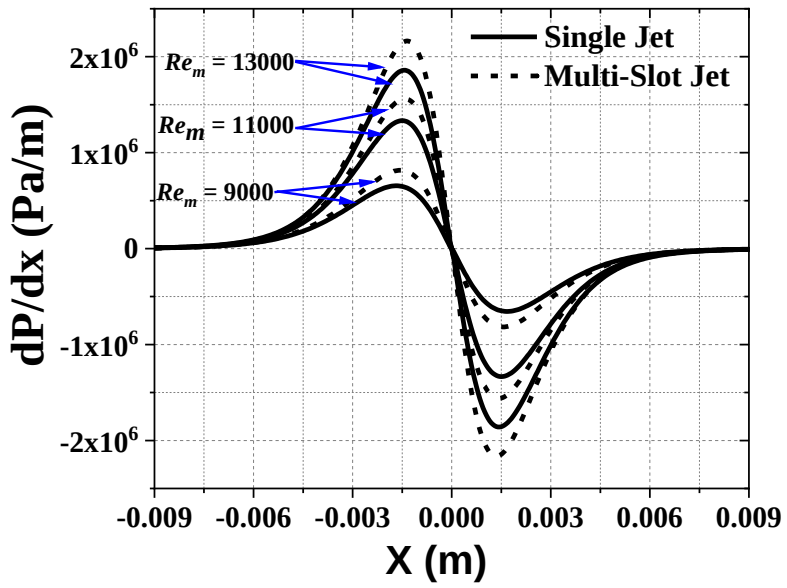

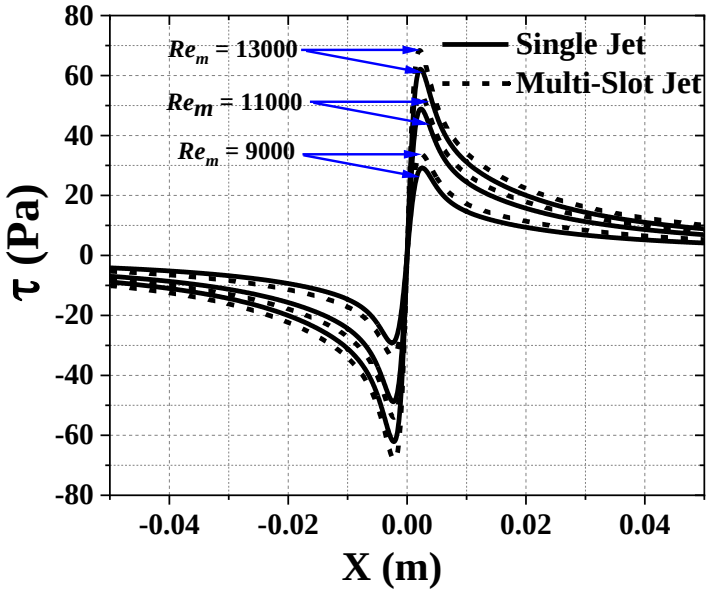

Figure 3-20. According to this Figure, the pressure gradient distribution and shear stress in the vicinity of the wiping region increased with increasing Re_m. Moreover, for each Re_m

the maximum pressure gradient and shear stress were larger for the modified multi-jet configuration versus the single slot air knife geometry.

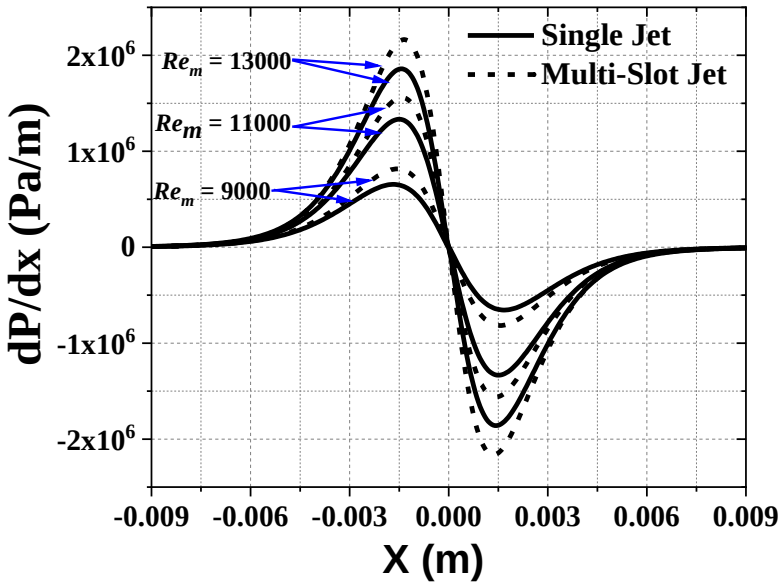

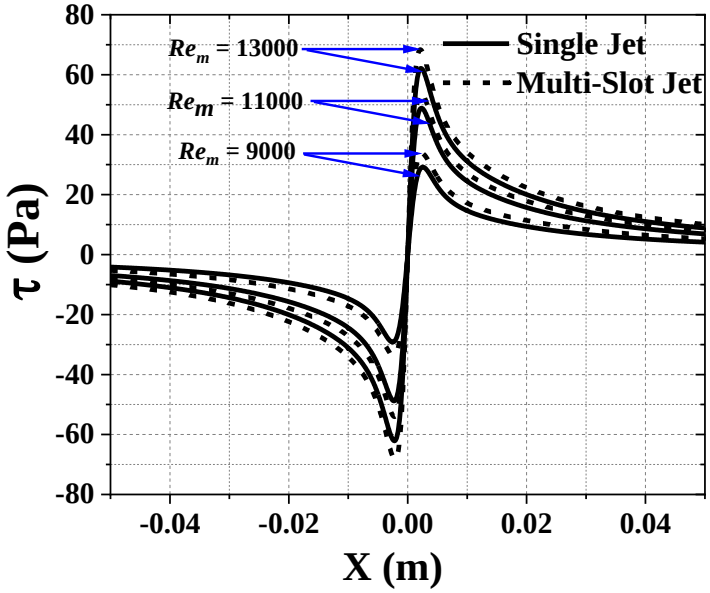

Figure 3-20) Effect of main jet Reynolds number on pressure gradient and shear stress distribution of the modified multiple slot jets for Z/D = 12, Re_a = 3000, D_a = 1.5 mm D = 1.5 mm, a = 1 mm, s = 0 mm, θ = 8°.

Figure 3-21 shows the coating weight on a moving substrate for various Re_m and V_s, with Re_a = 3000 and Z/D = 12, D_a = 1.5 mm D = 1.5 mm, a = 1 mm, s = 0 mm and θ = 8°. By increasing Re_m, the coating weight decreased for each V_s and increased with increasing strip velocity. The results for the multi-slot design were compared with the single slot jet coating weights. It was concluded that the coating weight for this configuration was lower for each Re_m and V_s in the case of the multi-slot air knife geometry.

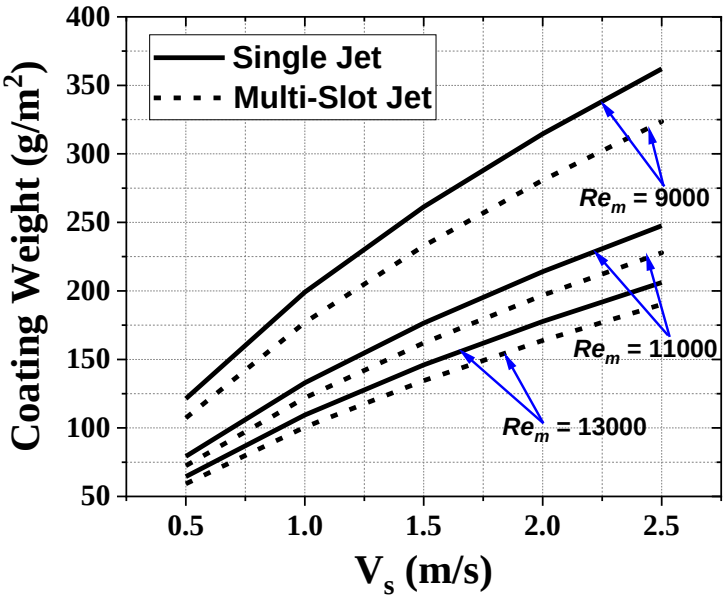

Figure 3-21) Coating weight of the single slot jet and modified multi-slot jet for various Re_m and V_s with Z/D = 12 and Re_a = 3000, D_a = 1.5 mm D = 1.5 mm, a = 1 mm, s = 0, θ = 8°.

3.8.7 Effect of auxiliary jet Reynolds number

In this section the effect of auxiliary jet Reynolds number on the coating weight was investigated numerically while the main slot Reynolds number was fixed at Re_m=11000. Figure 3-22 shows the wall pressure gradient and wall shear stress results for Re_a ranging between 3000 and 9000 with Re_m = 11000 and Z/D = 12, $D_a = D$ = 1.5 mm, a = 1 mm, s = 0 and θ = 8°. It can be seen that the maximum pressure gradient was sensitive to Re_a and decreased with increasing Re_a such that the pressure gradient distribution and shear stresses were higher than those of the single jet case for $Re_a \leq 6000$.

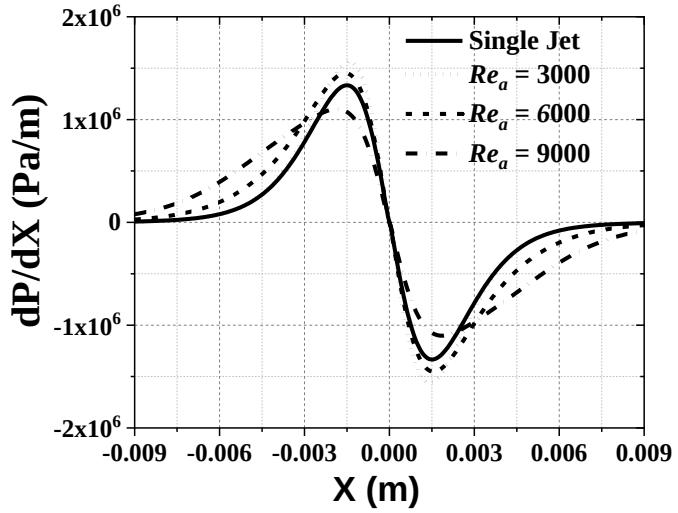

a)

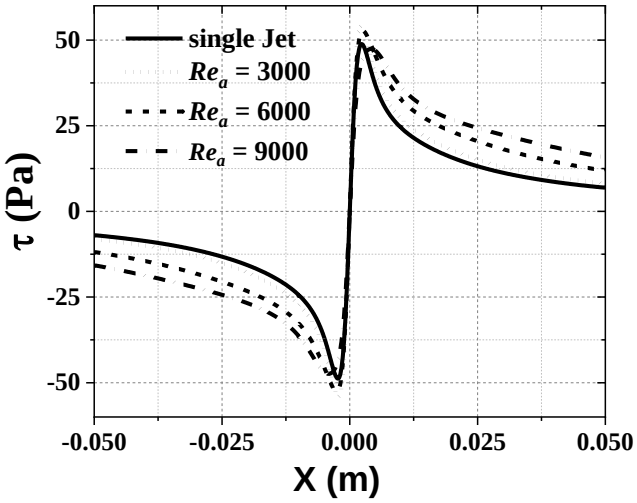

b)

Figure 3-22) Effect of auxiliary jet Reynolds number on wall pressure gradient and wall shear stress for the modified multi-slot jet with Re_m = 11000 and Z/D = 12, D_a = 1.5 mm D = 1.5 mm, a = 1 mm, s = 0, $\theta = 8^o$.

According to Figure 3-23 for high Re_a the auxiliary jet flow particles with higher velocities collide to the main jet flow and decrease its strength in the impingement region. Therefore, it decreases the wiping ability of the main jet. However for lower Re_a the low velocity particles of the auxiliary jet mix with the flow in the jet centerline region and increase the speed of the flow that imping on the substrate. This velocity increment is a main cause in increasing the wall shear stress and pressure gradient for this configuration in comparison with the conventional single-impinging slot jet case.

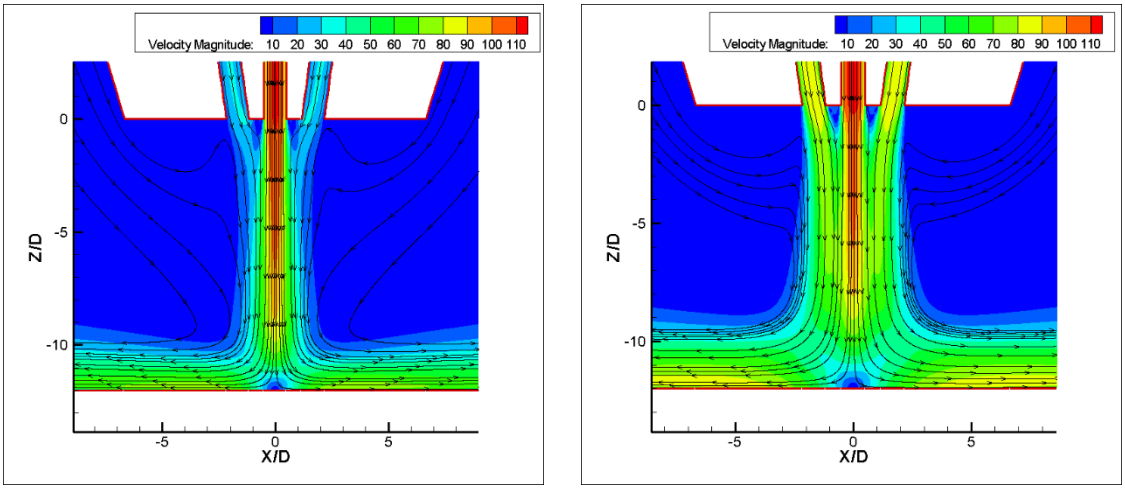

Figure 3-23) Pressure contour and streamlines for a) Re_a = 3000 and b) Re_a = 9000 where Z/D = 12, Re_m = 11000, D_a = 1.5 mm D = 1.5 mm, a = 1 mm, s = 0.

Figure 3-24 shows the effect of auxiliary jets Reynolds number on coating weight. It was observed that the coating weight increased with increasing Re_a for each strip velocity. It can be concluded that when the auxiliary jet Reynolds number is a fraction of the main jet Reynolds number (i.e. 25% - 55%), the multi-slot jet geometry can yield lighter coating weights.

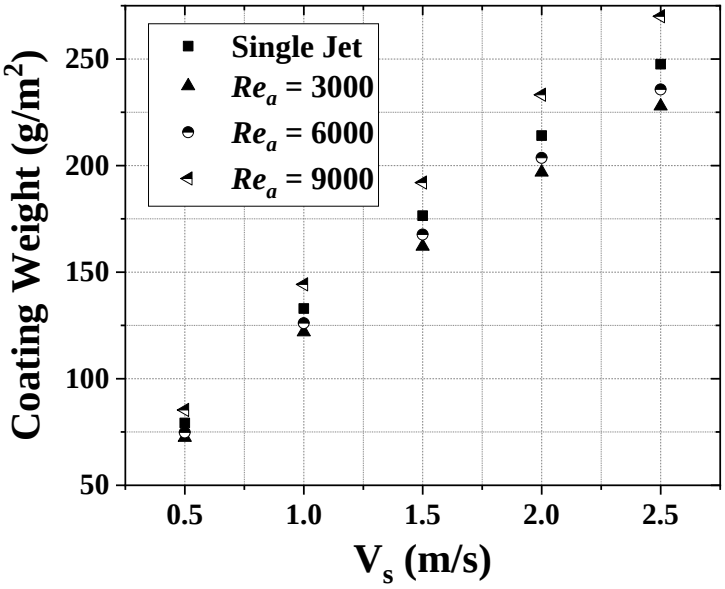

Figure 3-24) Coating weight for different Re_a and V_s with Z/D = 12 and Re_m = 11000.

3.9 Conclusion

A novel configuration for a multi-slot air-knife which can be applicable for the continuous hot dip galvanizing process as an alternative for the conventional single slot jet was investigated numerically.

Wall pressure and wall shear stress results from the numerical simulations were used as boundary conditions in the analytical solution of the liquid film thickness in order to estimate the final coating weight on a moving substrate. In the current study, the sensitivity of the wall pressure distribution to air knife geometry changes was investigated and a modified arrangement for the multi-slot jet configuration was obtained based on the CFD results. The parametric study showed that for obtaining lower coating weights, the arrangement for the multi-slot air-knife should be in a way that the main and auxiliary jet

centerlines coincide at a same point on the impingement wall. Also by decreasing the distance between the main jet and auxiliary jets and auxiliary jet width lower coating weight can be obtained. In the next step, the effects of jet to wall distance, auxiliary jet Reynolds number, strip velocity and main jet Reynolds number on the coating thickness were investigated by numerical simulations of the modified multi-slot air-knife design and compared to the traditional single jet geometry. It was observed that for $Z/D \geq 8$, a thinner coating thickness for higher strip velocities can be achieved by the modified multi-slot air-knife, particularly when the auxiliary jet Reynolds number was set as a fraction of the main jet Reynolds number. Also by increasing the main jet Reynolds number, multi-slot air knife showed better results in terms of coating thickness reduction compared to the conventional single slot air knife.

3.10 References

[1] Marder, A. R. ‘Metallurgy of zinc-coated steel’. Prog. Mater. Sci. 45, 191–271 (2000).

[2] Thornton, J. A. , Graff, H. F. ‘An analytical description of the jet’ finishing process for hot-dip metallic coatings on strip. Metall. Trans. B 7, 607–618 (1976).

[3] Tuck, E. O. ‘Continuous coating with gravity and jet stripping’. Phys. Fluids 26, 2352 (1983).

[4] Ellen, C. H. , Tu, C. V. ‘An analysis of jet stripping of molten metallic coatings’. Eight Australas. Fluid Mech. Conf. 106, (1983).

[5] Myrillas, K. P. Rambauda, J.M. Mataigneb, P. Gardinb, S. Vincentc, J.M. Buchlina. ‘Numerical modeling of gas-jet wiping process’. Chem. Eng. Process. Process Intensif. 68, 26–31 (2013).

[6] Tu, C. V , Wood, D. H. ‘Wall pressure and shear stress measurements’. Exp. Therm. Fluid Sci. 13, 364–373 (1996).

[7] Gosset, A., Rambaud, P., Castellano, L., Dubois, M. & Buchlin, J. M. ‘Modeling of gas-jet wiping at small standoff distances’. in 6th European Coating Symposium, (2005).

[8] Guo, Y., Wood, D. H. ‘Measurements in the vicinity of a stagnation point’. Exp. Therm. Fluid Sci. 25, 605–614 (2002).

[9] Naphade, P., Mukhopadhyay, A., Chakrabarti, S. ‘Mathematical modelling of jet finishing process for hot-dip zinc coatings on steel strip’. ISIJ Int. 45, 209–213 (2005).

[10] Elsaadawy, E. aA., Balthazaar, A.K.S, McDermid, J.R., Hrymak, A.N. ‘Coating weight model for the continuous hot-dip galvanizing process’. Metall. Mater. Trans. B Process Metall. Mater. Process. Sci. 38, 413–424 (2007).

[11] Lacanette, D., Gosset, A., Vincent, S., Buchlin, J. M. , Arquis, E. ‘Macroscopic analysis of gas-jet wiping: Numerical simulation and experimental approach’. Phys. Fluids 18, (2006).

[12] Dubois, M. ‘Review on Wiping : A Key Process Limiting CGL Productivity’. in Galvatech 2011 Conference Proceedings: HDG Process Technologies 1847–1859 (2011).

[13] Kim, G. Y., Park, H. D., Lee, D. E. , Chung, W. C. ‘Gas wiping apparatus having multiple nozzles’. US patent 20100031879, (2008).

[14] Launder, B. E. , Sharma, B. I. ‘Application of the energy dissipation model of turbulence to the calculation of flow near a spinning disc’. Lett. Heat Mass Transf. 131–138 (1974).

[15] Alibeigi, S., Mcdermid, J. R., Ziada, S. , Goodwin, F. E. ‘Effect of Air Knife Geometry on Coating Weight Control in the Continuous Galvanizing Line’. in Galvatech 2013 Conference Proceedings: HDG Process Technologies 437–440 (2013).

[16] Ritcey, A., Mcdermid, J. R. , Ziada, S. ‘Wall shear stress under an impinging planar jet using the razor blade technique’. in ICFMFA 2015 : 17th International Conference on F luid Mechanics and Flow Analysis (2015).

Chapter 4: Experimental and Numerical Study of Coating Thickness using Multi-Slot Air-Knives

Ali Yahaee Soufiani, Joseph R. McDermid, Andrew N. Hrymak, Frank E. Goodwin, Metallurgical and Materials Transactions B (MMTB), 2019, (DOI: 10.1007/s11663-019-01666-1)

In this paper, the wiping apparatus was designed and manufactured by me. Moreover, all the experimental measurements and numerical simulations were carried out by me under the supervision of Dr. McDermid and Dr. Hrymak. The manuscript was initially drafted by me and reviewed to the final version by Dr. McDermid and Dr. Hrymak. Dr. Goodwin was included as an author in this paper as a courtesy for his provision of industrial sponsorship.

4.1 Abstract

Gas jet wiping is a widely employed production technology for controlling the final zinc coating thickness on a moving substrate during continuous hot-dip galvanizing. This paper presents an experimental investigation and numerical analysis of a prototype multi-slot air-knife, which offers an increase in wiping efficiency relative to the traditional single-slot jet geometry in the continuous galvanizing process.

The applicability of the analytical coating weight model of Elsaadawy et al. [1] to predict the final coating weight was determined for the multi-slot geometry, where particular focus was devoted to the effect of geometric parameters. Experimental measurements under a variety of knife geometry and process conditions agreed with the coating weight predictions of the analytical model. It was also shown that the air knife geometric parameters had a significant effect on the pressure profile and shear stress distribution applied by the air-knives to the moving substrate. It was determined that the final coating thickness was significantly affected by the auxiliary jet width, D_a, where lighter coating weights at higher strip velocities (up to 5.4 % at V_s = 1.5 m/s) could be achieved by using the multi-slot air-knives prototype versus the conventional single-slot configuration.

4.2 Nomenclature

c	Speed of sound (m/s)
D	Main jet width (m)
D_a	Auxiliary jet width (m)
g	Gravitational acceleration (m/s^2)
G	Non-dimensional pressure gradient
h_f	Final film thickness (m)
h	Local film thickness (m)
H	Non-dimensional film thickness
L	Computational domain length (m)
L_s	Strip width (m)
$\dot{m}$	Mass flow rate of removed oil (kg/s)
P	Static pressure (Pa)
P_s	Nozzle static pressure (Pa)
P_∞	Ambient pressure (Pa)
q	Withdrawal flux (m^2/s)
Q	Non-dimensional withdrawal flux
R	Universal gas constant (J/mol.K)
Re	Jet Reynolds number $\left(\mathrm{Re} = \frac{\rho u D}{\mu} \right)$
S	Non-dimensional shear stress
s	Auxiliary jet offset distance (m)
T	Temperature (K)
U	Fluid velocity (m/s)
V_s	Strip velocity (m/s)
Z	Main jet exit to wall distance (m)
μ	Fluid dynamic viscosity (kg/m.s)
μ_t	Turbulent viscosity (kg/m.s)
ρ_{cl}	Coating liquid density (kg/m^3)
γ	Ratio of specific heats of air
τ	Shear stress (Pa)
ρ	Density of gas (kg/m^3)
ρ_{cl}	Density of coating liquid (kg/m^3)

4.3 Introduction

In the steel industry, the continuous hot-dip galvanizing (CHDG) process is broadly used in order to protect the underlying steel substrate from the effects of environmental degradation. The CHDG process includes a molten zinc (Zn) bath, usually held at 733 K (460°C), in which the steel substrate is constantly submerged, resulting in deposition of the liquid Zn-Al-Fe alloy on the steel substrate [2]. Upon exiting the bath, the substrate is coated with a rather thick layer of liquid zinc because of viscous drag forces [3][14]. In order to control the coating layer thickness on the steel, a pair of impinging gas jets (referred to as air knives in the industry), generally in the single-slot configuration, are located above the bath (Figure 4-1). These air knives remove the excess zinc by applying a pressure gradient (dp/dx) and shear stress (τ) to the coating layer and return the excess molten Zn liquid to the bath[14]. In this manner, the desired final film thickness (h_f), which is a function of the nozzle pressure P_s, the strip velocity V_s, the nozzle to moving sheet distance Z, the jet width D, and the viscosity and density of the liquid zinc [4], can be obtained after the wiping action of the air-knives.

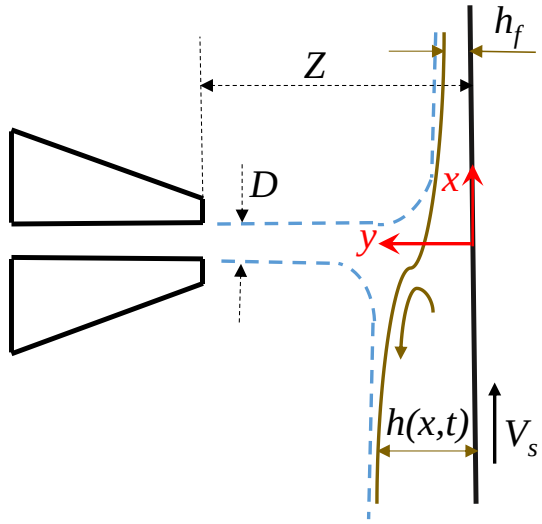

Figure 4-1) Schematic of the conventional single-slot gas jet wiping process for coating control.

Steel sheet products are generally used by the automotive industry for either structural members or closure panels. A recent trend within the automotive industry has been to reduce the Zn coating weight applied to the steel sheet in order to reduce the overall mass of the automotive body-in-white, thereby increasing fuel efficiency and reducing costs [5]. Furthermore, the industry is motivated to reduce the local variability of the zinc coating thickness in order to mitigate the practice of "over-coating", also with the objective of reducing costs. There are several studies available in the literature on using a single-slot turbulent impinging gas jet for controlling the liquid zinc coating thickness on the metal strip during continuous galvanizing [3, 4, 6-8]. The early work on modelling the gasjet wiping process to predict final coating thicknesses – usually expressed as coating weights (e.g. g/m^2) – assumed a decoupled model – i.e. a thin liquid coating film with boundary

conditions on the surface that related to the impinging flow field (i.e. pressure profile gradient and shear stress gradient).

A fundamental analytical coating weight model has been presented by Thornton and Graff [3] to predict the coating film thickness after wiping by a single-slot air-knife. They postulated that only the maximum wall pressure gradient played a significant role in determining the final film thickness. The proposed model predicted the final coating thickness as a function of nozzle-to-substrate distance, strip velocity, momentum flux of the jet, and jet width. In a later modification to the Thornton and Graff [3] coating weight model, Ellen and Tu [4] employed the shear stress applied on the film surface by the jet in their analysis of the gas jet wiping process. Their model improved the prediction of final coating thickness and correlated well with coating thickness measurements taken from an industrial continuous galvanizing line [3]. Subsequent studies on the influence of zinc liquid surface tension on the predicted coating weight showed a negligible contribution of surface tension with the pressure gradients typical of continuous galvanizing gas jet wiping as the jet action overcame the capillary force on the coating liquid [7],[9]. Through their experimental measurements, Tu and Wood [8] studied the effect of jet Reynolds number ($3000 \leq Re \leq 11000$) and jet-to-wall standoff distances ($2 \leq Z/D \leq 20$) on the wall pressure profile and wall shear stress distribution under an impinging jet. The experimental correlations of wall shear stress and wall pressure gradient [10] were then used in the coating weight model developed by Ellen and Tu [4] to successfully predict the final Zn coating thickness on the moving substrate. Hrymak et al. [11] subsequently used computational methods to develop a coating weight model to optimize operating conditions

for a targeted coating weight. The coating weights studied lay between 45-75 g/m^2 while the jet Z/D ratios ranged from $2 \leq Z/D \leq 6$. The computational results were benchmarked against industrial coating weight data and excellent agreement was found between the model and the line data with the highest deviation being approximately 8%. Gosset et al. [12] studied the properties of a gas jet at small standoff distances (i.e. $Z/D \leq 8$) and observed that the final coating thickness remained relatively constant for $Z/D < 7$, i.e. in the jet potential core. Elsaadawy et al. [1], proposed a coating weight model based on the work of Ellen and Tu [4] as a function of gas jet operating conditions, where improved correlations of shear stress and pressure gradient were found by Elsaadawy et al. [1] by employing both experimental measurements and numerical analysis using the k-ε turbulence model in (FLUENT^{TM}). The model predictions were in good agreement with industrial continuous galvanizing line data for coating weights of less than 75 g/m^2 for which the average error between the model predictions and measured coating thicknesses were about 8%.

Although single slot jets are widely used in continuous galvanizing lines (CGLs) to control the coating thickness, the current configuration of single-slot jet air-knives are very close to their limit with respect to having the capability of wiping to coating weights of less than 40 g/m^2 at higher line speeds [5]. In order to lower coating weights using single-slot air-knives at reasonable strip velocities, the wiping pressure could be significantly increased. However, higher wiping pressures can lead to industrial difficulties such as higher noise generation ([13], [14]), splashing [15] and coating non-uniformity [5]. Currently, to cope with such problems and achieve the desired lower coating weights, the

steel strip typically moves at lower speeds, which adversely affects the productivity of the line.

In order to address some of these challenges, Kim et al. [16] proposed a multi-slot air knife design to mitigate the splashing problem and enhance coating quality. Their multi-slot configuration consisted of one main jet and four side jets blowing air at reduced velocities relative to the main jet. However, the effect of the proposed configuration on the wall pressure profile and wall shear stress distribution, and consequently the final coating thickness, were not determined.

Tamadonfar et al. [17,18] numerically simulated a multi-slot jet composed of a main jet and two symmetrically inclined jets adjacent to the main jet. The range of simulated flow conditions in the studies of Tamadonfar et al. [17,18]were limited to one slot jet gap and one specific geometry of the multiple slot jet. For the range of operating parameters explored, the multi-slot air-knives did not produce a thinner coating thickness in comparison to a single slot air-knife. Alibeigi et al. [19] later experimentally investigated the wall pressure distribution of the multi-slot jet design under different operating conditions (i.e. Re_m, Re_a, Z/D) and compared the results with the numerical simulations of Tamadonfar et al. [17, 18]. The comparisons showed some disagreement on the maximum wall pressure and pressure distribution between the two studies. Finnerty et al. [20], through the acoustic measurements, later showed that the auxiliary jets of the Tamadonfar et al. [17] design had the ability to eliminate the high-intensity acoustic tones associated with aeroacoustics feedback, implying that the main jet had been stabilized by the action of the auxiliary jets. McDermid et al. [21] later showed *via* PIV measurements that, when

operating the auxiliary jets such that the auxiliary jet velocity was approximately 40% of the main jet velocity did, indeed, stabilize the main jet by significantly reducing main jet flapping associated with the aeroacoustics feedback relative to that observed for the single jet design [22] by largely eliminating the vortical structures associated with the high shear gradients between the main jet and bulk environment.

More recently, Yahyaee Soufiani et al. [23] investigated the fluid flow for the prototype multi-slot configuration. Computational fluid dynamics were applied to predict the wall pressure profile and wall shear stress distributions arising from the multi-slot air knives, and the results were then used in the analytical coating weight model developed by Elsaadawy et al. [1] to predict the liquid zinc coating thickness on the moving strip. The authors showed that a specific arrangement for the multiple slot air knife, where the main and auxiliary jet centerlines coincided at a same point on the impingement wall (i.e. the steel strip), led to lower coating weights compared to a single-slot air knife working under the same operating conditions. The coating weight results of Yahyaee Soufiani et al. [23] for the multiple slot air-knives, were not, however, verified by experimental measurements.

The current contribution focuses on determining the applicability of the Elsaadawy et al. [1] coating weight model for gas jet wiping using the prototype multi-slot air knife and to determine the effects of jet geometry and jet operating parameters on the final coating weight. In this study, the conventional single slot jet design was used as a base case for comparing the coating weight data to those derived from the multi-slot air-knives.

4.4 Analytical model of film thickness

For the convenience of the reader, the key equations and concepts of the analytical coating weight model used in the present work are reviewed below. The final coating thickness is determined by solving the simplified two-dimensional momentum equation for a liquid film. The pressure across the liquid film was assumed to be constant as the film velocity perpendicular to the plate was negligible in comparison with the velocity parallel to the substrate [4]. Using the above assumptions and the x-y co-ordinate system specified in Figure 4-1, the film momentum equation was reduced to:

$$\mu\frac{\partial^2 u}{\partial y^2}-\left(\rho g+\frac{dp}{dx}\right)=0 \tag{4-1}$$

where the boundary conditions for the solution of equation (4-1) were:

$$u=V_s \qquad at \;\; y=0 \tag{4-2}$$

$$\mu\left(\frac{\partial u}{\partial y}\right)=\tau \qquad at \;\; y=h \tag{4-3}$$

The velocity profile can then be obtained through equations (4-1) – (4-3) such that:

$$u=V_S\left[1+\frac{y}{h}SH-\frac{y}{h}\left(2-\frac{y}{h}\right)\frac{GH^2}{2}\right] \tag{4-4}$$

where $H=h\sqrt{\frac{\rho g}{\mu V_S}}$, $S=\frac{\tau}{\sqrt{\rho\mu V_S g}}$ and $G=1+\frac{1}{\rho g}\frac{dp}{dx}$. Integrating equation (4-4) yields the volumetric flux of the liquid, *q*, as:

$$q=\int_0^h u dy=V_s h\left(1+\frac{SH}{2}-\frac{GH^2}{3}\right) \tag{4-5}$$

where the non-dimensional withdrawal flux, $Q = \frac{q}{V_S}\sqrt{\frac{\rho g}{\mu V_S}}$, can be derived from equation (4-5) such that:

$$Q = -\frac{GH^3}{3} + \frac{SH^2}{2} + H \tag{4-6}$$

The non-dimensional film thickness, *H*, then can be determined by setting $\frac{dQ}{dH} = 0$ [6] and solving for *H* such that:

$$H = \frac{S \pm \sqrt{S^2 + 4G}}{2G} \tag{4-7}$$

Upon solidification of the liquid Zn alloy, the film velocity is equal to the strip velocity (V_s) and the coating thickness, h_f, can be determined *via*:

$$h_f = \frac{q}{V_S} = \frac{Q_{\max}}{\sqrt{\frac{\rho g}{\mu V_S}}} \tag{4-8}$$

The pressure profile gradient and shear stress profile can be used with equations (4-7) and (4-8) in predicting the final coating weight. An examination of equations (4-6) through (4-8) will show that higher maximum values for the *dp/dx* and τ distributions near the wiping region will result in lighter coating weights. Thus, in the present work, the wall shear stress and pressure gradient distributions applied by a conventional single-slot and from the prototype multi-slot gas jet designs were predicted through numerical simulations. The predicted final coating thickness on a moving substrate was then compared with experimental measurements, as will be described in section 4-6.

4.5 Numerical modeling

Numerical simulation of the impinging slot jets – both in the single and multi-slot geometries –on a flat plate were performed using FLUENT 15.0. For all simulations, a double precision pressure-based solver was used while for the pressure-velocity coupling the SIMPLE method was applied. The Reynolds-Averaged Navier-Stokes (RANS) equations (equations (4-9) and (4-10)) were used for the air flow determination.

$$\frac{\partial \rho}{\partial t} + \frac{\partial \left(\rho \overline{u}_i \right)}{\partial x_i} = 0 \tag{4-9}$$

$$\frac{\partial \rho \overline{u}_i}{\partial t} + \frac{\partial \rho \overline{u}_i \overline{u}_j}{\partial x_i} = -\frac{\partial p}{\partial x_i} + \frac{\partial}{\partial x_i}\left[\mu \left(\frac{\partial \overline{u}_i}{\partial x_j} + \frac{\partial \overline{u}_j}{\partial x_i} \right) - \rho \overline{u_i' u_j'} \right] \tag{4-10}$$

The Reynolds stress was modeled using the Boussinesq hypothesis, which relates it to the mean velocity gradient *via* the turbulent viscosity, μ_t (equation (4-11)):

$$-\rho \overline{u_i' u_j'} = \mu_t \left(\frac{\partial \overline{u}_i}{\partial x_j} + \frac{\partial \overline{u}_j}{\partial x_i} \right) \tag{4-11}$$

In the present study, the two-equation model of the standard *k-ε* turbulence model was used to determine the turbulent viscosity, μ_t. In this model, two transport equations are required to be solved for turbulent kinetic energy and rate of turbulent dissipation. The transport equations are as follows:

$$\frac{\partial \rho k}{\partial t} + \frac{\partial \rho k u_i}{\partial x_i} = \frac{\partial}{\partial x_j}\left[\left(\mu + \frac{\mu_t}{\sigma_k} \right) \frac{\partial k}{\partial x_j} \right] + G_k - \rho \varepsilon \tag{4-12}$$

$$\frac{\partial \rho \varepsilon}{\partial t} + \frac{\partial \rho \varepsilon u_i}{\partial x_i} = \frac{\partial}{\partial x_j}\left[\left(\mu + \frac{\mu_t}{\sigma_\varepsilon} \right) \frac{\partial \varepsilon}{\partial x_j} \right] + C_{1\varepsilon} \frac{\varepsilon}{k} (G_k) - C_{2\varepsilon} \rho \frac{\varepsilon^2}{k} \tag{4-13}$$

$$\mu_t = \rho C_\mu k^2 / \varepsilon \tag{4-14}$$

where C_μ is a model constant. For the pressure term, the standard method for the pressure and a first-order winding-up method was used to determine the turbulent dissipation rate (ε), the turbulent kinetic energy (k) and the momentum. The discretized equations were iterated until the root-mean-square (RMS) residuals for all governing equations were less than 10^{-6}.

Schematics of the single and multi-slot nozzle configurations are shown in Figure 4-2. The pressure profile and shear stress CFD results were validated *via* the experimental measurements of Ritcey et al. [24] and Alibeigi [25]. The CFD boundary conditions were a defined pressure inlet at the nozzle inlets, the no slip condition at the nozzle walls and at the impingement surface, and a defined pressure outlet at the edge of the computational domain. The inlet pressure (P_s), was used to estimate the flow velocity at the nozzle exit using equation (4-15) [26]:

$$U = c\sqrt{\frac{2}{\gamma - 1}\left[\left(\frac{P_s + P_\infty}{P_\infty}\right)^{\gamma-1/\gamma} - 1\right]} \tag{4-15}$$

where c is the speed of sound (343 m/s), γ is the ratio of specific heats of air , and P_∞ is the ambient pressure. A combination of quadrilateral and triangular meshes were used for the jet simulation. The mesh was refined near the wall region and grid clustering was also performed along the jet centerline. Four grids with 252,000 to 393,000 nodal points, depending on the plate-to-main jet width (Z/D, Figure 4-2) ratio, were examined to ensure mesh independence of the results. Mesh refinement along the wall was such that the first

grid was placed in the viscous sub-layer (y+∼1) where the mesh dimension near the wall was on the order of 4 µm.

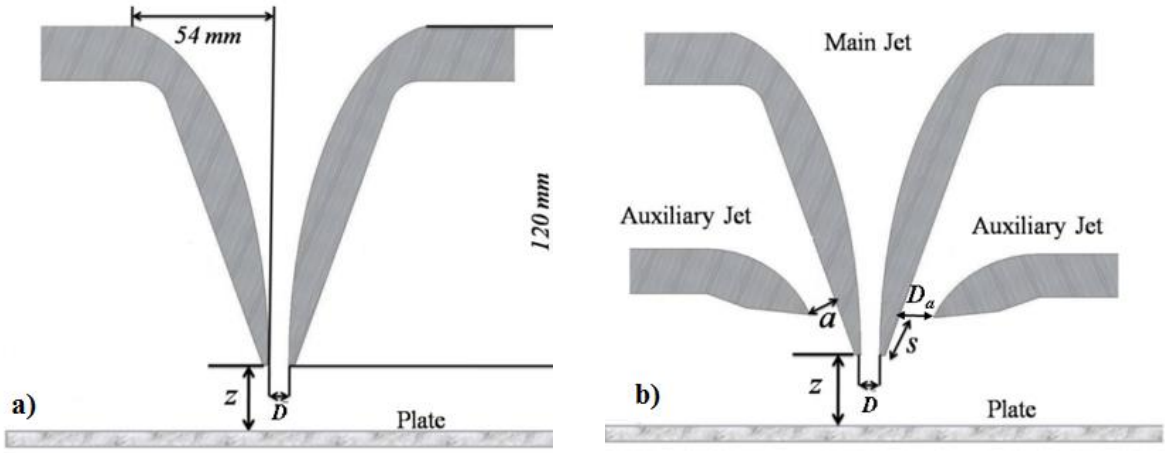

Figure 4-2) Schematic of a) the single and b) multi-slot air-knife geometries.

The numerical simulations in the current study were benchmarked against the experimental wall pressure distributions of Alibeigi [25] and Ritcey et al. [24] for $4 < Z/D < 12$ at $Re_m = 11000$. Figure 4-3 compares the numerically-derived non-dimensional wall pressure profiles from the present study versus the experimental data of Ritcey et al. [24] for the single-slot jet configuration as a function of jet to wall distance. Figure 4-3 illustrates that the numerically simulated pressure profile matches well with the experimental measurements. Figure 4-4 shows a similar comparison of several numerically-derived wall pressure profiles from this work versus the experimental data of Alibeigi [25] for the multi-slot air-knives where $Re_m = Re_a = 11000$. According to Figure 4-4, the predicted non-dimensional wall pressure profiles agree, within experimental error, with experiment.

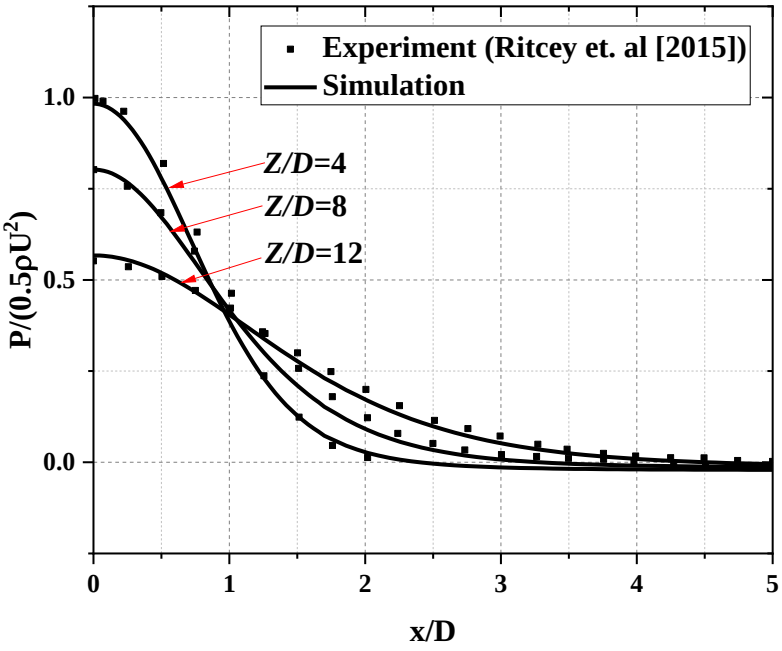

Figure 4-3) Comparison of non-dimensional wall pressure profiles at Re=11000 and 4 < *Z/D* < 12 with the experimental measurements of Ritcey et al. [24].

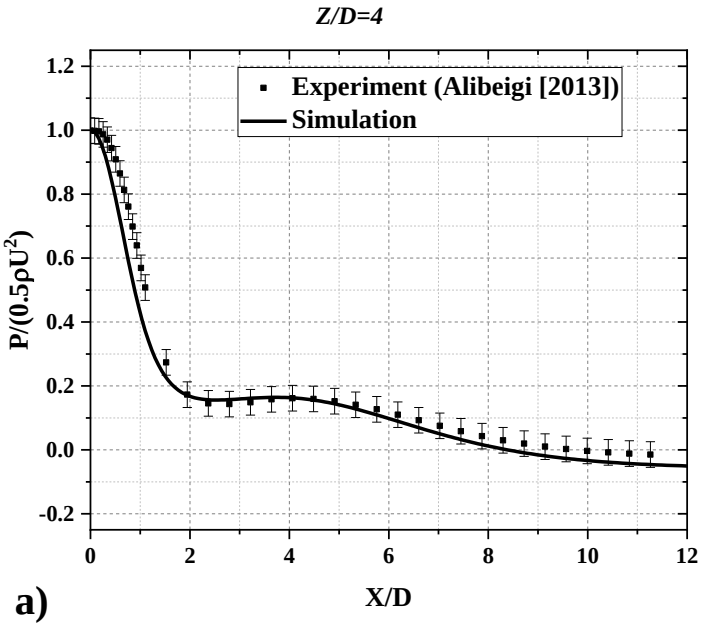

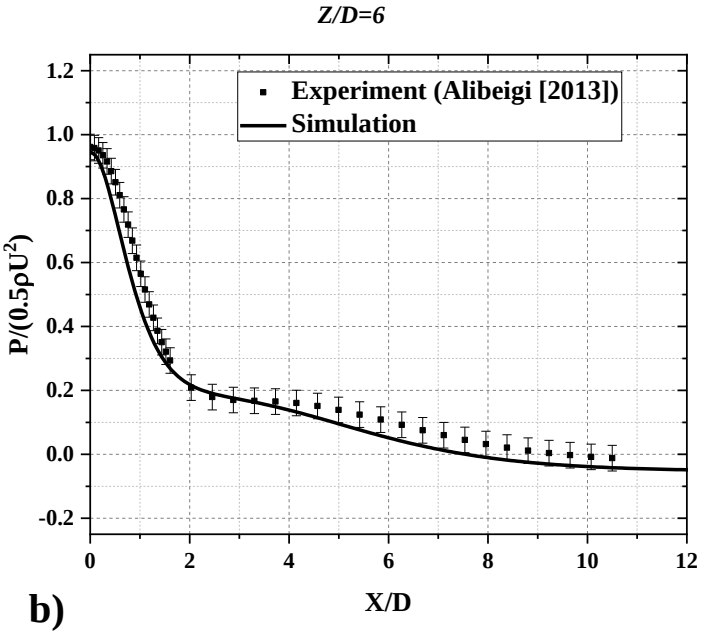
Z/D=6
Experiment (Alibeigi [2013])
Simulation
P/(0.5ρU²)
X/D
1.2
1.0
0.8
0.6
0.4
0.2
0.0
-0.2
0
2
4
6
8
10
12

b)

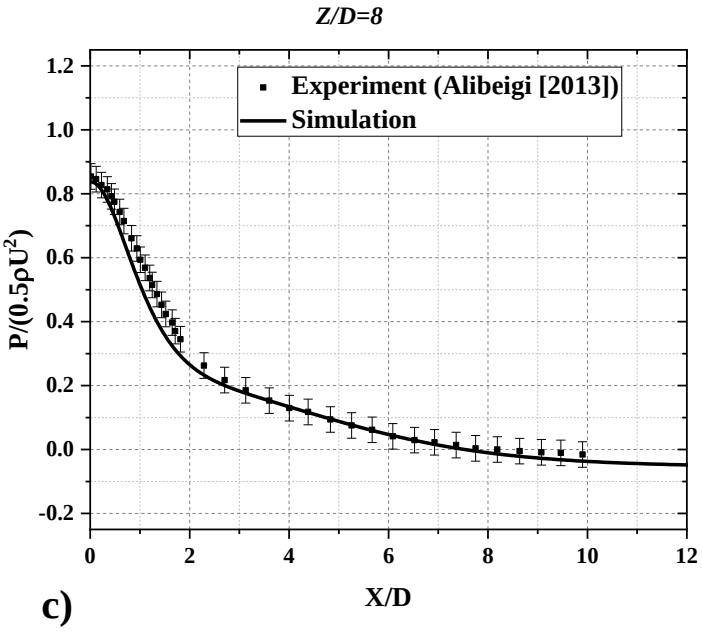
Z/D=8
Experiment (Alibeigi [2013])
Simulation
P/(0.5ρU²)
X/D
1.2
1.0
0.8
0.6
0.4
0.2
0.0
-0.2
0
2
4
6
8
10
12

c)

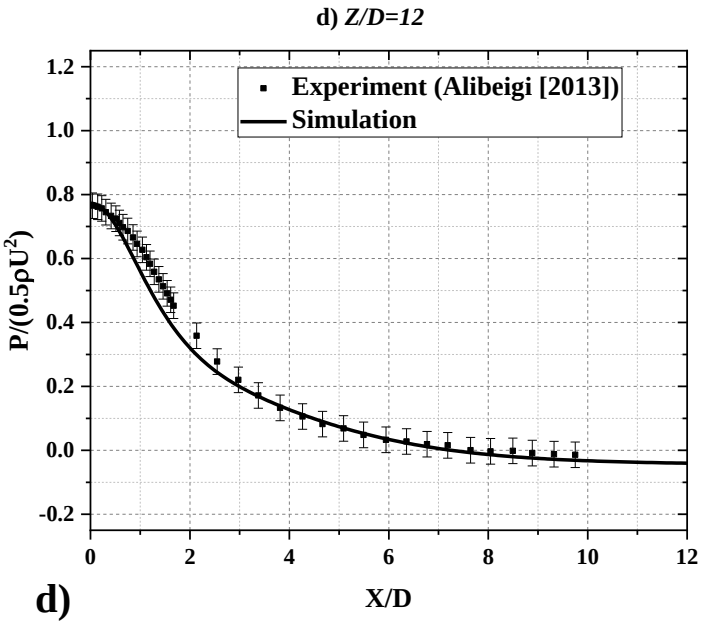

Figure 4-4) Comparison of numerical wall pressure distribution results with the experimental measurements of Alibeigi [25] for the multi-slot air knife geometry (Figure 4-2)) at Re_m=11000, Re_a=11000 and a) *Z/D* = 4, b) *Z/D* = 6, c) *Z/D* = 8, d) *Z/D* = 12.

4.6 Test facility

4.6.1 Air-Knives

A schematic of the prototype multi-slot impinging jet used in the experimental measurements is presented in Figure 4-5. The multi-slot air knives consists of three jets, one main jet and two inclined auxiliary jets symmetrically located on each side of the main jet. The main jet was perpendicular to the moving strip and the auxiliary jets were inclined at 20° from the main jet centerline. The prototype multi-slot air knives have three separate inlet chambers and each has an individual plenum and valve to allow independent control of the plenum pressure for each nozzle. Compressed air from a 550 kPa blower was used

to feed the auxiliary jets and the main jet was fed with a resident 550 kPa compressed air line. For the main jet, air was passed through a regulator and two filters to prevent any particulates entering the main jet plenum and nozzle. An electric valve was also used immediately after the filter to adjust the main jet pressure using an in-house computer program. In the case of the auxiliary jets, the air supply was passed through a 5 cm regulator valve, a 5 cm ball valve and a 5 cm gate valve prior to entering a T manifold, where three 2.5 cm globe valves were used to adjust the pressure for each of the auxiliary nozzles. For all of the nozzles, air entered into the applicable plenum *via* a 25.4 mm diameter pipe at the top of the plenum, was passed through a flow distributor tube (Figure 4-5)) and then through a series of mesh screens located upstream of the nozzle contraction in order to break up any large-scale turbulent structures (Figure 4-5). The screens comprised stainless steel cloth with 28 wires/cm. Finally, air exited the nozzle at 90° to its inlet direction. To adjust the distance between the nozzle and the plate – i.e. the Z/D ratio – the prototype multi-jet air-knife was mounted on a computer controlled traverse system consisting of a VXM-3 Velmex™ power supply with a Slo-syn stepper motor with a least division of 5 μm. A Validyne DP-15 pressure transducer was used to measure the plenum pressures and the data was logged using a conventional data acquisition system and LabVIEW software. The plenum pressure was measured at the centerline of each jet, upstream of the nozzle contraction.

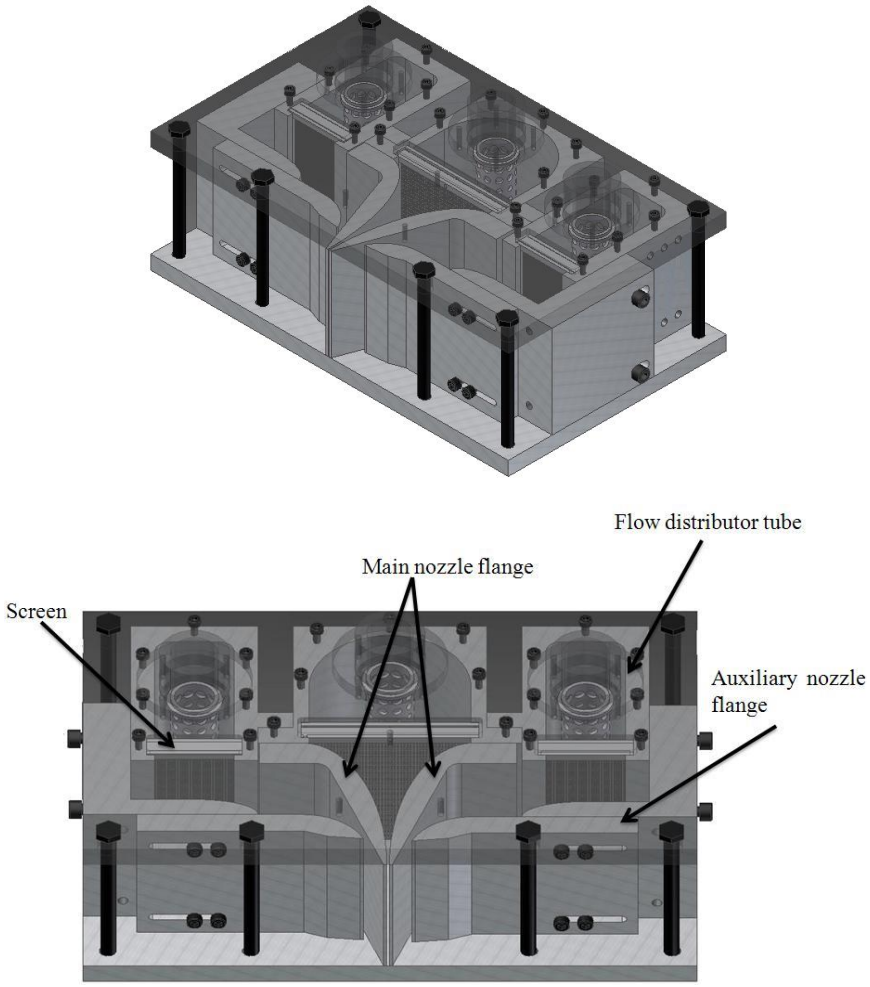

Figure 4-5) Isometric view of the multi-slot air knives.

4.6.2 6.2. Wiping apparatus

The molten zinc temperature commonly employed in the industrial continuous galvanizing process is 733 K (460°C). A cold laboratory-scale model of the continuous galvanizing gas jet wiping process was designed and manufactured (Figure 4-6) with the objective of verifying the numerically modelled coating weights for the prototype multi-jet air knife.

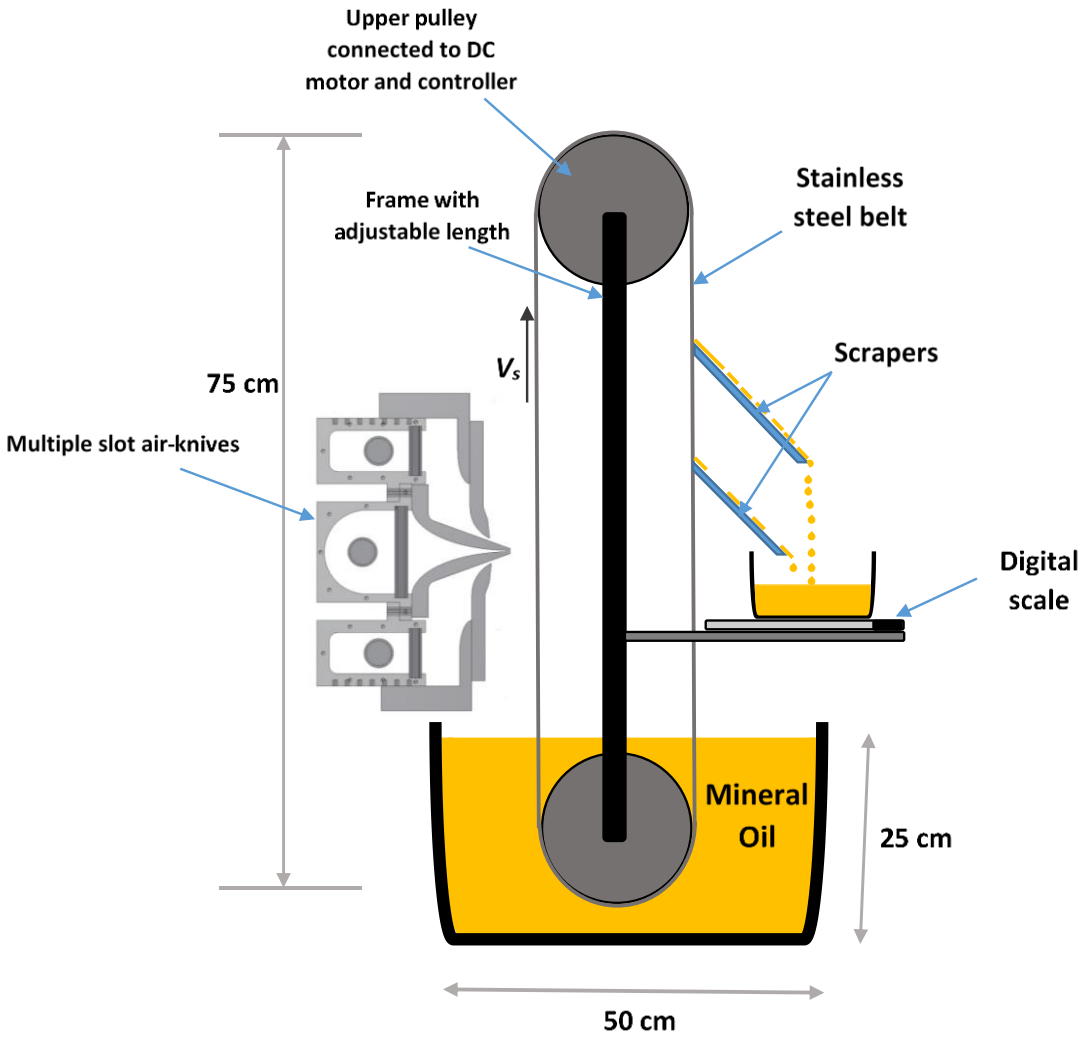

Figure 4-6) Schematic of the experimental multi-slot jet wiping apparatus.

The apparatus consists of a vertical stainless steel strip, 75 cm long and 5 cm wide, stretched between two rolls. An electric motor connected to the upper shaft and the upper roll provided the strip motion. The strip velocity was adjusted in the range of 0.5-3.5 m/s by means of an AC to DC speed controller connected to an electric motor. The strip velocity was measured by means of optical and mechanical tachometers with an accuracy of ± 0.05

m/s and a resolution of 0.1 rpm (for the test range of 2 to 999.9 rpm). The lower roll was designed to be adjustable to allow for the provision of adequate tension of the strip. The lower roll was immersed in the model working fluid, mineral oil, with density of 865 kg/m^3 and kinematic viscosity of 10 cSt. The gas jet wiping devices tested using this apparatus were the single and multi-slot air-knives shown schematically in Figure 4-5and discussed in the previous section. The multi-slot air knives were positioned 50 cm above the free surface of the liquid bath perpendicular to the strip. The air-knives were 5 cm longer than the strip width to avoid edge effects. The wiping mechanism was studied on one side of the strip only. To ensure good stability of the strip in the jet impingement region, the rear face of the strip slid on a rubber damper lubricated by the mineral oil liquid coating. The main jet to substrate distances and strip velocities used in the experiments were $8 \leq Z/D \leq 12$ and $0.25 \leq V_s \leq 1.5$ m/s.

After the substrate passed the wiping region, the liquid film was removed by two inclined rubber blades or “squeegees”. A digital balance with an accuracy of ±0.01 g measured the mass of the collected liquid while the collection period was measured by a chronometer. The mean liquid film thickness, h_f, was determined through the mass flow rate of liquid removed from the strip during the 300 s collection period using equation (4-16):

$$h_f = \dot{m}_{cl} / (\rho_{cl} L_s V_s) \tag{4-16}$$

Each experiment was repeated four times and the results reported are an average of these four experimental runs. According to Coleman and Steels [27], the overall uncertainty of a

dependent variable r (δr), which is function of j independently measured variables X_i can be found by using the Kline and McClintok method, given by:

$$\delta r = \sqrt{\sum_{i=1}^{j} \left(\theta_i \left(\delta X_i\right)\right)^2} \tag{4-17}$$

where $\theta_i = \frac{\partial r}{\partial X_i}$ and δX_i are the uncertainty for each measured variable. The uncertainty in the mean value of a measured X_i is given by $U_{X_i} = \sqrt{B_{X_i}^2 + P_{X_i}^2}$, where B is the instrumental bias error and P is the precision (random) error. The random error was calculated through the student t-distribution at the 95% confidence level and the instrumental bias error was determined through the manufacturers' specifications. Moreover, two additional sources of bias error were observed for the wiping apparatus depicted in Figure 4-6, namely: 1) inefficiency of the wiping scrapers in removing all the oil from the belt and 2) splashing of oil from the belt, largely at the belt upper roll turnover. The latter source of error was not observed for the lower strip velocities of V_S = 0.25 m/s and V_S =0.5 m/s. It was estimated that 1.8% of the mineral oil was left behind on the strip due to scraper inefficiency and the contribution of splashing was 3.2%-5.8% (depending on the strip velocity) to the discrepancy between the experimental measurements versus the analytical model.

4.7 Results and discussion

In order to assess the viability of the wiping apparatus (Figure 4-6), experimental measurements were first benchmarked against the analytical coating model of Thornton

and Graff [3] and the Elsaadawy et al. model [1] for a free meniscus coating and single gas jet wiping, respectively.

4.7.1 Free meniscus coating

An analytical solution for the free meniscus coating thickness can be determined by solving equations (1) – (5) and setting $dp/dx = 0$ as there is no gas jet acting on the liquid film[14].

Figure 4-7 presents a comparison of the free meniscus experimental data versus the analytical model of Thornton and Graff [3]. From this, it can be seen that the measured values of the free meniscus coating weight compare favorably with the corresponding predictions of the analytical model. It can be seen that there was a slight under-prediction in the experimental measurements versus the analytical model for $V_S \geq 0.75$ m/s. This discrepancy is attributed to two sources of bias error, discussed previously: 1) inefficiency of the wiping scrapers in removing all the oil from the belt and 2) splashing of oil from the belt, particularly at the belt turnover.

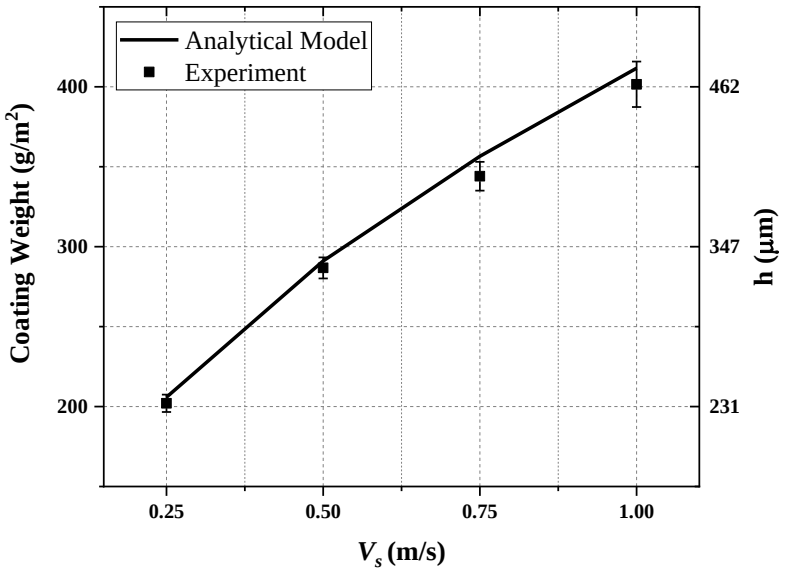

Figure 4-7) Comparison of experimental measurements of coating thickness for free meniscus coatings with the analytical model of Thornton and Graff [3].

4.7.2 Single jet wiping

Figure 4-8 compares the experimentally measured coating weights with the predictions of the Elsaadawy et al. [1] model for single slot gas jet wiping as a function of strip velocity (V_s) for Z/D = 12, Re = 9000 and Re = 11000. From Figure 4-8) , it can be seen that the predicted coating weight was, generally, in agreement with the experimental measurements for all strip velocities for a main jet Re = 9000. However, it can be seen that the measured final coating weight was slightly lower than the predicted values for Re = 11000, especially at higher strip velocities (V_S). This is due to the fact that splashing inevitably increased as the strip speed increased. Experiments were also run at a variety of strip-to-knife distances (Z/D) and strip speeds such that $8 \leq Z/D \leq 12$ and $0.25 \leq V_S \leq 1.5$ m/s, respectively, for Re = 9000 and Re = 11000. According to Gosset et al. [12], coating thickness for the single jet

wiping strongly depends on the nozzle to strip distance for Z/D ≥ 7. That's mainly because for Z/D ≤ 6, the potential core of the jet would impinge to the strip. For multi-slot jet wiping, the numerical investigation of Yahyaee et al. [23] also showed that for Z/D ≥ 8, a lighter coating weight can be achieved through the use of multi-slot jet. In the other hand, in the galvanizing industry, the upper *Z/D* ratio is usually limited to *Z/D* = 12; because for a given coating thickness, increasing *Z/D* results in increasing plenum pressure which causes industrial difficulties such as higher noise generation, splashing and coating non-uniformity [18]. In terms of strip velocity, Dubois [5] showed that the main reason leading to non-uniform coating was the high strip velocity of $V_s \geq 100$ m/min (~$V_s > 1.5$ m/s), when Z/D ≥ 7. In the other hand, lower line speeds ($V_s \leq 1$ (m/s)) in the galvanizing industry typically occurs for high temperature annealing or thick strip sheet [5].

The results of these experiments in comparison to the predictions of the Elsaadawy et al. [1] model are shown in Figure 4-9. It can be seen that for all *Z/D* and V_S explored, the measured coating weight values agreed with the predictions of the Elsaadawy et al. [1] model.

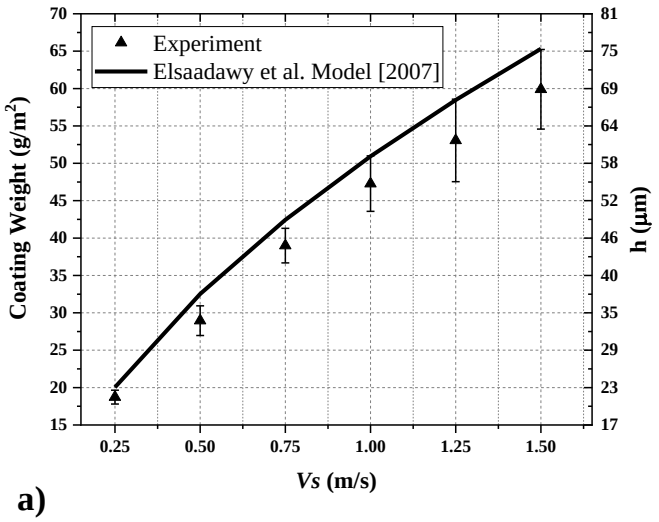

a)

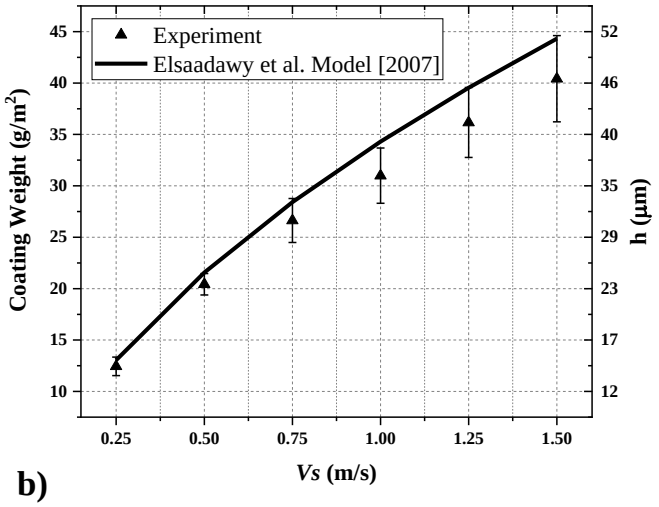

b)

Figure 4-8) Comparison of measured and predicted measurements for single jet wiping with the Elsaadawy et al [1] coating weight model for Z/D = 12, a) Re = 9000 b) Re = 11000.

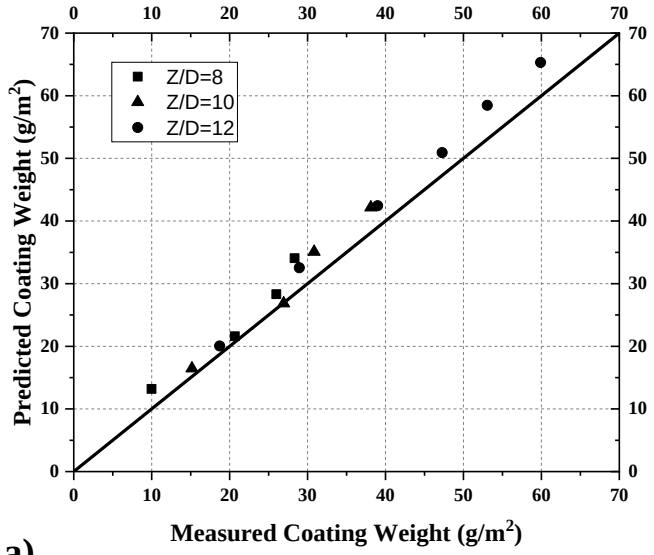

a)

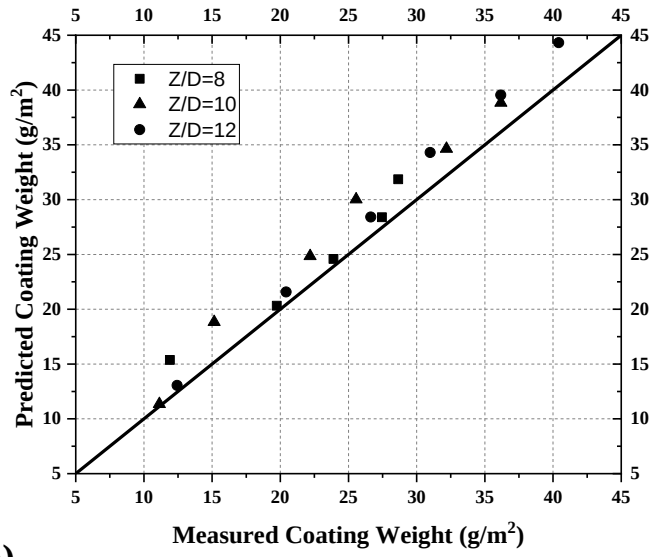

b)

Figure 4-9) Comparison of measured and predicted coating weights using the Elsaadawy et al. [1] model at $0.25 \leq V_s \leq 1.5$ m/s for $8 \leq Z/D \leq 12$, a) $Re = 9000$ and b) $Re = 11000$.

4.7.3 Multi-slot jet wiping

In this section, the multi-slot jet configuration, shown in Figure 4-5, was applied as the wiping actuator in the experimental setup and the effect of varying its geometry on the final coating thickness was determined. Figure 4-10 shows the experimental versus predicted final coating weight per Elsaadawy et al.[1] for different values of the auxiliary jet width, D_a, for a constant main jet Reynolds number of $Re_m = 11000$, auxiliary jet Reynolds number of $Re_a = 5000$, $D = 1.5$ mm and $Z/D = 12$. According to Figure 4-10, the predicted coating thickness using the Elsaadawy et al. model [1] agreed with the experimental measurements. It can be also seen that reducing the auxiliary jet width reduced the coating weight. This can be explained by studying the effect of the auxiliary jet width, D_a, on the pressure, pressure gradient (i.e. dp/dx) and shear stress profiles applied by the multi-slot air knife. It can be seen that the pressure profile (Figure 4-11) was broader and possessed a distinct shoulder for $D_a/D = 3$ versus the $D_a/D \leq 1$ pressure profiles. This sharper pressure distribution for $D_a/D \leq 1$ resulted in a greater wall pressure gradient and wall shear stress compared with the $D_a/D = 3$ case, as shown in Figure 4-12. Thus, lower coating weights can be achieved by decreasing the auxiliary jet width, D_a, such that $D_a/D \leq 1$. This can also be seen in Figure 4-13, where the predicted coating weights are enumerated as function D_a for strip velocities of $0.25 \leq V_s \leq 1.5$ m/s. It can be seen that, at each strip velocity, the multi-slot jets having $D_a/D \leq 1$ resulted in lower coating weights compared to the single slot jet configuration (i.e. $D_a/D = 0$).

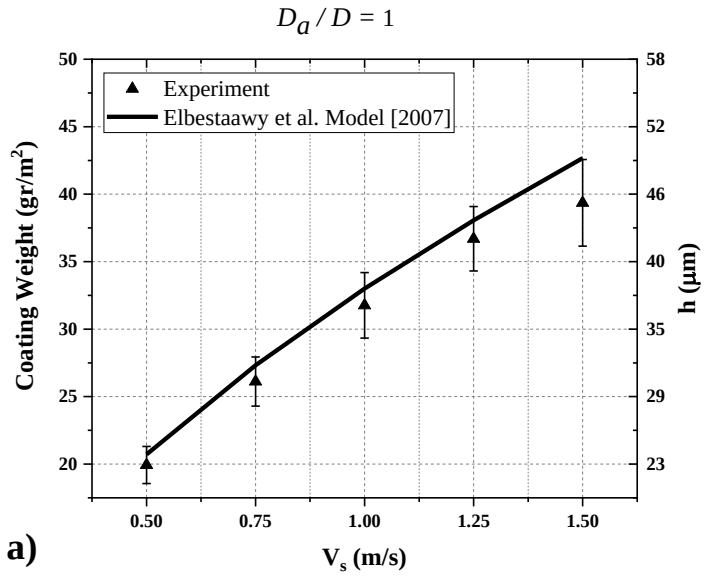
D_a / D = 1
Experiment
Elbestaawy et al. Model [2007]
Coating Weight (gr/m^2)
h (μm)
V_s (m/s)
50
45
40
35
30
25
20
58
52
46
40
35
29
23
0.50
0.75
1.00
1.25
1.50

a)

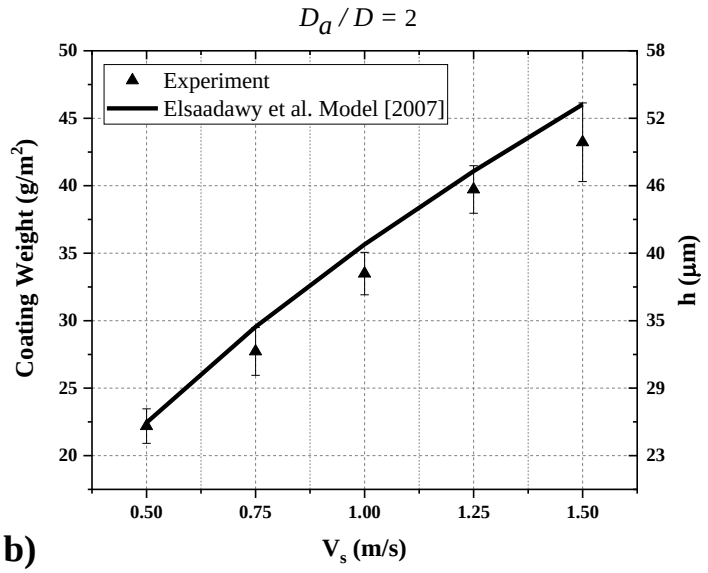
D_a / D = 2
Experiment
Elsaadawy et al. Model [2007]
Coating Weight (g/m^2)
h (μm)
V_s (m/s)
50
45
40
35
30
25
20
58
52
46
40
35
29
23
0.50
0.75
1.00
1.25
1.50

b)

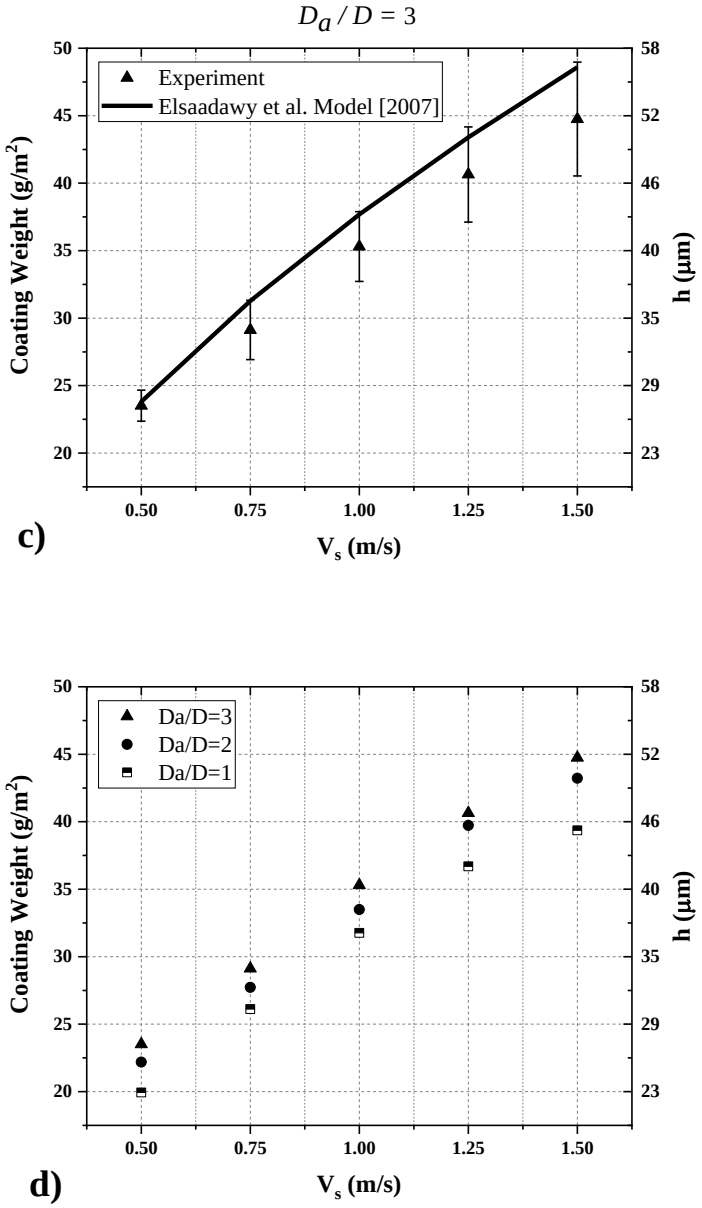

Figure 4-10) Comparison of experimental and predicted measurements using the Elsaadawy et al. [1] model for the multi-slot jet where Z/D = 12, Re_m = 11000, Re_a = 5000, D = 1.5 mm and s = 10 mm for a) D_a / D = 1, b) D_a / D = *2*, c) D_a / D = *3* and d) comparison of experimental measurements for $1 \leq D_a / D \leq 3$.

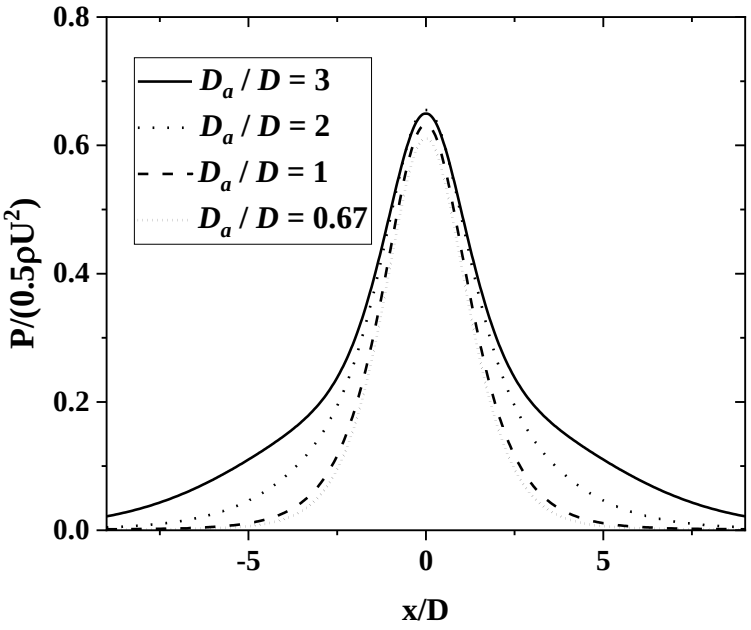

Figure 4-11) Non-dimensional wall pressure distribution for $0.67 \leq D_a/D \leq 3$ with Re_m = 11000, Re_a = 5000, Z/D = 12, D = 1.5 mm and s=10 mm.

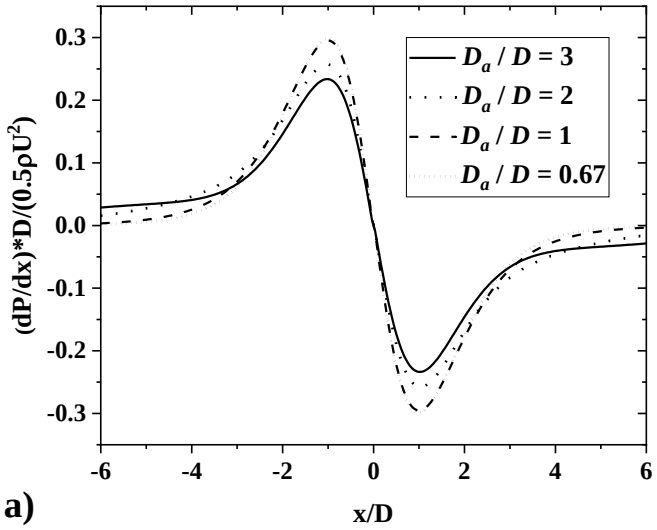

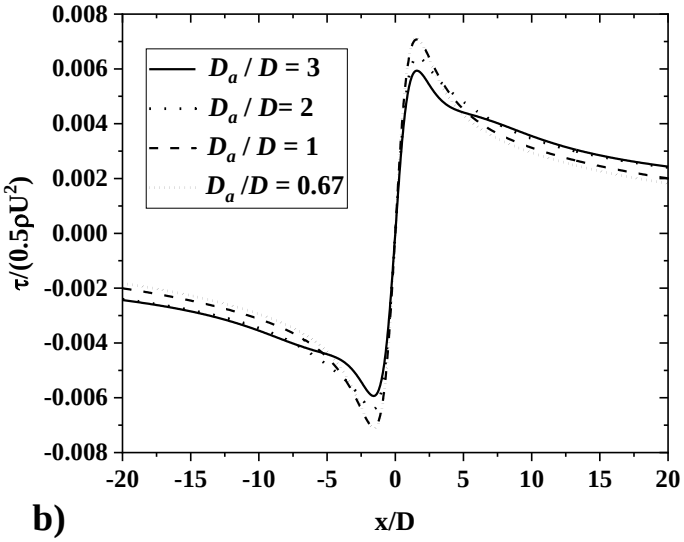

Figure 4-12) Non dimensional a) wall pressure gradient and b) wall shear stress for $0.67 \leq D_a/D \leq 3$, with $Re_m = 11000$, $Re_a = 5000$, $Z/D = 12$, $D = 1.5$ mm and $s = 10$ mm.

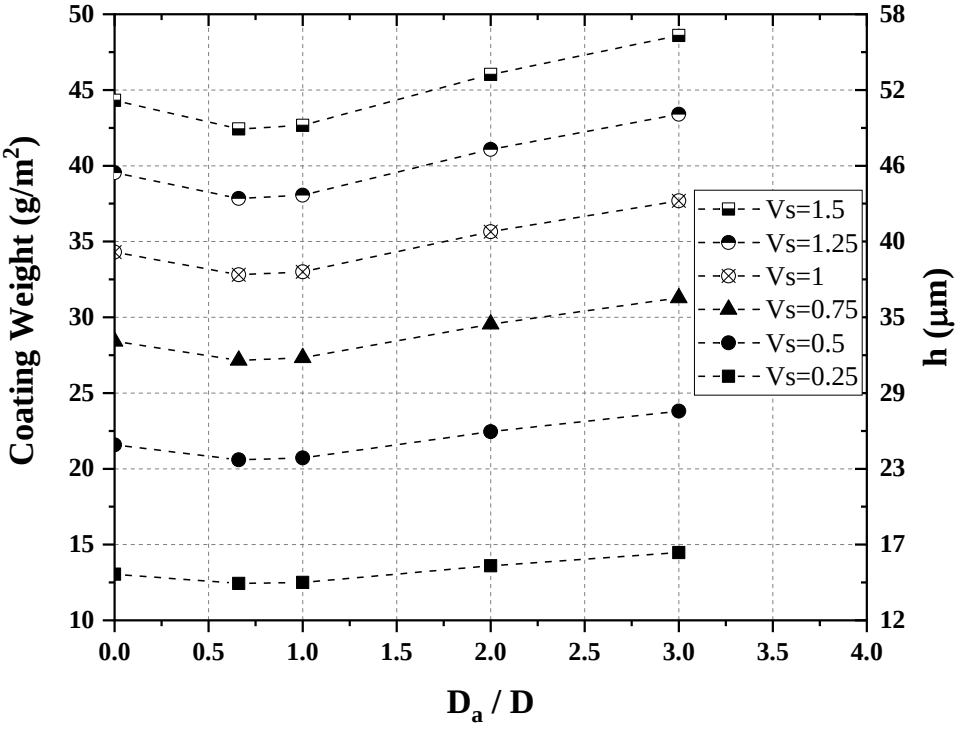

Figure 4-13) Effect of auxiliary jet width on final coating thickness as a function of strip velocity for Z/D = 12, Re_m = 11000, Re_a = 5000 and s = 10 mm.

The effect of auxiliary jet offset distance, s, on the final coating thickness was investigated for s = 10 mm and s = 0 mm for $D = D_a$ = 1.5 mm (i.e. D_a/D = 1), Re_m = 11000, Re_a = 5000 and Z/D = 12. Figure 4-14 provides the experimentally measured coating weights versus the predicted coating weights using the Elsaadawy et al. model [1]. It can be seen that the experimental coating weights agreed well with the predictions of the Elsaadawy et al. model [1] for all values of s explored. Figure 4-15 shows the compiled coating weight variations as a function of strip velocity for $0 \leq s \leq 10$ mm. From Figure 4-15, it can be seen that the final coating weight was not a significant function of the auxiliary jet offset, s, for $0 \leq s \leq 10$ mm. Comparison of the wall pressure gradient and wall

shear stress (Figure 4-16) also confirmed the negligible effect of changing the auxiliary jet offset on the resultant coating weight.

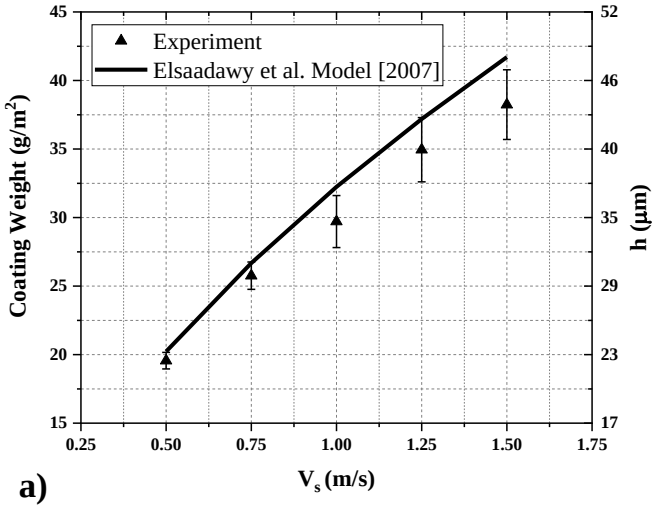

a)

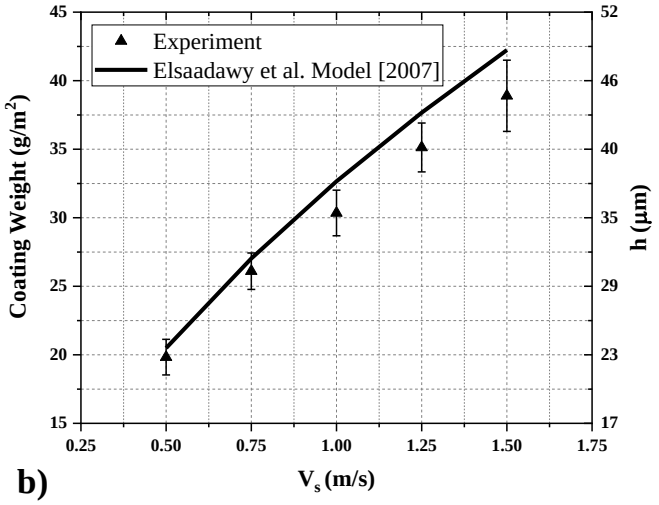

b)

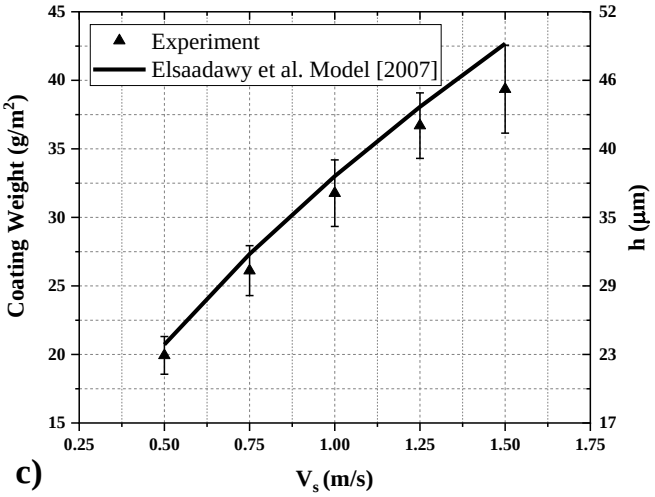

Figure 4-14) Comparison of coating weight model with experimental measurements for a) s = 0 mm, b) s = 5 mm c) s = 10 mm with Z/D = 12, Re_m = 11000, Re_a = 5000and D_a = 1.5 mm.

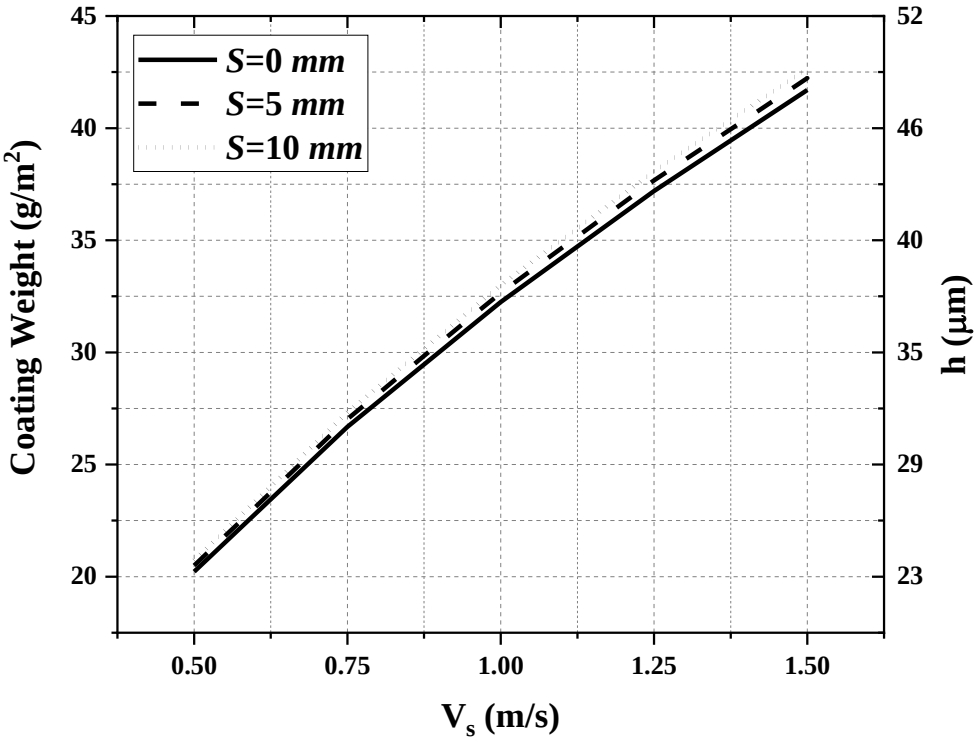

Figure 4-15) Effect of auxiliary jet offset, *s*, on the final coating thickness for different strip velocities where Z/*D* = 12, Re_m = 11000, Re_a = 5000 and *D* = D_a = 1.5 mm.

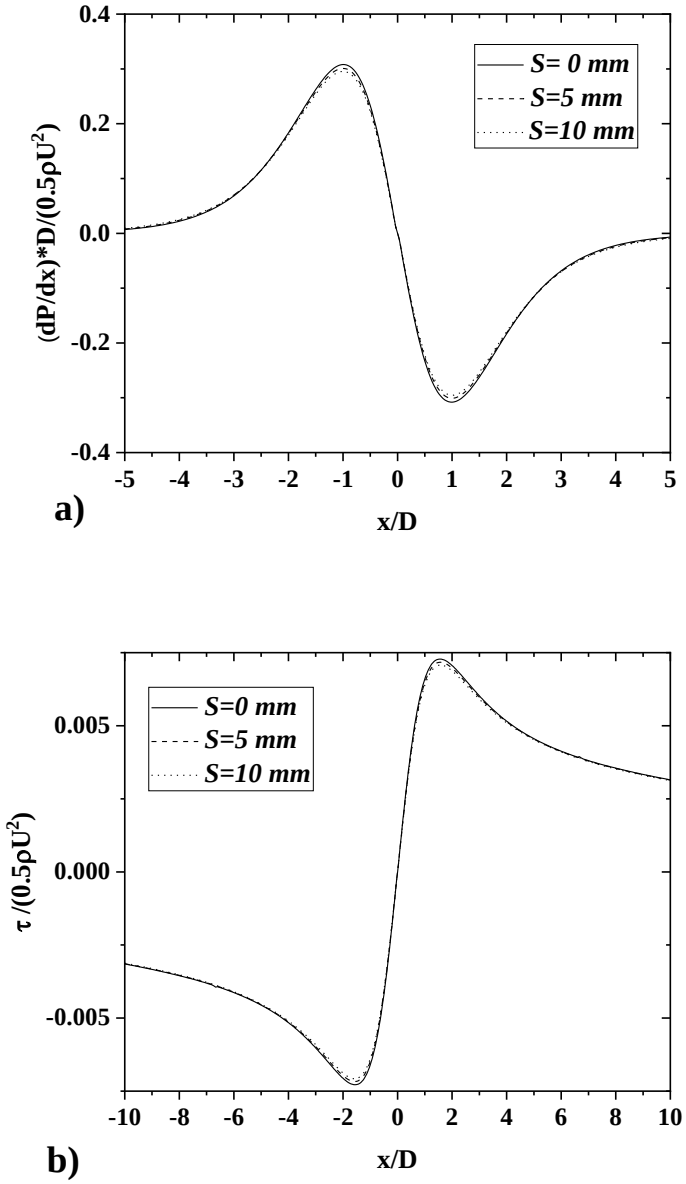

Figure 4-16) Non dimensional a) wall pressure gradient and b) wall shear distribution for different *s* with Re_m = 11000, Re_a = 5000, *Z/D* = 12 and D_a = 1.5 mm.

Figure 4-17 shows a comparison of the coating weights for the single jet and multi-slot jets as a function of strip velocity, V_s, with *Z/D = 12*, $D = D_a$= 1.5 mm (i.e. D / D_a = 1),

Re_m = 11000 and Re_a = 5000 held constant. According to Figure 4-17, by increasing the strip

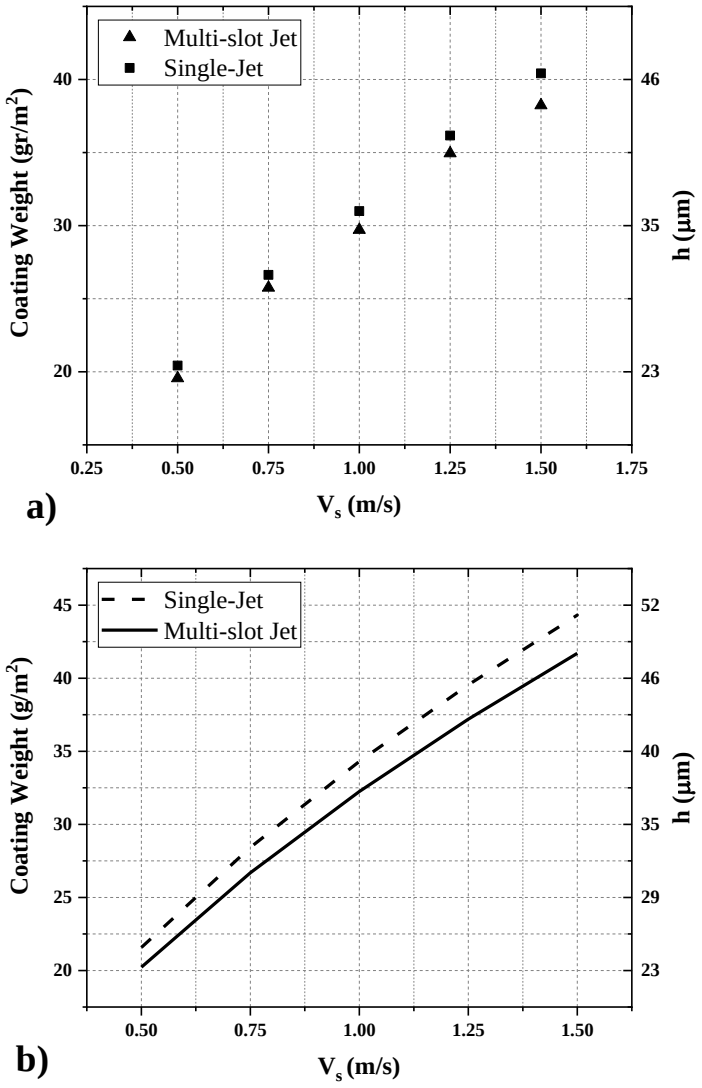

Figure 4-17) Comparison of a) experimentally measured and b) predicted final coating weight of single jet wiping with Re_m=11000, Z/D = 12 and D = 1.5 mm with the multi-slot jet wiping at different strip velocities with Re_m = 11000, Re_a = 5000, Z/D = 12 and D = D_a = 1.5 mm.

velocity, the coating weight increased significantly and it was shown that, for each strip velocity V_s, the predicted coating weight for this multi-slot air knife geometry was lower than the traditional single-slot jet configuration, with the largest difference being about 5.4% for V_s =1.5 *m/s*.

4.8 Conclusions

A novel configuration for a multi-slot air-knife, which can be effectively used in the continuous galvanizing gas jet wiping process, was investigated through experiments and computational fluid dynamics simulations. The experimental measurements of the final coating weights were compared with previously developed models for single gas jet wiping and free meniscus coating.

It was determined that the experimental coating weight measurements agreed with the predictions of the Ellen and Tu [3] and Elsaadawy et al. [1] models. Experiments were also conducted for different geometries of the multi-slot configuration and, in all cases, the experimental coating weight measurements agreed with the predicted values by the Elsaadawy et al. [1] model. It was observed that the final coating thickness was not sensitive to the auxiliary jet stand-off distance. However, the auxiliary jet width had a significant impact on the wall pressure gradient, the wall shear stress distribution and, consequently, on the final coating weight. Results showed that, for $D_a/D \leq 1$, the width of wall pressure distribution decreased while the maximum pressure remained constant. This resulted in higher values of the wall pressure gradient and shear stress in the vicinity of wiping zone and lower final coating thicknesses for the multi-slot air-knife versus the single-slot

geometry under the same operating conditions, particularly at higher strip velocities (with the highest difference of 5.4% at V_s = 1.5 m/s).

4.9 Acknowledgment

The authors gratefully acknowledge the financial contributions of the International Zinc Association Galvanized Autobody Partnership (IZA-GAP) members and the Natural Sciences and Engineering Research Council of Canada (NSERC, grant CRDPJ 446105-2012) to the success of this research.

4.10 References

[1] E.A. Elsaadawy, G.S. Hanumanth, A.K.S. Balthazaar, J.R. McDermid, A.N. Hrymak, and J.F. Forbes: Metall. Mater. Trans. B Process Metall. Mater. Process. Sci., 2007, vol. 38, pp. 413–24.

[2] A.R. Marder: Prog. Mater. Sci., 2000, vol. 45, pp. 191–271.

[3] J.A. Thornton and H.F. Graff: Metall. Trans. B, 1976, vol. 7, pp. 607–18.

[4] C.H. Ellen and C. V. Tu: J. Fluids Eng., 1983, vol. 106, pp. 399–404.

[5] M. Dubois: in Galvatech 2011 Conference Proceedings: HDG Process Technologies, Genova, 2011, pp. 1847–59.

[6] E.O. Tuck: Phys. Fluids, 1983, vol. 26, pp. 2352–8.

[7] H. Yoneda: Master of Applied Science Thesis , Uneversity of Minnesota, USA, 1993.

[8] C. V Tu and D.H. Wood: Exp. Therm. Fluid Sci., 1996, vol. 13, pp. 364–73.

[9] E.O. Tuck and J.-M. Vanden Broeck: AIChE J., 1984, vol. 30, pp. 808–11.

[10] C.V. Tu and D.H. Wood: Exp. Therm. Fluid Sci., 1996, vol. 13, pp. 364–73.

[11] A.N. Hrymak, E.A. Elsaadawy, G. Hanumanth, J.R. McDermid, and F.E. Goodwin: AISTech Proceedings, vol. II, 2005, pp. 393–401.

[12] A. Gosset, P. Rambaud, L. Castellano, M. Dubois, and J.M. Buchlin: in 6th European Coating Symposium, Bradford, United Kingdom, 2005.

[13] J.-R. Park: Ironnmaking Steelmak., 2001, vol. 28, pp. 53–7.

[14] D. Arthurs and S. Ziada: J. Can. Acoust. Assoc., 2007, vol. 35, pp. 28–9.

[15] K. Myrillas, A. Gosset, P. Rambaud, M. Anderhuber, J.M. Mataigne, and J.M. Buchlin: Chem. Eng. Process. Process Intensif., 2011, vol. 50, pp. 466–70.

[16] G.Y. Kim, H.D. Park, D.E. Lee, W.C. Chung, US 2010/0031879 A1: 2008.

[17] P. Tamadonfar, J.R. McDermid, A.N. Hrymak, and F.E. Goodwin: in AISTech - Iron and Steel Technology Conference Proceedings, Pittsburgh, 2010, pp. 517–25.

[18] P. Tamadonfar, J.R. McDermid, A.N. Hrymak, and F.E. Goodwin: in 8th International Conference of Zinc and Zinc Alloy Coated Steel Sheet (GalvaTech 2011), Genova, Italy, 2011.

[19] S. Alibeigi, J.R. McDermid, S. Ziada, and F.E. Goodwin: in Galvatech 2013: 9th International Conference on Zinc and Zinc Alloy Coated Steel Sheet & 2nd Asia-Pacific Galvanizing Conference, Beijing, 2013, pp. 437–40.

[20] D. Finnerty, J. McDermid, F. Goodwin, and S. Ziada: in Galvatech 2017: 11th International Conference on Zinc and Zinc Alloy Coated Steel Sheet, Tokyo, 2017, pp. 307–13.

[21] J.R. McDermid, D. Finnerty, S. Ziada, and F.E. Goodwin: in 109th Meeting of the Galvanizer's Association, Troy, MI, 2017.

[22] D. Arthurs and S. Ziada: J. Fluids Struct., 2012, vol. 34, pp. 236–58.

[23] A. Yahyaee Soufiani, J.R. McDermid, A.N. Hrymak, and F.E. Goodwin: J. Coatings Technol. Res., 2017, vol. 14, pp. 1015–28.

[24] A. Ritcey, J.R. McDermid, and S. Ziada: in ICFMFA 2015 : 17th International Conference on Fluid Mechanics and Flow Analysis, 2015.

[25] S. Alibeigi: Master of Applied Science Thesis, McMaster University, McMaster University, Canada, 2013.

[26] F. M.White: Fluid Mechanics, fourth ed., McGraw-Hill, Boston, 2003, 866.

[27] H.W. Coleman and W.G. Steele: Experimentation and Uncertainity Analysis for Engineers, Second ed., JOHN WILEY & SONS, INC., New York, 1999, 271.

Chapter 5: A Parametric Study of a Multi-Slot Air Knife for Coating Thickness Reduction

Ali Yahaee Soufiani, Joseph R. McDermid, Andrew N. Hrymak, Frank E. Goodwin, This chapter has been submitted to journal of The Iron and Steel Institute of Japan (ISIJ) International. The following Chapter is the as-submitted version of the article.

In this paper, all the experimental measurements and numerical simulations were carried out by me under supervision of Dr. McDermid and Dr. Hrymak. The manuscript was initially drafted by me and reviewed to the final version by Dr. McDermid and Dr. Hrymak. Dr. Goodwin was included as an author in this paper as a courtesy for his provision of industrial sponsorship.

5.1 Abstract

This paper presents an investigation of the gas jet wiping process, which is used in the continuous galvanizing line (CGL) to control the Zn-alloy coating thickness on steel substrates. In this study, a novel configuration of a multi-slot air knife was used as the wiping actuator in a parametric study of the gas jet wiping process. The main goal of the study was to identify the operating window in which lighter coating weights can be achieved with the multi-slot air knife at higher strip velocities. A laboratory scale wiping apparatus was designed and manufactured and the effects of various operating conditions, such as: main jet Reynolds number (Re_m), auxiliary jet Reynolds number (Re_a) and jet-to-substrate distance (Z/D) on the final coating thickness were determined experimentally. Numerical simulations of multi-slot jet wiping were also performed under the same operating conditions using computational fluid dynamics to estimate the pressure and shear stress profiles along with analytical models of the coating thickness to compare with the experimental measurements.

It was observed that the experimental measurements, under different operating conditions for the multi-slot air-knives, agreed with the coating weight predictions of analytical models available from the literature. The results showed that the coating weight produced by the multi-slot air knife, with a relatively low flow for the auxiliary jet (i.e. $Re_a/Re_m \leq 0.5$), was lower than the final coating weight under similar main jet Re from a single slot nozzle. Conversely, when $Re_a/Re_m \sim 1$, the width of the pressure distribution increased, thereby decreasing the pressure gradient distribution found in the vicinity of the

wiping region and, consequently, increased the coating thickness versus that predicted for the single slot geometry.

5.2 Nomenclature

c	Speed of sound (m/s)	Q	Non-dimensional withdrawal flux
D	Main jet width (m)	R	Universal gas constant (J/mol.K)
D_a	Auxiliary jet width (m)	Re	Jet Reynolds number ($\mathrm{Re} = \frac{\rho u D}{\mu}$)
g	Gravitational acceleration (m/s^2)	S	Non-dimensional shear stress
G	Non-dimensional pressure gradient	s	Auxiliary jet offset distance (m)
h_f	Final film thickness (m)	T	Temperature (K)
h	Local film thickness (m)	U	Fluid velocity (m/s)
h_o	Free meniscus film coating (m)	V_s	Strip velocity (m/s)
h_m	Final film thickness of multi-slot jet (m)	We	Weber number ($We = \frac{\rho_{cl} u_{cl}^2 h_f}{\sigma}$)
h_m	Final film thickness of single jet (m)	Z	Main jet exit to wall distance (m)
H	Non-dimensional film thickness	μ	Fluid dynamic viscosity (kg/m.s)
L	Computational domain length (m)	μ_t	Turbulent viscosity (kg/m.s)
L_s	Strip width (m)	ρ_{cl}	Coating liquid density (kg/m^3)
$\dot{m}$	Mass flow rate of removed oil (kg/s)	γ	Ratio of specific heats of air
P	Static pressure (Pa)	τ	Shear stress (Pa)
P_s	Nozzle static pressure (Pa)	ρ	Density of gas (kg/m^3)
P_∞	Ambient pressure (Pa)	ρ_{cl}	Density of coating liquid (kg/m^3)
q	Withdrawal flux (m^2/s)	σ	Surface tension (N/m)
q_a	Air volume flow rate (m^3/s)		

5.3 Introduction

In the steel manufacturing industry, ferrous substrates are protected against corrosion by applying a sacrificial layer of zinc to the steel surface through continuous hot dip galvanizing. In this process, the substrate is continuously immersed in a bath of molten zinc at 460°C [1] and, when it is withdrawn from the bath, the strip will be covered with a relatively thick liquid film. In order to reduce the coating thickness of the film to the target thickness, a pair of impinging slot gas jets (or air knives) are located above the bath to remove the excess zinc from the steel strip (Figure 5-1). The pressure gradient (*dp/dx*) and shear stress (τ) applied to the liquid film by the gas jets controls the final film thickness above the air knife, and most of the liquid returns to the bath as a runback flow. The gas jet wiping process leads to a relatively thin coating thickness – typically on the order of 10 – 20 μm in the case of automotive applications – with a relatively smooth surface. The final coating thickness, h_f ,depends on the steel strip velocity (V_s), wiping pressure (P_s), nozzle exit to strip standoff distance (Z), the nozzle slot width (D) and liquid properties such as density (ρ_{cL}) and viscosity (μ) [2-4].

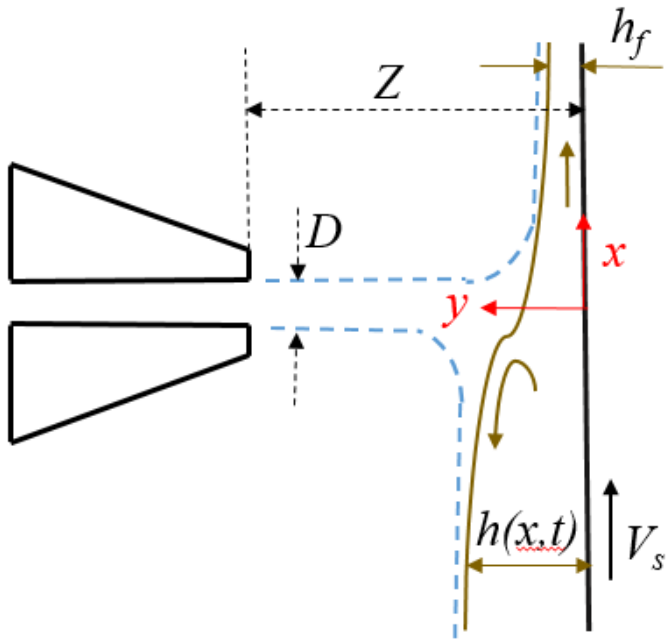

Figure 5-1) Schematic of the gas jet wiping process.

Thin steel sheet products are generally used by the automotive industry for either structural members or closure panels. A recent trend within the automotive industry has been to reduce the zinc coating weight applied to the thin sheets as part of industry efforts to reduce the overall mass of the body-in-white and reduce costs [5]. Currently, a single slot air knife configuration is commonly used as the wiping actuator in continuous galvanizing lines (CGLs) for controlling the film coating thickness. There are numerous experimental and numerical studies available in the literature to model and characterize the wiping ability of the conventional single slot impinging jet ([2-4], [6-8]). The wiping pressure must be increased significantly to obtain lower coating weights using the single slot air knife at reasonable strip velocities. However, increasing the pressure can cause some industrial difficulties such as higher tonal noise generation [9,10], splashing [11] and

coating non-uniformity [5]. Currently, to cope with such problems, the steel strip velocity is limited to lower values in the CGL, which can adversely affects CGL productivity and costs.

As an alternative approach, the multi-slot air knife has been recently investigated as the wiping actuator in the CGL instead of the traditional single slot jet. In order to modify the final coating quality and stabilize the substrate to lessen lateral vibrations between the jets, Tu [12] filed a patent and proposed a variety of new air knife designs with dual nozzles for application in the CGL. In all instances, the apparatus comprised a primary stripping jet for wiping and an adjacent smoothing jet. In this patent, the smoothing jet stream impinged on the coating at a low pressures sufficient to smooth the coating whereas the stripping jet impinged at higher pressures sufficient to reduce the thickness of the smoothed layer to a desired target thickness.

Two of the proposed configurations, a main jet with an inclined auxiliary impinging slot jet and two parallel impinging slot jets [12], were studied numerically by Tamadonfar et al. [13]. The maximum wall pressure gradient and shear stress distribution profiles were obtained for these two configurations. These were then implemented in the coating model developed by Elsaadawy et al. [14] in order to calculate the final coating thickness. Tamadonfar et al.'s numerical results [13] did not show any advantage in using these novel configurations over the single slot air knife in term of coating thickness reduction.

Kim et al. [15] subsequently proposed an innovative multi-slot jet design for application in the CGL to address the splashing problem and reduce surface irregularities due to jet fluctuations. The proposed air knife consisted of one main jet and four symmetrically

situated, inclined auxiliary jets discharging air at lower velocities versus the main slot jet. The intent of the patent claim was that, in the proposed multi-slot design, the gas discharged from the main and auxiliary jets provided the necessary force for wiping excess molten zinc from the sheet, where the auxiliary jets were used to prevent splashing by mixing the gas streams of the main jet and auxiliary jets, resulting in a lower speed of the jet wall along the length direction of the substrate.

Tamadonfar et al. [16] subsequently numerically simulated a multi-slot jet composed of a main jet and two symmetrically situated auxiliary jets adjacent to the main jet. The range of simulated flow conditions in the studies of Tamadonfar et al. [16] were limited to one slot jet gap, and one main and auxiliary jet Reynolds number (Re = 11000). In this case, no significant benefits with respect to coating weight reduction were realized as this configuration decreased both the maximum pressure gradient and maximum wall shear stress applied to the coating.

Alibeigi et al. [17] experimentally investigated the wall pressure distribution of the multi-slot jet configuration of Tamadonfar et al. [16] under wider variety of operating conditions (Re_m, Re_a, Z/D) and compared the results with the numerical simulations of Tamadonfar et al. ([13],[16]), where appropriate. The comparison showed some disagreements on the maximum wall pressure and pressure distribution between the two studies. The simulated stagnation pressure was higher than the experimentally derived value and the simulated maximum pressure gradient was also higher than the experimental result.

Finnerty et al. [18], experimentally studied the effect of auxiliary jets on tonal noise reduction originating from aeroacoustics feedback using the multi-slot air knife geometry of Alibeigi et al. [17]. In this study, the main jet velocity was held at 250 *m/s* for all experiments and auxiliary jet flows were varied between zero and 60 *m/s* in 20 *m/s* intervals. The authors showed that the prototype multi-slot air knife was able to decrease the magnitude of the tonal noise to the point of near complete suppression when the auxiliary jet velocity was set at 0.25 V_m or greater [18]. They also showed that the auxiliary jets also introduced broadband noise at low frequencies which was not of sufficient magnitude to present a hazard to CGL workers.

Yahyaee Soufiani et al. [19] investigated the fluid flow of the prototype multi-slot jet configuration of Alibeigi et al. [17] discharging air on a moving substrate. Computational fluid dynamics were applied to predict the wall pressure and wall shear stress distributions of the multi-slot air knife, and the results were then used in the analytical model of Elsaadawy et al. [14] to estimate the final liquid zinc thickness on the substrate. Takeda et al. [20] also investigated the gas wiping process using a three-slot air knife. This study focused on the mixing process of the jets and the distribution of the impinging pressure of the mixed jet. Both studies determined that, at high auxiliary jet velocities, the impinging pressure gradient became more moderate and the wiping performance deteriorated. However, the wall pressure gradient for the Alibeigi et al. [17] multi-slot nozzle using low auxiliary jet velocities (35% of the main jet velocity) increased and made it possible to reduce the coating weight versus the single slot jet configuration ([19],[20]). A similar trend

was reported for the shear stress distribution in the wiping region with lower auxiliary jet velocities which reduced the final coating thickness ([19], [20]).

More recently, Yahyaee Soufiani et al. [21] experimentally investigated the applicability of the Elsaadawy et al. [14] analytical coating weight model for wiping via the multi-slot jet geometry and examined the effects of the multi-jet geometry process variables on the final coating thickness. The experimental measurements, under different knife geometries and process conditions, agreed with the coating weight predictions of the analytical model of Elsaadawy et al [14]. Under the investigated operating conditions, it was determined that decreasing the auxiliary jet width such that $D_a/D \leq 1$ and operating the auxiliary and main jets such that $Re_a/Re_m \sim 0.5$, increased the pressure gradient through providing a higher pressure gradient while the maximum pressure remained constant and resulted in a lower final coating thicknesses for the multi-slot air knife wiping versus the single slot geometry.

As mentioned above, the multi-slot jet proposed by Alibeigi et al. [17] has been shown to be a promising design alternative to overcome some of the limitations of the single slot air knife. However, the effect of operating conditions for the proposed multi-slot jet air knife on final coating thickness have not been determined. The current research focuses on determining the effect of the operating conditions of the multi-slot jet on the final coating weight. In this study, the conventional single slot jet geometry was used as a base case for comparing the coating weight data on a moving substrate with those obtained using the multi-slot air knife configuration.

5.4 Film thickness model

The final film thickness can be predicted based on lubrication theory, in which the inertia term in the momentum equation is assumed negligible compared to pressure, gravity and viscosity [2]. The Navier-Stokes equation can be then further simplified based on the following assumptions:

The coating flow can be assumed to be incompressible, steady state and with constant viscosity ([2], [3]). The effects of oxidation, surface tension and surface roughness are also assumed to be negligible [1] and the no-slip condition for the liquid on the steel strip is assumed applicable. The simplified momentum equation, as a result, balances viscous forces with pressure and gravity forces (equation 5-1)

$$\mu\frac{\partial^2 u}{\partial y^2}-\left(\rho g+\frac{dp}{dx}\right)=0 \tag{5-1}$$

By applying the no slip condition at the strip and the jet shear stress at the liquid surface as the boundary conditions, the velocity profile of the coating liquid can be written as:

$$u=\frac{1}{2}\frac{\rho g}{\mu}y^2-\frac{\rho g h}{\mu}y+V_s \tag{5-2}$$

By introducing the non-dimensional film thickness $\left(H=h\sqrt{\frac{\rho g}{\mu V_S}}\right)$, non-dimensional shear stress, $\left(S=\frac{\tau}{\sqrt{\rho\mu V_S g}}\right)$, and non-dimensional pressure gradient, $\left(G=1+\frac{1}{\rho g}\frac{dp}{dx}\right)$, the non-dimensional liquid volumetric flux, *Q*, can be derived as [19]:

$$Q=-\frac{GH^3}{3}+\frac{SH^2}{2}+H \tag{5-3}$$

The non-dimensional film thickness, *H*, corresponding to the maximum withdrawal flux $(Q_{\max})$ can be determined by setting $\frac{dQ}{dH}=0$ and employing the quadratic formula [6] to solve for *H*, such that:

$$H=\frac{S\pm\sqrt{S^2+4G}}{2G} \tag{5-4}$$

Upon solidification of the coating liquid, the film velocity is equal to the substrate velocity (V_s) and the final coating thickness, h_f, is given by:

$$h_f=\frac{q}{V_S}=\frac{Q_{\max}}{\sqrt{\frac{\rho g}{\mu V_S}}} \tag{5-5}$$

The shear stress distribution and pressure gradient along the wall can be used with equations (5-4) and (5-5) to estimate the final coating thickness on a moving substrate. In the present work, the pressure gradient and shear stress distributions induced in a static wall by a conventional single-slot and the prototype multi-slot air knife designs were predicted through numerical simulations. The predicted final coating thickness was then compared with experimental measurements, to be described in section 5-6.

5.5 Numerical modeling

For determination of the air flow through the slot jets, the Reynolds-Averaged Navier-Stokes (RANS) equations (equations (5-6) and (5-7)) were used with the pressure-based solver and the SIMPLE method for pressure-velocity coupling.

$$\frac{\partial\left(\rho\overline{u}_i\right)}{\partial x_i}=0 \tag{5-6}$$

$$\frac{\partial\rho\overline{u}_i\overline{u}_j}{\partial x_i}=-\frac{\partial p}{\partial x_i}+\frac{\partial}{\partial x_i}\left[\mu\left(\frac{\partial\overline{u}_i}{\partial x_j}+\frac{\partial\overline{u}_j}{\partial x_i}\right)-\rho\overline{u_i'u_j'}\right] \tag{5-7}$$

The Reynolds stress $-\rho\overline{u_i'u_j'}$ was modeled using the Boussinesq hypothesis, and the two-equation model for the standard k-ε model was used to determine the turbulent viscosity, μ_t .The discretized equations were iterated until the root-mean-square (RMS) residuals for all governing equations were less than 10^{-6}.

Schematics of the single and multi-slot nozzle geometries used are illustrated in Figure 5-2. In order to validate the numerical modelling results with the experimental measurements of Tu and Wood [7] and the previous multi-slot jet experiments of Alibeigi et al. [17], the following geometric parameters were fixed: auxiliary jet width (D_a) at 3 mm, the distance between the exit of the main and auxiliary jets (s) at 20 mm, and the main jet slot width (D) at 1.5mm. The inclination of the auxiliary jets relative to the main jet centerline was 20°. The boundary conditions were the no slip condition at the impingement surface and nozzle walls, a pressure inlet at the nozzle inlets and a pressure outlet at the exit of the computational domain. The inlet pressure (P_s), was used to estimate the flow velocity of the jet exiting the nozzle using equation (5-8) [22].

$$U=c\sqrt{\frac{2}{\gamma-1}\left[\left(\frac{P_s+P_\infty}{P_\infty}\right)^{\gamma-1/\gamma}-1\right]} \tag{5-8}$$

Where P_∞ is the ambient pressure, γ is the ratio of specific heats of air and c is the speed of sound (343 m/s).

The mesh used for the impinging jets was comprised of a mixture of quadrilaterals and triangles. Grid clustering was used adjacent to the wall and around the jet centerline, where large gradients in the velocity field, pressure field and turbulent parameters were expected. Four grids with 252,000 to 393,000 nodal points, depending on the nozzle plate-to-main jet width (*Z/D*, Figure 5-2) ratio [19], were tested to verify the mesh independence of the numerical results. In the near wall region, the mesh was refined such that the first node was located in the viscous sub-layer (y+∼1) and the mesh size near the wall was approximately 4 µm. The computational domain size was defined as $-85 \leq X/D \leq +85$.

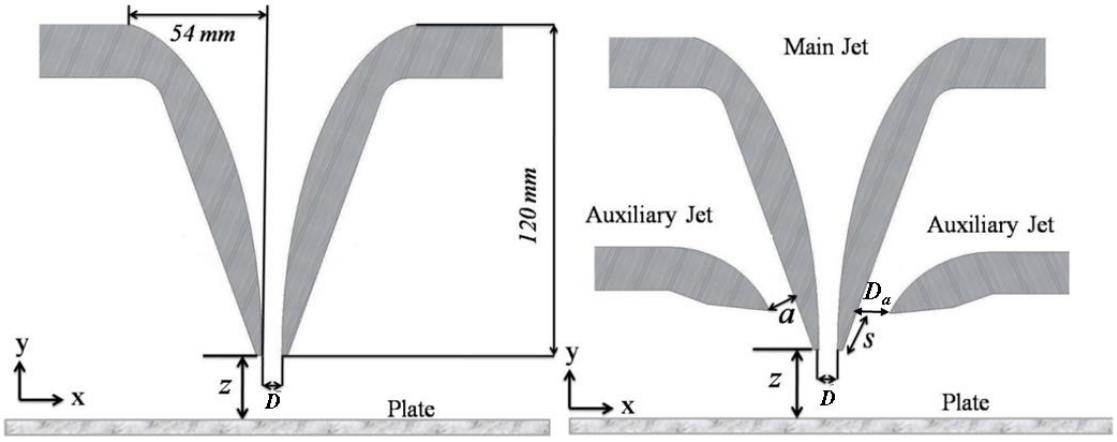

Figure 5-2) Schematic of the single-slot (left) and multi-slot air knife (right) with definitions for the jet geometric parameters.

Numerical simulations were benchmarked against experimental wall pressure distribution for different wall to jet ratios ($4 \leq Z\,D \leq 12$) at $Re_m = 11000$. Figure 5-3 presents

a comparison of numerical non-dimensional wall pressure profiles versus the experimental data of Tu and Wood [7] for a single-slot planar impinging jet as function of *Z/D*. It can be seen that the predicted pressure distributions were in good agreement with the experimental data. Figure 5-4 shows a comparison of the numerical wall pressure profile versus the experimental data of Alibeigi et al. [17] for a the multi-slot impinging jet where $Re_m = Re_a$ = 11000. From Figure 5-4, it can be seen that the numerical models of the multi-slot jet geometry also agreed with the experimental measurements.

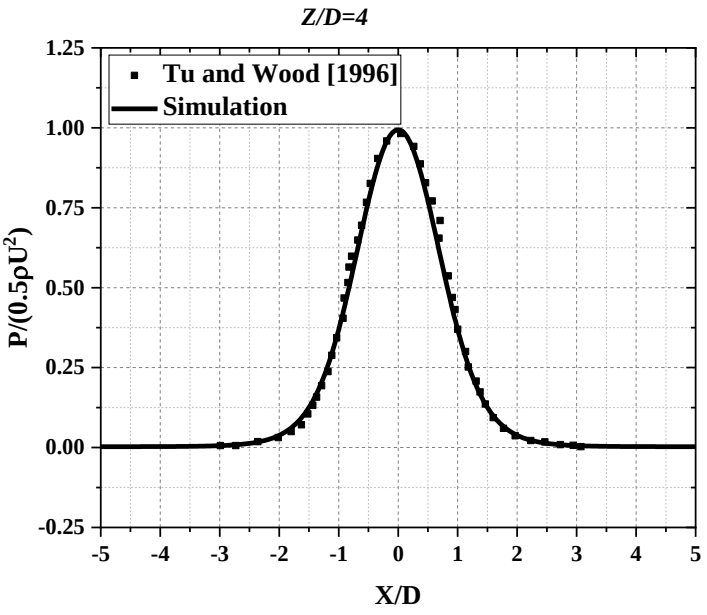

a)

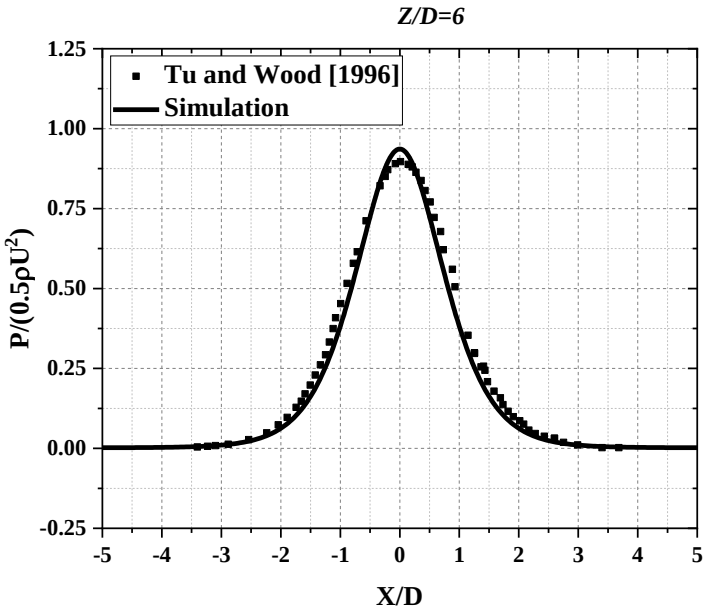
Z/D=6
Tu and Wood [1996]
Simulation
P/(0.5ρU²)
X/D
1.25
1.00
0.75
0.50
0.25
0.00
-0.25
-5
-4
-3
-2
-1
0
1
2
3
4
5

b)

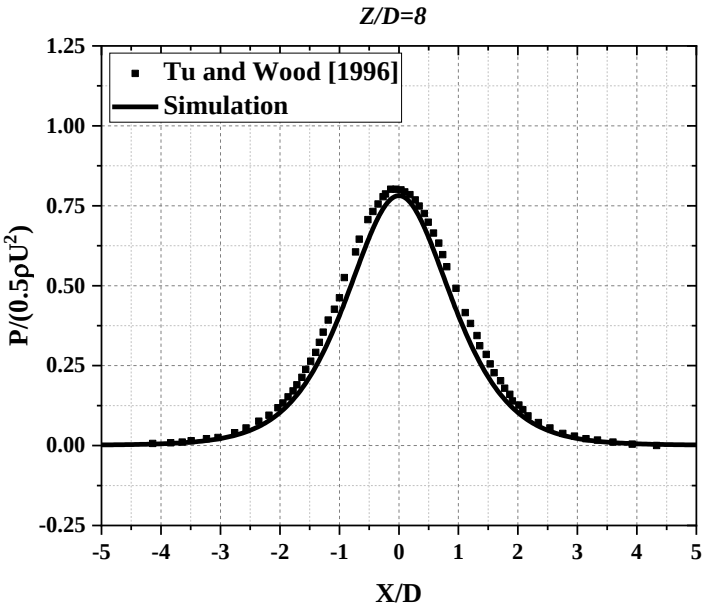
Z/D=8
Tu and Wood [1996]
Simulation
P/(0.5ρU²)
X/D
1.25
1.00
0.75
0.50
0.25
0.00
-0.25
-5
-4
-3
-2
-1
0
1
2
3
4
5

c)

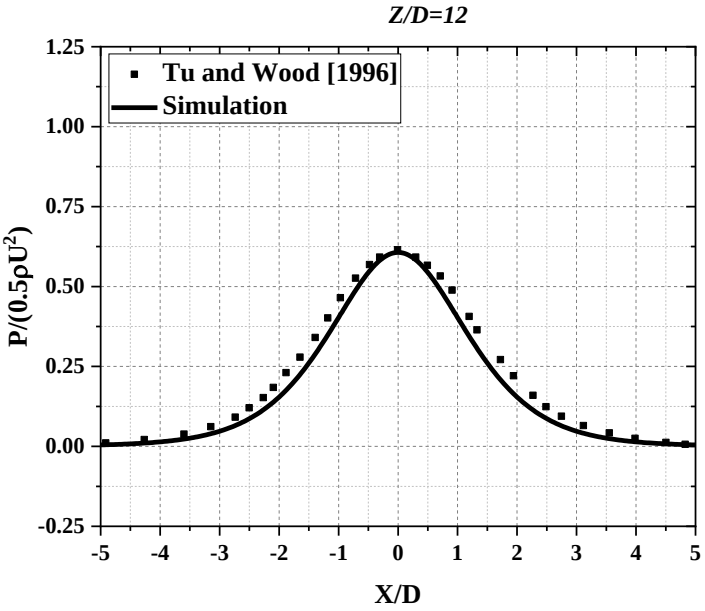

d)

Figure 5-3) Comparison of numerical non-dimensional wall pressure profiles at Re = 11000 and $4 \leq Z/D \leq 12$ with the experimental measurements of Tu and Wood [7].

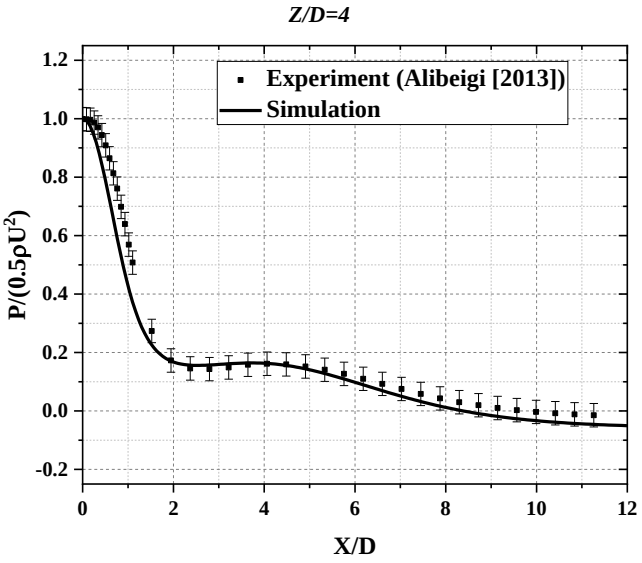

a)

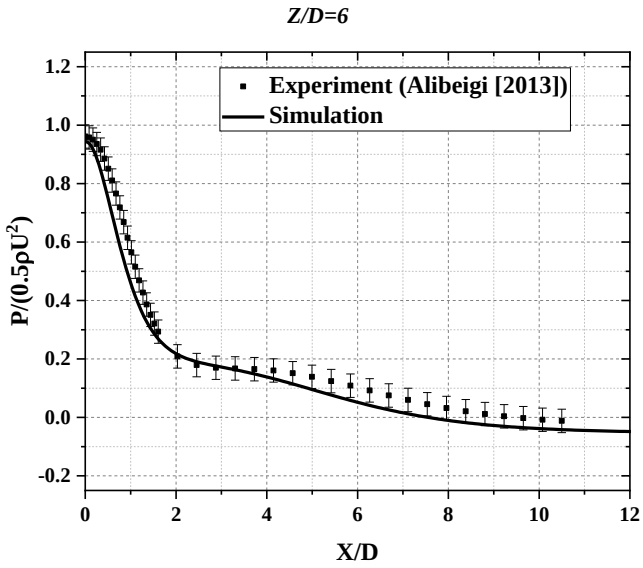
Z/D=6
Experiment (Alibeigi [2013])
Simulation
P/(0.5ρU²)
X/D
1.2
1.0
0.8
0.6
0.4
0.2
0.0
-0.2
0
2
4
6
8
10
12

b)

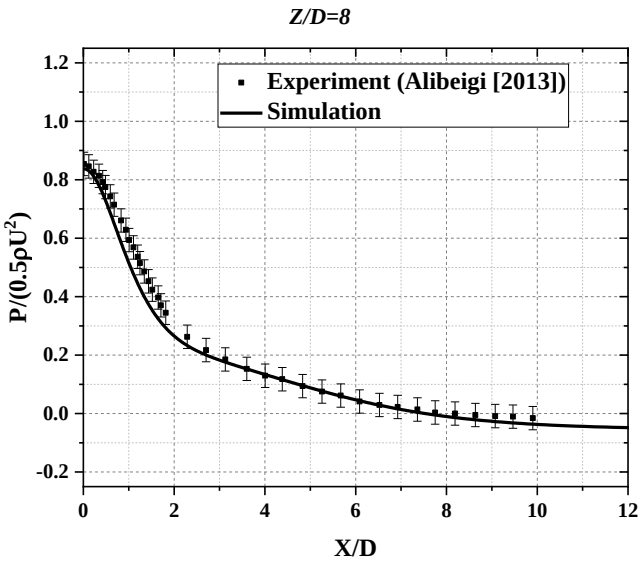
Z/D=8
Experiment (Alibeigi [2013])
Simulation
P/(0.5ρU²)
X/D
1.2
1.0
0.8
0.6
0.4
0.2
0.0
-0.2
0
2
4
6
8
10
12

c)

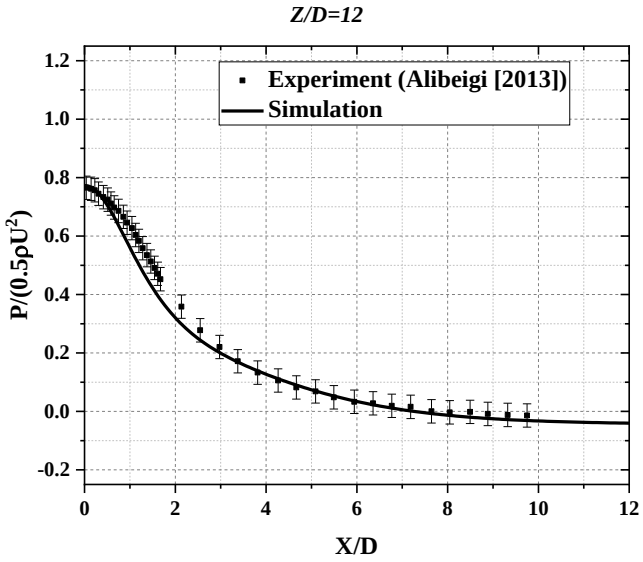

d)

Figure 5-4) Comparison of numerical wall pressure distributions with experimental measurements of Alibeigi [17] for multi-slot air knife at Re_m = 11000, Re_a = 11000 and 4 ≤ Z/D ≤ 12.

5.6 Experimental facility

A schematic of the prototype multi-slot air knife used in the experimental measurements is presented in Figure 5-5. The multi-slot air knife consists of three jets, one main jet and two auxiliary jets symmetrically located on each side of the main jet. The main jet was situated perpendicular to the moving strip and the auxiliary jets were inclined at 20° from the main jet centerline. The prototype multi-slot air knife had three separate chambers and each had an individual plenum and valve to allow independent control of the plenum pressure of each nozzle. Compressed air from a 550 kPa blower was used to feed the auxiliary jets and the main nozzle was supplied with a resident 550 kPa compressed air line. For the main jet, air was passed through a regulator and two filters to prevent any particulates entering the main nozzle. An electric valve was also used immediately after the filter to adjust the main jet pressure. In the case of the auxiliary jets, the air supply was passed through a 5 cm regulator valve, a 5 cm ball valve and a 5 cm gate valve prior to entering a T manifold, where three 2.5 cm globe valves were used to adjust the pressure for each of the auxiliary nozzles. For all of the nozzles, air entered each plenum *via* a 25.4 mm diameter pipe at the top of the plenum, passed through a flow distributor tube (Figure 5-5) and then passed through a series of mesh screens located upstream of the nozzle contraction in order to break up any large-scale turbulent structures (Figure 5-5), where the screens comprised stainless steel cloth with a density of 28 wires/cm. Finally, the air exited the nozzle at 90° to its inlet direction. To adjust the distance between the nozzle and the plate – i.e. the Z/D ratio – the prototype multi-slot air knife was mounted on a computer controlled traverse system consisting of a VXM-3 Velmex™ power supply with a Slo-syn

stepper motor with a minimum step division of 5 μm. Validyne DP-15 pressure transducers were used to measure the plenum pressure upstream of each jet centerline and prior to the nozzle contraction (Figure 5-5) and the data logged using a conventional data acquisition system and a LabVIEW program.

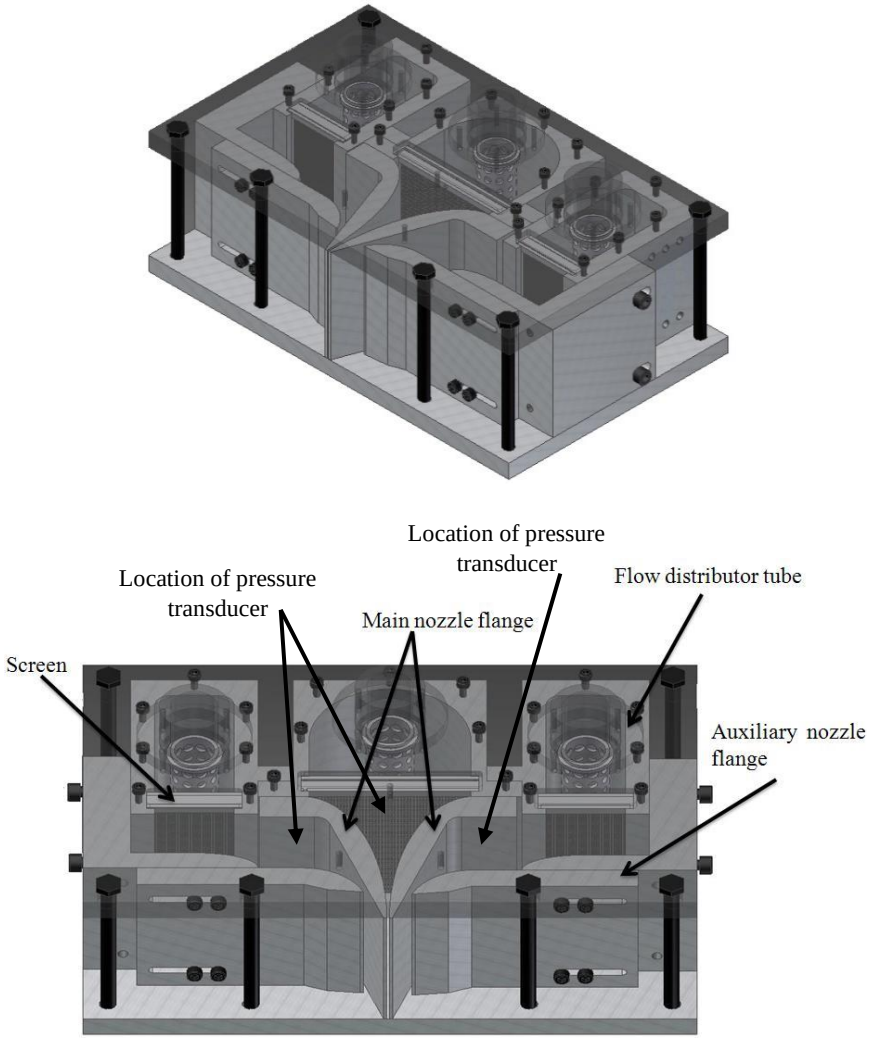

Figure 5-5) Isometric view of the prototype multi-slot air knife.

A cold laboratory-scale model of the continuous galvanizing gas jet wiping process was designed and manufactured (Figure 5-6) with the objective of validating the numerically modelled coating weights for the prototype multi-slot air knife.

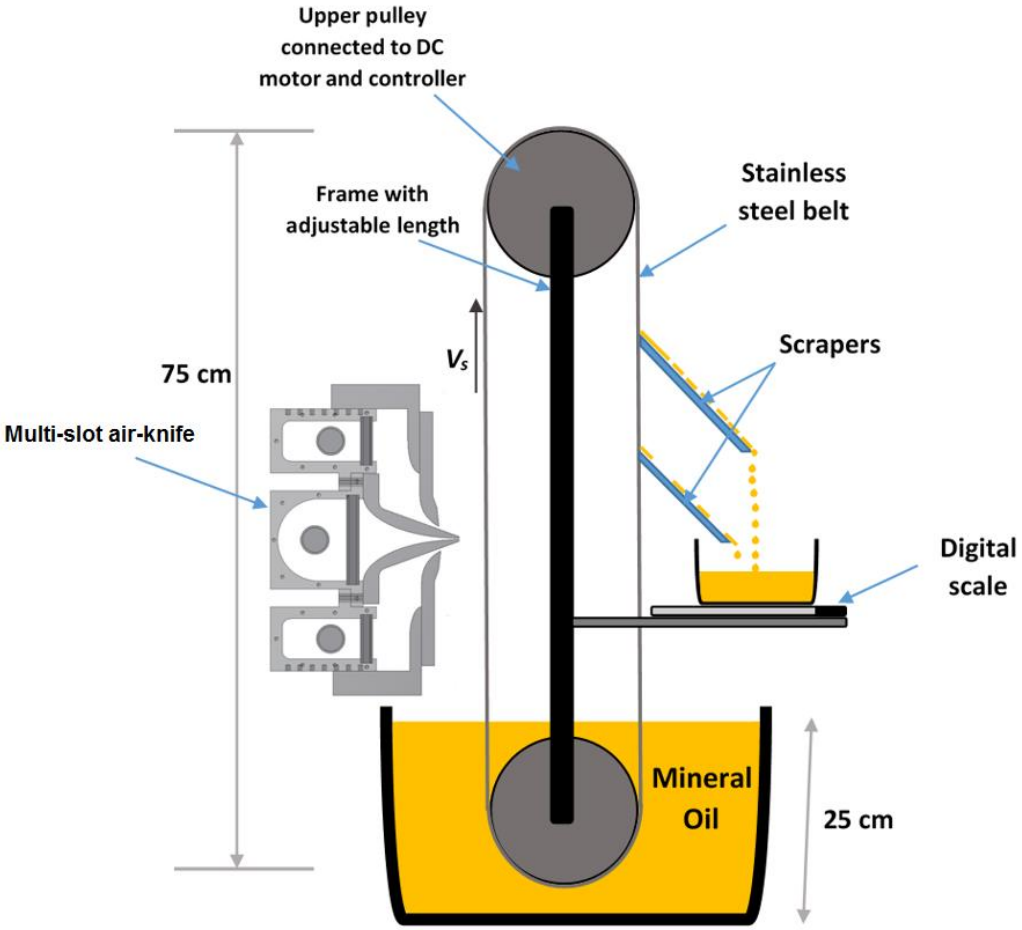

Figure 5-6) Schematic diagram of the experimental setup.

The experimental gas jet wiping apparatus consisted of a vertical stainless steel strip, 75 cm long and 5 cm wide, stretched between two rolls. An electric motor connected to the upper shaft and the upper roll provided the strip motion. The strip velocity was adjusted in the range of 0.5-3.5 m/s by means of an AC to DC speed controller connected to the electric

motor. The strip velocity was measured by means of optical and mechanical tachometers with an accuracy of ± 0.05 % and a resolution of 0.1 rpm (for the test range of 2 to 9999.9 rpm). The lower roll was designed to be adjustable to allow for the provision of adequate strip tension. The lower roll was immersed in the model working fluid – mineral oil – the properties of which are documented in Table 5-5-1. Table 5-2 compares the range of non-dimensional parameters characteristic of the molten Zn bath used in continuous galvanizing line [23] versus the apparatus used in the current study. It can be seen that the range of parameters are in satisfactory agreement and, thus, sufficient dynamic similarity was thought to have been established between the laboratory apparatus and the continuous galvanizing line.

The gas jet wiping devices tested using this apparatus were the single and multi-slot air knife discussed in the previous section and pictured in Figure 5-5 and Figure 5-6. The multi-slot air knife was positioned 50 cm above the free surface of the liquid bath perpendicular to the strip. The air-knife width was 5 cm longer than the strip width to avoid edge effects. The mineral oil was wiped on only one side of the strip, as pictured in Figure 5-6. The main jet to substrate distances and strip velocities used in the experiments were $8 \leq Z/D \leq 12$ and $0.25 \leq V_s \leq 1.5$ m/s.

After the substrate passed the through the wiping region, the liquid film remaining on the steel strip was removed by two inclined rubber blades or “squeegees” (Figure 5-6). Once steady-state was stablished, a digital balance with an accuracy of ± 0.01 g measured the mass of the collected liquid during the 300 s collection period, as measured by a

chronometer. The mean liquid film thickness, h_f, was determined through the mass flow rate of liquid removed from the strip during the collection period using equation (5-9):

$$h_f = \dot{m}_{cl} / \left(\rho_{cl} L_s V_s \right) \tag{5-9}$$

Each experiment was repeated four times. According to Coleman and Steels [24], the overall uncertainty of a discrete dependent variable (r), which is function of j independent measured variable X_i can be found using the Kline and McClintok method, given as:

$$\delta r = \sqrt{\sum_{i=1}^{j} \left(\theta_i \left(\delta X_i \right) \right)^2} \tag{5-10}$$

where $\theta_i = \dfrac{\partial r}{\partial X_i}$ and δX_i are the uncertainty for each measured variable. The uncertainty in the mean value of a measured X_i is given by $U_{X_i} = \sqrt{B_{X_i}^2 + P_{X_i}^2}$ where B is the instrumental bias error and P is precision (random) error. The random error of the mean was calculated through the student t-distribution at the 95% confidence level and instrumental error was found through manufacturers' specifications.

Table 5-5-1) Working liquid properties in the experimental facility [25].

Liquid	Density (kg/m^3)	Kinematic Viscosity (m^2/s)	Surface Tension (N/m)
Mineral Oil	865	10^{-5}	0.0323

Table 5-5-2) Non-dimensional characteristic parameters for the experimental working fluid and the molten Zn alloy used in industrial CGLs.

Similarity Parameters	Continuous Galvanizing Line [23]	Experimental Apparatus
G	35-200	77-296
S	1-10	3.9-6.7
h/h_o	0.02-0.06	0.019-0.055
Re_{film}	20-100	1.9-10.2
We	0.3-1.5	0.51-1.48

5.7 Results and discussion

In this section, the properties of the prototype multi-slot air knife shown in Figure 5-5 were experimentally determined. The effect of the plate-to-nozzle ratio (*Z/D*), which ranged between 8 and 12, the main jet Reynolds number of between 7000 and 11000, and the auxiliary jet Reynolds number of between 3000 and 11000 on the final coating weight will be discussed. The main jet width (*D*), auxiliary jet width (D_a) and the auxiliary jet offset (*s*) were fixed at D = 1.5 mm, D_a = 1.5 mm (i.e. D_a/D = 1) and s = 10 mm, respectively, as it had been previously shown by the present authors that this configuration of the multi-slot air knife led to lighter coating weights compared to the traditional single slot air knife [21]. By adjusting the pressure of the jet nozzles, P_s, the velocity of main jet was changed from 70 m/s to 110 m/s, and the velocity of auxiliary jets were changed from 30 to 110 m/s. The

total wiping energy per unit time and unit length of strip, E_w (equation 5-11), was used for comparing the different case studies.

$$E_w = P_s q_a = P_s V_j A \tag{5-11}$$

where A is the nominal jet exit cross sectional area, V_j is the jet exit velocity and q_a is the volumetric air flow rate for each jet. The energy taken into account for the multi-slot air knife (E_{total}) is the algebraic sum of the energies of the main and the auxiliary jets.

5.7.1 Effect of auxiliary jet Reynolds number (Re_a)

The effect of Re_a on the coating weight was investigated experimentally and results are compared with analytical model developed by Elsaadawy et al. [14]. Re_a was varied between 3000 and 9000 whilst the main slot jet Reynolds number was fixed at Re_m = 11000. According to Figure 5-7, the Elsaadawy et al. [14] model predicted the trends seen in the experimental measurements. The slight discrepancy between the model and the experimental measurements (especially at higher strip velocities) can be attributed to two sources of systematic errors; 1) the inefficiency of the wiping scrapers in removing all of the oil from the belt and 2) the splashing of oil from the belt, particularly at the upper pulley (Figure ?? – apparatus schematic). The latter source of error was observed for strip velocities of $V_s \geq 0.75$ m/s. Based on a comparison of the free meniscus coating measurements versus the analytical model developed by Thornton and Graff [2], it was estimated that 1.8% of the oil was left behind due to scraper inefficiency and that the contribution of splashing was 3.2%-5.8% (depending on the strip velocity) to the observed discrepancies between of the experimental measurements versus the analytical model.

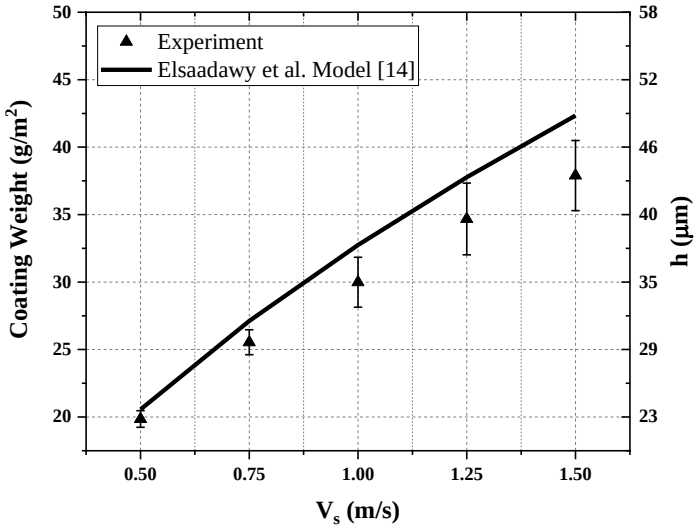
Experiment
Elsaadawy et al. Model [14]
Coating Weight (g/m^2)
h (μm)
V_s (m/s)
50
45
40
35
30
25
20
58
52
46
40
35
29
23
0.50
0.75
1.00
1.25
1.50

a)

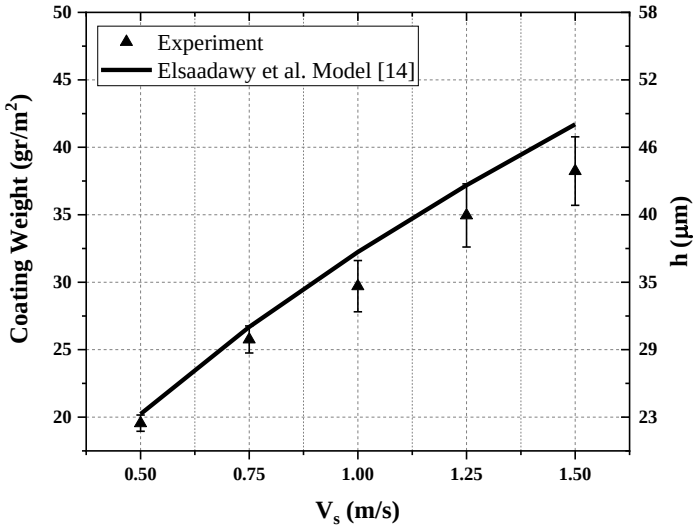
Experiment
Elsaadawy et al. Model [14]
Coating Weight (gr/m^2)
h (μm)
V_s (m/s)
50
45
40
35
30
25
20
58
52
46
40
35
29
23
0.50
0.75
1.00
1.25
1.50

b)

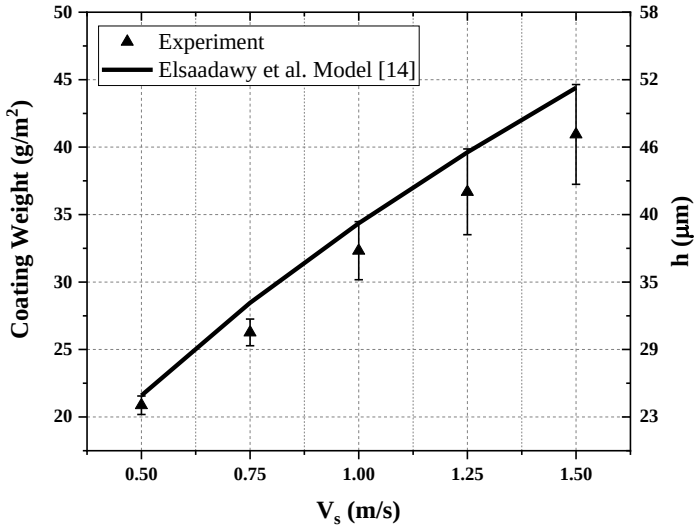

c)

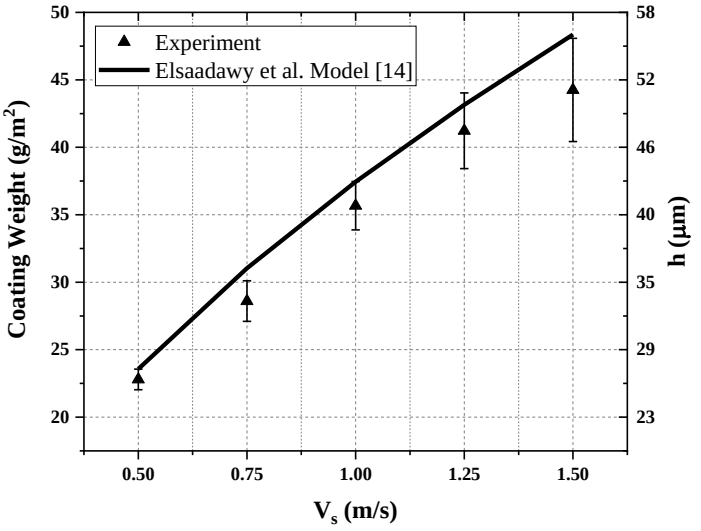

d)

Figure 5-7) Effect of auxiliary jet Reynolds number on final coating weight at Re_m = 11000, Z/D = 12, D = 1.5 mm, D_a = 1.5 mm and s = 10 mm for a) Re_a = 3000, b) Re_a = 5000, c) Re_a = 7000 and d) Re_a = 9000.

Figure 5-8 shows the non-dimensional predicted final coating thickness (h_m/h_s) using the Elsaadawy et al. model [14] as a function of Re_a for the experimental range of strip

velocities (V_s). In Figure 5-8, h_m and h_s represent the predicted final coating thickness for the multi-slot and single-slot jets, respectively. According to the shaded area shown in Figure 5-8, there was an operating window at lower auxiliary jet Reynolds numbers- i.e. Rea/Rem ≤ 0.6 – which resulted in lower coating weights compared to the single slot jet (i.e. $h_m/h_s < 1$) for the same main jet Reynolds number and the same main jet slot width. It should also be noted that this trend was insensitive to changes in strip velocity within the range explored experimentally (Figure 5-8).

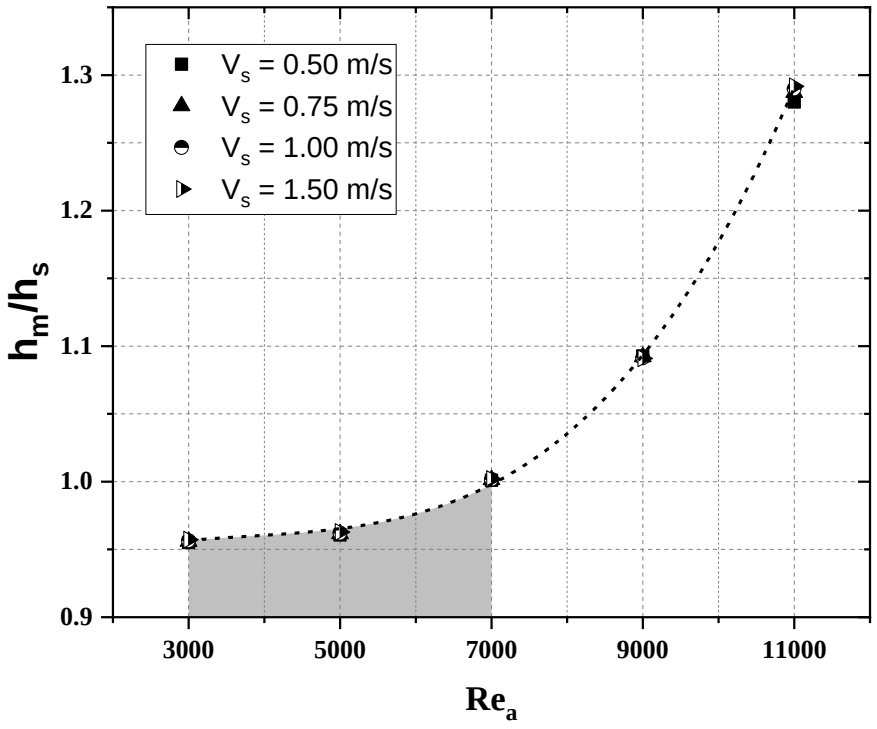

Figure 5-8) Predicted final coating weight using the Elsaadawy et al. model [1]) as a function of Re_a for Re_m = 11000, Z/D = 12, D = 1.5 mm, D_a = 1.5 mm and s = 10 mm and $0.5 \leq V_s \leq 1.5$ m/s.

This can be explained by examining Figure 5-9and Figure 5-10, which compare the wall pressure profiles, the wall pressure gradient and the wall shear stress distributions for the single and multi-slot air knife at different $Re_{a,}$, respectively. It can be seen that, at higher Re_a, a greater value for the maximum non-dimensional pressure can be achieved for the multi-slot air knife (Figure 5-9). However, by increasing Re_a the wall pressures for ($X/D \geq 1$) also increased and led to a wider pressure profile (Figure 5-9). Thus, the value of the wall pressure profile gradient was decreased in the vicinity of the wiping region at higher Re_a (Figure 5-10a). The same trend can be observed in Figure 5-10b for the wall shear stress distribution. Conversely, at the lower Re_a of 3000, the auxiliary jets contributed to the wiping action by increasing of the maximum pressure while the pressure profile gradient was very similar to that of the single jet profile for the $X/D \geq 1$ region (Figure 5-10). Furthermore, Figure 5-10 shows that a higher maximum pressure gradient and maximum wall shear stress were be achieved for lower values of Re_a (Figure 5-10) and, therefore, lower coating weights would be expected.

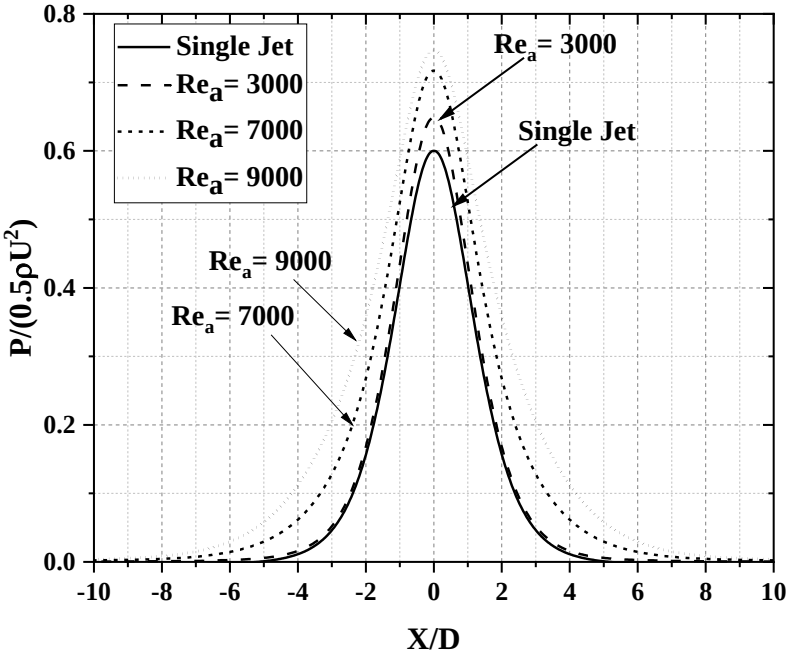

Figure 5-9) Non-dimensional wall pressure distributions for different Re_a, with Re_m = 11000, Z/D = 12, D = 1.5 mm, D_a = 1.5 mm and s = 10 mm.

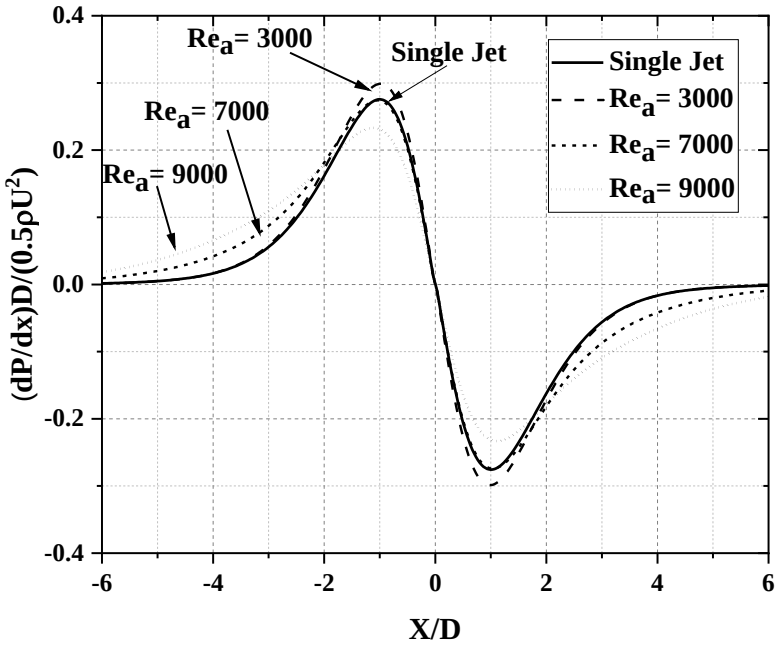

a)

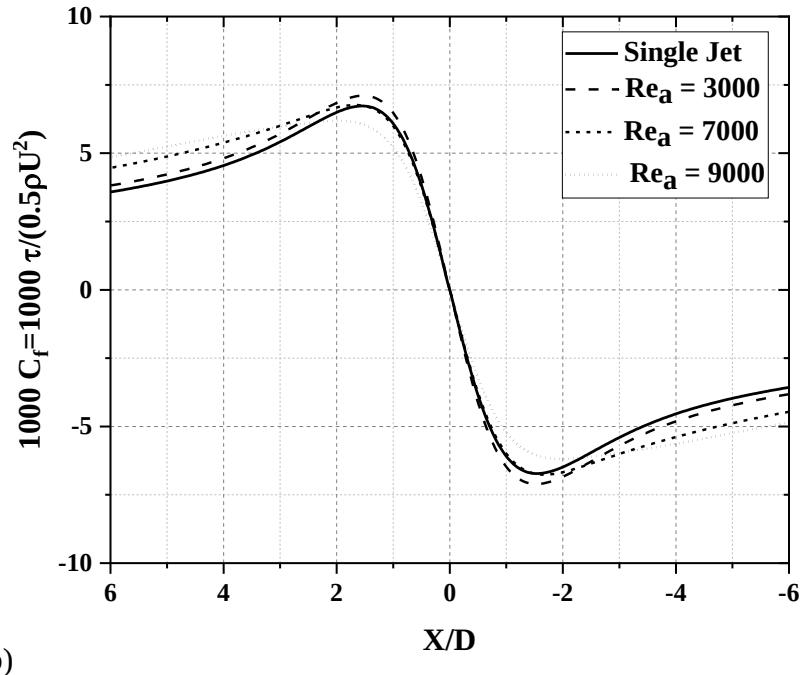

b)

Figure 5-10) Non-dimensional a) wall pressure gradient distributions and b) shear stress distribution for different Re_a, with Re_m = 11000, Z/D = 12, D = 1.5 mm, D_a = 1.5 mm and s = 10 mm.

Figure 5-11 compares the experimentally measured coating weights at different strip velocities as a function of auxiliary jet Reynolds number (Re_a) for Re_m = 11000 and Z/D = 12. Figure 5-11 also confirms that lower coating weights can be obtained with a relatively low Re_a. Conversely, when the auxiliary jet Reynolds numbers approached that of main jet, the wiping ability of the multi-slot jet decreased and, consequently, the final coating weight increased versus the single-slot jet configuration. This can be attributed to the higher pressure gradient and the higher wall shear stress in the wiping region for $Re_a/Re_m \leq 0.5$ which was observed in Figure 5-10. It can also be seen from Figure 5-11 that for all Re_a the coating weight increased with increasing substrate velocity.

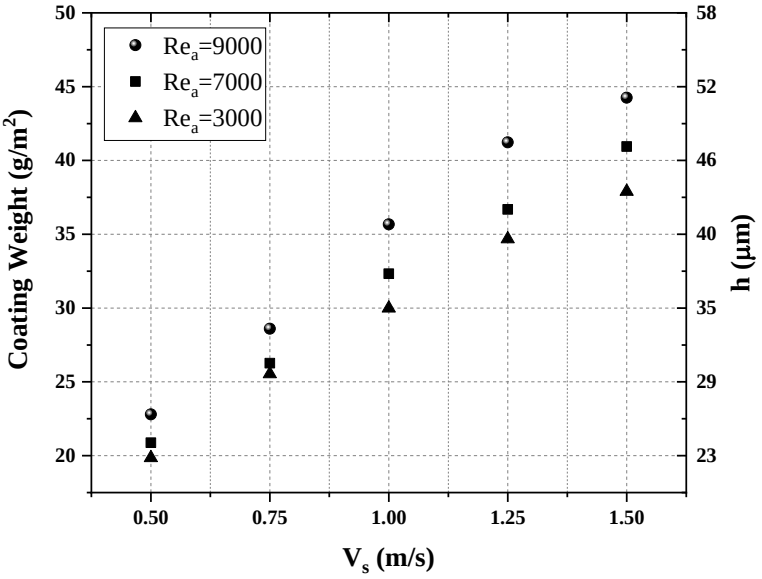

Figure 5-11) Effect of auxiliary jet Reynolds number on experimentally measured coating weights at Re_m = 11000, Z/D = 12, D = 1.5 mm, D_a = 1.5 mm, s = 10 mm and 3000 ≤ Re_a ≤ 9000.

Figure 5-12 shows the experimentally measured coating weights on the moving strip as a function of strip velocity (V_s) and auxiliary jet Reynolds number, Re_a, for Re_m = 11000 and Z / D = 12. According to Figure 5-12, the experimentally measured coating weight data also confirmed that, for the lower auxiliary jet Reynolds number of Re_a = 3000, at higher strip velocities (V_s = 1.5 m/s), lighter coating weight can be achieved compared to the single slot air knife.

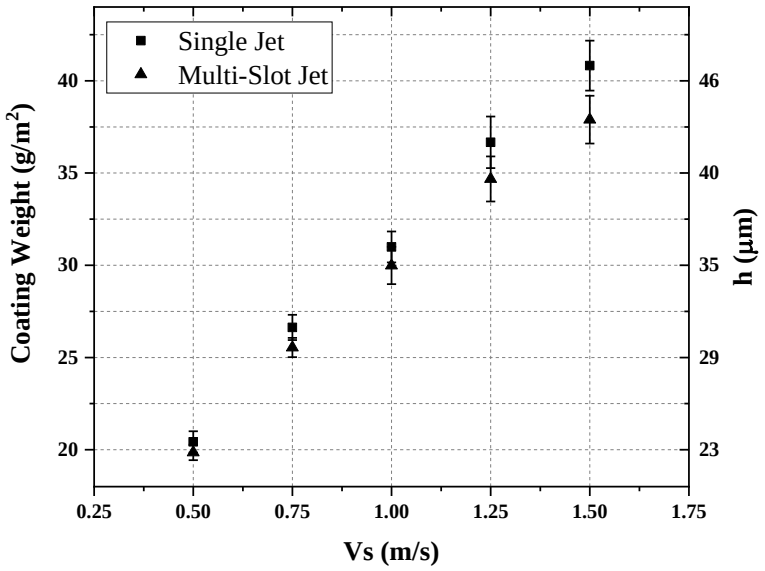

Figure 5-12) Comparison of experimentally measured coating weight for multi-slot jet at different strip velocities, Re_m = 11000, Re_a = 3000, Z/D = 12, D = 1.5 mm, D_a = 1.5 mm and s = 10 mm with single slot jet at Re_m = 11000, D = 1.5 mm and Z/D = 12.

The coating thickness reduction observed at the low auxiliary jet Reynolds number can be discussed from the energy point of view. Figure 5-13 shows the final coating weight versus the non-dimensional total input wiping energy in the multi-slot air knife calculated using equation 5-11. In this figure, the main jet Reynolds number was fixed at Re_m= 11000 while the auxiliary jet Reynolds number was varied between 3000 to 11000. The total energy of the multi-slot air knife was normalized to that of the main jet. The results of Figure 5-13 show that coating weight reductions can be realized by having the input energy of the auxiliary jets being less than 5% of the main jet wiping energy (i.e. $E_{total}/E_{main} < 1.05$) compared to the single slot air knife (i.e. $E_{total}/E_{main} = 1$)

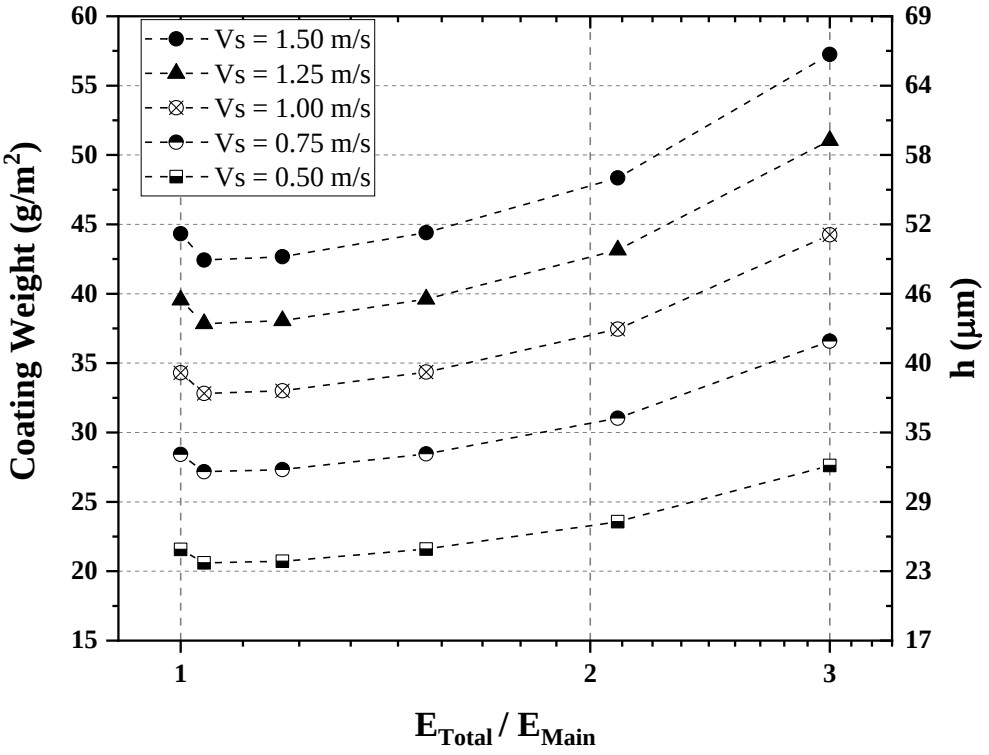

Figure 5-13) Final coating weight as a function of the total input energy of the multi-slot air knife for Re_m = 11000, Z/D = 12, D = 1.5 mm, D_a = 1.5 mm and s = 10 mm, $0.5 \leq V_s \leq 1.5$ m/s and $3000 \leq Re_a \leq 11000$.

5.7.2 Effect of main jet Reynolds number (Re_m)

The effect of the main jet Reynolds number (Re_m) on the final coating weight is presented in this section. Re_m was varied between 7000 and 11000 while Re_a was fixed at 3000 for these experiments. That is, the main jet velocity changed from 70 to 110 m/s, whereas the auxiliary jet velocity was fixed at 30 m/s. The main jet width (D), auxiliary jet width (D_a), jet to strip distance (Z/D) and the auxiliary jet offset (s) were fixed at D = 1.5 mm, D_a = 1.5 mm (i.e. D_a/D = 1), Z/D=12 and s = 10 mm, respectively. The experimentally measured final coating weight for the multi-slot jet as a function of strip velocity as a

function of Re_m is shown in Figure 5-14. According to this figure, the predicted values of the final coating thickness using the Elsaadawy et al. model [1] agreed with the experimental measurements at each Re_m. Figure 5-15 compares the coating weights for the multi-slot air knife with the single slot jet coating weight data for $7000 \leq Re_m \leq 11000$ at fixed Re_a = 3000 and Z/D = 12. According to Figure 5-15, at higher strip velocities the coating weight from the multi-slot jet configuration was lower compared to that of the single slot jet for the investigated range of main jet Reynolds numbers. Coating weight estimates from the Elsaadawy et al. [1] model also confirmed this trend for coating thickness reduction (Figure 5-16), where the highest difference was observed at V_s=1.5 *m/s* for all of investigated main jet Reynolds numbers ($7000 \leq Re_m \leq 11000$).

Figure 5-17 shows the CFD derived wall pressure gradient distribution at Z/D = 12 and Re_a = 3000 for both the single and multi-slot air knives. It can be seen that adding lower velocity auxiliary jets beside the main jet led to an increase in the maximum non-dimensional pressure gradient and also increased the wiping region pressure gradient for this configuration versus the single-impinging slot jet case. A similar trend can be seen in Figure 5-18 for the wall shear stress profile for Re_m = 9000 and Re_m = 11000 while Re_a = 3000 and Z/D = 12.

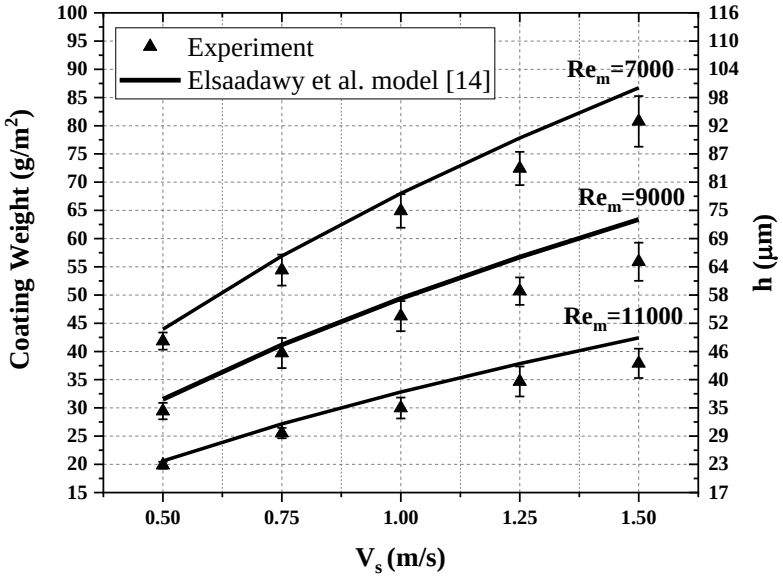

Figure 5-14) Final coating weight for the multi-slot jet at different strip velocities and Re_m, with Re_a = 3000, Z/D = 12, D = 1.5 mm, D_a = 1.5 mm and s = 10 mm.

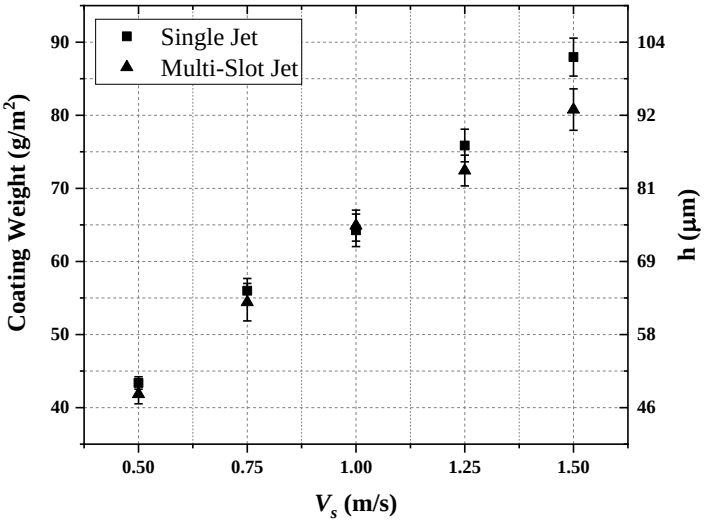

a)

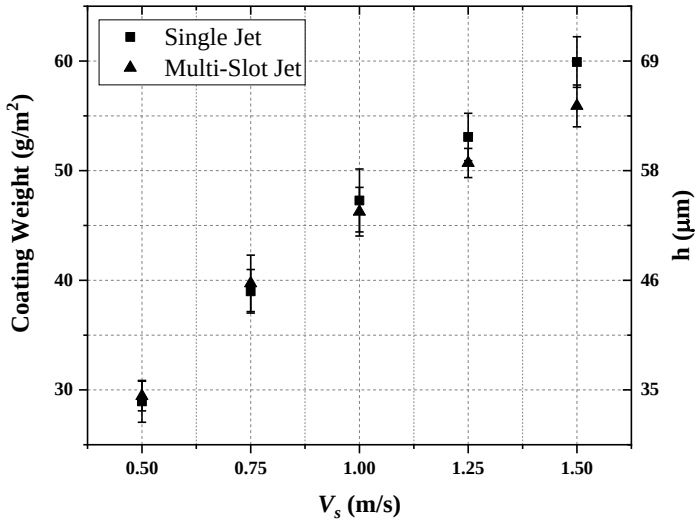

b)

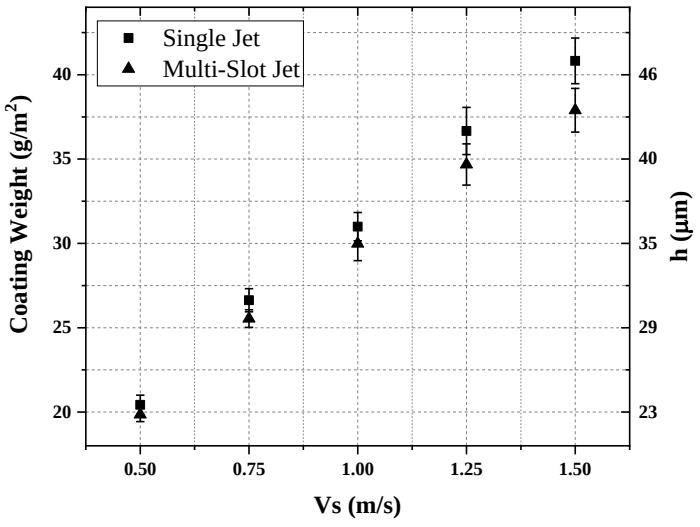

c)

Figure 5-15) Comparison of experimentally measured coating weights for the single and multi-slot air knife at a) Re_m = 7000, b) Re_m = 9000, c) Re_m = 11000 for Z/D = 12, Re_a = 3000, D = 1.5 mm, D_a = 1.5 mm and s = 10 mm.

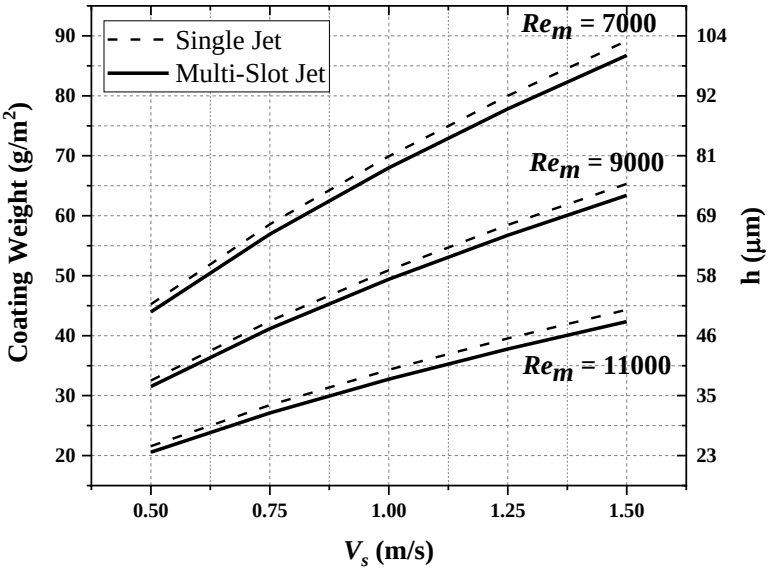

Figure 5-16) Comparison of predicted final coating weight for the single and multi-slot air knife using the Elsaadawy et al. model [14] at $7000 \leq Re_m \leq 11000$ for Z/D = 12, Re_a = 3000 D = 1.5 mm, D_a = 1.5 mm and s = 10 mm.

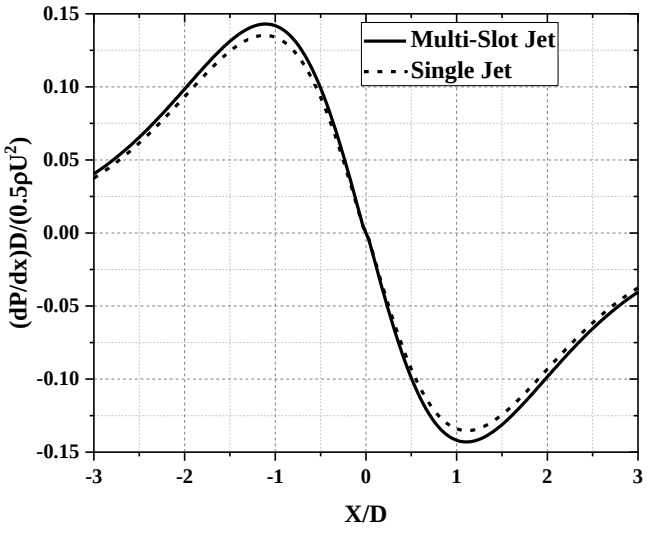

a)

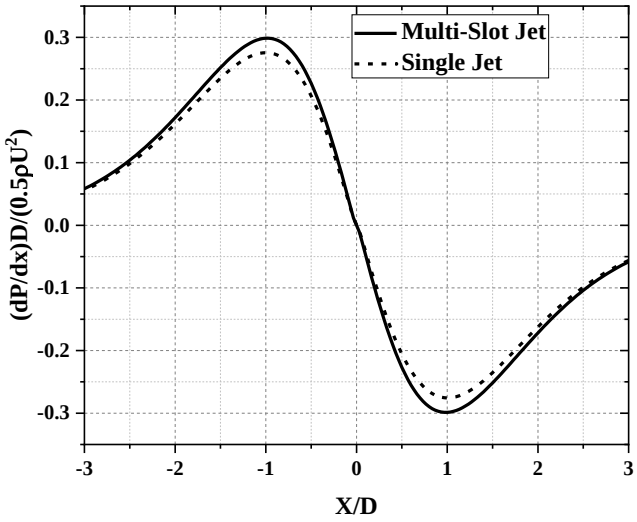

b)

Figure 5-17) Comparison of non-dimensional wall pressure gradient for the single and multi-slot air knife at a) Re_m = 9000 and b) Re_m = 11000 for Z/D = 12, Re_a = 3000, D = 1.5 mm, D_a = 1.5 mm and s = 10 mm.

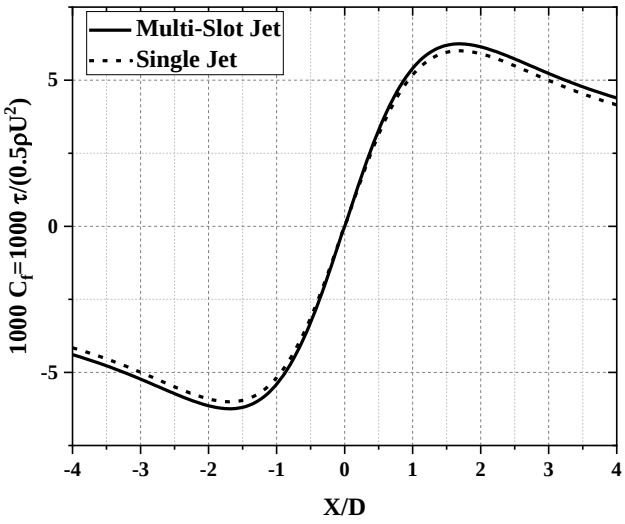

a)

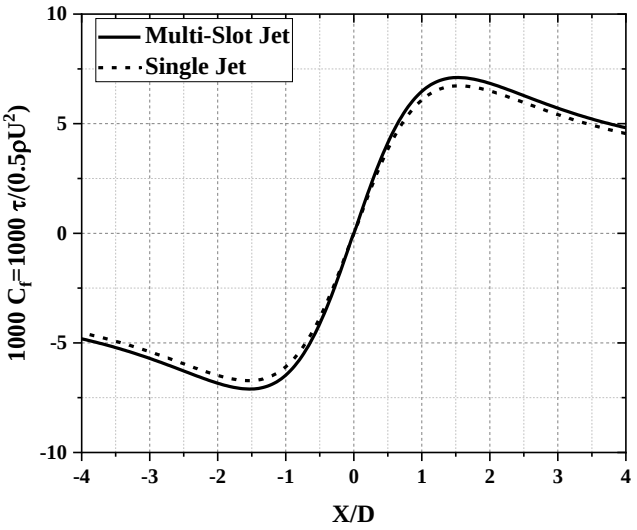

b)

Figure 5-18) Comparison of non-dimensional wall shear stress distribution for single and multi-slot air knife at a) Re_m = 9000 and b) Re_m = 11000 for Z/D = 12, Re_a = 3000, D = 1.5 mm, D_a = 1.5 mm and s = 10 mm.

5.7.3 Effect of *Z/D*

The effect of the strip to nozzle ratio (Z/D) on the coating weight on a moving substrate was investigated at Re_m = 11000, Re_a = 3000, D = 1.5 mm, D_a = 1.5 mm, s = 10 mm and $0.5 \leq V_s \leq 1.5$. The results were compared with the results of the conventional single slot jet working at the same main jet Reynolds number. Figure 5-19 represents the final coating thickness for the multi-slot jet wiping as a function Z/D for Re_m = 11000, Re_a = 3000 and $0.5 \leq V_s \leq 1.5$. It is shown that the predicted coating weight was sensitive to the Z/D ratio and increased with increasing Z/D. Figure 5-20 compares the predicted coating weight by the Elsaadawy et al. model [14] as a function of V_s and Z/D ratio for the single jet working at Re_m = 11000 versus the multi-slot jet working at Re_m = 11000 and Re_m = 3000. According

to Figure 5-20, for $Z/D \geq 10$, the coating weight for the multi-slot configuration was lower than the single slot jet case for all strip velocities ($0.5 \leq V_s \leq 1.5$), with the largest difference being about 4.7% for $V_s = 1.5$ m/s.

For the single slot jet at $Z/D = 12$, since the potential core was absorbed before impingement, there would be a significant decrease in the maximum wall pressure versus the low Z/D case where the potential core was impinging on the wall. By using the multi-slot configuration under the specific arrangement in this study, the momentum loss of the main jet could be decreased as the auxiliary jet flow merged with that of the main jet without affecting the jet width. The merged jet with higher momentum and with the same width resulted in higher pressure gradient (Figure 5-10a) and shear stresses (Figure 5-10b) at the coating surface and, consequently, the coating thickness decreased for the multi-slot jet. However, at lower Z/D, since the potential core of the main jet impinged on the strip, the additional flow coming from the auxiliary jet did not have a significant effect on the pressure gradient or shear stress and no significant coating thickness reduction was observed.

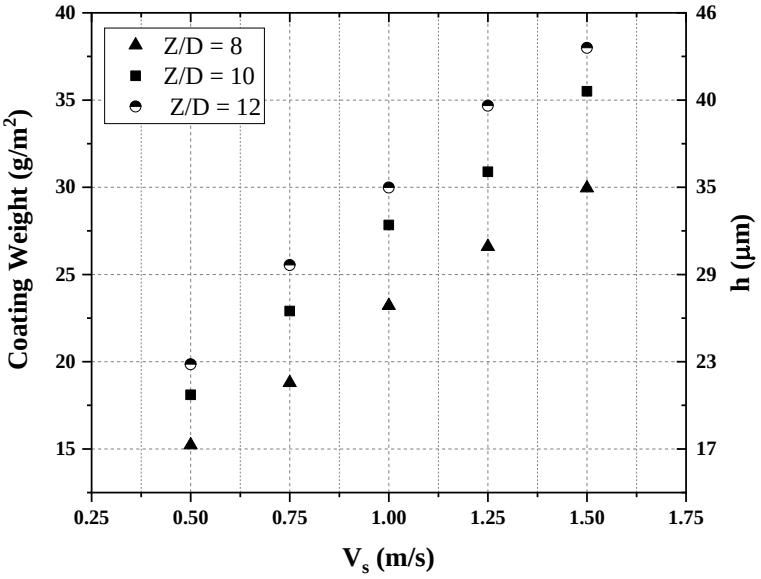

Figure 5-19) Experimental measurements of final coating thickness as a function of *Z/D* at different strip velocities, Re_m = 11000, Re_a = 3000, D = 1.5 mm, D_a = 1.5 mm and s = 10 mm.

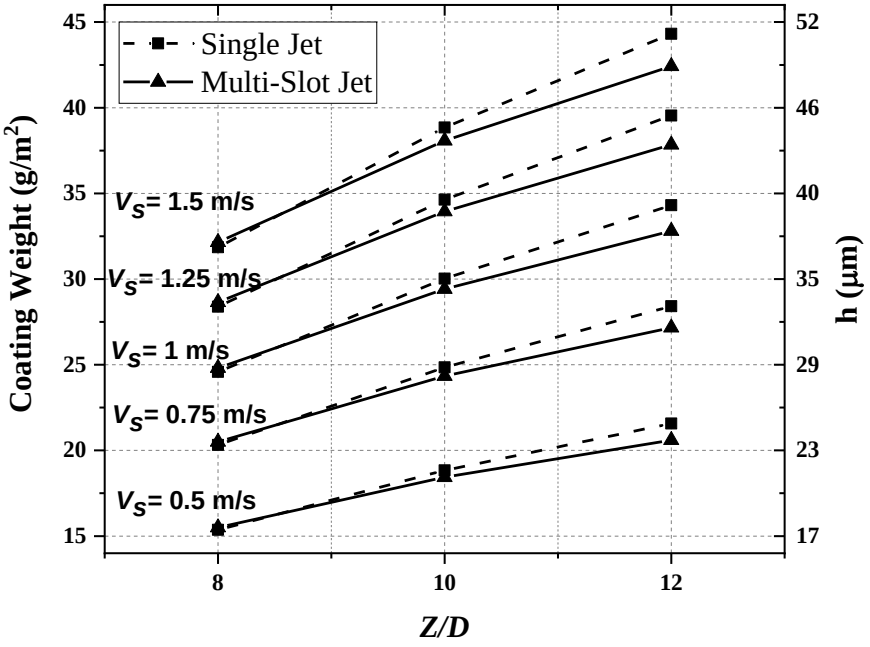

Figure 5-20) Comparison of coating weight predicted by Elsaadawy et al. model [14] for a single jet working at Re_m = 11000, D = 1.5 mm and multi-slot jet wiping working at Re_m = 11000 and Re_a = 3000, D = 1.5 mm, D_a = 1.5 mm and s = 10 mm.

5.8 Conclusions

The final coating weight during gas jet wiping in the continuous galvanizing process by means of a novel prototype multi-slot air knife over a variety of operating conditions was measured experimentally. Numerical simulations for the same operating conditions were also carried out to estimate the wall pressure and shear stress profiles for the purpose of predicting the coating weight on the moving substrate using a 2-D steady-state analytical model. Based on a previous study by the authors [21], the geometry of the multi-slot jet

was set such that $D_a/D = 1$ and $s = 10$ mm for the experimental measurements and numerical simulations.

The sensitivity of the final coating weight to the main and auxiliary jet Reynolds numbers were determined. It was observed that at higher strip velocities, slightly lighter coating weights could be achieved by using the multi-slot air knife configuration when such that the auxiliary jets were operated at a fraction of main jet Reynolds number (i.e. $Re_a/Re_m \leq 0.5$). It was also shown that the experimentally measured coating weights were in good agreement with the predicted coating weights using the analytical liquid film coating weight model of Elsaadawy et al. [14] at different auxiliary jet Reynolds number ($3000 \leq Re_a \leq 9000$) for a fixed main jet Reynolds number of $Re_m = 11000$ and $Z/D = 12$.

The effect of the main jet Reynolds number ($7000 \leq Re_m \leq 11000$) for a fixed auxiliary jet Reynolds number ($Re_a = 3000$) and jet to strip distance of $Z/D = 12$ was also experimentally investigated. The measurements were benchmarked against the analytical model of Elsaadawy et al. [1]) and showed that the experimental data agreed with the predicted results. Moreover, for each main jet Reynolds number ($7000 \leq Re_m \leq 11000$), it was confirmed that with $D_a/D = 1$ and $Re_a = 3000$, slightly lighter coating weights at higher strip velocities could be achieved using the multi-slot air knife.

In the last part of this paper, the sensitivity of coating weight to the jet to wall distance (Z/D) ration was investigated for $D_a/D = 1$, $Re_m = 11000$ and $Re_a = 3000$. The experimental results showed the effectiveness of using the multi slot air knife for $Z/D \geq 10$, as the flow of the auxiliary jets reduced the momentum loss of the main jet without increasing the jet

width. Therefore, the higher wall pressure gradient and shear stress upon impingement at the coating surface resulted in lighter coating weights.

5.9 Acknowledgments

The authors gratefully acknowledge the financial support of the International Zinc Organization Galvanized Autobody Partnership (IZA-GAP) members, Dofasco Global R&D Hamilton and the Natural Sciences and Engineering Research Council of Canada (NSERC grant CRDPJ 446105-2012).

5.10 References

[1] A. R. Marder, Prog. Mater. Sci., 45(2000), 191.

[2] J. A. Thornton and H. F. Graff, Metall. Trans. B, 7(1976), 607.

[3] C. H. Ellen and C. V. Tu, J. Fluids Eng., 106(1983), 399.

[4] A. N. Hrymak, E. A. Elsaadawy, G. Hanumanth, J. R. McDermid, and F. E. Goodwin, in AISTech Proceedings, (2016), 393.

[5] M. Dubois, in Galvatech 2011 Conference Proceedings: HDG Process Technologies, 2011, 1847.

[6] E. O. Tuck, Phys. Fluids, 26(1983), 2352.

[7] C. V Tu and D. H. Wood, Exp. Therm. Fluid Sci., 13(1996), 364.

[8] D. Lacanette, A. Gosset, S. Vincent, J. M. Buchlin, and E. Arquis, Phys. Fluids, 18(2006),1.

[9] J.-R. Park, Ironnmaking Steelmak., 28(2001), 53.

[10] D. Arthurs and S. Ziada, J. Can. Acoust. Assoc., 35(2007), 28.

[11] K. Myrillas, A. Gosset, P. Rambaud, M. Anderhuber, J. M. Mataigne, and J. M. Buchlin, Chem. Eng. Process. Process Intensif., 50(2011),466.

[12] C. V Tu, (1994), Patent number: US005360641A.

[13] P. Tamadonfar, J. R. McDermid, A. N. Hrymak, and F. E. Goodwin, in AISTech - Iron and Steel Technology Conference Proceedings, (2010), 517.

[14] E. A. Elsaadawy, G. S. Hanumanth, A. K. S. Balthazaar, J. R. McDermid, A. N. Hrymak, and J. F. Forbes, Metall. Mater. Trans. B Process Metall. Mater. Process. Sci., 38(2007), 413.

[15] G. Y. Kim, H. D. Park, D. E. Lee, and W. C. Chung, , (2008), Patent number: US0031879 A1.

[16] P. Tamadonfar, J. R. McDermid, A. N. Hrymak, and F. E. Goodwin, in 8th International Conference of Zinc and Zinc Alloy Coated Steel Sheet (Galvatech 2011), (2011).

[17] S. Alibeigi, J. R. McDermid, S. Ziada, and F. E. Goodwin, in Galvatech 2013: 9th International Conference on Zinc and Zinc Alloy Coated Steel Sheet & 2nd Asia-Pacific Galvanizing Conference, (2013), 437.

[18] D. Finnerty, J. R. McDermid, F. Goodwin, and S. Ziada, in 11th International Conference on Zinc and Zinc Alloy Coated Steel Sheetß (Galvatech 2017), 2017.

[19] A. Yahyaee Soufiani, J. R. McDermid, A. N. Hrymak, and F. E. Goodwin, J. Coatings Technol. Res., 14(2017), 1015.

[20] G. Takeda, H. Takahashi, and K. Kabeya, Tetsu-to-Hagane, 102(2016), 576.

[21] A. Y. Soufiani, J. R. McDermid, A. N. Hrymak, and F. E. Goodwin, Submitt. to Metall. Mater. Trans. B Process Metall. Mater. Process. Sci., (2019).

[22] F. M. White, Fluid Mechanics, fourth ed., McGraw-Hill, Boston, (2003), 866.

[23] J. M. Buchlin, Modeling of gas-jet wiping. In Thin Liquid Films and Coating Processes, Von-karman institute, Waterloo, Belgium, (1997),141.

[24] H. W. Coleman and W. G. Steele, Experimentation and Uncertainity Analysis for engineers, Second ed. JOHN WILEY & SONS INC., New York, (1999), 271.

[25] M. J. Neale, The Tribology Handbook, seconnd ed., Butterworth-Heinemann, Oxford, (1995), 640.

Chapter 6: Experimental study on coating thickness and noise reduction via multi-slot jet

Ali Yahaee Soufiani, Joseph R. McDermid, Andrew N. Hrymak, Frank E. Goodwin. (This paper will be submitted for publication shortly)

In this paper, all the experimental measurements were carried out by me under supervision of Dr. McDermid and Dr. Hrymak. The manuscript was initially drafted by me and reviewed to its final version by Dr. McDermid and Dr. Hrymak. Dr. Goodwin was included as an author in this paper as a courtesy for his industrial sponsorship.

6.1 Abstract

Gas jet wiping is an effective hydrodynamic method to control coating thickness of liquid zinc on a moving steel substrate within a continuous hot dip galvanizing line. One of the industrial problems associated with the gas jet wiping process is the generation of high intensity tonal noise, which could cause difficulties in the workplace for operators especially in vicinity of the galvanizing line. In this study, the ability of a novel configuration of multi-slot jet in noise elimination and coating thickness reduction during gas jet wiping process was experimentally investigated. The wiping process via traditional single slot jet was also studied to compare the results with multi-slot jet data. Noise and coating weight measurements were carried out over a wide range of operating conditions to quantify the trends of noise generated and final coating thicknesses.

It was found that when the auxiliary jet velocity is a fraction of the main jet velocity such that, $Re_a/Re_m \leq 0.5$, the multi-slot jet has the ability to either attenuate or eliminate the high intensity tonal noise generated during single jet wiping. Moreover, for the same operating conditions (i.e. $Re_a/Re_m \leq 0.5$) it was observed that lighter coating weights can be achieved through using multi-slot air jet compared to the single slot jet wiping.

These findings indicate that the multi-slot design can be applied effectively as the wiping actuator in a continuous hot dip galvanizing line to produce lighter coating weights with less intensity tonal noise compared to the traditional single-slot jet design.

6.2 Nomenclature

D	Main jet width (m)
D_a	Auxiliary jet width (m)
D_{EB}	Edge baffle distance (m)
f	Frequency (Hz)
h_f	Final film thickness (m)
h	Local film thickness (m)
L_s	Strip width (m)
$\dot{m}_{cl}$	Mass flow rate of removed oil (kg/s)
P_o	Nozzle static pressure (Pa)
Re	Jet Reynolds number ($\mathrm{Re} = \frac{\rho u D}{\mu}$)
Re_m	Main jet Reynolds number
Re_a	Auxiliary jet Reynolds number
Re	Jet Reynolds number ($\mathrm{Re} = \frac{\rho u D}{\mu}$)
s	Auxiliary jet offset distance (m)
V_s	Strip velocity (m/s)
V_j	Nozzle exit velocity (m/s)
Z	Main jet exit to wall distance (m)
ρ_{cl}	Coating liquid density (kg/m^3)
α	Main jet inclination angle
ε	Impingement plate inclination angle
ρ_{cl}	Density of coating liquid (kg/m^3)

6.3 Introduction

The process of gas jet wiping has employed in various industries such as forming of plastic, drying of paper, cooling of electronic devices, photograph production and cooling of turbine blades. This process is also widely used in a continuous hot dip galvanizing line (CHDG) to control coating thickness of liquid zinc on the steel substrates. In CHDG, steel sheet is continuously immersed into a molten zinc bath and withdrawn vertically. The sheet is then passed through a pair of opposing gas jets (which are referred as to air-knives) which impinge air on the sheet. In this manner, the excess zinc is stripped away and returns to the bath as a runback flow and a uniform thin layer of zinc remains on the substrate. Figure 6-1 shows a schematic figure of the gas jet wiping process for a single slot jet.

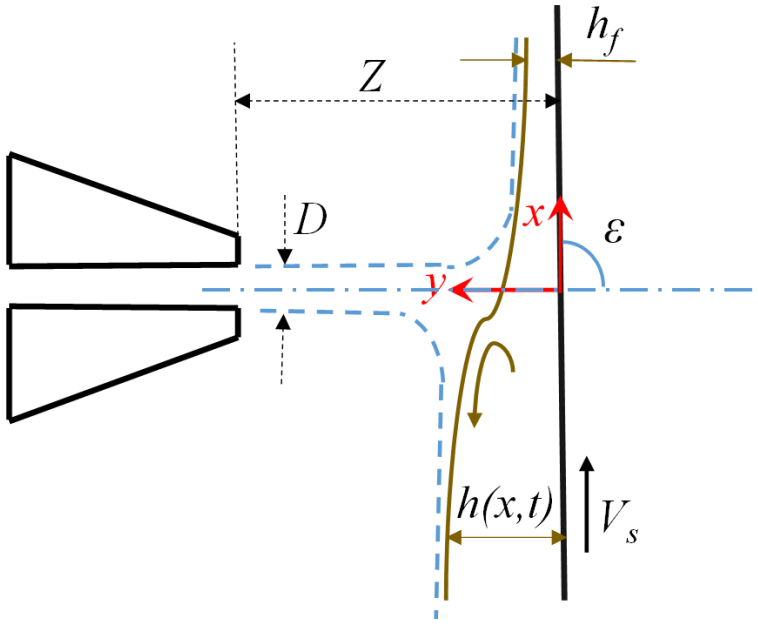

Figure 6-1) Schematic of the gas jet wiping process.

Currently a traditional configuration of single slot jet is used as the wiping actuators in the continuous hot dip galvanizing line. Although gas wiping via a single jet is a reliable process for controlling coating thickness of liquid zinc on the steel sheets, there are some industrial difficulties associated with this technique. One of the main issues during single slot jet wiping process is the generation of high tonal noise at higher wiping pressure, which is a limiting factor in the galvanized steel production rates and increase production costs. In order to have a lower coating thickness as the line speed is increased, the nozzle pressure and consequently the jet exit velocity must be increased significantly. The noise generation is acknowledged to be proportional to the impinged jet velocity [1]. Therefore, as the line speed increases, the noise generation by the gas wiping process also increases. Hygienic limitations which restricts worker to exposure to high sound levels, restrain the production line to reach the maximum speed for a desired coating thickness. This is a more serious issue for the automotive industry which is always demanding galvanized steel sheet with lower coating weights [2].

A number of studies have experimentally investigated the noise generation by impingement of a gas jet on a solid surface ([3]-[6]). Less attention in the literature has been paid to the noise generation due to impingement of planar jet in comparison with axisymmetric jets.

In an experimental investigation Petrie [3] studied noise generated by impingement of an axisymmetric air jet on a flat plate. In this study the jet velocity varied between V_j = 82 and 213 m/s while the nozzle diameter was set between D = 19 mm and 38 mm. The sound pressure level in this study was found to be inversely proportional to jet to plate ratio (Z/D),

and a distinct tonal noise up to 27 dB above the noise of a free jet was reported. The other parameter investigated in this study was the effect of jet to plate impingement angle on the acoustic tones. The plate was first set normal to the impinging jet, and then it was slowly inclined to the axis of the jet. 10 dB decrease was observed in the sound pressure level for inclination angles of $\varepsilon = 30°$, and further reductions in sound pressure level was reported by increasing the inclination angle up to $\varepsilon = 60°$.

Thornton and Graff [4] showed that by using air instead of superheated steam as the working fluid during wiping process, the overall sound pressure level around the coating pot can be decreased by 5 dB. They reported that by this substitution, more than 90% of the product line at their production facility could be finished at 90 dB. However, the investigated line speed was relatively low ($V_s < 1$ m/s) and the obtained coating weights was quite high (around 300 g/m^2) in the study of Thornton and Graff [4]. The generation noise would increase for a given low coating weight at higher line speeds.

Nosseir and Ho [7] investigated the noise generation and feedback mechanism [8] of an axisymmetric jet impinging on a flat plate in two separate studies. It was reported that a feedback mechanism existed for jet to plate ratio of $Z/D < 7.5$ for axisymmetric jets impinging on the flat plate. The authors attributed the noise generation to this feedback mechanism, which was comprised of coherent structures produced within the jet shear layer. The coherent structures move toward the plate and the subsequent impingement results in pressure fluctuations and distortion of the vorticity field. The pressure fluctuations move upstream to the nozzle lip and excite the perturbations in the shear layer. Therefore, the feedback cycle completes and results in generation of acoustic tonal noise. The authors

showed that the frequency of the generated tonal noise was a function of the speed of sound, and speed of coherent structures travelling downstream to the plate.

Park [5] studied the noise generation and edge over-coating during the gas jet wiping process through various experimental measurements. The study was carried out on an actual continuous galvanizing line with the focus on analyzing total noise level, main noise frequency and a main noise level of the dominant acoustic tone. Park [5] observed that the noise level decreased with increasing sheet width from 900 mm to 1200 mm, which resulted in decreasing the jet-jet impingement length. The author concluded that during the gas jet wiping process, most of the noise was generated at the edge of the steel strip where the opposing jets impinge and thus turbulence increases. The study also acknowledged the effect of the impinged jet velocity on the overall sound pressure level and the frequency and sound pressure level of tonal noises.

Dubois [6] carried out an extensive set of experiments in order to characterize noise generation during the gas jet wiping process. The effects of edge baffle, nozzle pressure (P_o), jet width to wall distance ratio (Z/D), jet inclination angle (α) and edge baffle distance (D_{EB}) on the noise generation were investigated. The experiments in this study were performed in both a laboratory environment and also in an actual production line with the main focus on the effect of the edge baffles and their effects with other parameters. Dubois [6] comprehensively analyzed the spectral content and the frequency response of acoustic tones produced during gas wiping.

An experimental study of noise generation in the gas wiping process was carried out by Arthurs and Ziada [1] to understand the effect of the various process parameters on overall

noise levels and the generation of discrete acoustic tones. The effect of plenum pressure and impingement ratio on the noise generated by gas wiping was investigated. Semi-empirical models was developed to predict the frequency of the tones based on the process parameters used. Moreover, noise maps of tone intensity were constructed to aid manufacturers in optimizing gas wiping process to minimize noise production. The authors reported that there were no significant tones generated for the pressure runs of 1.0 and 1.5 psi. Significant acoustic tones were present for plenum pressures of P_o = 2.0 psi and greater starting at an impingement ratio of Z/D = 6. The generation of this tone occurs for successively larger ranges of impingement ratio for increasing pressures and seems to occur over two distinct regions.

Finnerty et al. [9], experimentally studied the effect of auxiliary jets on noise reduction by using a multi-slot jet. In this study, the main jet velocity was held at 250 m/s for all experiments and auxiliary jet flows were varied between zero and 60 m/s in 20 m/s intervals. The authors showed that the multi-slot jets were able to decrease the magnitude of the tonal noise to the point of near complete suppression when the auxiliary jet velocity was set as the quarter velocity of the main jet. They also showed that the auxiliary jets also introduced broadband noise at low frequencies which is not of a sufficient magnitude to present a hazard to workers on continuous galvanizing lines.

In another study, Finnerty et al. [10], through particle image velocimetry (PIV) measurements, showed that the auxiliary jets had the ability to stabilize the main jet flapping. McDermid et al. [11] later studied stabilizing effect of auxiliary jets via PIV measurements. The authors showed that, operating the auxiliary jets such that the auxiliary

jet velocity was approximately 40% of the main jet velocity did, indeed, stabilize the main jet by significantly reducing main jet flapping [11]. The jet flapping associated with the aeroacoustics feedback relative to that observed for the single jet design [12] decreased, by largely eliminating the vortical structures associated with the high shear gradients between the main jet and bulk environment [11].

For the current study, measurements have been performed on a scaled galvanizing simulator in a laboratory environment. Single slot jet and multi-slot jet were used as the wiping actuators. A set of experiments over a wide range of gas wiping parameters such as main jet Reynolds number (Re_m), auxiliary jet Reynolds number (Re_a), jet to strip ratio (Z/D) and strip velocity were performed in order to provide an overview of noise generation in the gas wiping process. The experiments with the same operating conditions were repeated to measure final coating thicknesses after the action of gas wiping and the results of multi-slot jet were compared with that of single slot jet. An analysis of simultaneous ability of multi-slot jet on noise elimination and coating thickness reduction were performed for the purpose of higher production rates and efficiency.

6.4 Test facility

A schematic of the prototype multi-slot jet used in the experimental measurements is presented in Figure 6-2. The multi-slot jet consists of three jets, one main jet slot and two auxiliary jet slots symmetrically located on each side of the main jet slot. The main jet was perpendicular to the moving strip and the auxiliary jets were inclined at 20° from the main jet centerline. The prototype multi-slot jet have three separate chambers, and each has an

individual plenum and valve to allow independent control of the plenum pressure of each slot. Compressed air from a 550 kPa blower was used to feed the auxiliary jets and the main slot was supplied with a resident 550 kPa compressed air line. For the main jet air was passed through a regulator and two filters to prevent any rust or particulates to get into the main slot. An electrical valve is also used right after the filter to adjust the main jet pressure using an in-house computer program. In the case of the auxiliary jets, the air supply was passed through a 5 cm regulator valve, a 5 cm ball valve and a 5 cm gate valve prior to entering a T manifold, where three 2.5 cm globe valves were used to adjust the pressure for each of the auxiliary slot. For all of the slots, air entered into each plenum *via* a 25.4 mm diameter pipe at the top of the plenum, passed through a flow distributor tube (Figure 6-2) and then passes through a series of mesh screens located upstream of the nozzle contraction in order to break up any large-scale turbulent structures (Figure 6-2). These screens comprised stainless steel cloth with a density of 28 wires/cm. Finally, air exited the slot at 90° to its inlet direction. To adjust the distance between the slot and the plate – i.e. the Z/D ratio – the prototype multi-slot jet was mounted on a computer controlled traverse system consisting of a VXM-3 Velmex™ power supply with a Slo-syn stepper motor with a minimum division of 5 μm. A Validyne DP-15 pressure transducer was used to measure the pressures in the plenums and the data was logged using a conventional data acquisition system and a LabVIEW program. The plenum pressure was measured at the centerline of each jet, upstream of the nozzle contraction.

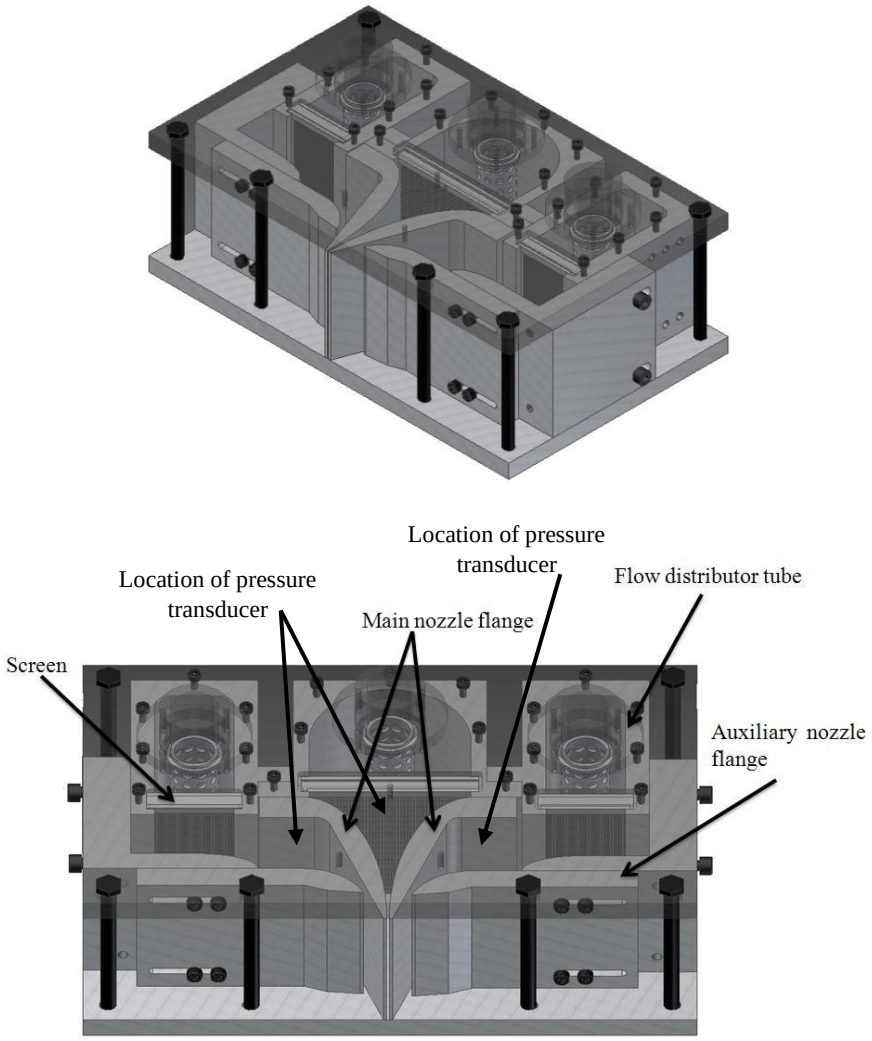

Figure 6-2) Isometric view of the multi-slot jet.

The molten zinc temperature commonly employed in the industrial continuous galvanizing process is 733 K (460°C). A cold laboratory scale model of the continuous galvanizing gas jet wiping process was designed and manufactured (Figure 6-3) with the objective of verifying the numerically modelled coating weights for the prototype multi-slot jet.

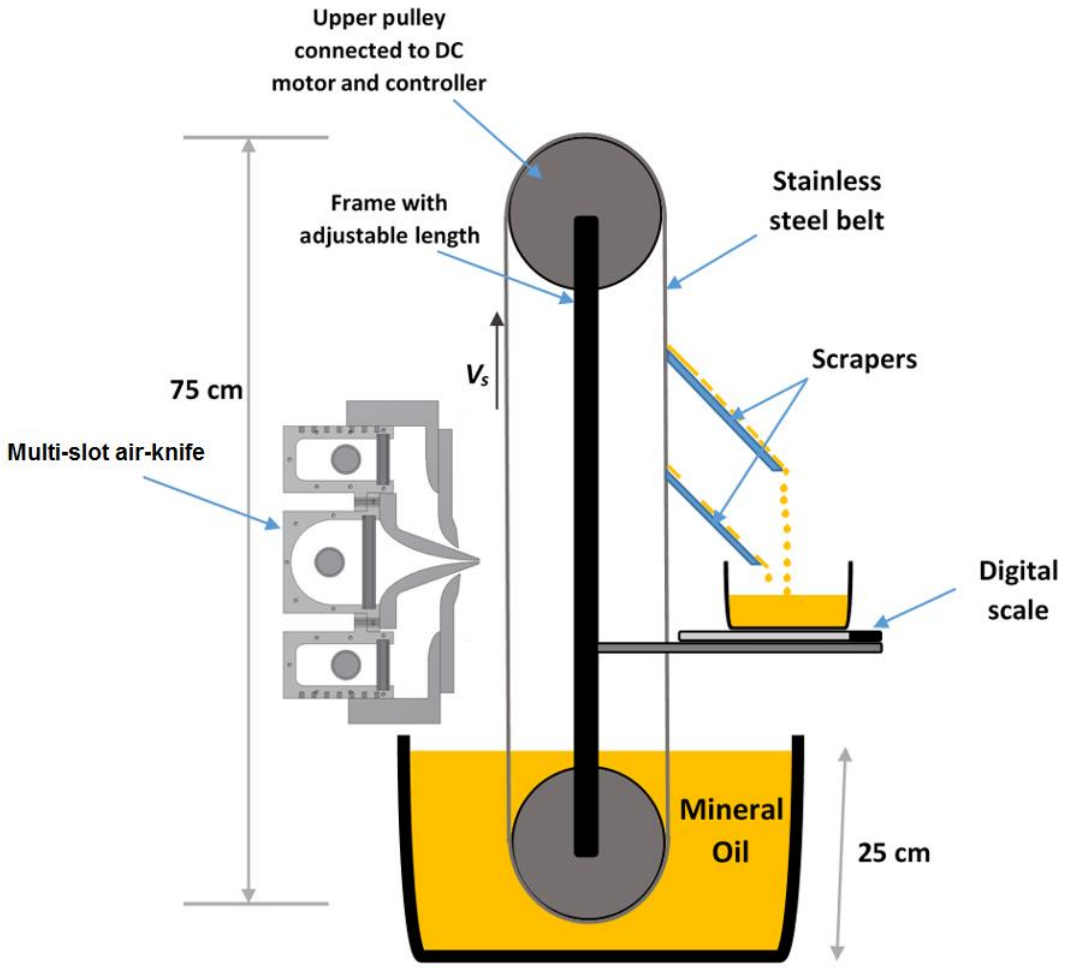

Figure 6-3) Schematic diagram of the experimental setup.

The apparatus consists of a vertical stainless-steel strip, 75 cm long and 5 cm wide, stretched between two rolls. An electric motor connected to the upper shaft and the upper roll provides the strip motion. The strip velocity can be adjusted in the range of 0.5-3.5 m/s by means of an AC to DC speed controller connected to the electric motor. The strip velocity was measured by means of optical and mechanical tachometers with an accuracy of ± 0.05 % and a resolution of 0.1 rpm (for the test range of 2 to 9999.9 rpm). The lower roll was designed to be adjustable to allow for the provision of adequate tension of the strip.

The lower roll was immersed in the model working fluid, mineral oil, the properties of which are documented in Table 6-1. The gas jet wiping devices tested using this apparatus were the single and multi-slot jet discussed in the previous section. The multi-slot jet are positioned 50 cm above the free surface of the liquid bath perpendicular to the strip. The air-knives were 5 cm longer than the strip width to avoid edge effects. The wiping mechanism was studied only on one side of the strip. To ensure good stability of the strip in the jet impingement region, the rear face of the strip slid on a rubber damper lubricated by the coating liquid. The main jet to substrate distances and strip velocities used in the experiments were $8 \leq Z/D \leq 12$ and $0.25 \leq V_s \leq 1.5$ m/s.

After the substrate passed the wiping region, the liquid film was removed by two inclined rubber blades or "squeegees". A digital balance with an accuracy of 0.01 g measured the mass of the collected liquid while the collection period was measured by a chronometer. The mean liquid film thickness, h_f, was determined through the mass flow rate of liquid removed from the strip during the collection period of 300 seconds using equation (6-1):

$$h_f = \dot{m}_{cl} / (\rho_{cl} L_s V_s) \tag{6-1}$$

An articulating arm was used to hold the microphone used for acoustics measurements in the desired location. A ½" GRAS pressure microphone was used for all testing in conjunction with a National Instruments 9233 USB based data acquisition card with 24-bit resolution and a hardware based anti-aliasing filter. All data was collected using LabView® in the form of amplitude spectra, power spectra and power spectral density at a sample rate of 25,000 Hz. Data was averaged using a linear averaging scheme for a total of 50 one

second averages. In addition, an integrated peak-hold type sound pressure level (SPL) meter was used to determine the maximum overall sound pressure level. Microphone calibration was performed using a G.R.A.S. Type 42 AB pressure calibrator prior to each day of measurements and the calibration was re-checked at the conclusion of a measurement set to ensure no drift had occurred.

The acoustic signal was acquired with a 40BP GRAS microphone and then it was amplified with a 26AB preamplifier and a 12AA power supply. The data acquisition for the experiments was performed using a National Instruments NI-4452 4 channel data card. A National Instruments LabView program was used for recording the data.

Each experiment repeated four times. According to Coleman and Steels [13], the overall uncertainty in dependent variable (r), which is function of j independent measured variable X_i can be found by using the Kline and McClintok method given as:

$$\delta r = \sqrt{\sum_{i=1}^{j} \left(\theta_i \left(\delta X_i\right)\right)^2} \tag{6-2}$$

Where $\theta_i = \frac{\partial r}{\partial X_i}$ and δX_i is the uncertainty for each measured variable. The uncertainty in the mean value of a measured X_i is given by $U_{X_i} = \sqrt{B_{X_i}^2 + P_{X_i}^2}$ where B is the instrumental error and P is random error. The random error was calculated through t-student distribution with 95% confidence level and instrumental error was found through manufacturers' specifications.

Table 6-1. Working liquid properties in the experimental facility [14].

Liquid	Density (kg/m^3)	Kinematic Viscosity (m^2/s)	Surface Tension (N/m)
Mineral Oil	865	10^{-5}	0.0323

6.5 Results and discussion

In this study, sound measurements were performed for jet to strip distances of $8 \leq Z/D \leq 16$, main jet Reynolds number of $20000 \leq Re_m \leq 24000$, auxiliary jet Reynolds number of $5000 \leq Re_a \leq 10000$ and strip velocity of $0 \leq V_s \leq 1.5$ m/s. The range for the main jet Reynolds number was selected to produce significant tone over the range of investigated parameters. The main jet width, D, and auxiliary jets width, D_a, were fixed at 1.5 mm. The auxiliary jets offset distances for these experiments were s = 10 mm. Figure 6-4 illustrates an acoustic spectrum of a single slot jet as a function of jet to strip distance (Z/D) for the strip velocity of V_s = 0.5 m/s and Re_m = 20000. As shown in Figure 6-4, there was a constant background sound pressure of 60 dB with a tonal noise which manifests itself as a sharp peak of high sound pressure level (acoustic intensity) generated for Z/D = 11, Z/D = 14 and Z/D = 15. For more clarification of noise spectrum of the single slot jet, Figure 6-5 illustrates acoustic intensity-frequency plots for $11 \leq Z/D \leq 15$. The tonal peak noises were clearly identifiable in Figure 6-5 at frequencies of approximately f = 4000, 3000 and 3000 reaching sound pressure levels of 89, 84 and 87 for Z/D = 11, Z/D = 14 and Z/D = 15, respectively.

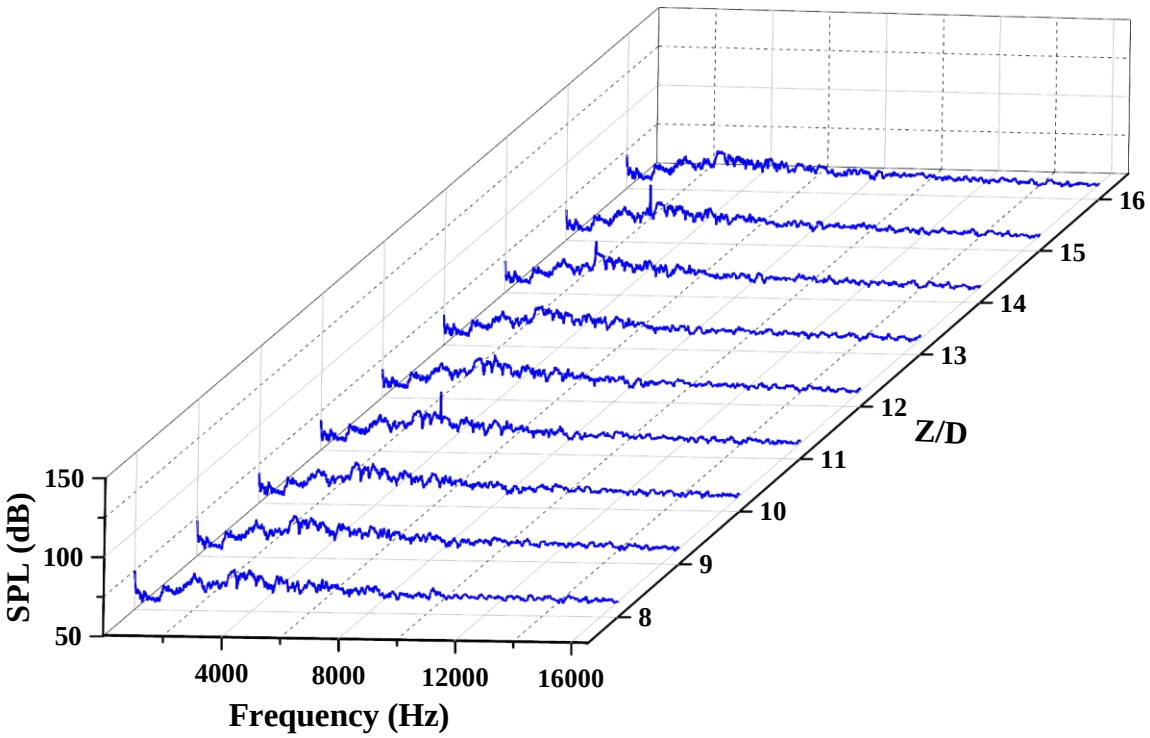

Figure 6-4) Sound pressure level of a single slot jet as a function of jet to strip distance (Z/D) for the strip velocity of V_s = 0.5 m/s and Re_m = 20000.

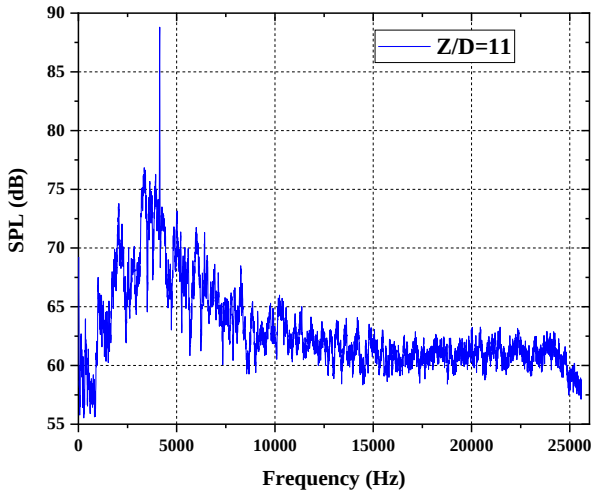

a)

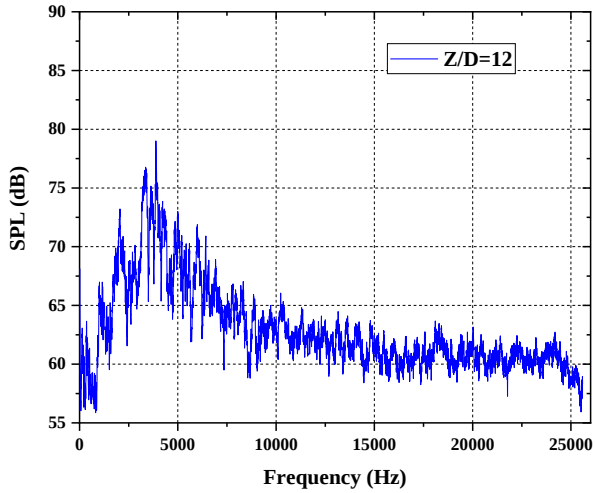
Z/D=12
SPL (dB)
Frequency (Hz)
90
85
80
75
70
65
60
55
0
5000
10000
15000
20000
25000

b)

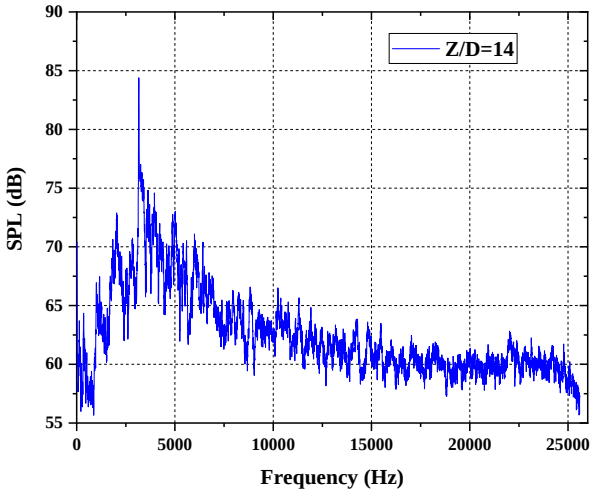
Z/D=14
SPL (dB)
Frequency (Hz)
90
85
80
75
70
65
60
55
0
5000
10000
15000
20000
25000

c)

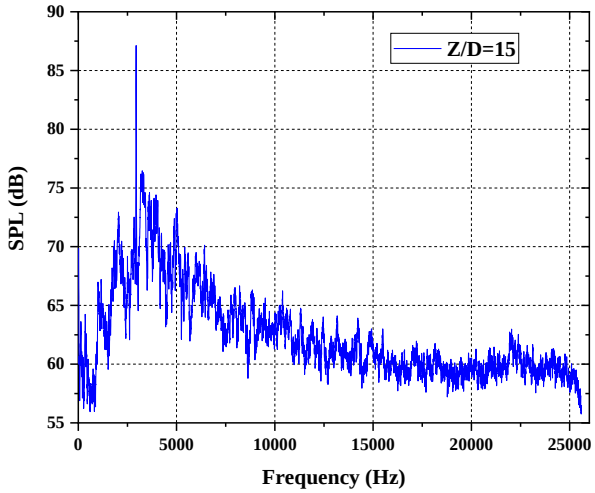

d)

Figure 6-5) Sound pressure level of a single slot jet for a) Z/D = 11, b) Z/D = 12, c) Z/D = 14 and Z/D = 15 at Re_m = 20000 and V_s = 0.5 m/s.

Figure 6-6 shows the sound intensity plots for the multi-slot jet with Re_m = 20000 m/s while the auxiliary jet was set at Re_a = 5000 m/s. Comparison of Figure 6-6 to the noise produced by single slot jet in Figure 6-5 revealed that the tonal peaks of single slot jet were completely eliminated by using multi-slot jet. This tonal suppression can be attributed to the decrease in growth rate of vortices, which are moving from the nozzle toward the strip [11]. The use of auxiliary jets at lower velocities compared the main jet, reduced the velocity differences of the main jet stream and the ambient air [10]. Therefore larger distances are needed for the coherent structures to be established and generate acoustic pressure waves once impinging on the strip [10]. The sound spectrum was also investigated for higher auxiliary jet Reynolds number of Re_a = 10000 as it is shown in Figure 6-7. It was

observed that tonal peaks of sound pressure level observed for the single jet in Figure 6-5, were completely suppressed (Figure 6-7).

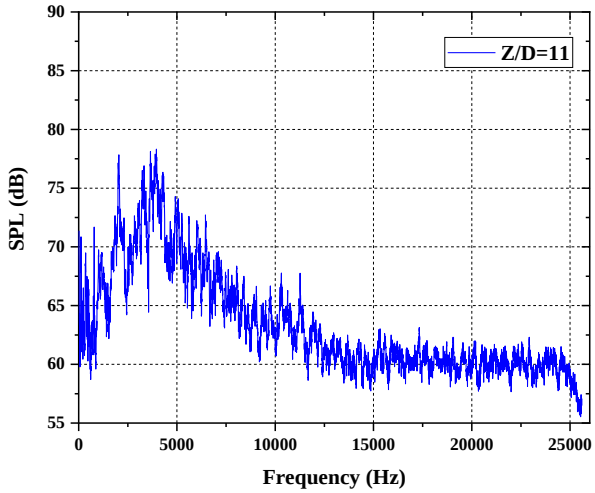

a)

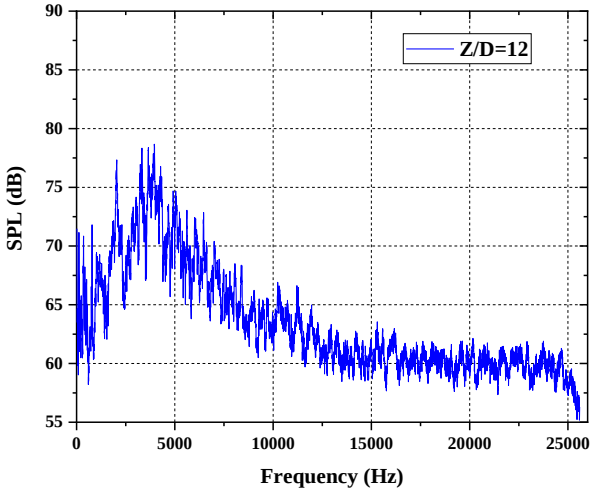

b)

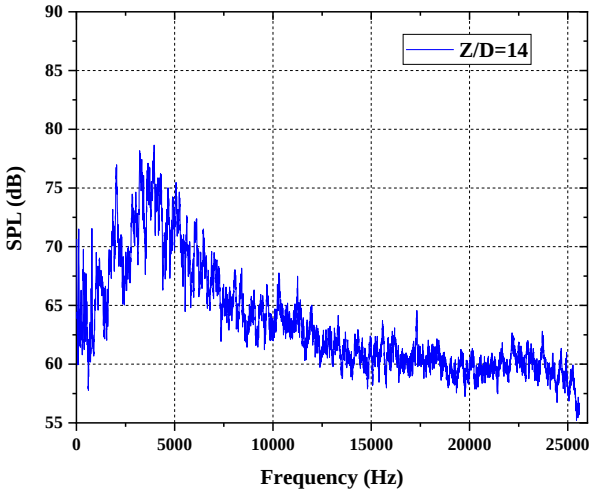

c)

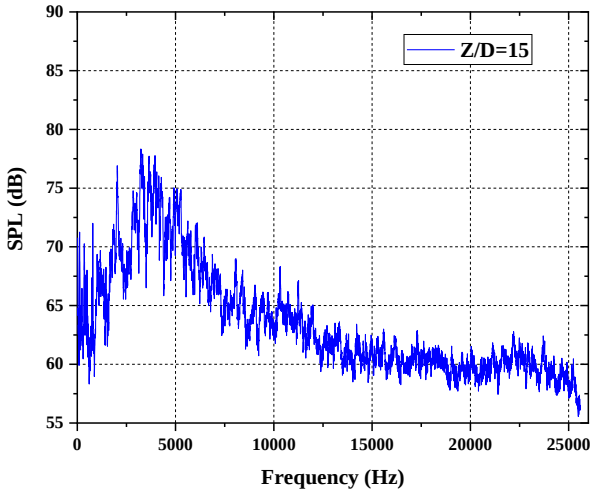

d)

Figure 6-6) Sound pressure level of the multi-slot jet for a) Z/D = 11, b) Z/D = 12, c) Z/D = 14 and Z/D = 15 at Re_m = 20000, Re_a = 5000 and V_s = 0.5 m/s with geometrical configuration of $D = D_a$ = 1.5 mm and s = 5 mm.

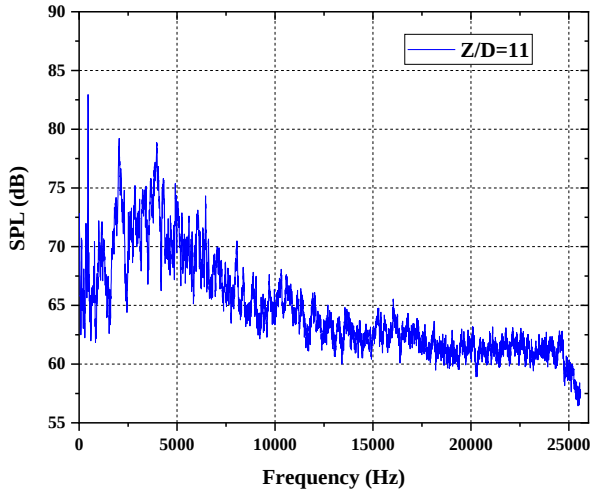
Z/D=11
SPL (dB)
Frequency (Hz)
90
85
80
75
70
65
60
55
0
5000
10000
15000
20000
25000

a)

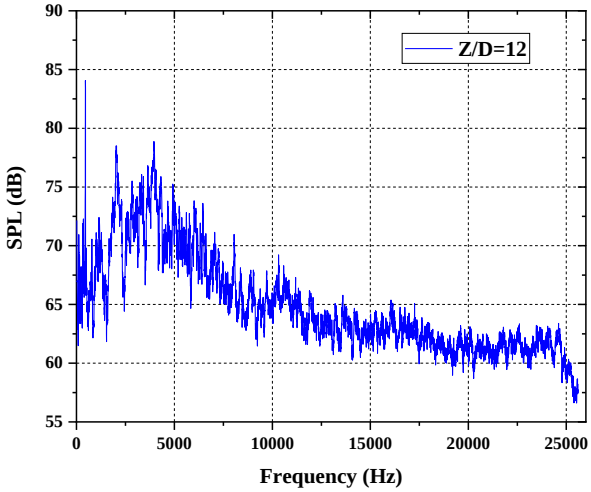
Z/D=12
SPL (dB)
Frequency (Hz)
90
85
80
75
70
65
60
55
0
5000
10000
15000
20000
25000

b)

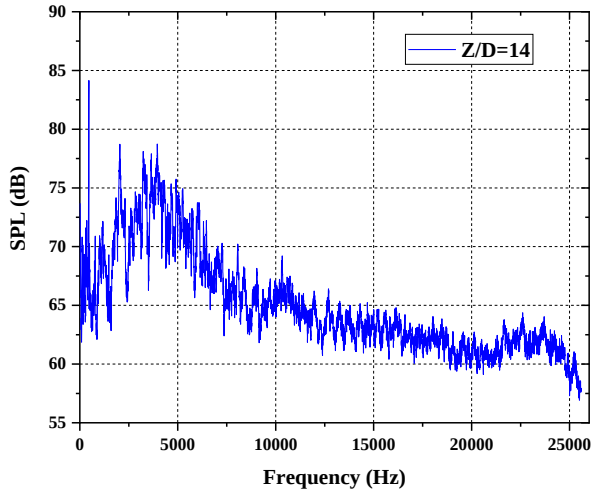

c)

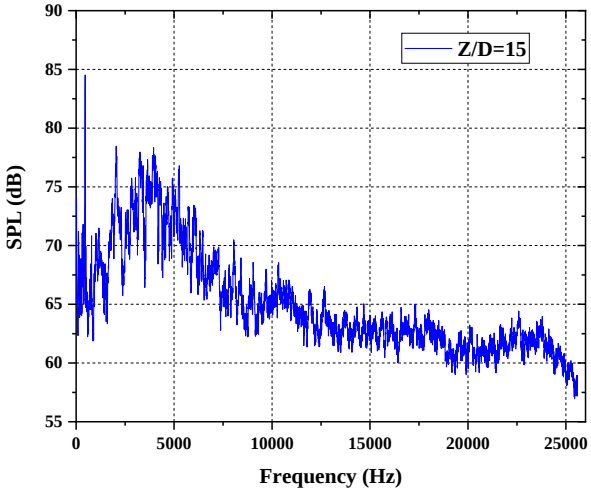

d)

Figure 6-7) Sound pressure level of the multi-slot jet for a) Z/D = 11, b) Z/D = 12, c) Z/D = 14 and Z/D = 15 at Re_m = 20000, Re_a = 10000 and V_s = 0.5 m/s with geometrical configuration of $D = D_a$ = 1.5 mm and s = 10 mm.

The experimental investigation on the acoustic pressure level of gas jet wiping process was also performed for higher main jet Reynolds number (Re_m). Figure 6-8 illustrates the sound spectrum of a single slot jet with the main jet Reynolds number of Re_m = 24000

impinging to the strip moving at velocity V_s = 0.5 m/s and for the jet to strip distances of 8 ≤ Z/D ≤ 16. As it can be seen from Figure 6-8, there were several harmonic series of high intensity tonal peaks for frequencies of less than 14 kHz with varying Z/D. It can also be observed that at Re_m = 24000, high intensity tonal noises were generated even at low jet to strip distances (Z/D ≤ 9) which was not the case for lower main jet Reynolds number of Re_m = 20000 discussed in Figure 6-5. This can be explained with the increased velocity difference between the main and auxiliary gas streams. In this case, vortices can obtain the coherence required to generate acoustic pressure wave at shorter distances and therefore, tonal noise can be exists at lower jet to strip distances [9]. The effect main jet Reynolds number is shown with further clarification in Figure 6-9 which compares the sound pressure level spectrum of a single slot jet for three different main jet Reynolds numbers of Re_m = 20000, 22000 and 240000 at V_s = 0.5 m/s and Z/D = 8, 12 and 15. According to Figure 6-9, the tonal peaks were present at lower jet to strip distance (i.e. Z/D = 8) only at higher main jet Reynolds numbers and decreasing the main jet Reynolds number, delayed onset of tonal noise generation to higher wall to jet distances.

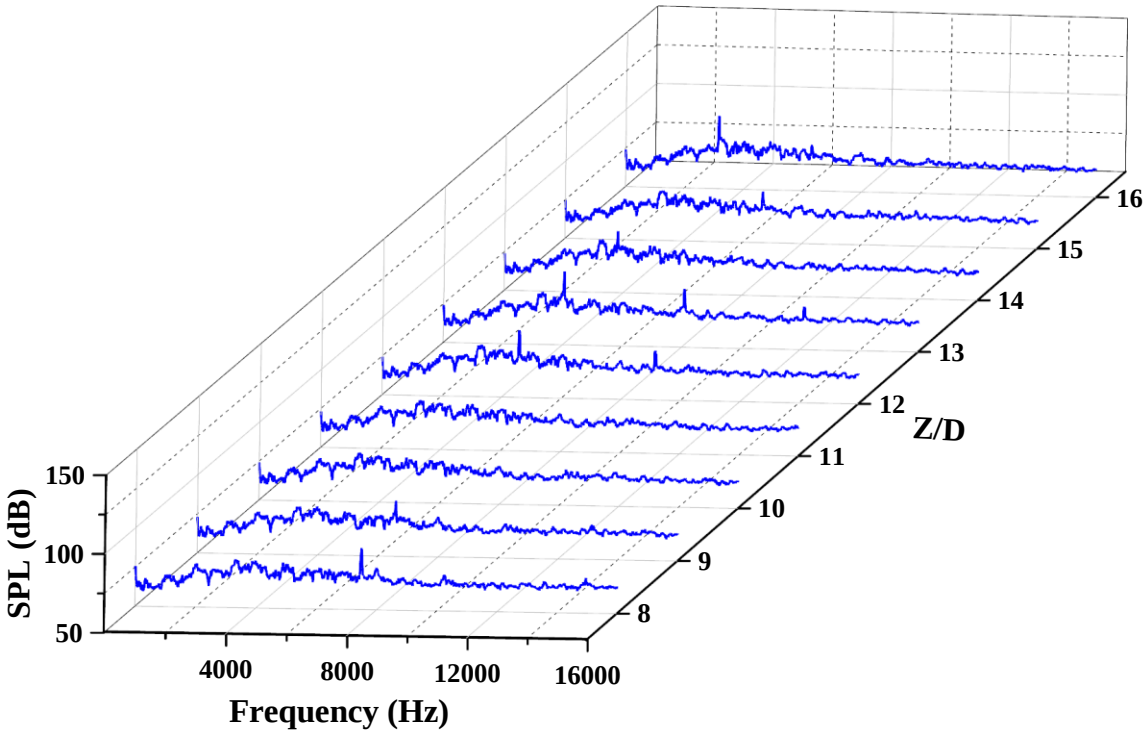

Figure 6-8) Sound pressure level of a single slot jet as a function of jet to strip distance (Z/D) for the strip velocity of V_s = 0.5 m/s and Re_m = 24000.

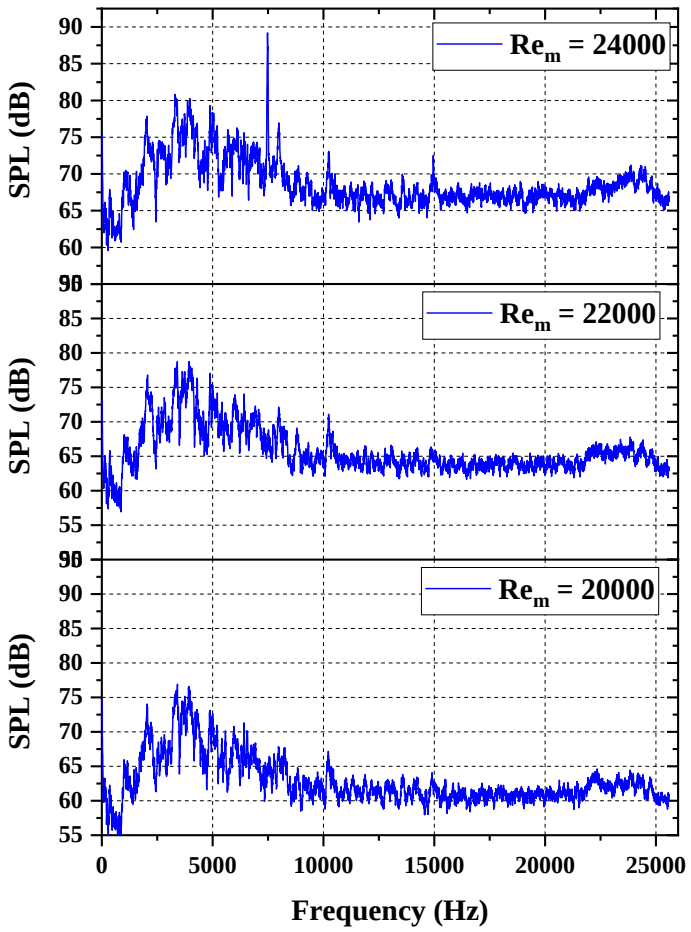
Re$_m$ = 24000
Re$_m$ = 22000
Re$_m$ = 20000
SPL (dB)
Frequency (Hz)
0
5000
10000
15000
20000
25000

a)

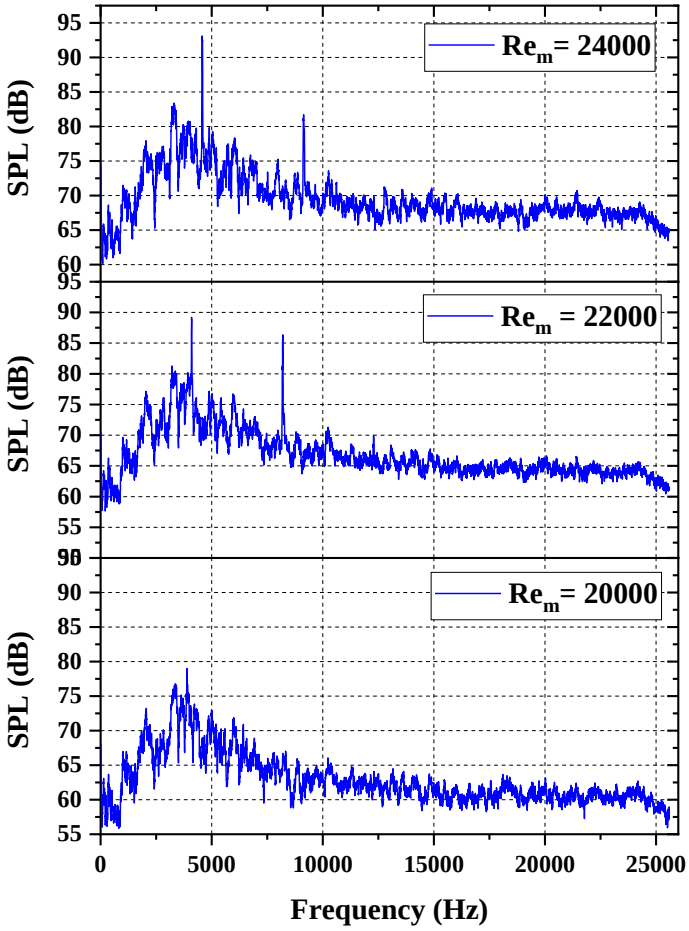
Re$_m$= 24000
Re$_m$ = 22000
Re$_m$= 20000
SPL (dB)
Frequency (Hz)
0
5000
10000
15000
20000
25000

b)

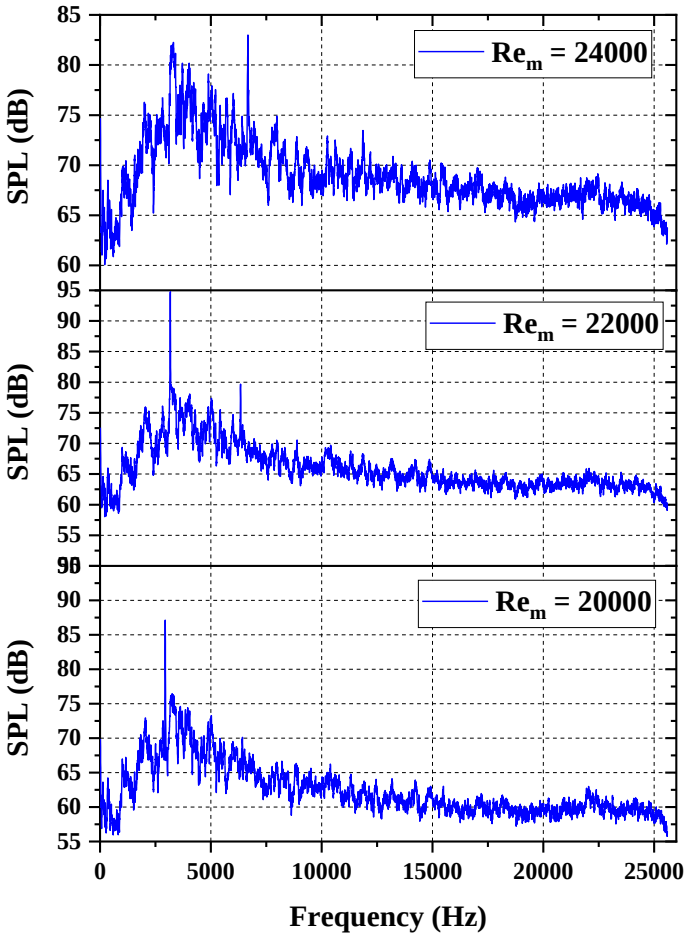

c)

Figure 6-9) Sound pressure level spectrum of a single slot jet for $20000 \leq Re_m \leq 240000$ at V_s =0.5 m/s and a) Z/D = 8, b) Z/D = 12, c) Z/D = 15.

Effect of auxiliary jets on the sound pressure level spectrum at a main jet Reynolds number of Re_m = 24000 is shown in Figure 6-10 for the auxiliary jet Reynolds number of Re_a= 5000, V_s = 0.5 m/s and $8 \leq Z/D \leq 16$. As it is shown in Figure 6-10, there was a constant background sound pressure of 60 dB with a tonal noise which manifests itself as a sharp peak of high sound pressure level (acoustic intensity) generated for Z/D = 11, Z/D = 14 and Z/D = 15. It can be seen that the tonal noise observed for the single jet (Figure 6-8) is completely eliminated for all the jet to strip distances.

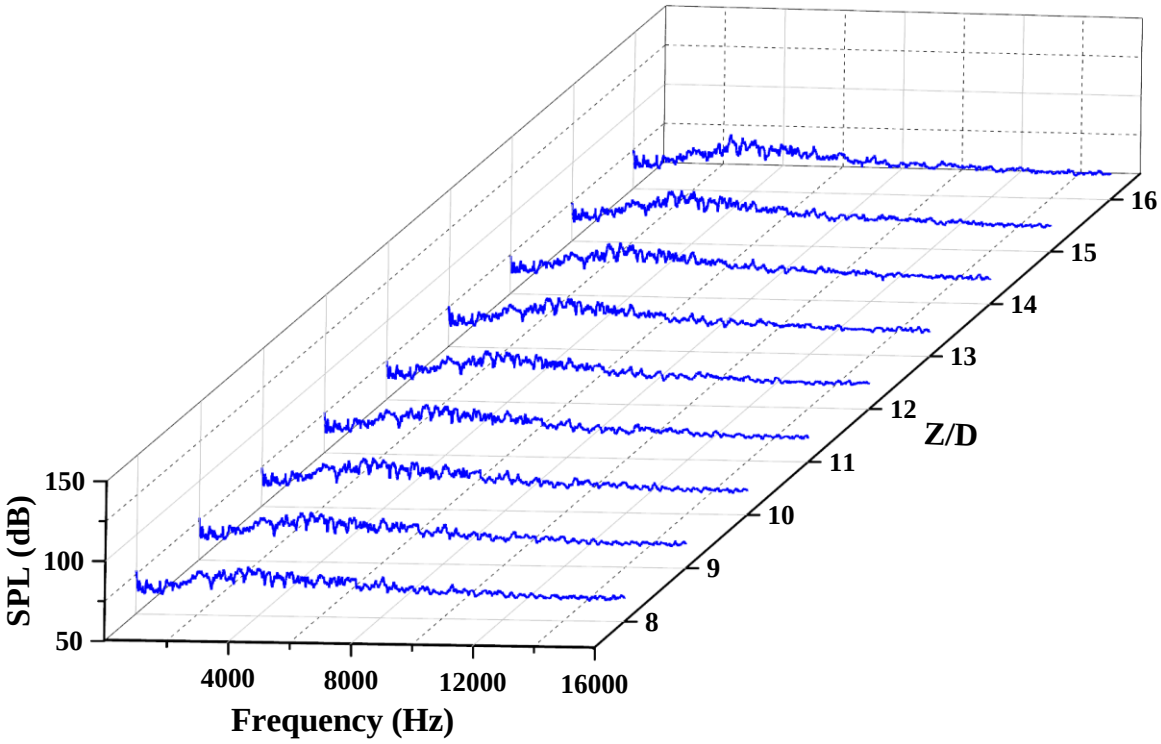

Figure 6-10) Sound pressure level of the multi-slot jet as a function of jet to strip distance (Z/D) for Re_m = 24000, Re_a = 5000 and V_s = 0.5 m/s with geometrical configuration of D = D_a = 1.5 mm and s = 10 mm.

The experiments were also run for different strip velocities (V_s). Figure 6-11 shows acoustic intensity spectrum for the single slot jet with Z/D = 15, Re_m = 20000 and $0 \leq V_s \leq$ 1.5 m/s. As it can be seen from Figure 6-11, the tonal peak noise presented for all the investigated strip velocities with highest amount of 90 dB at frequency of f = 3000 Hz for V_s = 0. The tonal noise with the same frequency was observed for higher strip velocities, however, the highest sound pressure level is slightly lower compared with when V_s = 0. Figure 6-12 shows sound pressure level spectrum for the multi-slot jet at Re_m = 20000, Re_a = 5000 and Z/D = 15 for $0 \leq V_s \leq$ 1.5 m/s. It can be seen from Figure 6-12 that the elimination of tonal noise happened for all the investigated strip velocities in this study through use of multi-slot jet.

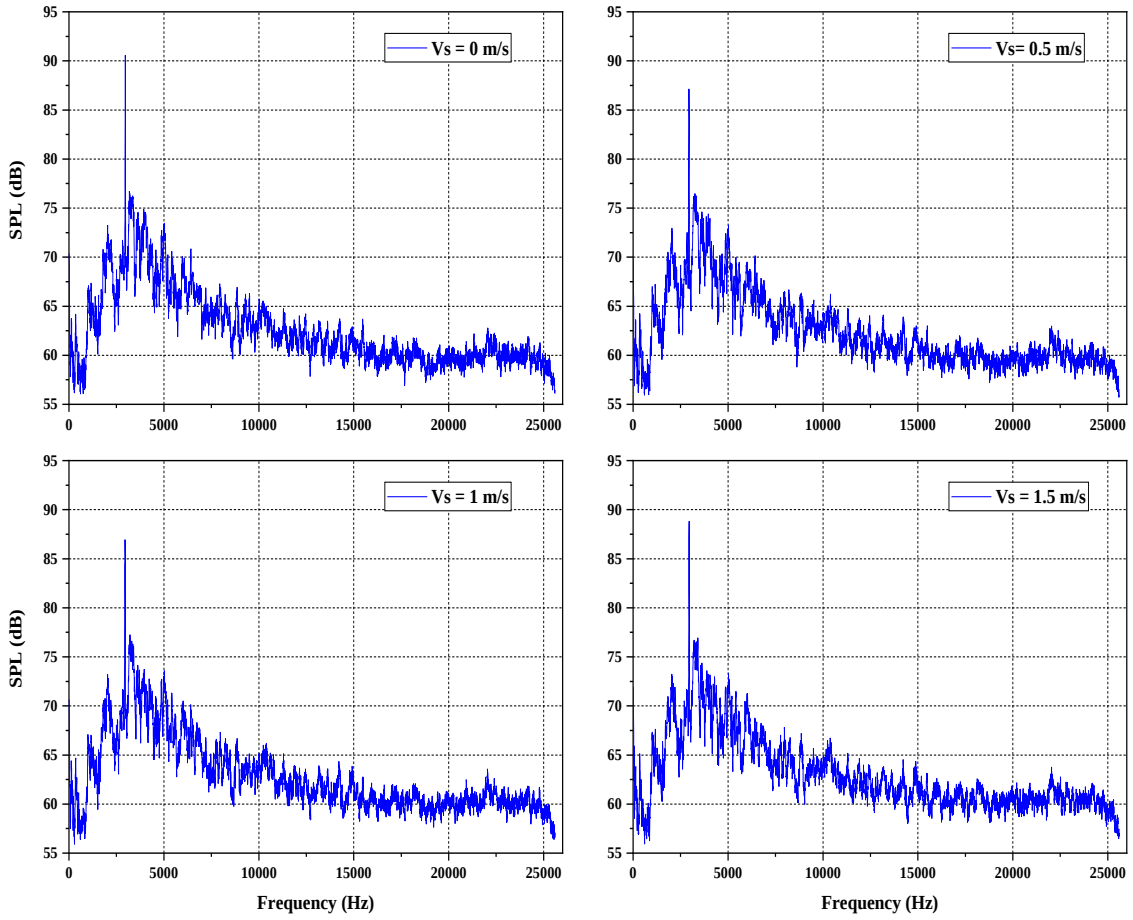

Figure 6-11) Sound pressure level spectrum of a single slot jet for Re_m = 20000 at Z/D = 15 and $0 \leq V_s \leq 1.5$ m/s.

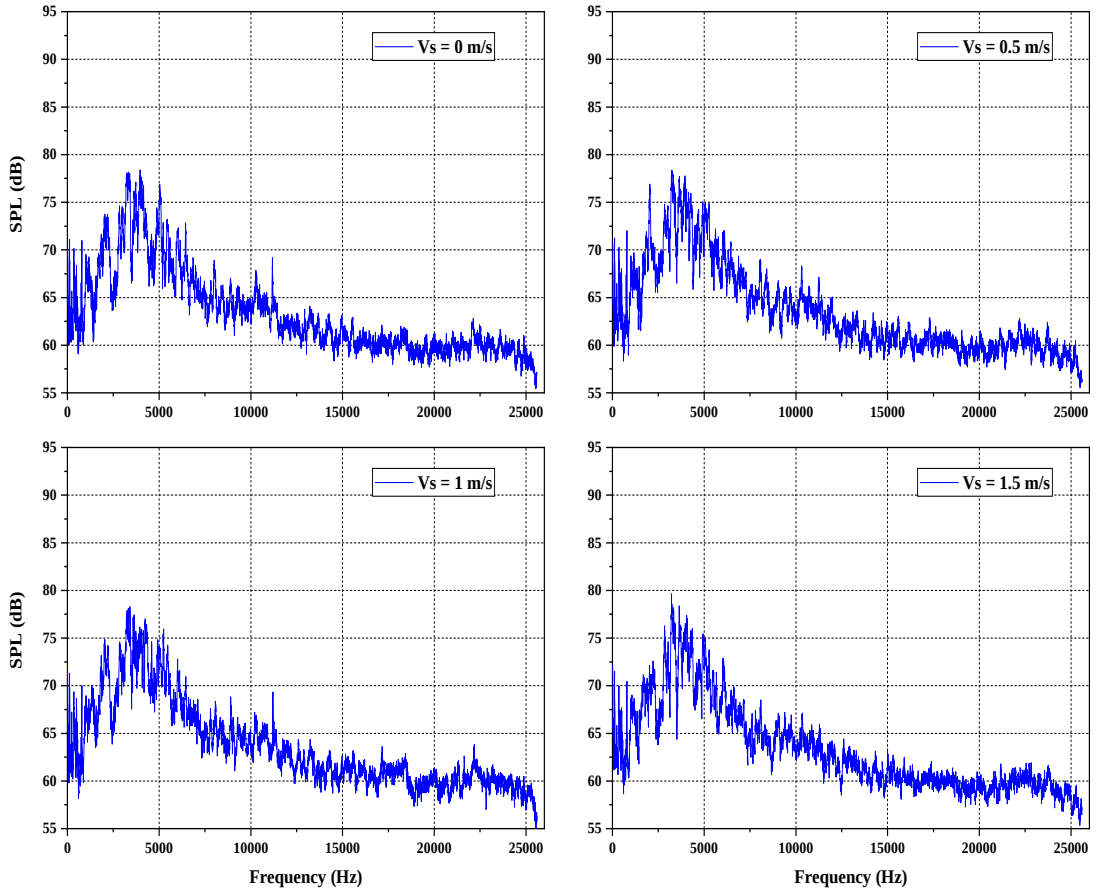

Figure 6-12) Sound pressure level spectrum of the multi-slot jet for Re_m = 20000, Re_a = 5000 at Z/D = 15 and $0 \leq V_s \leq 1.5$ m/s with geometrical configuration of $D = D_a$ = 1.5 mm and s = 10 mm.

Figure 6-13 compares the effect of auxiliary jet Reynolds number (Re_m) at different strip velocities (V_s). By comparing Figure 6-11 and Figure 6-13, it can be seen Figure 6-13 that for all the cases, the sharp peak observed for the single slot jet at f = 3000 Hz was eliminated through use of auxiliary jets for both of Re_a = 5000 and Re_a = 10000, however, a tonal noise at very low frequency of f = 250 Hz generated for Re_a = 10000 which was not observed for Re_a = 50000.

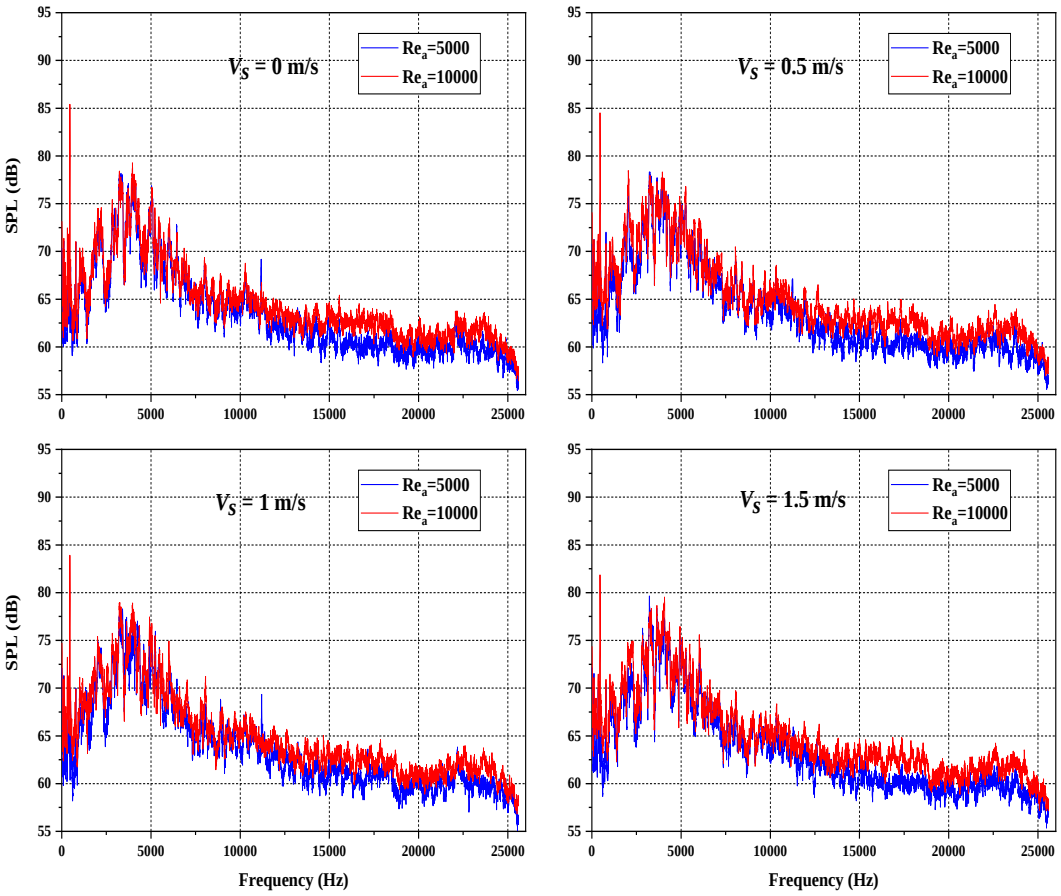

Figure 6-13) Sound pressure level spectrum of the multi-slot jet for Re_m = 20000, 5000 ≤ Re_a ≤ 10000, Z/D = 15 and 0 ≤ V_s ≤ 1.5 m/s with geometrical configuration of D = D_a = 1.5 mm and s = 10 mm.

In the next step, the prototype of multi-slot jet shown in Figure 6-2 was used to determine coating thickness reduction. The effect of the plate-to-nozzle ratio (Z/D), for Z/D =12 and Z/D =15 with main jet Reynolds number of Re_m = 20000, auxiliary slot jets Reynolds number of 5000 ≤ Re_a ≤ 10000 and 0.5 ≤ V_s ≤ 1.5 m/s, on the final coating weight will be discussed. The main jet width (D), auxiliary jet width (D_a) and the auxiliary jet offset (s)

were fixed at D = 1.5 mm, D_a = 1.5 mm (i.e. D_a/D = 1) and s = 10 mm, as it has been previously shown by the present authors that this configuration of multi-slot jet leads to lighter coating weight compared to the traditional single slot jet ([15], [16]).

Figure 6-14 compares the experimentally measured coating weights via single slot jet with multi-slot jet data as a function of strip velocity (V_s) at Z/D = 12, Re_m = 20000 and auxiliary jet Reynolds number of Re_a = 5000. According to Figure 6-14, no significant differences were observed between the coating weights obtained via multi-slot jet and the single slot jet data at Z/D = 12.

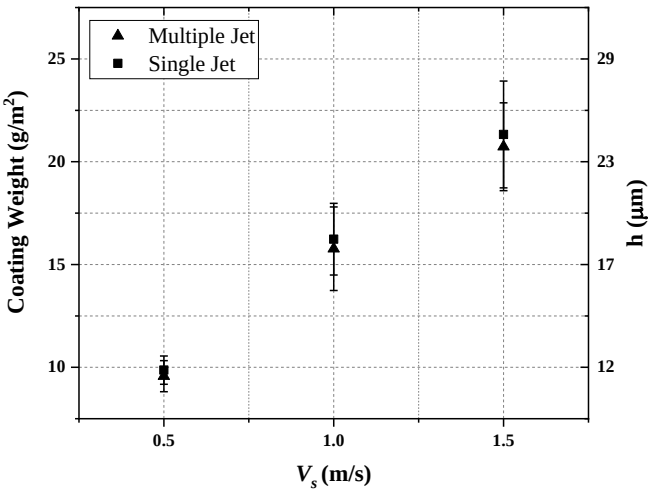

Figure 6-14) Comparison of experimentally measured coating weight for multi-slot jet at different strip velocities, Re_m = 20000, Z/D = 12, D = 1.5 mm, D_a = 1.5 mm and s = 10 mm for a) Re_a = 5000 and b) Re_a = 10000 with single slot jet at Re_m = 20000, D = 1.5 mm and Z/D = 12.

The experiments were also performed for higher jet to strip distance of Z/D = 15. Figure 6-15 shows coating weight obtained through use of single slot jet and multi-slot jet as a

function of strip velocity (V_s) at Z/D = 15, Re_m = 20000 and auxiliary jet Reynolds number of 5000 ≤ Re_a ≤10000. According to Figure 6-15, by having a relatively low auxiliary jet Reynolds number such that ($Re_a/Re_m \leq 0.5$) lower coating weights at higher strip velocity (Vs) can be obtained by using multi-slot jet compared to the single slot jet. This can be attributed to the higher pressure gradient and the higher wall shear stress in the wiping region for $Re_a/Re_m \leq 0.5$ which explained by Yahyaee et al. [16].

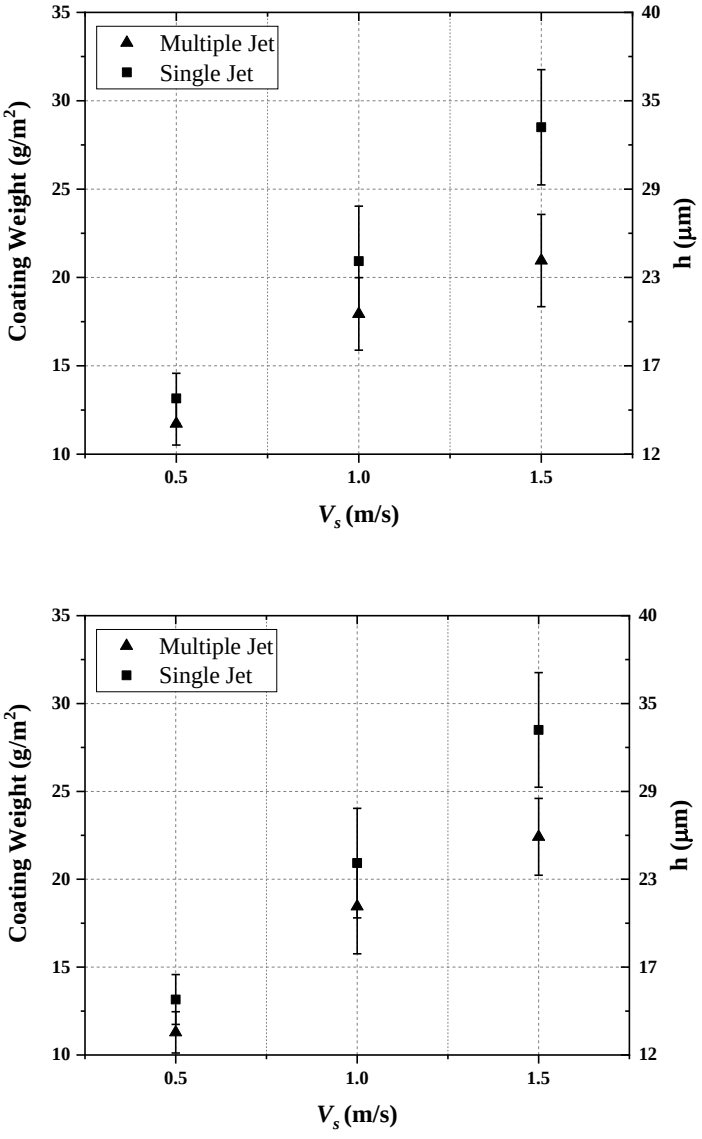

Figure 6-15) Comparison of experimentally measured coating weight for multi-slot jet at different strip velocities, Re_m = 20000, Z/D = 15, D = 1.5 mm, D_a = 1.5 mm and s = 10 mm for a) Re_a = 5000 and b) Re_a = 10000 with single slot jet at Re_m = 20000, D = 1.5 mm and Z/D = 15.

6.6 Acknowledgment

The authors gratefully acknowledge the financial support of the International Zinc Organization Galvanized Autobody Partnership (IZA-GAP) members, Arcelor Mittal Dofasco Global R&D Hamilton and the Natural Sciences and Engineering Research Council of Canada (NSERC, grant CRDPJ 446105-2012).

6.7 Conclusions

In the current study effect of auxiliary jets on coating thickness reduction and noise elimination during gas jet wiping process was experimentally investigated. It was observed that for the single jet wiping there is high tonal noise in the human audible range which can be a risk for the workers' health and safety. The experiments were performed under various operating conditions such as main jet Reynolds number (Re_m), Auxiliary jet Reynolds number (Re_a), jet to strip distance (Z/D) and strip velocity (V_s).

This study shows that the tonal noise generated in single jet wiping can be either attenuated or eliminated through the use of auxiliary jets especially when auxiliary jets velocity is a fraction of the main jet velocity such that ($Re_a/Re_m \leq 0.5$). The coating thickness measurements were performed under the same operating conditions and it was observed a lighter coating thickness can be achieved by using multi-slot jet as the wiping

actuator in gas jet wiping process. Therefore, despite its more complicated geometry can be operated with benefit to lower coating weights and noise elimination. This has positive implications for both industrial hygiene and impart additional wiping energy to the coating, thereby allowing for further reductions of coating weight versus the traditional single-slot jet design.

6.8 References

[1] D. Arthurs and S. Ziada, J. Can. Acoust. Assoc., vol. 35, no. 3, pp. 28–29, 2007.

[2] M. Dubois, in Galvatech 2011 Conference Proceedings: HDG Process Technologies, 2011, pp. 1847–1859.

[3] A. M. Petrie, Appl. Acoust., vol. 7, no. 2, pp. 117–126, 1974.

[4] J. A. Thornton and H. F. Graff, Metall. Trans. B, vol. 7, no. 4, pp. 607–618, 1976.

[5] J.-R. Park, Ironnmaking Steelmak., vol. 28, no. 1, pp. 53–57, 2001.

[6] M. Dubois, Part 1. & Part 2. Galvanizers Meeting- 2001. ILZRO, 2001.

[7] N. S. Nosseir and C. M. Ho, J. Fluid Mech., vol. 116, pp. 379–391, 1982.

[8] C. M. Nossier, S. M., Ho, J. Fluid Mech., vol. 105, pp. 119–142, 1981.

[9] D. Finnerty, J. McDermid, S. Ziada, and F. Goodwin, AISTech 2016 Proc., no. 905, pp. 2075–2082, 2016.

[10] D. Finnerty, J. McDermid, F. Goodwin, and S. Ziada, in Galvatech 2017: 11th International Conference on Zinc and Zinc Alloy Coated Steel Sheet, 2017, pp. 307–313.

[11] J. R. McDermid, D. Finnerty, S. Ziada, and F. E. Goodwin, in 109th Meeting of the Galvanizer's Association, 2017.

[12] D. Arthurs and S. Ziada, J. Fluids Struct., vol. 34, pp. 236–258, 2012.

[13] H. W. Coleman and W. G. Steele, Experimentation and Uncertainity Analysis for Engineers, Second Ed. JOHN WILEY & SONS, INC., 1999.

[14] Michael J Neale, The Tribology Handbook, Second Ed.. Oxford: Butterworth-Heinemann, 1995.

[15] A. Yahyaee Soufiani, J. R. McDermid, A. N. Hrymak, and F. E. Goodwin, J. Coatings Technol. Res., vol. 14, no. 5, pp. 1015–1028, 2017.

[16] A. Y. Soufiani, J. R. McDermid, A. N. Hrymak, and F. E. Goodwin, Metall. Mater. Trans. B Process Metall. Mater. Process. Sci., 2019 (DOI: 10.1007/s11663-019-01666-1).

Chapter 7: Global Discussion

The results presented in the papers that formed Chapters 3 to 6 were discussed in detail in each chapter. The current chapter contains a brief, global discussion to integrate the results of each of these chapters within the context of the global objective of this thesis, focussing on the effects of the multi-slot air knife geometry and the wiping operating conditions on the wall pressure profile, shear stress distribution and final coating thickness.

The sensitivity of the wall pressure and shear stress distributions to multi-slot air knife geometry changes were first determined through numerical simulations. For validation purposes, the numerical results were benchmarked against the experimental measurements of Ellen and Tu [15], Alibeigi et al. [48], [50] and Ritcey et al. [51] (Figures 3-3,3-4, 3-5, 4-3, 4-4, 5-3 and 5-4). It was shown that the CFD results were in good agreement with the experimental data.

The simulations were then expanded to study the effect of flow and air knife geometric parameters in order to determine the air knife parameters required to produce lighter coating weights versus the traditional single slot air knife design. The effects of various geometric parameters such as auxiliary jet width (D_a), distance between the main jet and auxiliary jet (a) exits, auxiliary jet offset distance (s) and inclination angle of the auxiliary jets (θ) were numerically investigated. A schematic of the above parameters, as applied to the current multi-slot air knife, are provided in Figure 7-1 as a reminder to the reader. The traditional model of a single slot jet was used as a base case for comparing the wall pressure results, wall shear stress distributions and the coating weight on the moving substrate.

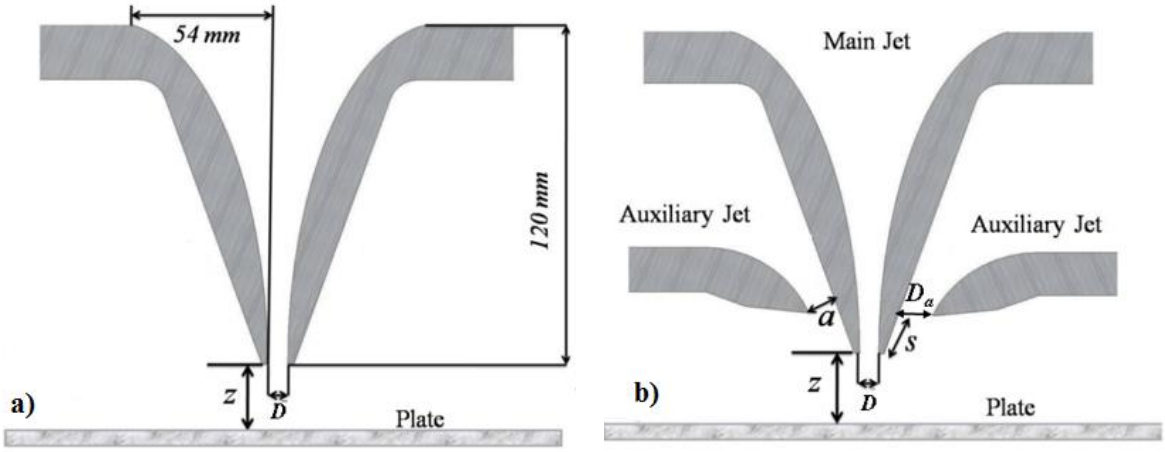

Figure 7-1) Schematic of a) the single and b) multi-slot air-knife geometries.

Comparison of the numerically obtained wall pressure profiles for different auxiliary jet widths showed that the wall pressure profile was sensitive to changes in the auxiliary jet width (D_a) (Figures 3-9, 4-11). It was determined that, by decreasing the auxiliary jet width (D_a), a sharper pressure profile could be achieved. Thus, decreasing the auxiliary jet width led to an increased wall pressure gradient and wall shear stress in the vicinity of the wiping region (Figures 3-11, 4-12a, 4-12b). By applying the wall pressure and shear stress distributions in the analytical model of Elsaadawy et al. [1], it was determined that, in the range of the experimentally explored strip velocities ($0.25 \leq V_s \leq 1.5$ m/s), by using the multi-slot air-knife with $D_a/D \leq 1$, lower coating weights (up to 4.7%) could be achieved versus the traditional single slot air knife (Figure 7-2).

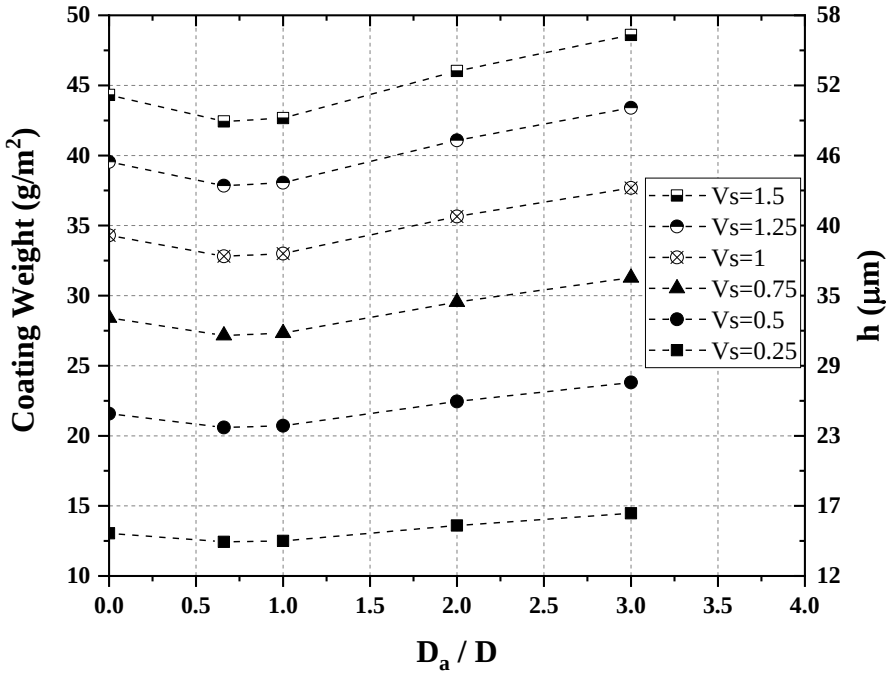

Figure 7-2) Effect of auxiliary jet width on final coating thickness as a function of strip velocity for Z/D = 12, Re_m = 11000, Re_a = 5000 and s = 10 mm.

Also, it was shown that decreasing the distance between the main jet and auxiliary jet exit (a) led to a higher wall pressure gradient (Figure 3-13) with lower coating weights being obtained for $a/D < 1$. However, it should be noted that $a/D < 1.5$ was maintained for all of the experiments documented in chapter 4 where lower coating weights were obtained versus the single slot design. Thus, it can only be concluded that $a/D < 1.5$ should be maintained for the multi-slot air knife.

For the range of geometric and operating parameters studied, the effect of auxiliary jet offset distance (s) did not significantly affect the wall pressure and shear stress distributions and, consequently, the final coating weights (Figures 3-14, 4-15 and 4-16). For the inclination angle (θ) at which the main and auxiliary jet centerlines were coincident at a

same point on the impingement wall, the highest maximum wall pressure was obtained (Figure 3-12). Thus, the optimum inclination angle for the auxiliary jets for a given air knife geometry and *Z/D* can be found through Equation (7-1):

$$\theta = \text{Arctan}\left(\frac{\frac{a}{D} + \frac{D_a}{2D} + \frac{1}{2}}{\frac{Z}{D}} \right) \tag{7-1}$$

Based on the above results, a modified geometry for the multi-slot air-knife was proposed and this configuration was then used as the wiping actuator in a more extensive parametric investigation of the multi-jet design. The shear stress and pressure gradient distributions were used in the analytical model developed by Elsaadawy et al. [1] (discussed in section 3.4) to estimate the coating thickness under various operating conditions.

With the objective of validating the numerically modelled coating weights for the multi-jet air knife configuration, a cold laboratory-scale model of the continuous galvanizing multi-slot gas jet wiping process was designed, manufactured (Figure 4-6) and tested. The prototype multi-slot air knife (Figure 4-5) was used as the wiping actuator in the wiping apparatus. Experimental measurements were benchmarked against the analytical coating models of Thornton and Graff [14] and Elsaadawy et al. [1] for a free meniscus coating, single gas jet and multi-slot jet wiping. It was determined that for all parameters explored (i.e. D_a, s, Re_m, Re_a, Z/D and V_s) the experimentally measured final coating weights compared favorably with the corresponding predictions of the analytical models (Figures 4-7, 4-8, 4-9, 4-10, 4-14, 5-7, 5-14). Therefore, the applicability of the Elsaadawy et al. [1] model for prediction of the final coating thickness for the multi-slot air knife was determined.

The experimental measurements and numerical simulations were then expanded to identify the operating window in which lighter coating weights can be achieved with the multi-slot air knife at higher strip velocities. The effect of the plate-to-nozzle ratio (*Z/D*), which ranged between 6 and 12, the main jet Reynolds number, Re_m, which ranged between 7000 and 24000, and the auxiliary slot jets Reynolds number, Re_a, which ranged between 3000 and 10000, on the final coating weight were investigated.

It was found that at each strip velocity, through the use of the multi-slot air knife, lower coating weights could be achieved compared to the conventional single slot jet for $Z/D > 8$ (Figures 3-19, 5-20). It was shown that, using the multi-slot air knife at $Z/D > 8$ led to a higher maximum pressure gradient and maximum shear stress compared to that of the single slot jet (Figure 3-18). This was justified based on the length of the potential core of the main jet and wall to air-knife distance (*Z/D*) (Figures 3-15, 3-16 and 3-17). For the single slot jet at $Z/D > 8$, since the potential core was absorbed before impingement, there would be a significant decrease in the maximum wall pressure versus the low *Z/D* case where the potential core was impinging on the wall. It was shown that by using the multi-slot configuration the momentum loss of the main jet was decreased as the auxiliary jet flow merged with that of the main jet. The merged jet with a higher momentum resulted in a higher pressure gradient and shear stresses at the coating surface and, consequently, the coating thickness decreased for the multi-slot jet.

It was also determined that, for the range of strip velocities explored ($0.5 \leq V_s \leq 1.5$ m/s) and the investigated main jet Reynolds numbers ($7000 \leq Re_m \leq 24000$), there was an operating window at lower auxiliary jet Reynolds numbers of $Re_a/Re_m \leq 0.5$, which led to

lighter coating weights for wiping with multi-slot air knife in comparison with the conventional single slot jet geometry (Figures 3-21, 3-24, 4-17, 5-12, 5-15, 5-16, 6-15). Figure 7-3 illustrates the non-dimensional predicted final coating thickness (h_m/h_s) as a function of Re_a for the strip velocities of $0.5 \leq Vs \leq 1.5$ m/s and Rem = 11000 where Da/D = 1 for all experiments. In Figure 7-3, h_m and h_s represent the predicted final coating thickness for the multi-slot and single-slot jets, respectively. As can be seen from Figure 7-3, there was an operating window at $Re_a/Re_m \leq 0.5$ for the multi-slot air knife working at $Re_m = 11000$ which resulted in lower coating weights compared to the single slot jet (i.e. $h_m/h_s < 1$). Similar trends were observed for the range of main jet Reynolds numbers investigated ($7000 \leq Re_m \leq 24000$).

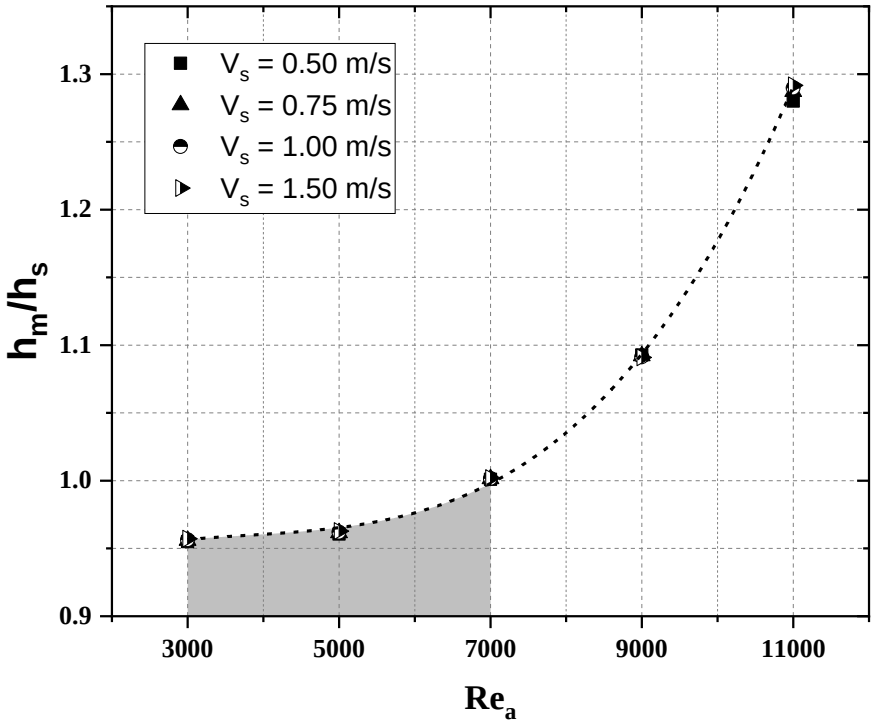

Figure 7-3) Predicted final coating weight using the Elsaadawy et al. model [1] as a function of Re_a for Re_m = 11000, Z/D = 12, D = 1.5 mm, D_a = 1.5 mm and s = 10 mm and $0.5 \leq V_s \leq 1.5$ m/s.

The findings summarized in Figure 7-3 were attributed to the wall pressure profiles at lower auxiliary jet Reynolds numbers (i.e. $Re_a/Re_m \leq 0.5$) being found to be sharper compared to that of the single slot jet .Thus, in the vicinity of wiping region, higher values of the pressure gradient and wall shear stress could be achieved by using the multi-slot air knife (Figures 3-20, 3-22, 5-9, 5-10, 5-17 and 5-18), which resulted in lower coating weights. Conversely, a wider wall pressure profile was found when the auxiliary jet Reynolds number approached that of main jet (i.e. $Re_a/Re_m \geq 0.8$) for the range of studied main jet Reynolds numbers ($7000 \leq Re_m \leq 24000$) . Consequently, lower values of the wall

pressure gradient and wall shear stress were found in the wiping region, which led to higher coating weights (Figures 3-24, 5-8 and 5-11).

By analyzing the input energy of the jets (Equation 5-11), it was determined that at relatively low wiping energy ratios over that of the conventional single slot jet {$E_{Total}/E_{main} \leq 1.05$), lighter coating weights could be achieved through use of the multi-slot air knife (Figure 7-4).

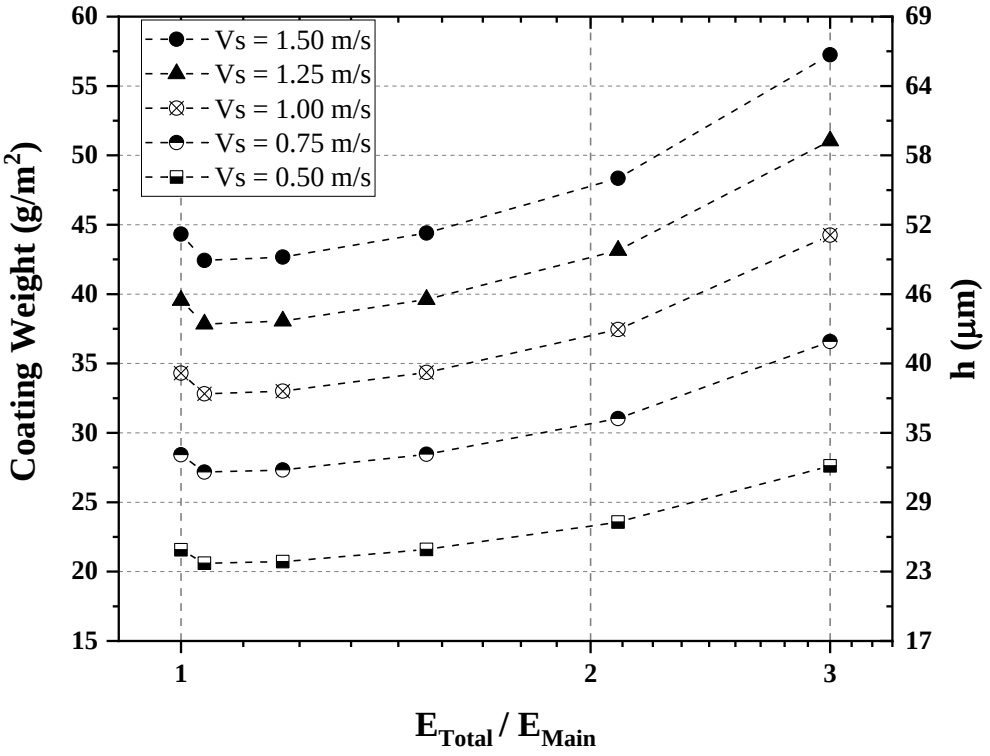

Figure 7-4) Final coating weight as a function of the total input energy of the multi-slot air knife for Re_m = 11000, Z/D = 12, D = 1.5 mm, D_a = 1.5 mm and s = 10 mm, $0.5 \leq V_s \leq 1.5$ m/s and $3000 \leq Re_a \leq 11000$.

Based on the discussed numerical results and experimental measurements documented in Chapters 3-7, the operating and geometry parameters for the multi-slot air knife which

could lead to lower coating weights compared to the single slot jet are summarized in Table 7-1.

Table 7-1) Summary of operating and geometry parameters which led to lighter coating weights using the multi-slot air knife *versus* the single slot air knife

Re_m	V_s (m/s)	Re_a/Re_m	D_a/D	Z/D	s/D	a/D
7000	0.5-1.5	≤ 0.5	≤ 1	6-12	0-6	≤ 1
9000	0.5-1.5	≤ 0.5	≤ 1	8-12	0-6	≤ 1
11000	0.5-1.5	≤ 0.5	≤ 1	8-12	0-6	≤ 1
20000 -24000	0.5-1.5	≤ 0.5	≤ 1	15	0-6	≤ 1

Sound intensity measurements were conducted for the gas jet wiping process using the single and multi-slot air knives at various operating conditions such as the main jet Reynolds numbers ($20000 \leq Re_m \leq 24000$), auxiliary jet Reynolds numbers (Re_a = 5000 and Re_a = 10000), strip to nozzle ratios ($8 \leq Z/D \leq 16$) and strip velocities ($0 \leq V_s \leq 1.5$ m/s).

It was shown that, for the single jet wiping, there was a constant background sound pressure of 60 dB for all explored strip to nozzle ratios ($8 \leq Z/D \leq 16$) (Figures 6-4 and 6-5). For Z/D =11, Z/D =14 and Z/D =15 a tonal noise was also observed for single jet wiping (Figures 6-5a, 6-5c and 6-5d). Investigation of the noise generation showed that the tonal noise produced by the single slot jet was completely eliminated by using the multi-slot jet at Re_m = 20000 when the auxiliary jet was set at $Re_a/Re_m \leq 0.5$ (Figures 6-6a, 6-6b, 6-6c, 6-6d, 6-7a, 6-7b, 6-7c, 6-7d, 6-13a, 6-13b, 6-13c, 6-13d and Figure 7-5).

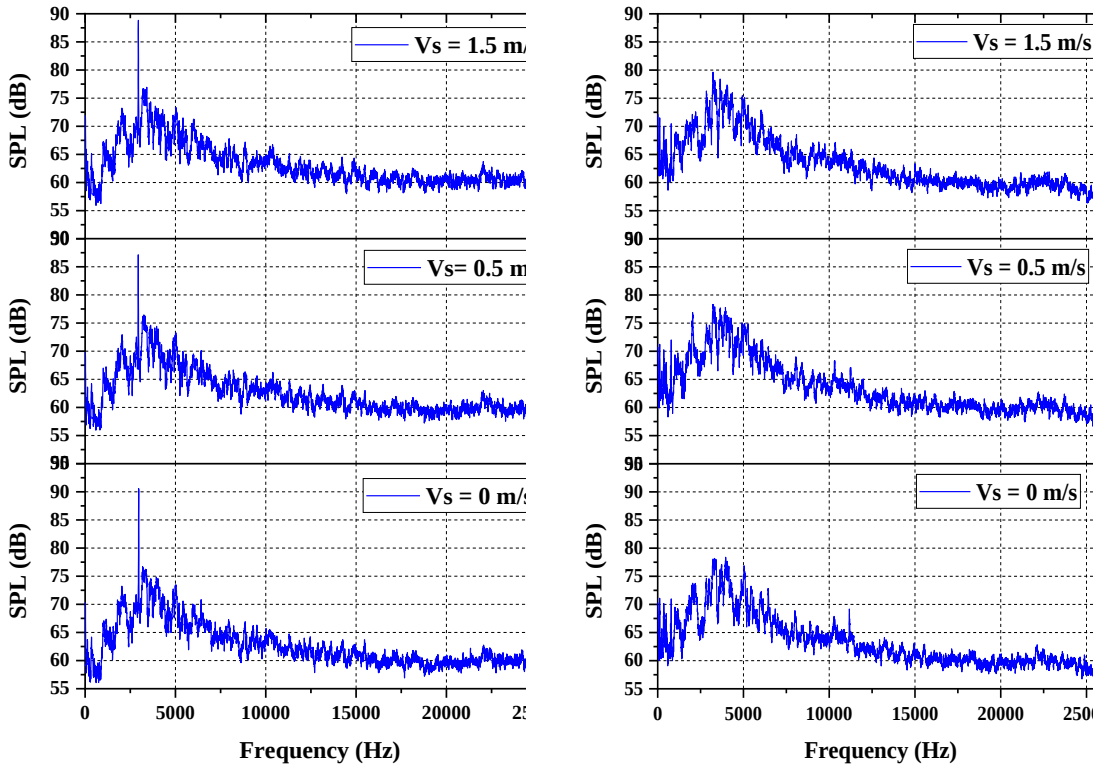

a) b)

Figure 7-5) Sound pressure level spectrum of a) single slot jet for Re_m = 20000 at Z/D = 15 and $0 \leq V_s \leq 1.5$ m/s and b) the multi-slot jet for Re_m = 20000, Re_a = 5000 at Z/D = 15 and $0 \leq V_s \leq 1.5$ m/s with $D_a/D = 1$.

The tonal noise was also observed for the single slot jet at higher main jet Reynolds numbers of Re_m = 22000 and Re_m = 24000 (Figures 6-8, 6-9a, 6-9b and 6-9c). For all cases, it was observed that by operating the auxiliary jets at $Re_a/Re_m \leq 0.5$, the tonal noise could be completely eliminated (Figure 6-10). This noise reduction through use of the multi-slot jet was observed for strip velocities ranging from $0 \leq V_s \leq 1.5$ m/s (Figures 6-11a, 6-11b, 6-11c, 6-11d, 6-12a, 6-12b, 6-12c and 6-12d) and is consistent with one of the identified operating parameters to produce lighter coating weights (Table 7-1).

Based on the analysis of noise reduction, the gas wiping parameters were set at Re_m = 20000, $Re_a/Re_m \leq 0.5$ and $D_a/D = 1$ (which was found to be beneficial in term of coating thickness reduction) and coating thickness measurements were performed. It was found that for the multi-slot jet operating at $Z/D = 15$, not only can the prototype multi-slot air knife eliminate tonal noise, but also it can also produce lighter coating weights compared the single slot air knife (Figure 6-15a and 6-15b).

The single slot air-knives which are currently used as the wiping actuators in the continuous galvanizing lines (CGLs), are usually set to operate at Re_m = 11000 while the knife to strip ratio (Z/D) is set to $Z/D \geq 10$ to avoid the nozzle blockage due to strip vibrations and slot clogging by Zn droplets. Improvements of the annealing section (Figure 2-1) have allowed the production line speed to be increased up to 100 m/min (~ 1.5 m/s). However, as discussed in Chapter 2, the single air knife configuration is close to its limit to produce lighter coating weights at higher line speeds. From a practical point of view, multi-slot air knives could be a promising, practical alternative to the tradition single air knife technology. It was shown in this study that under the specified geometry parameters and operating window illustrated in Table 7-1, using the multi-slot air knife could lead to lower coating weights at higher strip velocities and the tonal noise which are the source of hygiene issues could be attenuated.

Chapter 8: Conclusions and Future Direction

8.1 Conclusions and contributions to knowledge

- Based on the sensitivity analysis on wall pressure gradient, wall shear stress distribution and final coating weight, a modified arrangement for a prototype multi-slot jet air knife was proposed. It was shown that lighter coating weights could be achieved for the arrangement of the multi-slot air knife in which the main and auxiliary jet centerlines coincided at a same point on the impingement wall with $D_a/D \leq 1$ and $a/D < 1$.
- Experimental measurements under a variety of knife geometry and process conditions were compared with the coating weight predictions of the analytical model developed by Elsaadawy et al. [1]. Good agreement was found between the experimental coating weight measurements and the predictions of the analytical model, which proved the applicability of the analytical model [1] for prediction of final coating weight via multi-slot air knife.
- An operating window was determined for the multi-slot jet design which could result in lower coating weights at higher strip velocities compared to that of single slot air knife. It was shown that in the range of strip velocities $0.5 \leq V_s \leq 1.5$ m/s and $7000 \leq Re_m \leq 24000$, by setting the auxiliary jet Reynolds number such that $Re_m/Re_a \leq 0.5$, lower coating weights could be achieved through use of multi-slot air knife for $Z/D > 8$ while $D_a/D \leq 1$.

- An energy analysis was carried out to compare the overall input energy for the multi-slot jet with that of single slot jet. The calculations showed that it is only required to have less than 5% of the main jet wiping energy as the auxiliary jets wiping energy in order to obtain lighter coating weights via the multi-slot jet design.
- It was observed that, over the range of geometric and jet operating parameters studied, the tonal noise generated by the single jet during gas jet wiping process was either attenuated or completely eliminated through the use of the multi-slot air knife. The measured coating weights also confirmed the ability of the multi-slot air knife to produce lower coating thicknesses compared the single jet wiping simultaneous with the tonal noise elimination.

In summary, it was shown that, the multi-slot jet configuration, in spite of its more complicated geometry and need for a multi-part air distribution system, can be operated with benefit to lower coating weights at reasonable strip velocities and also attenuation of high intensity tonal noise. This has positive implications for industrial hygiene and the possibility of being able to impart additional wiping energy to the coating, thereby allowing for further reductions of coating weight versus the traditional single-slot jet design.

8.2 Recommendations for future work

- Using the light absorption technique and high speed camera downstream of the multi-slot jet wiping region in order to determine the coating thickness uniformity.

- Investigate the ability of auxiliary jets on delaying of splashing phenomenon and determine if using the multi-slot jet design allows additional reductions in the final film thickness in some cases where the limitation of splashing will not permit stronger wiping with a single jet.
- Numerically simulate multi-slot jet wiping using two-phase flow methods in which the liquid side can be modeled on the moving substrate. In this case the shape of the liquid film can be predicted using different turbulent impinging slot jet configurations.
- The flow field can also be obtained through use of particle image velocimetry (PIV) method and later compared with the numerical velocity and vorticity fields.

Appendix A

Enhanced wall treatment for the RANS K-ε Model:

The fidelity of a numerical solution depends significantly on the near wall modeling as walls are the main source of mean vorticity and turbulence. Within the near-wall region, the solution variables have large gradients, and significant momentum and other scalar transports occur. Not only is the mean velocity affected through the no-slip condition that must be satisfied at the wall, but the nature of the turbulence is also changed by the presence of the wall in non-trivial ways. In the vicinity of the wall, the tangential velocity fluctuations and the normal fluctuations are reduced due to viscous damping and kinematic blocking, respectively.

Toward the outer part of the near-wall region, the turbulence is rapidly augmented by the production of turbulence kinetic energy due to the large gradients in mean velocity [12]. Thus, accurate representation of the flow in the near-wall region determines the successful prediction of wall-bounded turbulent flows.

A.1. Wall Functions vs. Near-Wall Model

According to Schlichting [12], the near-wall region can be divided into three layers. In the innermost layer, known as the “viscous sublayer”, the flow is almost laminar, and the (molecular) viscosity plays a dominant role in momentum and heat or mass transfer. In the outer layer, called the fully turbulent layer, turbulence plays a major role. In the

intermediate region between the viscous sublayer and the fully turbulent layer, the effects of molecular viscosity and turbulence are equally important [12].

There are two major approaches to modeling the near-wall region. In one approach, the viscous sublayer and buffer layer are not resolved, and semi-empirical formulae, commonly referred to as "wall functions", are used to bridge the viscosity-affected region between the wall and the fully turbulent region (Figure A-1). Thus, the need to modify the turbulence models in the fully turbulent region to account for the presence of the wall is obviated. The main shortcoming of all wall functions is that the numerical results deteriorate under refinement of the grid in the wall normal direction. Y+ values ($Y^+ = \frac{\rho u_\tau y}{\mu}$ where u_τ is the frictional velocity defined as $u_\tau = \sqrt{\frac{\tau_w}{\rho}}$ and y is the distance from the wall) of below 15 will result in unbounded errors in the wall shear stress and wall heat transfer values. Moreover, wall functions tend to become less reliable when the flow situation departs from the ideal conditions that are assumed in their derivation. Among others, the constant-shear and local equilibrium assumptions are the ones that most restrict the universality of the standard wall functions. Accordingly, in complex flows involving separation, reattachment, and impingement where the mean flow and turbulence are subjected to rapid changes, and when the flows are in strong non-equilibrium, the quality of the predictions is likely to be compromised through the use of the wall functions.

In another approach, which has been used throughout this study and is referred to as the near wall modeling approach, the turbulence models are modified to enable the viscosity-affected region to be resolved with an appropriate meshing strategy all the way to the wall,

including the viscous sublayer. Figure A-1, schematically illustrates the two approaches discussed above.

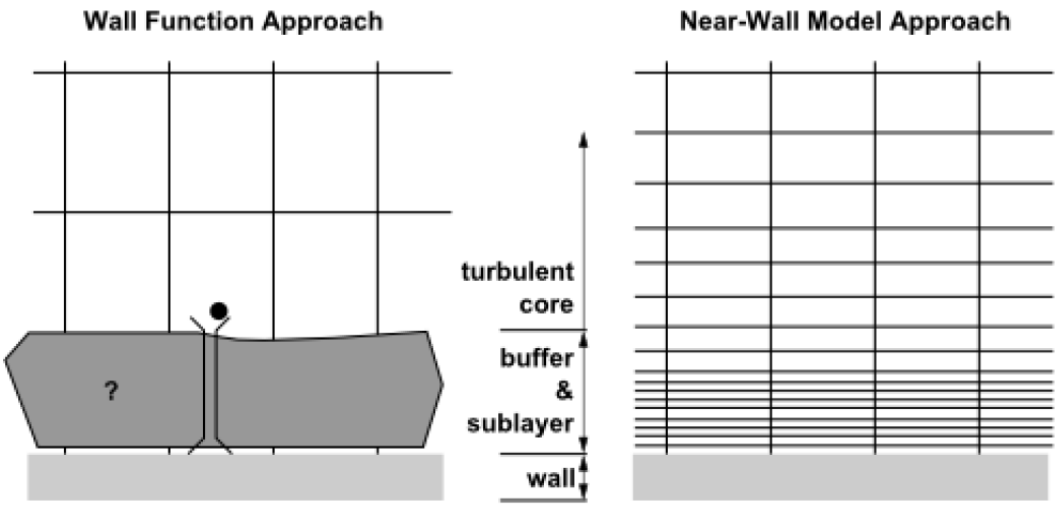

Figure A-1) Wall function approach vs near wall modelling approach [52].

A.2. Enhanced Wall Treatment

The Enhanced Wall Treatment is a near-wall modeling method that combines a two-layer model with enhanced wall functions. In this approach, the near-wall mesh must be sufficiently fine in the vicinity of the wall, which imposes higher computational costs in comparison with the wall function method. However, as the viscous sub-layer is totally resolved with the modified turbulent models in this approach, the non-physical results of the wall function approach can be avoided.

In this approach, the whole domain is subdivided into a viscosity-affected region and a fully turbulent region and the viscosity-affected near-wall region is completely resolved all the way to the viscous sublayer. The demarcation of the two regions is determined by a wall-distance-based turbulent Reynolds number, Re_y, defined as

$$Re_y = \frac{\rho y \sqrt{k}}{\mu}$$

A-1

where y is the wall-normal distance calculated at the cell centers.

In the fully turbulent region ($Re_y \geq Re_y^*$, $Re_y^* = 200$), the k-ε model is employed. While, in the viscosity-affected near-wall region ($Re_y < Re_y^*$), the one equation model of Wolfstein [53] is employed. In the one-equation model, the momentum equations and the k equation are retained as described in Chapters 3-5, however, the turbulent viscosity, $\mu_{t,Viscous}$ is computed using:

$$\mu_{t,Viscous} = \rho C_\mu l_\mu \sqrt{k}$$

A-2

The formulation for the turbulent viscosity described above is used as a part of the enhanced wall treatment, in which the viscosity defined in Equation A-2, is smoothly blended with the high-Reynolds number, μ_t from the outer region, as proposed by Jongen [54]:

$$\mu_{t,enh} = \lambda_\varepsilon \mu_t + (1 - \lambda_\varepsilon)\mu_{t,Viscous}$$

A-3

A blending function, λ_ε, is defined in such a way that it is equal to unity away from walls and is zero in the vicinity of the walls. The blending function has the following form:

$$\lambda_\varepsilon = \frac{1}{2}\left[1 + tanh\left(\frac{-Re_y}{A \quad y^*}\right)\right]$$

A-4

where the constant *A* determines the width of the blending function.

The ε field in the viscosity-affected region is computed from:

$$\varepsilon = \frac{k^{3/2}}{l_\varepsilon} \qquad \text{A-5}$$

The length scales that appear in Equation A-5 are computed from Chen and Patel [55]:

$$l_\varepsilon = y C_l^* \left(1 - e^{-Re_y/A_\varepsilon}\right) \qquad \text{A-6}$$

where $C_l^* = \kappa C_\mu^{-3/4}$, $A_\varepsilon = 2C_l^*$.

If the entire flow domain is inside the viscosity-affected region ($Re_y < Re_y^*$), ε is not obtained by solving the transport equation; it is instead obtained algebraically from Equation A-5. Otherwise, a procedure for blending of ε that is similar to the μ_t-blending is used in order to ensure a smooth transition between the algebraically specified ε in the inner region and the obtained ε from solution of the transport equation in the outer region.

References

(Used in Chaspter 1, Chapter 2, Chapter 7 and Chapter 8)

[1] E. A. Elsaadawy, G. S. Hanumanth, A. K. S. Balthazaar, J. R. McDermid, A. N. Hrymak, and J. F. Forbes, "Coating weight model for the continuous hot-dip galvanizing process," *Metall. Mater. Trans. B Process Metall. Mater. Process. Sci.*, vol. 38, no. 3, pp. 413–424, 2007.

[2] A. R. Marder, "'Metallurgy of zinc-coated steel,'" *Prog. Mater. Sci.*, vol. 45, no. 3, pp. 191–271, 2000.

[3] C. Gau and C. C. Lee, "Impingement cooling flow structure and heat transfer along rib-roughened walls," *Int. J. Heat Mass Transf.*, vol. 35, no. 11, pp. 3009–3020, 1992.

[4] A. R. P. S. A. SARKAR, N. NITIN, M.V. KARWE, "Fluid Flow and Heat Transfer in Air Jet," *J. Food Sci. Crh113*, vol. 69, no. 4, pp. 113–122, 2004.

[5] K. Kataoka, M. Suguro, H. Degawa, K. Maruo, and I. Mihata, "The effect of surface renewal due to large- scale eddies on jet impingement heat transfer," vol. 30, pp. 559–567, 1987.

[6] S. A. Strieg and T. E. Diller, "An analysis of the effect of entrainment temperature on jet impingement heat transfer," *J. Heat Transfer*, vol. 106, no. 4, pp. 804–810, 1984.

[7] C.-N. Li, H-L., Chiang, H-W. D., Hsu, "Jet impingement and forced convection cooling experimental study in rotating turbine blades," *Int. J. Turbo Jet Engines*, vol. 28, pp. 147–158, 2011.

[8] S. Polat, "HEAT AND MASS TRANSFER IN IMPINGEMENT DRYING," *Dry. Technol.*, vol. 11, no. 6, pp. 1147–1176, 1993.

[9] B. R. Hollworth and M. Durbin, "Impingement cooling of electronics," *J. Heat Transfer*, vol. 114, no. 3, pp. 607–613, 1992.

[10] S. Maurel and C. Solliec, "A turbulent plane jet impinging nearby and far from a flat plate," *Exp. Fluids*, vol. 31, no. 6, pp. 687–696, 2001.

[11] S. Beltaos and N. Rajaratnam, “Plane turbulent impinging jet,” *J. Hydraul. Res.*, vol. 11, no. 1, pp. 29–59, 1973.

[12] H. Schlichting, *Boundary Layer Theory*, Seventh Edition. McGraw-Hill, New York, 1979.

[13] Frank B. Incropera, Liquid Cooling of Electronic Devices by Single-Phase Convection. New York, Wiley-Interscience, 1999.

[14] J. A. Thornton and H. F. Graff, “‘An analytical description of the jet’ finishing process for hot-dip metallic coatings on strip,” *Metall. Trans. B*, vol. 7, no. 4, pp. 607–618, 1976.

[15] C. H. Ellen and C. V. Tu, “‘An analysis of jet stripping of molten metallic coatings,’” *J. Fluids Eng.*, vol. 106, no. December 1984, pp. 399–404, 1983.

[16] P. Naphade, A. Mukhopadhyay, and S. Chakrabarti, “‘Mathematical modelling of jet finishing process for hot-dip zinc coatings on steel strip,’” *ISIJ Int.*, vol. 45, no. 2, pp. 209–213, 2005.

[17] A. N. Hrymak, E. A. Elsaadawy, G. Hanumanth, J. R. McDermid, and F. E. Goodwin, “Air Knife Coating Weight Models,” in *AISTech Proceedings*, vol. II, no. April 2016, pp. 393–401, 2005.

[18] M. Dubois, “‘Review on Wiping : A Key Process Limiting CGL Productivity,’” in *Galvatech 2011 Conference Proceedings: HDG Process Technologies*, pp. 1847–1859, 2011.

[19] A. Gosset and J.-M. Buchlin, “Jet Wiping in Hot-Dip Galvanization,” *J. Fluids Eng.*, vol. 129, no. 4, pp. 466–475, 2007.

[20] E. O. Tuck and J.-M. Vanden Broeck, “Influence of Surface Tension on Jet-Stripped Continuous Coating of Sheet,” *AIChE J.*, vol. 30, no. 5, pp. 808–811, 1984.

[21] H. Yoneda, Master of Applied Science Thesis, “Analysis of air-knife coating,” Uneversity of Minnesota, USA, 1993.

[22] C. V Tu and D. H. Wood, “‘Wall pressure and shear stress measurements,’” *Exp. Therm. Fluid Sci.*, vol. 13, no. 4, pp. 364–373, 1996.

[23] A. N. Hrymak, J. F. Forbes, E. Elsaadawy, A. Balthazaar, Q. Hu, and J. Knight, ZCO-2-3: Improving Coating Weight Consistency. Final Report. McMaster University & University of Alberta. 2004.

[24] J.-M. Buchlin, "Modeling of gas-jet wiping. In Thin Liquid Films and Coating Processes, Von Karman Institute Lecture Series," in *Von Karman Institute Lecture Series*, Belguium, 1997.

[25] A. Gosset, P. Rambaud, L. Castellano, M. Dubois, and J. M. Buchlin, "'Modeling of gas-jet wiping at small standoff distances,'" in *Proc. of European Coating Symposium*, September 2005.

[26] Y. H. Kweon and H. D. Kim, "Study on the wiping gas jet in continuous galvanizing line," *J. Therm. Sci.*, vol. 20, no. 3, pp. 242–247, 2011.

[27] D. Lacanette, S. Vincent, and É. Arquis, "A numerical experiment on the interaction between a film and a turbulent jet," *Comptes Rendus Mécanique*, vol. 333, no. 4, pp. 343–349, 2005.

[28] D. Lacanette, A. Gosset, S. Vincent, J. M. Buchlin, and É. Arquis, "Macroscopic analysis of gas-jet wiping: Numerical simulation and experimental approach," *Phys. Fluids*, vol. 18, no. 4, 2006.

[29] Z. Yang and A. Bandivadekar, *Light-duty vehicle greenhouse gas and fuel economy standards*. International Council on Clean Transportation, 2017.

[30] H. G. Yoon and M. K. Chung, "Development of Novel Air-knife System to Prevent Check-mark Stain on Galvanized Strip Surface," *ISIJ Int.*, vol. 50, no. 5, pp. 752–759, 2010.

[31] T.-S. Cho, Y.-D. Kwon, and S.-B. Kwon, "A study of the influence of air-knife tilting on coating thickness in hot-dip galvanizing," *J. Therm. Sci.*, vol. 18, no. 3, pp. 262–267, 2009.

[32] S. Kim, J. Cho, K. Ahn, and M. Chung, "Numerical analysis of edge over-coating in continuous hot-dip galvanizing," *ISIJ Int.*, vol. 43, no. 10, pp. 1495–1501, 2003.

[33] K. J. Ahn and M. K. Chung, “A noble gas wiping system to prevent the edge overcoating in continuous hot-dip galvanizing,” *Isij Int.*, vol. 46, no. 4, pp. 573–578, 2006.

[34] M. A. Mendez, “A Research Methodology to Study Jet Wiping Processes,” no. May 2016, pp. 2–6, 2015.

[35] H. So, H. G. Yoon, and M. K. Chung, “Large eddy simulation of flow characteristics in an unconfined slot impinging jet with various nozzle-to-plate distances,” *J. Mech. Sci. Technol.*, vol. 25, no. 3, pp. 721–729, 2011.

[36] C. Pfeiler, W. Eßl, G. Reiss, C. K. Riener, G. Angeli, and A. Kharicha, “Investigation of the Gas-Jet Wiping Process − Two-Phase Large Eddy Simulations Elucidate Impingement Dynamics and Wave Formation on Zinc Coatings,” *Steel Res. Int.*, vol. 88, no. 9, pp. 1–10, 2017.

[37] “A Guide to the Noise Regulation (O. Reg. 381/15) under the Occupational Health and Safety Act,” *Ontario-Ministary of labour*, 2016. .

[38] M. Dubois, “Characterization of noise generated by gas wiping,” Part-1, Galvanizers Meeting- 2001. ILZRO, 2001.

[39] A. M. Petrie, “An experimental investigation of the noise produced by air jet impingement on flat plates,” *Appl. Acoust.*, vol. 7, no. 2, pp. 117–126, 1974.

[40] N. S. Nosseir and C. M. Ho, “Dynamics of an impinging jet. Part 2. The noise generation,” *J. Fluid Mech.*, vol. 116, pp. 379–391, 1982.

[41] D. Arthurs and S. Ziada, “Noise Generated by Impingement of a Planar Jet on a Flat Plate,” *J. Can. Acoust. Assoc.*, vol. 35, no. 3, pp. 28–29, 2007.

[42] D. Finnerty, J. McDermid, S. Ziada, and F. Goodwin, “A Parametric Study of Auxiliary Air Knives for the Purpose of Noise Reduction,” *AISTech 2016 Proc.*, no. 905, pp. 2075–2082, 2016.

[43] J. R. McDermid, D. Finnerty, S. Ziada, and F. E. Goodwin, “Properties of a Novel Air-Knife Design – Part II,” in *109th Meeting of the Galvanizer’s Association*, 2017.

[44] C. V Tu, “Stripping liquid coatings,” no. 18, p. 5, 1994.

[45] P. Tamadonfar, J. R. McDermid, A. N. Hrymak, and F. E. Goodwin, "Numerical investigation of air knives with multiple-impinging slot jets in continuous hot-dip galvanizing," in *AISTech - Iron and Steel Technology Conference Proceedings*, pp. 517–525, 2010.

[46] G. Y. Kim, H. D. Park, D. E. Lee, and W. C. Chung, "'Gas wiping apparatus having multiple nozzles,'" US 2010/0031879 A1, 2008.

[47] P. Tamadonfar, J. R. McDermid, A. N. Hrymak, and F. E. Goodwin, "Study of a multi-slot air knife in the wiping process of liquid zinc coatings," in *8th International Conference of Zinc and Zinc Alloy Coated Steel Sheet (GalvaTech 2011)*, 2011.

[48] S. Alibeigi, J. R. McDermid, S. Ziada, and F. E. Goodwin, "Effect of Air Knife Geometry on Coating Weight Control in the Continuous Galvanizing Line," in *Galvatech 2013: 9th International Conference on Zinc and Zinc Alloy Coated Steel Sheet & 2nd Asia-Pacific Galvanizing Conference*, 2013, pp. 437–440.

[49] K. Myrillas, A. Gosset, P. Rambaud, M. Anderhuber, J. M. Mataigne, and J. M. Buchlin, "Technique for delaying splashing in jet wiping process," *Chem. Eng. Process. Process Intensif.*, vol. 50, no. 5–6, pp. 466–470, 2011.

[50] S. Alibeigi, Master of Applied Science Thesis, "Experimental investigation of air-knife geometry in continuous hot-dip galvanizing," McMaster University, Canada, 2013.

[51] A. Ritcey, J. R. McDermid, and S. Ziada, "'Wall shear stress under an impinging planar jet using the razor blade technique,'" in *ICFMFA 2015 : 17th International Conference on Fluid Mechanics and Flow Analysis*, 2015.